POLYMER BASED NANOCOMPOSITE ELECTROLYTES FOR Li-ION BATTERIES

Ph.D. THESIS

by

RAJNI SHARMA

DEPARTMENT OF METALLURGICAL AND MATERIALS ENGINEERING
INDIAN INSTITUTE OF TECHNOLOGY ROORKEE
ROORKEE - 247 667 (INDIA)
JULY, 2015

POLYMER BASED NANOCOMPOSITE ELECTROLYTES FOR Li-ION BATTERIES

A THESIS

Submitted in partial fulfilment of the requirements for the award of the degree of

DOCTOR OF PHILOSOPHY

in

METALLURGICAL AND MATERIALS ENGINEERING

by

RAJNI SHARMA

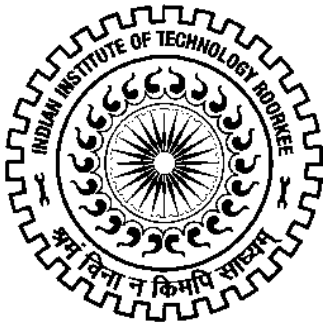

DEPARTMENT OF METALLURGICAL AND MATERIALS ENGINEERING
INDIAN INSTITUTE OF TECHNOLOGY ROORKEE
ROORKEE - 247667 (INDIA)
JULY, 2015

INDIAN INSTITUTE OF TECHNOLOGY ROORKEE
ROORKEE

CANDIDATE'S DECLARATION

I hereby certify that the work which is being presented in the thesis entitled **POLYMER BASED NANOCOMPOSITE ELECTROLYTES FOR Li-ION BATTERIES** in partial fulfilment of the requirements for the award of the Degree of Doctor of Philosophy and submitted in the Department of **Metallurgical and Materials Engineering** of the Indian Institute of Technology Roorkee is an authentic record of my own work carried out during a period from **July, 2010** to **July, 2015** under the supervision of **Dr. Anjan Sil, Professor** and **Dr. Subrata Ray, Professor**, Department of **Metallurgical and Materials Engineering**, Indian Institute of Technology Roorkee, Roorkee.

The matter presented in the thesis has not been submitted by me for the award of any other degree of this or any other Institute.

(RAJNI SHARMA)

This is to certify that the above statement made by the candidate is correct to the best of our knowledge.

(Anjan Sil)
Supervisor
Date:

(Subrata Ray)
Supervisor

The Ph.D. Viva-Voce Examination of **Mrs. RAJNI SHARMA**, Research Scholar, has been held on _____

Chairman, SRC

Signature of External Examiner

This is to certify that the student has made all the corrections in the thesis.

Signature of Supervisors

Head of the Department

To my parents (Prem Sharma and Saroj Sharma) and husband (Dr. Manvinder Tejpal) whose support has been a continuous source of motivation

and

To my teachers, for giving me the opportunity to spend the best of my life playing with the fascinating material in the world

Abstract

Novel studies of Wright and Armand in the late 1970s on ionically conducting polymers known as "polymer electrolytes" have opened an area of materials research with potential application in the power industry. The electrolytes have been known by their technological applications in the areas of energy conversion and storage. As compared to liquid electrolytes, the polymer electrolytes have several merits such as these materials have no leakage problem, ability to operate with highly reactive electrodes over a wide range of temperature and the possibility of miniaturization of device assembly. These advantages have drawn many researchers attention towards the development of lithium polymer batteries and other electrochemical devices such as electrochromic windows, supercapacitors, sensors etc.

The polymer electrolytes create a new market of the secondary battery and 'Sony' is the number one worldwide in the production of lithium-ion gel polymer batteries. The utilization of the lithium-ion gel polymer battery has been supported by the technical innovation of polymer electrolyte materials. Batteries based on polymer electrolytes are the subject of active research and development. In order to keep abreast with the rapid development of portable electronic equipment, improving the performance of polymer electrolytes has therefore become a goal of research. The polymers to act as electrolyte are desirable to possess the following characteristics: (i) high ionic conductivity, (ii) good dimensional stability, (iii) high cationic transport number, (iv) improved mechanical stability, (v) high chemical, electrochemical and thermal stability and (vi) compatibility with the materials of both anode and cathode.

The Ph.D. thesis deals with the synthesis and characterization of gel polymer electrolytes (GPEs) based on (i) PMMA-(PC+DEC)-$LiClO_4$ and (ii) P(VdF-HFP)-(PC+DEC)-$LiClO_4$ systems. Dispersoids used are multi-walled carbon nanotube (MWCNT), carbon nanofiber (CNF), silicon dioxide (SiO_2) nanofiber and titanium dioxide (TiO_2) nanofiber for the preparation of nanocomposite gel polymer electrolytes (NCGPEs). The various categories of polymer electrolytes are (a) Conventional dry/solid polymer electrolytes, (b) Plasticized solid polymer electrolytes, (c) Rubbery electrolytes, (d) Polyelectrolytes, (e) Gel polymer electrolytes and (f) Composite polymer

electrolytes. Each type is differentiated from another by a characteristic conductivity range. Gel polymer electrolytes have a relatively higher ionic conductivity and therefore are contemplated to be a potential candidate for application in high performance lithium ion battery. Though various researchers have conducted investigations on gel cast electrolytes, however, the primary focus of their studies are on achieving higher ionic conductivity of these materials.

In the present study, the GPEs and NCGPEs have been synthesized in the form of film by solution casting technique. An attempt has been made to integrate the investigation on mechanical characteristics such as strength of the films with desired ionic conductivity and thermal stability. It is needless to mention that mechanical strength is an essential requirement for the films to be inserted in the cell assembly. Different types of nanofiller (carbon and oxide based) were selected and for each type of nanofiller, several compositions were used to study the effect of filler quantity on the various properties of the NCGPEs. Dispersion of nanofiller in precursor polymer solution was made using ultrasonic probe. While the stress-strain characteristics were measured for the individual films, the ionic conductivity of MWCNT and CNF dispersed films were measured by adopting three-layer-film fabrication. The central layer of MWCNT/CNF dispersed layer was sandwiched both sides with filler free gel cast polymer layers. Such arrangement ensures the avoidance of electrical shorting for the electrical conductivity measurements.

The presentation of the entire thesis has been divided in six chapters.

Chapter I presents the introduction of the work stating the objective of the Ph.D. dissertation.

Chapter II presents the literature survey describing the state of the art of different types of polymer electrolytes in general and nanocomposite gel polymer electrolytes in particular. A brief description of ion transport models has also been made. The justification of taking up the problem has been highlighted.

Chapter III presents the properties of constituent materials viz. polymers (PMMA and P(VdF-HFP)), plasticizers (PC+DEC), salt ($LiClO_4$) and inorganic fillers (MWCNT, CNF, SiO_2 nanofiber and TiO_2 nanofiber) used in preparing GPEs and NCGPEs. Synthesis techniques for the preparation of GPEs and NCGPEs by solution casting method have been explained. Principles of various characterization tools and instruments employed to characterize the GPEs and NCGPEs in

the present work have been briefly explained. The ionic, mechanical, thermal characteristics and electrochemical analysis of the GPEs and NCGPEs have also been discussed.

Chapter IV presents results and discussion on the synthesis of the GPEs based on (i) PMMA-(PC+DEC)-$LiClO_4$ and (ii) P(VdF-HFP)-(PC+DEC)-$LiClO_4$ systems along with their physical, chemical and electrochemical characteristics.

Chapter V presents results and discussion on the synthesis of various types of NCGPEs dispersed with different types of nanofillers viz. MWCNTs, CNFs, SiO_2 nanofiber and TiO_2 nanofiber in both the systems i.e PMMA-(PC+DEC)-$LiClO_4$ and P(VdF-HFP)-(PC+DEC)-$LiClO_4$. The enhancement in the mechanical, thermal and electrochemical properties that has been observed for all the NCGPE films with respect to their GPE counterpart has been discussed.

Chapter VI outlines the major conclusions drawn from the work done. The future scope of the related field is also briefly stated.

List of Publications

Peer Reviewed Journals:

[1] R. Sharma, A. Sil and S. Ray, "Characterization of Plasticized PMMA-$LiClO_4$ Solid Polymer Electrolytes". Advanced Materials Research, 585 (2012) 185-189.

[2] A. Sil, R. Sharma and S. Ray, "Mechanical and thermal characteristics of PMMA-based nanocomposite gel polymer electrolytes with CNFs dispersion". Surface and Coatings Technology, 271 (2015) 201-206.

[3] R. Sharma, A. Sil and S. Ray, "Effect of Carbon Nanotube Dispersion on Electrochemical and Mechanical Characteristics of Poly(methyl methacrylate)-based gel polymer electrolytes". Polymer Composites, 2015. (DOI 10.1002/pc.23372)

[4] A. Sil, R. Sharma and S. Ray, "Carbon nanofibers reinforced P(VdF-HFP) based gel polymer electrolyte for lithium-ion battery application". World Academy of Science, Engineering and Technology, 9 (2015).

[5] R. Sharma, A. Sil and S. Ray, "Poly(methyl methacrylate) based nanocomposite gel polymer electrolytes with enhanced safety and performance". Journal of Polymer Research, Under Review.

[6] R. Sharma, A. Sil and S. Ray, "Mechanical and electrochemical properties of poly(methyl methacrylate) based composite gel polymer electrolytes reinforced with nano-sized TiO_2 ceramic fibers". Journal of Polymer Testing, Under Review.

[7] R. Sharma, A. Sil and S. Ray, "Development of P(VdF-HFP) based nanocomposite polymer electrolytes reinforced with multiwalled carbon nanotubes". Journal of Dispersion Science and Technology, Communicated.

[8] R. Sharma, A. Sil and S. Ray, "Dispersibility of TiO_2 nanofibers on the performance of P(VdF-HFP) based composite polymer electrolytes for Li-ion batteries". Energy Storage Materials, Communicated.

Conference Proceedings/Symposium:

[9] R. Sharma, A. Sil and S. Ray, "Investigation of Ionic Conduction in PMMA-$LiClO_4$-(PC-DEC) Polymer Gel Electrolytes", Global Challenges- Role of Science and Technology in Giving Their Solutions (GC-RSTS). March 3-4, 2012; TITS Bhiwani.

[10] R. Sharma, A. Sil and S. Ray, "Characterization of Plasticized PMMA-$LiClO_4$ Solid Polymer Electrolytes", Advances in Materials and Processing Challenges and Opportunities (AMPCO). Nov 2-4, 2012; IIT Roorkee.

[11] R. Sharma, A. Sil and S. Ray, "Ionic Conduction in P(VdF-HFP)-(PC+DEC)-$LiClO_4$ Gel Polymer Electrolytes", International Symposium for Research Scholars (ISRS). Dec 13-15, 2012; IIT Madras.

[12] R. Sharma, A. Sil and S. Ray, "Synthesis and Characterization of 0.60P(VdF-HFP):0.15(PC+DEC):0.10$LiClO_4$ gel polymer electrolyte", Advances in Material Science for Energy Applications (AMSEA). Jan 9-10, 2014; UPES Dehradun.

[13] R. Sharma, A. Sil and S. Ray, "Conductivity and thermal behavior of P(VDF-HFP) based nanocomposite polymer electrolytes", International Conference on Functional Materials (ICFM). Feb 5-7, 2014; IIT Kharagpur.

[14] R. Sharma, A. Sil and S. Ray, "Conductivity, infrared and thermal studies on plasticized polymer electrolytes with nano-sized ceramic fillers", 17th Punjab Science Congress (PSC). Feb 14-16, 2014; PTU Jalandhar.

[15] A. Sil, R. Sharma and S. Ray, "Mechanical and thermal characteristics of PMMA based nanocomposite gel polymer electrolytes with CNFs dispersion" 8th International Conference on Surfaces, Coatings and Nanostructured Materials (NANOSMAT). Sept 8-11, 2014; Dublin, Republic of Ireland.

[16] R. Sharma, A. Sil and S. Ray, "Preparation and Characterization of Nanocomposite Polymer Electrolytes Based on Poly(Methyl Methacrylate) with Nano-sized Ceramic Fillers". Materials Science & Technology 2014 (MS&T). Oct 12-16, 2014; Pittsburgh, USA.

[17] R. Sharma, A. Sil and S. Ray, "Structural, thermal and ionic properties of PVDF-HFP based nanocomposite gel polymer electrolytes dispersed with CNTs for li-ion batteries". 6th International Conference on Advancements in Polymeric Materials (APM). Feb 20-22, 2015; IISc Bangalore.

[18] R. Sharma, A. Sil and S. Ray, "P(VdF-HFP) based gel polymer electrolytes reinforced with SiO_2 nanofibers for Li-ion Batteries". 19th Punjab Science Congress. Feb 07-09, 2016; SUSGOI Mohali (Accepted).

Acknowledgements

Any doctoral thesis is not possible without the help and support of many people and to thank or even to acknowledge all of them is not possible within few pages. But I would like to mention as many as I can.

First and foremost, my utmost gratitude goes to Almighty God for giving me patience and courage to successfully complete my thesis work. I am eternally grateful to my family for their unremitting support. It goes without saying that none of this would have been possible without them.

I owe a sincere word of gratitude to my respected supervisors Prof. Anjan Sil and Prof. Subrata Ray whose excellent guidance, invaluable encouragement and support has made me complete my project. They have been a constant source of inspiration to me. They have also molded my outlook towards the science of materials. With all that they gave me even after that if I felt lost or dejected sometime they was always ready to boost my morale and helped me with my work. Their comprehensive knowledge and incisive insight in this field of research had inspired many critical ideas in this project. Besides the guidance in research they were always with me throughout my Ph.D. They were always available whenever I need advices and help. Needless to say, I shall be highly obliged to them for all the time.

I am deeply indebted to the Head, Department of Metallurgical and Materials Engineering, Indian Institute of Technology Roorkee, for his help and providing the facilities in the department for the research work. Sincere thanks to the Head, Institute Instrumentation Centre, for their co-operation in providing excellent facilities during the entire course of my experimental work.

I would like to acknowledge the other members of my Ph.D. committee, Prof. S. K. Nath, Dr. R. K. Dutta and Prof. B. S. S. Daniel, who monitored my work and took effort in reading and providing me with valuable comments on earlier versions of this thesis.

I wish to place my sincere thanks to the technical and administrative staff of the Department of Metallurgical and Materials Engineering, especially to Mr. Dhanprakash, Mr. R. K. Sharma, Mr. Rajinder Sharma, Mr. Dharam Pal, Mr. Satish Kr. Sharma, Mr. N. S. Rathod, Mr. Shakti Gupta, Mr. Kuldeep, Mr. Narendra, Mr. Shadiram who have helped in many ways during the course of

my Ph.D. Thanks are also due to Mr. Ramveer Singh, our departmental librarian and to Mr. S. D. Sharma, Mr. A. Saini, Mr. Shivkumar, Mr. Gotian, Mr. Mahaveer of IIC, for providing all the necessary help.

There are several people who deserve special thanks for providing help in my research. Some of them are Dr. Koushik Ghosh, Department of Chemistry; Prof. Anil Kumar, Head, Department of Chemistry.

I convey my sincere gratitude and thanks to Prof. O. P. Pandey, Dr. Bhupendra Chudasama and Dr. Punit Sharma for encouraging me to enter into the field of research.

I had the distinct pleasure of working with Dr. Kevin Knowles and his student Samantha O'Callaghan, University of Cambridge, UK during their visit at IIT Roorkee. I enjoyed both the professional and personal interactions with them.

I would also like to thank my many senior colleagues and lab mates for creating an interacting and enthusiastic research atmosphere. I am especially grateful to Dr. Kuldeep Singh Rana, Dr. Kuntal Maiti, Dr. Priti Singh, Dr. Gurpreet Singh and Dr. Vinay Pratap Singh. They gave me valuable comments and suggestions in completing this thesis work. I sincerely acknowledge the help received from Dr. Malay Jana with whom I had plenty of fruitful discussions at various stages. He has always been very supportive and caring. I would like to thank Dr. M. Deka for his help and encouraging words. My special and extended thanks to Sobhit, Siddhartha, Abhishek, Pritha, Hari Raj, Nitish, Sayeed, Ankit for being there always.

During my stay in IIT Roorkee, I was associated with several friends and colleagues. I appreciate each one of them for their moral support and cooperation which helped to keep things in perspective. Thanks to Ram, Kaushal, Sunil, Tilak, Himanshu, Manjit, Arun.

My hostel mates Alka and Snigdha were like my family members in Roorkee. We shared lot of happy experiences like traveling, party, dining. I will always remember those happy days of hostel life in Roorkee when we were together. The hostel life in Roorkee which includes some friends from the junior batch was strength for me ever. Thanks to Manisha, Ankita, Archana, Yash, Vimal, Niharika……there are a lot, thanks to them also.

Last but not the least I would like to acknowledge the financial support from Ministry of Human Resource & Development (MHRD), Government of India, Indo-Australia Strategic Research Fund (IASRF) of the Department of Science and Technology (DST), Government of India and UK-India Education and Research Initiative (UKIERI) for carrying out this work.

During the tenure of this thesis work, I was accompanied and supported by many people. So, I would like to express my gratitude to all those who helped me in completing my thesis.

(RAJNI SHARMA)

Contents

List of Abbreviations

AC	Alternating Current
Al_2O_3	Aluminium Oxide
$BaTiO_3$	Barium Titanate
BS	Backscattering
CeO_2	Cerium Oxide
CNF	Carbon Nanofiber
CPE	Composite Polymer Electrolyte
DC	Direct Current
DBP	Dibutyl Phthalate
DEC	Diethyl Carbonate
DIEPIG	Diepoxy Polyethylene Glycol
DMC	Dimethyl Carbonate
DME	Dimethoxyethane
DSC	Differential Scanning Calorimetry
DTG	Differential Thermogravimetric
EC	Ethylene Carbonate
EDAX	Energy Dispersive X-ray Analysis
EV	Electrical Vehicle
FESEM	Field Emission Scanning Electron Microscope
FTIR	Fourier Transform Infrared Spectroscopy
GPE	Gel Polymer Electrolyte
HEV	Hybrid Electrical Vehicle
$LiAlO_2$	Lithium Aluminate
$LiAsF_6$	Lithium Hexafluoro Arsenide
$LiCF_3SO_3$	Lithium Trifluoromethane Sulfonate
$LiClO_4$	Lithium Perchlorate
$LiN(CF_3SO_2)_2$	Lithium Bis(trifIuoromethanesulfonimide)
$LiNBO_3$	Lithium Niobate
$LiPF_6$	Lithium Hexafluorophosphate
MMT	Montmorillonite
MWCNT	Multi Walled Carbon Nanotube
$NaClO_4$	Sodium Perchlorate

NaOH	Sodium Hydroxide
NaSCN	Sodium Thiocyanate
NCPE	Nanocomposite Polymer Electrolyte
NCGPE	Nanocomposite Gel Polymer Electrolyte
NH_4SCN	Ammonium Thiocyanate
NMR	Nuclear Magnetic Resonance
PAN	Poly(acrylonitrile)
PAni	Polyaniline
$PbTiO_2$	Lead Titanate
PC	Propylene Carbonate
PEG	Poly(ethylene glycol)
PEO	Poly(ethylene oxide)
PMMA	Poly(methyl methacrylate)
PPO	Poly(propylene oxide)
PVA	Poly(vinyl alcohol)
PVB	Poly(vinyl butyl)
PVC	Poly(vinyl chloride)
PVdF	Poly(vinylidene fluoride)
P(VdF-HFP)	Poly(vinylidene fluoride-hexafluoropropylene)
RT	Room Temperature
SAD	Selected Area Diffraction
SAP	Silica Aerogel Powder
SAXS	Small Angle X-ray Scattering
SE	Secondary Electron
SEI	Surface Electrolyte Interphase
SEM	Scanning Electron Microscopy
SHI	Swift Heavy Ion
SiO_2	Silicon Dioxide
SPE	Solid Polymer Electrolyte
SS	Stainless Steel
TCNQ	Tetracyanoquinodimethane
TEM	Transmission Electron Microscopy
TEP	Triethyl Phosphate
TGA	Thermogravimetric Analysis

TiO_2	Titanium Dioxide
TMP	Trimethyl Phosphate
VTF	Vogel-Tamman-Fulcher
WLF	William-Landel-Ferry
XRD	X-ray Diffraction
ZrO_2	Zirconium Dioxide

List of Figures

List of Tables

Chapter 1

Introduction

Chapter 1

Introduction

Modern life requires steady and reliable energy supplies, which, in the present days, should be clean and renewable so as to ensure sustainability. Though fossil fuels have been and are still the major energy resources, but future availability and limitation of greenhouse gas emission and other pollutants are worrying aspects of the current energy scenario. Unless alternative energy sources emerge, global warming caused by greenhouse gases may eventually threaten our existence. There is an extensive exploration of alternate ways of generating energy and also the feasibility of the energy storage, which is required, may be at different times. Also, the storage of energy is required for mobile power sources as in non-polluting electric vehicles and mobile tools. The lithium ion batteries, in particular, are at the forefront amongst the contenders for high power applications because of their higher performance and being light in weight, making it superior to either lead acid, nickel cadmium or nickel metal hydride battery systems. There is a significant success of lithium ion battery in consumer electronics. However, the current commercial lithium-ion batteries may still be improved considerably in respect of specific energy density to provide power for electric vehicle (EV) and hybrid electric vehicle (HEV). Thus, there is continuing search for lithium-ion batteries with higher ionic conductivity, thermal, mechanical and better dimensional stability. Just like any other types of batteries, a lithium-ion battery also consists of major three components which are an anode, a cathode and the electrolyte between the electrodes and it works by converting the chemical potential to the electrical energy through the electrochemical reaction which includes the heterogeneous process of charge transfer that occurs at an electrode surface.

Nearly 150 years have passed since the discovery of ionic conduction in Ag_2S and PbF_2 which are non-metallic solids by Faraday in 1839 (Faraday, 1839). A lot of continuous efforts have been devoted to develop newer ion conducting materials for electrochemical devices such as electrochromic windows, supercapacitors, high energy density batteries, micro/nano-electromechanical sensors etc. by the researchers worldwide. Till now various ion conducting materials like glasses, ionic salts, ceramics etc. have been tried out for the electrochemical device applications but the ion conducting polymers called “polymer electrolytes” are receiving

remarkable attention (Agrawal et al, 2008). The reason of using such polymeric electrolytes over liquid and other solids lies in the free standing consistency which reduces the cost, easy handling, conformability to the electrodes and improved safety hazards (Fergus, 2010).

One of the most important steps in understanding of polymer electrolytes is that the ionic conductivity is a property of amorphous elastomeric phases (Berthier et al, 1983). Amorphous polymers having high molecular weight above their glass transition temperature may exhibit mechanical properties similar in most ways to those of a true solid, which is a result of cross linking and chain entanglement of different types of polymer. At microscopic level, however, local relaxation of polymer chain processes may still provide liquid like degree of freedom somewhat similar to that in an ordinary molecular liquid. Ionically conducting phases, free from low molecular weight solvents, based on the dissolution of salts in suitable ion coordinating polymers are the key components in new types of batteries for electric cars and portable electronic devices in which cations are transported from the anode to the cathode through the polymer electrolyte medium i.e. polymer itself is the medium in which ion conduction occurs. The application of polymer electrolytes in batteries requires following characteristics: high ionic conductivity, good dimensional stability, improved thermal, chemical and electrochemical compatibility with the material of both anode and cathode with good mechanical strength.

The development of various types of polymer electrolytes has mainly passed the following three different stages: (a) dry/solid polymer electrolytes (DPEs/SPEs), (b) gel polymer electrolytes (GPEs) and (c) composite polymer electrolytes (CPEs). The present study mainly focuses on two types of gel polymer electrolytes. One type is Poly(methyl methacrylate) (PMMA) based electrolytes giving rise to good ionic conductivity because of its beneficial effect on stabilization of the lithium-electrolyte interface and other type is Poly(vinylidenefluoride-co-hexafluoropropylene) (P(VdF-HFP)) having high dielectric constant, low crystallinity and low glass transition temperature with an excellent chemical stability due to VdF unit and plasticity due to HFP unit. However, GPEs exhibit various drawbacks, such as increased reactivity with lithium-metal electrode, volatility because of its beneficial effect on stabilization of the lithium-electrolyte interface and poor mechanical stability. In order to retain the physical and chemical properties of GPEs, the gel films have to be hardened either by physical or chemical curing (high energy radiation) which requires high processing cost. Alternatively, addition of nano-sized filler to the

polymer electrolytes has become an ever increasing attractive approach due to the enhanced ionic conductivity, improved mechanical and thermal stability with enhanced electrode-electrolyte interface stability by forming filler network into the polymer host, inhibiting crystallization, reorganization of the polymer chains and interacting with species of lithium ion (Croce et al, 1998). These types of materials are named as nanocomposite gel polymer electrolytes (NCGPEs) and are the main focus of present study.

Nanofiber and nanowire with their huge surface area to volume ratio, about a thousand times higher than that of a human hair, have the potential to improve material strength for various applications in energy materials. The large amount of surface area can have noticeable effect on the properties of the composite with the introduction of relatively a small amount of nano-sized reinforcement. Adding clay into polymer matrix improves the mechanical and thermal properties is one of the examples. Other kinds of nano-particulates may result in enhanced dielectric, optical, heat resistance or flame retardance and mechanical properties such as strength, stiffness and resistance to wear and damage. On the other hand, formation of nanocomposite electrolyte through the reinforcement by nanofiller having dimensions less than 100 nm into polymer matrix finds various important applications for the development of lithium polymer battery. The nanofillers for reinforcement can be of spherical shape as well as for plate-like and fibrous nanofiller with their high aspect ratio that exhibits a stronger effect on the performance. As a result, nanofiller because of their excellent thermal and mechanical properties coupled with very high aspect ratio theoretically are the ideal candidates for reinforcing a polymer matrix. The main challenge in this case lies in the fact of increased specific surface area due to the small size of the dispersing fillers and consequently forces per unit mass resulting from interactions between these surfaces and surrounding area become more pronounced. As a result, dispersion of nanofiller into the polymer matrix with different surface energy is quiet tough. However a strong interface between the reinforcing phase and the polymer matrix is always desirable in order to achieve desirable properties. Therefore, NCGPEs have attracted great interest due to their improved properties compared with the bare polymer and other conventional electrolytes.

This work focuses on current issues of polymer electrolytes related to enhancement of mechanical, thermal and electrochemical behaviour without affecting their ionic properties using various types of dispersoids (MWCNT, CNF, SiO_2 nanofiber and TiO_2 nanofiber) which are synthesized by

solution casting method which may be more suitable for application in the polymer electrolyte of lithium ion batteries in terms of performance and cost. The study reported in the thesis is divided into two segments. In the first segment the synthesis of gel polymer electrolytes by solution casting process has been discussed. In the second segment of this investigation, different types of nanofiller have been introduced so as to produce nanocomposite gel polymer electrolytes and correlated to their physical and chemical properties in order to assess the possibility for the application of the NCGPEs in lithium ion battery replacing the presently used liquid electrolytes which may be more suitable in terms of performance and cost.

Chapter 2

Literature Review

Chapter 2

Literature Review

This chapter describes the definitions of various types of polymer electrolytes viz. SPEs, GPEs and CPEs and their developments. A brief description of ion conduction mechanisms that explain the ion transport kinetics in solvent-free, gel and nanocomposite electrolytes and their models have been presented. At the end definition of the problem and scope of the present work are stated.

2.1 Historical Developments of Polymer Electrolytes

The path breaking studies of ionic conduction in solids by Faraday has been known since 1803 (Faraday, 1839). Afterwards various researchers worldwide made efforts to develop newer ion conducting materials for electrochemical devices such as high energy density batteries, sensors, supercapacitors etc (Tubandt et al, 1920). Several ion conducting materials like ionic salts, ceramics particles etc. have been tried out for applications in electrochemical device but ionically conducting polymers known as "polymer electrolytes" are receiving major attention and have opened an novel area of materials research with potential application in the energy source industry (Fenton et al, 1973; Stephan, 2006). As compared to liquid electrolytes, the polymer electrolytes have various advantages such as no leakage problem, ability to operate with highly reactive electrodes over a wide range of temperature, and the possibility of miniaturization of device assembly. These advantages have drawn attention towards the development of lithium polymer batteries for portable electronic devices and electric cars.

The main reason for using polymer electrolytes over other types of electrolytes lies in their flexibility and compatibility to the electrodes. The need for high ionic conductivity arises from the fact that how fast or at what rate energy from a battery can be drained which mainly depends on the extent of ion mobility in the electrolyte. For battery applications, the electrolyte must be dimensionally stable since the polymer electrolyte works as a separator, providing electrical insulation between anode and cathode, which implies that it must be possible to process polymer electrolyte into free-standing film with adequate strength. Since the electrolyte film is inserted between the cathode and the anode, in order to avoid undesireable chemical reaction proceeding at

the electrode-electrolyte interfaces, it should possess a high chemical stability. Also polymer electrolytes must have an electrochemical stability domain ranging from 0 to as high as 4-5 V (Song et al, 1999).

The first work on ion conducting polymer: poly(ethylene oxide) (PEO) dissolved with alkali metal salt were carried out by Wright et al. (Fenton, 1973) in 1973. Armand realized initially that these materials could be used as electrolytes in battery applications (Armand et al, 1978). There after a large number of polymer electrolyte materials involving different kinds of transporting ions, namely, H^+, Li^+, Na^+, K^+, Ag^+, Mg^{2+} etc. have been reported. Various theoretical approaches have been adopted to understand the mechanism of ion transport in the polymer electrolytes as well as their physical and chemical processes which occur at the polymer electrolyte-electrode interfaces (Gray, 1991; Alamgir, 1994). A number of research papers/books/monographs have been published, which deal with materials designing aspects in polymer electrolyte system and also a variety of techniques usually employed for structural/thermal/ion transport characterization of the polymer electrolyte systems (MacCallum, 1987; Scrosati, 1993; Bruce, 1995).

2.2 Classification of Polymer Electrolytes

The development of polymer electrolytes has gone through various categories from DPEs to GPEs and CPEs as shown in Fig. 2.1. In dry polymer systems, the host polymer is used as the solvent along with lithium salt. The example of DPEs is the PEO based systems which has very low conductivity value of the order of 10^{-8} S cm^{-1} at ambient temperature (Armand et al, 1979). The second stage of polymer electrolyte is called ‘‘gel polymer electrolyte’’ which is neither solid nor liquid or we can say that conversely both solid and liquid (Song, 1999). Basically, gels possess cohesive properties of the solids and the diffusive property of liquids which makes them finding various important applications. The third one is “composite polymer electrolytes” which include inorganic solids with high surface area in proportion with a ‘dry polymer’ or ‘gel polymer’ system. Generally, particulate type filler with high surface area such as ZrO_2, Al_2O_3 and clay particles are incorporated into the polymer matrices and the combined systems are called “composite polymer electrolytes” (Lee et al, 2003). The advantages of adding inorganic fillers into the polymer matrix not only increase the ionic conductivity but also improves the mechanical strength as well as electrode-electrolyte interface stability (Stephan, 2005; Ray, 2008).

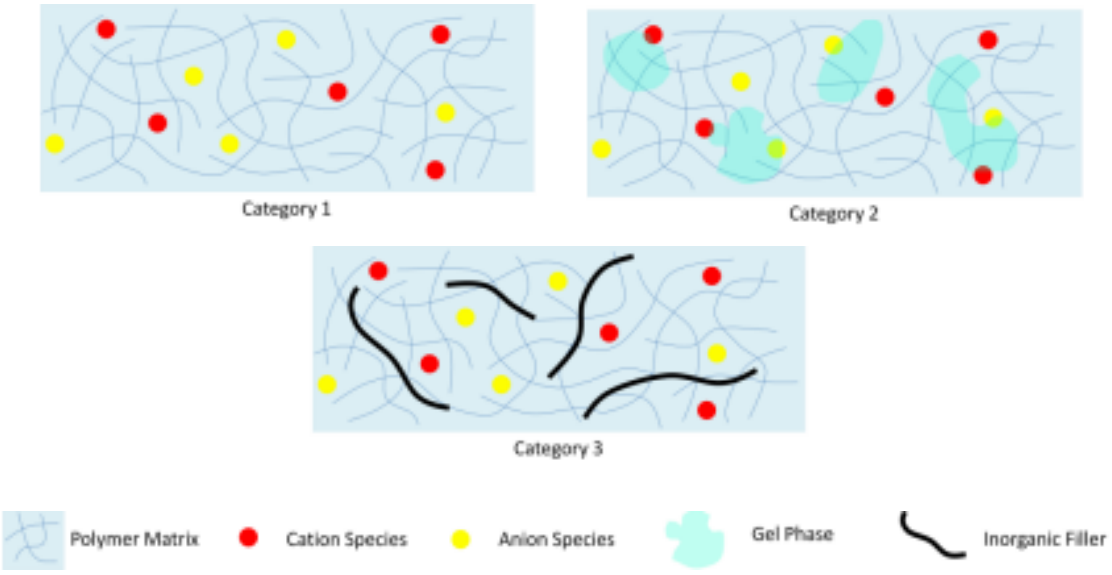

Fig. 2.1: Different categories of polymer electrolytes i.e. Category 1: Dry Polymer Electrolytes; Category 2: Gel Polymer Electrolytes and Category 3: Composite Polymer Electrolytes (Scrosati, 2000).

A detailed description on the above three types of polymer electrolytes are given below:

2.2.1 Solid Polymer Electrolytes

As already pointed out, after the discovery of the SPEs i.e. PEO with an alkali metal salt complex in 1973 followed by an experimental demonstration of the first all solid-state battery based on the PEO, Li^+ ion polymer electrolyte enhanced the activity in this area tremendously since 1979. The majority of SPEs reported so far are based on high molecular weight polymers i.e. PEO and/or poly (propylene oxide) (PPO) complexed with different lithium salts. The main reason for preferring PEO/PPO as the polymer host was due to the fact that they usually form stable dry complexes exhibiting a relatively higher ionic conductivity than with other solvating polymers. The oxyethylene group: $–CH_2–CH_2–O–$ and the polar groups: –O–, –H–, –C–H– present sequentially in the polymer chains have the ability to dissolve the ionic salts. In late 1970's, at Sheffield, Wright and his coworkers (Lee et al, 1982) carried out an investigation on morphology of polymer complexes and its relation with ionic conductivity. They found that fully saturated crystalline region of PEO complexes yield poor conductivity and amorphous region gives higher conductivity. At the same time Killis et al. (Killis et al, 1980) had independently reached similar conclusions regarding PEO (amorphous) with urethane based PEO networks. The branched or

comb polyphosphazenes developed by Shriver and coworkers (Blonsky et al, 1984) at Pennsylvania and development of methoxy copolymer at Manchester by Booth's group (Nicholas et al, 1988) were among the most successful of these. Torrel et al. (Torrel et al, 1988) discussed the relationship between ionic conductivity and relaxation time. At about the same time, various theories and mechanisms of ion transport in these materials were also developed which include the dynamic percolation model (Ratner et al, 1989). The correlation between glass transition temperature, ionic conductivity and mechanical relaxation was investigated by Cheradame et al. (Cheradame et al, 1982) and Watanabe et al. (Watanabe et al, 1987). After the realization that ionic conductivity in DPEs could be increased by (i) suppressing the crystalline part of the host polymer enhancing polymer chain mobility resulting in the fast cation movement and (ii) increasing the number of charge carriers. Various attempts have been made to find the optimal combination of host polymer and dopant salt for faster ionic movement. To suppress the crystallization of polymer in order to enhance the mobility of polymer chain, various efforts have been made which include co-polymerization, cross-linking, comb formation (side chain and dendritic polymers), polymer alloy (including interpenetrating network) and blending with inorganic fillers (Yamamoto, 2007). Killis et al. (Killis et al, 1984) in combination with cross-linking and co-polymerization were able to achieve ionic conductivity of 5×10^{-5} Scm^{-1} at ambient temperature by cross-linking co-polymers of EO and PO. In the comb formation, Hall et al. (Hall et al, 1986) added PEO side chain to polysyloxane chains and obtained an ionic conductivity of 2×10^{-4} Scm^{-1} at ambient temperature.

Increase of charge carriers can be realized by the use of highly dissociable salts or by increasing concentration of salt. Nature of salt i.e. size of cation and anion, organic/inorganic salt, its lattice energy etc., plays an important role in the determining behaviour of polymer electrolytes. It has been found that larger anion results in amorphous matrix and provides path for cation movement, which enhances the ionic conductivity. Vallee et al. (Vallee et al, 1992) obtained conductivity of 4×10^{-5} Scm^{-1} at ambient temperature by dissolving lithium trifluorosulfonyl imide in PEO, which is over two-orders of magnitude higher than that of NaI-PEO system. Fujinami et al. (Fujinami et al, 1997) achieved conductivity of 2×10^{-5} Scm^{-1} at 25 ºC with siloxy aluminate system. A new type of 'polymer-in-salt' material was proposed by Angell et al. (Angell et al, 1993) in which lithium salts are mixed with small proportions of polymer PPO and PEO and found the conductivity value in the order of 10^{-3} Scm^{-1}.

2.2.2 Gel Polymer Electrolytes

Gel polymer electrolytes are another type of polymer electrolytes of great interest, particularly with regard to achieving higher ionic conductivity. GPEs are formed by incorporation of substantial amount of plasticizers such as diethyl carbonate (DEC), ethylene carbonate (EC), propylene carbonate (PC) etc. into the polymer matrix. The conduction of ion takes place through the liquid electrolytes where the host polymer provides the structural support. Adding plasticizer into SPEs facilitates greater dissociation of ions which allows large number of charge carriers for ion transport with reduced crystalline content and increased segmental mobility of the polymer chains (Song et al, 1999). Ito et al. (Ito et al, 1987) first observed the increase of ionic conductivity due to the addition of low molecular weight plasticizer in SPEs (PEO) and were able to enhance the ionic conductivity of PEO-$LiCF_3SO_3$ complexes plasticized with PEG up to 10^{-3} Scm^{-1} at room temperature which was attributed to the increase in amorphous region of PEO. On the other hand, the enhancement in ionic conductivity is adversely accompanied by the poor interfacial properties which are present due to the hydroxyl end groups. In order to avoid this issue, a few researchers have eliminated hydroxyl end groups of PEG by methoxy groups which are less reactive (Sander et al, 1992). Nagasubramaniam and his co-workers (Nagasubramaniam et al, 1990) used crown ether as plasticizer and were able to obtain ionic conductivity of about 10^{-4} Scm^{-1} for the PEO-$LiBF_4$ complex. Shodai et al. (Shodai et al, 1994) studied the thermal stability of PEO-$LiCF_3SO_3$ using EC and PC as plasticizers in air as well as in argon atmosphere where they found that oxygen present in the air lowers the decomposition temperature of PEO and accelerates its decomposition rate. Kovac et al. (Kovac et al, 1994) examined the structural and electrochemical characterization of polymer electrolytes i.e. $(PEO)_nLiAl(SO_3Cl)_4$ (n = 2-12) containing a mixture of PC and 1, 2-dimethoxyethane (DME) as plasticizers. It was shown that a substantial amount of plasticizers (PC+DME) remain incorporated in the final polymer electrolyte and reduces the crystallinity of PEO by more than 50%. The PEO/PC/DME complex exhibited high ionic conductivity at lower temperatures (20 ºC to 60 ºC), while at higher temperatures (T > 60 ºC) without plasticizer showed better conductivity. Itoh et al. (Itoh et al, 2006) prepared two kinds of PEO based comb like polymer electrolytes with poly-4 of 3,5-bis(poly(ethylene glycol) methyl ether (350, n = 7.2) styrene and poly-4/TCNQ of 7,7,8,8-tetracyanoquinodimethane (TCNQ) as plasticizer and $LiN(CF_3SO_2)_2$ as salt to examine their ionic conductivity, mechanical, thermal and electrochemical properties. They showed that the polymer electrolytes containing an alternating copolymer poly-

4/TCNQ exhibited higher ionic conductivity, better mechanical and thermal properties than that of containing a homopolymer poly-4. An electrolyte consisting of PEO crosslinked with PPO as a host, PC as a plasticizer, and lithium perchlorate ($LiClO_4$) as salt was synthesized by Tien et al. (Tien et al, 2008) for double layer capacitors. Li et al. (Li et al, 2009) prepared PVB/$LiClO_4$ polymer electrolyte films by solution casting method with PEG_{200}, PEG_{400} and PEG_{600} as plasticizers. The bulk conductivity of the electrolyte films increased from 10^{-10} to 10^{-6} Scm^{-1} with the addition of plasticizers. PEG_{400} exhibited plasticizing function superior to PEG_{200} and PEG_{600} and the conductivity could reach up to 10^{-6} Scm^{-1} at 25 ºC by controlling the ratio of $[O]:[Li^+] = 8$ and also by adding 30 wt.% PEG_{400} with PVB.

Among the GPEs reported till very recently, poly(acrylonitrile) (PAN) based gel electrolytes have been extensively studied. Watanabe and co-workers (Watanabe et al, 1982 and 1983) reported PAN-$LiClO_4$ complex in which by increasing ratio of (EC+PC)/$LiClO_4$, they were able to increase the conductivity up to 10^{-4}-10^{-5} Scm^{-1} at 25 ºC. Since the conductivity is not related with PAN content so it did not play any role in the mechanism of ion transport but acted as a matrix for structural stability. Later Abraham et al. (Abraham et al, 1990) and Alamgir et al. (Alamgir et al, 1993) found conductivity of 1.7×10^{-3} Scm^{-1} at 20 ºC and 1.1×10^{-5} Scm^{-1} at –10 ºC for PAN based electrolytes comprising of 38 m/o EC, 33 m/o PC with 8 m/o $LiClO_4$ and 21 m/o of PAN. The electrochemical stability of PAN based electrolytes using various salts ($LiN(CF_3SO_2)_2$, $LiAsF_6$, $LiCF_3SO_3$ and $LiPF_6$) and plasticizers (EC+PC) was studied by Choe et al. (Choe et al, 1997) in which they observed oxidation stability more than 5.0 V vs Li^+/Li as revealed by cyclic voltammetry studies. A fully amorphous gel of PAN/$LiClO_4$/EC exhibits transference numbers of ion more than 0.5 because of the absence of oxygen atoms in the PAN polymer matrix which was studied by Appetecchi and his co-workers (Appetecchi et al, 1998). Carol et al. (Carol et al, 2011) used electrospinning technique to prepare the fibrous membrane of PAN and showed an ionic conductivity value of 1.7×10^{-5} Scm^{-1} at 20 ºC with good mechanical strength and porosity. The gelled membrane also exhibited stable charge-discharge characteristics when evaluated as a separator in Li-ion cells. Despite the several advantages of PAN based electrolytes like high ionic conductivity of the order of 10^{-3} Scm^{-1} at 20 ºC, transference number around 0.6 and good electrochemical stability of 4.5 V, its poor compatibility with lithium metal anode offsets from practical applications. Other studies clearly reveal that the lithium metal electrode undergoes

serious passivation when comes in contact with PAN based electrodes which further affects its cyclability leading to safety hazards (Song, 1999).

In 1985, Iijima and Toyoguchi (Iijima et al, 1985) found that PMMA could be used as a gelating agent. Thereafter, the material PMMA has attracted a lot of interest as GPEs. The research performed by Bohnke's group (Bohnke et al, 1992 and 1993) showed that atactic PMMA formed ionically conducting gel with $LiClO_4$ in PC, or mixture of PC and EC. The addition of PMMA in various proportions to $LiClO_4$-PC in electrolyte considerably increased the viscosity to reach a solid rubber like material. On the other hand, the conductivities at room temperature of these gels decreased very marginally and remained very close to the liquid electrolyte. At about 20 wt.% polymer concentrations, these gel possessed room temperature conductivities of the order 10^{-3} Scm^{-1}. This high ionic mobility could be explained by the existence of a continuous conduction path available through the solvent. Different characterization techniques showed that PMMA just acted as a matrix and no lithium solvation with PMMA was found. PMMA based electrolytes prepared by PC/EC-LiX (X = AsF_6, ClO_4 or $N(CF_3SO_2)_2$) was found to exhibit similar conductivity behaviour with a slight difference in the value of activation energy was examined by Appetecchi et al. (Appetecchi et al, 1995). Stallworth et al. (Stallworth et al, 1995) synthesized PMMA based electrolytes using various lithium salts ($LiAsF_6$, $LiClO_4$, $LiN(CF_3SO_2)_2$) and plasticizers (PC/EC) which exhibited single glass transition temperature with dramatic changes in Nuclear Magnetic Resonance (NMR) line width which occurred in the vicinity of transition. Rajendran et al. (Rajendran et al, 2000 and 2001) reported an enhancement in the mechanical property of PMMA by blending with poly(vinyl alcohol) (PVA). However, a decrease in conductivity at higher PVA content was observed due to increased viscosity. Kim and Oh (Kim and Oh, 2002) modified PMMA based gel electrolytes with interpenetrating networks of poly(ethylene glycol dimethacrylate) (PEGDMA) polymers with different numbers of repeating ethylene oxide units. The addition of PEGDMA resulted in increase in dimensional stability of electrolytes which is due to cross-linking effect exerted by the network former with enhanced ionic conductivity. This modification provides high donor number with high chain flexibility of the ethylene oxide units. Hashmi and his co-workers (Hashmi et al, 2007) carried out a study comprising of PMMA-(EC+PC)-(($LiClO_4$, $NaClO_4$ and $(C_2H_5)_4NClO_4$ ($TEAClO_4$)) salts with a view to using them as electrolytes in electrical double layer capacitors (EDLCs) based on electrodes of activated charcoal powder. The optimum composition of GPEs with PMMA (20

wt.%)-EC:PC(1:1 v/v)-1M salt exhibited high conductivity of the order ~10^{-3} Scm^{-1} at ambient temperature with good dimensional stability which is suitable for their application in EDLCs. The ionic conductivity and transference number of GPEs containing PMMA, EC, PC and $LiBF_4$ were studied by Osman et al. (Osman et al, 2012). The highest conductivity of 2.24×10^{-3} Scm^{-1} at room temperature was obtained for the sample having 20 wt.% of $LiBF_4$. The increase in the conductivity with increasing salt concentration was attributed to the increase in mobility and number of the charge carriers. The decrease in the conductivity at still higher concentration was due to the saturation of the salt resulting in the reduced number of charge carriers.

Another potential system of GPE based on poly(vinylidene fluoride) (PVdF) host has been investigated since the early 1980s (Watanabe et al, 1981). Tsuchida and his co-workers (Tsuchida et al, 1983) showed that the physically cross-linked gelled PVdF had a conductivity of 10^{-3} Scm^{-1} at ambient temperature. Jiang et al. (Jiang et al, 1997) synthesized a novel PVdF based gel electrolyte using plasticizers (EC+PC) and salts ($LiPF_6$, $LiCF_3SO_3$ or $LiN(SO_2CF_3)_2$) by thermal extrusion method. They reported that concentration of the charge carriers and the viscosity of the medium are directly related to the weight ratio of system which influence the conductivity of the electrolyte and also offered excellent electrochemical behaviour but this fluorinated polymer was not stable towards lithium metal leading to poor interfacial properties between lithium and fluorine. Choi et al. (Choi et al, 2007) prepared porous PVdF based membranes with a 3-D network structure, by electrospinning method using different mixed solvent compositions, which showed high porosity and large electrolyte solution uptake, excellent mechanical and electrochemical properties. FT-Raman data showed that the ions of lithium predominately associated with the molecules of EC indicating that Li^+ solvated EC is a major mobile ionic species. In addition, the PVdF chain showed good interaction that influenced the swelling of PVdF to form a gel phase and enhances electrochemical properties. Rajendran et al. (Rajendran et al, 2008) investigated the physical and thermal properties of blend based PVdF-PVC gel polymer electrolytes with composition PVdF(20) - PVC(5) - (60:40) wt. ratio of EC/PC(67) - $LiClO_4$(8) complex. The highest ionic conductivity was found 3.86×10^{-3} Scm^{-1} at ambient temperature.

Recently, P(VdF-HFP) (88:12) based GPEs has drawn attention of many researchers. This co-polymer comprising an amorphous phase of HFP helps in entrapping large amount of liquid electrolyte and the crystalline phase of PVdF acts as mechanical support for the polymer matrix.

Capiglia et al. (Capiglia et al, 2001) were able to increase the conductivity up to 10^{-2} Scm^{-1} in a system comprising of P(VdF-HFP) and a solution of EC, DEC as solvent and $LiN(CF_3SO_2)_2$ as salt by reducing the wt. ratio of P(VdF-HFP) and EC/DEC/$LiN(CF_3SO_2)_2$ to 20:80. Stephan et al. (Stephan et al, 2005) synthesized a series of P(VdF-HFP) based electrolytes using plasticizers (EC+PC) and salts ($LiCF_3SO_3$, $LiBF_4$ and $LiClO_4$). They observed that the sample containing $LiBF_4$ as salt exhibited the maximum ionic conductivity which was attributed to the low lattice energy of the salt. On the other hand the same sample exhibited poor compatibility with lithium anode due to the formation of LiF layer. A systematic study was done by Saikia et al. (Saikia et al, 2004) using PC+DEC and $LiClO_4$ on PVdF and P(VdF-HFP) based electrolytes separately and found that P(VdF-HFP) based electrolytes exhibited higher ionic conductivity than PVdF based gel electrolytes. Non-flammable gel electrolyte has been prepared by Lalia et al. (Lalia et al, 2009) by immobilizing 1M $LiBF_4$/(EC+DEC) + TEP (triethylphosphate) (55:25:20, v/v/v) solution in P(VdF-HFP) where TEP acts as a fire-retardant solvent in gel electrolyte. Electrochemical tests based on 1M $LiBF_4$/EC+DEC+TEP (55:25:20) polymeric gel electrolyte indicated the better performance of polymer electrolytes for both anode (graphite) and cathode materials ($LiMn_2O_4$) as compared to other gel electrolytes containing TMP (trimethyl phosphate) as a fire-retardant solvent. Good rate capability with the positive electrode was also observed.

It is worth mentioning here that the polymer electrolytes are usually synthesized by adding low molecular weight plasticizers like EC, PC, DMC, DEC etc. into the host polymer matrix along with the lithium salts. The films obtained by this synthesis route result in tacky and mechanically weak films. As a result, the enhancement in ionic conductivity is offset by a loss of mechanical behaviour which leads to poor compatibility with the lithium metal electrodes that result in serious problems in terms of safety and performance (Stephan et al, 2005). In order to retain the mechanical behaviour of GPEs which have to be hardened either by physical curing or by chemical curing that result in high processing costs. Besides, the main disadvantage of the above process lies in the fact that the process has to be carried out in completely moisture free atmosphere. On the other hand, Bellcore group (Tarascon et al, 1996) proposed a different method to synthesize GPEs wherein polymer film soaked in electrolyte solution. Advantages of this process lie in the fact that the critical moisture control is required at the time of assembling the cell and mechanical strength is retained as compared to that of solution cast films. The same group successfully launched a reliable and practical rechargeable lithium polymer battery using P(VdF-HFP) (Gozdz et al, 1997).

Several reports are available on the development of films using phase inversion method (Hwang et al, 2007; Xiao et al, 2009; Arvindan et al, 2011 and Kumar et al, 2012). Unfortunately the membranes prepared by this technique exhibit poor electrochemical properties i.e. rate-capability (Stephan et al, 2005).

2.2.3 Composite Polymer Electrolytes

Composite polymer electrolytes are prepared by reinforcing a small fraction of organic filler particles usually in micron size and/or inorganic (ceramic) into the conventional SPE or GPE host (Kumar, 2000; Lee et al, 2003; Zhou et al, 2003). Recent studies reveal that addition of fillers not only enhances the ionic conductivity but also improves the mechanical strength with their interfacial properties which are in contact with the lithium metal electrode (Shah et al, 2005; Roelofs et al, 2014). The idea of using inert fillers was first explained by Weston et al. (Weston et al, 1982) showing that the addition of α-$A1_2O_3$ to PEO-$LiClO_4$ produced a significant improvement in the mechanical strength of the material at temperatures in excess of 100 ºC. The characteristics of these materials were further explored by Liquan (Liquan, 1988). He reported that addition of α-$A1_2O_3$ powder to PEO-NaSCN complex not only improves the mechanical properties of the polymer electrolyte but also increases its ionic conductivity. He suggested that the extent of the latter phenomenon depends critically on the size of the particle/filler used. Improvements of the conductivity in the $A1_2O_3$ (and SiO_2)-(PEO)-NaI composite system were also found by Wieczorek et al. (Wieczorek et al, 1989). Later Scrosati et al. (Scrosati et al, 1990) showed that the dispersion of γ-$LiAlO_2$ ceramic powders to the PEO-$LiC1O_4$ led to the formation of homogeneous composite polymer membranes with an improved mechanical stability above the crystalline to amorphous transition temperature (~ 60 ºC) than pure PEO-$LiClO_4$ complex. In particular, the CPEs containing 10 wt.% of γ-$LiAlO_2$ ceramic powder shows a maximum conductivity beyond which effect of dilution became predominant and conductivity decreased (Capuano et al, 1991). Also the dispersion of γ-$LiAlO_2$ ceramic powder into PEO based electrolyte improves electrochemical property of the electrolyte which allows in obtaining a good cycling efficiency ~ 99% (Appetecchi et al, 2000). Due to the addition of ceramic filler within the polymer might affect the rate of crystallization by preventing the agglomeration of the polymer chains with further enhancement in ionic conductivity. Fast ion transport is an inherent property of the amorphous phase in PEO based electrolytes and thus addition of ceramic filler in polymer electrolyte prevents the polymer recrystallization and thus produces a positive effect on the ionic conductivity (MacCallum, 1987).

People also studied CPEs for other systems like PEO-NaH_4I-Al_2O_3 (Chandra et al, 1995), $NaClO_4$ (Wieczorek et al, 1994) etc.

Despite a common agreement on the effect of degree of crystallinity by the addition of inorganic or organic fillers, little was known about the mechanisms that are responsible for the improvements in the properties. Wieczorek et al. (Wieczorek et al, 1996) defined new theory on Lewis acid-base interaction to analyze the structure and conductivity of CPEs which are complexed with alkali metal salts. They incorporated different particles with different characters i.e. Lewis acid centres i.e. $AlCl_3$, Lewis base centres i.e. poly(N,N dimethylacrylamide) and amphoteric Lewis acid-base i.e. α-Al_2O_3 in the PEO-$LiClO_4$ complex. Since Li^+ cation has a Lewis acid and PEO has a Lewis base character so the phenomena occurring in them could be explained in terms of the equilibrium between various Lewis acid-base reactions. This eventually results in the reduction of ion coupling i.e. increases the dissociation of salt and the formation of Li^+ ion conducting pathways at the filler surface leading to an increase in conductivity and cation transport number. Enhancement in conductivity and electrochemical stability at room temperature have been reported by Sun et al. (Sun et al, 1999) for the other PEO based systems using different type of lithium salts ($LiBF_4$, $LiPF_6$, $LiCF_3SO_3$) reinforced with micron sized particles of ferroelectric materials i.e. $PbTiO_3$, $BaTiO_3$. Panero et al. (Panero et al, 1992) found that addition of 30 wt.% of γ-$LiAlO_2$ filler into PEG complexed with lithium salt could significantly enhance the mechanical properties while conductivity remained almost same with filler free electrolyte. On the other hand, the addition of commercially available fillers i.e. mesoporous SBA-15 into PEO-$LiClO_4$ electrolyte not only improved mechanical but also electrochemical and physicochemical properties of the electrolyte (Ji et al, 2003).

2.2.4 Nanocomposite Polymer Electrolytes

It has been observed, in general, that the size of the particle and the physical nature of the dispersoid used play a significant role. The term “nanocomposites” was first appeared in 1994 by Lan et al. (Lan et al, 1994). After that, a lot of research has been carried out on various types of nanofillers. The development of polymer nanocomposites is one of the most active areas of the development and application of nanomaterials. Nanocomposites represent the new generation of two-phase material, associating a basic matrix to nanofiller inserted between polymer chains (Wagemaker et al, 2013). Nanofiller can significantly adjust or improve the various properties of

the materials into which they are incorporated such as mechanical, ionic, thermal or fire-retardant properties, sometimes in synergy with the conventional nanofiller. The properties of composite can be influenced by the mixture ratio between the matrix and the nanofiller. Nanocomposites are considered to be as one family of nanomaterials where a nano-object is dispersed into a matrix/phase. The other families are mainly nanostructured materials which are classified in terms of their surface or volume. Fig. 2.2 demonstrates the classification of the nanomaterials according to their dimension.

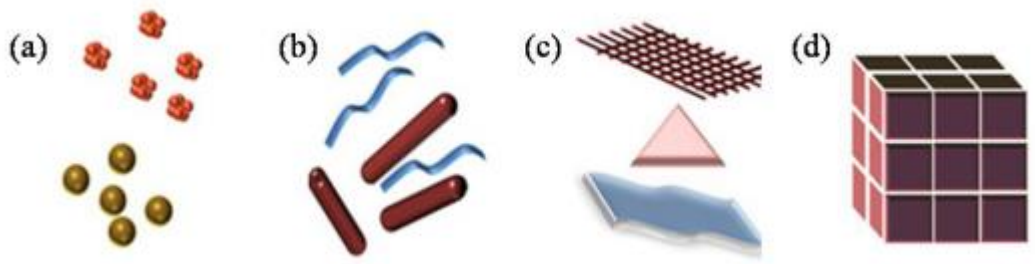

Fig. 2.2: Classification of Nanomaterials (a) 0-D spheres and clusters, (b) 1-D nanofibers, wires, and rods, (c) 2-D films, plates, and networks, (d) 3-D nanomaterials (Alagarasi, 2009).

Generally, smaller the particle size, larger the conductivity enhancement in the nanocomposite. The idea of using NCPEs is currently the main focus of various experimental and theoretical studies (Nan et al, 2003). Depending upon the nature of association, two kinds of nanocomposite electrolytes can be classified:

(i) Inorganic-in-organic, where inorganic nanoparticles are embedded in polymer matrix.

(ii) Organic-in-inorganic, where organic polymers are confined in inorganic templates such as layered silicates.

2.2.5 From Nanocomposites to Nanocomposite Gel Polymer Electrolytes

It is clear from foregoing discussion that GPEs exhibit high ionic conductivity at ambient temperature but their mechanical property at high plasticizer content is poor. Also the interfacial stability of GPEs with Li^+ metal electrode is very poor which results in short circuiting of the cell leading to premature battery failure. In contrast, CPEs exhibit very good interfacial stability with lithium electrode along with enhanced mechanical strength. However, their ionic conductivity is far from the practical applications. NCGPEs, on the other hand, combines the high room

temperature conductivity of conventional gel electrolytes with an excellent stability toward the lithium electrode and good mechanical strength (Jacob et al, 2003). Pradhan et al. (Pradhan et al, 2005) investigated the effect of PEG_{200} plasticizer on the change in the electrical and the stabilities of PEO-$NaClO_4$ dispersed with SiO_2 ceramic fillers. A substantial increase in the conductivity with two orders of magnitude at ambient temperature was noticed when compared with CPEs without any plasticizer. A similar kind of study was carried out by Kuila and his co-workers (Kuila et al, 2007) in which they used $LiMnO_3$ nanofiller. An enhancement in the conductivity about two orders of magnitude at ambient temperature was found on plasticization. A maximum conductivity of 2.6×10^{-4} Scm^{-1} at room temperature was observed for 30 wt.% of PEG as plasticizer compared to that for the pure PEO-$NaClO_4$ system which has conductivity of 1.05×10^{-6} Scm^{-1}. It was discussed on the basis of reduction in the energy barrier with enhancement of the amorphous phase leading to maximum segmental motion of Li^+ ions. NCGPEs based on PEO-EC-$LiCF_3SO_3$-Al_2O_3 complexes were successfully synthesized by Johan et al. (Johan et al, 2011). Wu et al. (Wu et al, 2006) carried out a comparative study with mesoporous zeolites and metal oxide fillers which were dispersed in the P(VdF-HFP) matrix comprising EC:PC (1:1 v/v) mixture as the plasticizer. Addition of nanofillers into the polymer electrolytes increased the conductivity from 1.2×10^{-3} Scm^{-1} to 2.1×10^{-3} Scm^{-1} because of the increased liquid electrolyte uptake and porosity. These electrolytes showed the electrochemical stability window up to 5.5 V. Composite porous membranes of P(VDF-HFP) with nano-silica were prepared by in-situ method based on hydrolysis of tetraethoxysilane and phase inversion (He et al, 2005). It was found that in-situ prepared nano-silica was dispersed homogeneously in the polymeric matrix further enhanced ionic conductivity and electrochemical stability against lithium electrodes. P(VdF-HFP) dispersed NCGPE films with aluminum oxyhydroxide ($AlO(OH)_n$) of different sizes 7 μm / 14 nm and $LiN(C_2F_5SO_2)_2$ as the lithium salt were prepared by solution casting method (Stephan et al, 2006). Dispersion of nanofiller increased the ionic conductivity. There are also recent report on the enhancement of conductivity due to the addition of MgO nanoparticles to P(VdF-HFP) based electrolytes (Kumar et al, 2011). Li et al. (Li et al, 2008) prepared microporous electrolytes based on P(VdF-HFP) by in-situ hydrolysis of $Ti(OC_4H_9)_4$ using a non-solvent-induced phase separation technique. Among various nanofiller, $BaTiO_3$ was observed to exhibit better ionic conductivity, highest electrolyte uptake and better compatibility with the lithium metal. NCGPEs based on the blend of P(VdF-HFP)/PVAc with plasticizer EC and salt $LiClO_4$ was prepared for various compositions of $BaTiO_3$ by Rajendran et al. (Rajendran

et al, 2012). The maximum ionic conductivity was found to be 2.56×10^{-3} Scm^{-1} with 8 wt.% of $BaTiO_3$ content at room temperature and was thermally stable up to 385 ºC. PAN based nanocomposite gel polymer electrolytes was synthesized by Hwang et al. (Hwang et al, 2002) using Montmorillonite (MMT) clay modified by quaternary alkyl ammonium salts, PC/EC co-solvent with salt $LiClO_4$. They showed a maximum ionic conductivity of 1.4×10^{-2} Scm^{-1} with superior film formation ability, plasticizer absorption and dimensional stability in addition to enhanced electrochemical stability as revealed by cyclic voltammetry study. Kim et al. (Kim et al, 2008) reported composite formation of a plasticized polymer electrolyte ($PEO_{16}LiClO_4$ + 50 wt.% EC) with organically modified Na-MMT. They observed an optimum conductivity of 10^{-5} Scm^{-1} at room temperature for the plasticized electrolyte and 10^{-4} Scm^{-1} for the composite using 10 wt.% modified MMT.

2.3 Ion Transport in Polymers: Mechanisms and Models

In solution, the polymer chains are randomly coiled but when it is solid, at least part of the material is amorphous i.e. randomness persists. When the polymer is solid, it is possible for the chains to align themselves in a systematic way by the formation of single or multiple helices or by chain folding for at least part of their length. The regions possess long range order are therefore known as crystalline. Crystallization is initiated at various locations within the polymer solid and the crystalline domains of each long chain molecules cannot be aligned within an individual crystalline region and these regions remain amorphous. In case of solvent free polymer electrolytes, such as PEO, salt gets dissolved into the polymer base because the lone pair electrons on the polymer chain oxygen atoms coordinate with the cations. The cation transport process in polymer electrolytes can be envisaged as a “roll-on” mechanism in which a cation is initially coordinated to several oxygen (or other) atoms (Linford, 1993). The linkages to one or more of the polymer segments that lie behind the direction of motion of the cation break and new linkages are formed in the forward direction. The cation motion is clearly facilitated by the flexing of the polymer chain segments, which allow old linkage to be broken and new attachment is made. For high molecular weight polymer hosts chain diffusion is small and makes little contribution to the mechanism for ion transport. Low barriers allow segmental motion to bond rotation thus providing a mechanism for ion transport in the polymer chain as conductivity is largely determined by the mobility of polymer segments. Fig. 2.3 shows the schematic representation of cation hopping of polymer electrolyte in different ways.

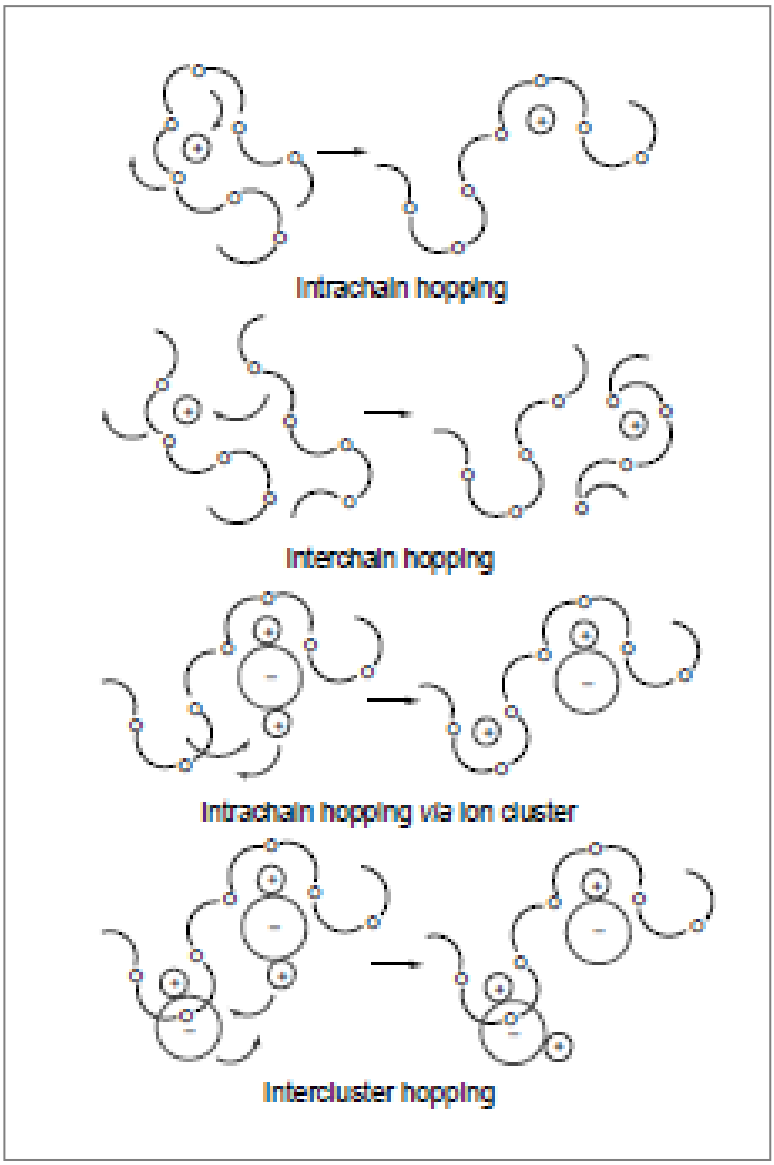

Fig. 2.3: Schematic diagram showing cation motion in polymer electrolytes (Gray, 1997).

For gel polymer electrolytes, polymer is an important constituent along with the plasticizer and salt. The salt provides ions for conduction and the plasticizer dissolves salt and provides the medium for ion conduction. The conductivity of gel electrolytes can be explained by 'Breathing polymeric chain model' which was proposed by Chandra et al. (Chandra et al, 2000). According to this, gel polymer electrolytes consist of free ions, ion aggregates and polymer chain dispersed in the gel matrix. The breathing of polymer by folding/unfolding up of its chains which results in density/pressure fluctuations at the microscopic level and assist the motion of ions along with dissociation of ion aggregates leading to the increase in ionic conductivity. The gel polymer

chains act on the ion pairs to effect on dissociation and the dissociated ions in the solvent are further solvated by the polymer chains results in a change in the carrier concentration and mobility.

2.3.1 Arrhenius Model

GPE is a semi-solid hybrid system in which conduction of ions is essentially occurs through liquid organic phase trapped in constantly flexing polymeric molecular chains above the glass transition temperature of polymer. Therefore, the Arrhenius relation for the conductivity of GPE systems expressed as:

$$\sigma = \sigma_0 = \exp(-\frac{E_a}{kT}) \tag{2.1}$$

where k is the Boltzmann constant, σ_0 is the pre-exponential factor and E_a is the activation energy, often provide a good representation of the conductivity-temperature relationship. Linear graph of log σ vs $1/T$ is often called as Arrhenius plot, as for an Arrhenius process the logarithm of the relevant performance parameter depends linearly on the reciprocal of temperature. The slope of the curve gives the activation energy of the process. In fact, diffusion rather than conductivity is the relevant activated transport process and the appropriate performance parameter is the diffusion coefficient. The Nernst-Einstien equation provides the link between diffusion and conductivity, but it reveals that D is proportional to (σT) rather than σ, and it would be more appropriate to plot log(σT) instead of log σ. For gel polymer electrolytes, the temperature range covered is often short and the variation in $1/T$ is substantially greater than the change in log T so that latter can be considered as approximately constant and (σT) can be replaced by log σ (Song et al, 2002).

2.3.2 Vogel-Tamman-Fulcher (VTF) Model

Solid electrolytes involve ion hopping between fixed sites, graph of log(σ) versus $1/T$ are straight lines whereas for the polymer based electrolytes the plots are often curved. Such behaviour would be seen in polymer electrolytes in which conduction occurs in the amorphous region and the conduction process is better describe by the VTF equation (Vogel, 1922; Tammann, 1926; Fulcher, 1925) given by:

$$\sigma = AT^{1/2} \exp\left[\frac{-E_a'}{k(T-T_0)}\right]$$

$$\text{Or, } \sigma = \sigma_0 \exp\left[\frac{-B}{k(T-T_0)}\right] \quad (2.2)$$

where B is a contant and its dimensions are that of energy, but which is not simply interpreted as an activation term. In configurational entropy terms, T_0 is the temperature at which the probability of configurational transition tends to zero, and is regarded as having a value between 20-50 K below the glass transition temperature (T_g). The value of conductivity becoming vanishingly small as T_0 approaches to T. If the conductivity versus temperature dependence curve is linear at large temperature range then it is Arrhenius. VTF (curved) behaviour can be modeled as Arrhenius behaviour by dividing the entire temperature range into the smaller temperature regions. The relation between Arrhenius and VTF behaviour of $\sigma(T)$ are widely reported in literature (MacCallum, 1987). This behaviour is rationalized by arguing that since the Arrhenius dependence is governed by the energy kT and VTF dependence by the energy interval $k(T-T_0)$, for $T \rangle\rangle T_0$ i.e. when T_0 is quite smaller than T, the curvature of conductivity versus temperature plot becomes small. Therefore, VTF equation approaches Arrhenius equation (Singh et al, 2002).

2.3.3 William-Landel-Ferry (WLF) Model

In amorphous polymer above its glass transition temperature, a single empirical function describes the temperature dependence of all the mechanical and electrical relaxation processes. The temperature dependence at a number of relaxation and transport processes can be describe by WLF equation given below (Williams et al, 1955).

$$\log\left[\frac{\eta(T)}{\eta(T_S)}\right] = \log a_T = -\frac{C_1(T-T_S)}{C_2 + T - T_S} \quad (2.3)$$

where a_T is the mechanical shift factor (express the fluidity or relaxation rate), η is the viscosity, T_S is reference temperature (usually $T_S = T_g + 50$ K) and C_1 and C_2 are the constants.

2.3.4 Dynamic Bond Percolation (DBP) Model

Nernst-Einstien relation and Kohlrausch summation do not fit well in the polymer ionics and deviation become more significant as the concentration of salt increases. In the former case, ions move by a local liquid like process rather than by hopping from site to site in an ordered polymer host. To describe conduction mechanism in polymers adequately, it is important to model it microscopically. DBP theory is a microscopic model for the disordered diffusion in dynamical systems (Druger et al, 1983). The model assumed that mobile ions move from one site to another site within the host polymer and the sites lie on a regular lattice. Assuming first-order hopping chemical kinetics for the movement of ion, the probability of finding an ion at site *j* can be written as:

$$\frac{dP_i}{dT} = \sum_j (P_j W_{ji} - P_i W_{ij}) \tag{2.4}$$

where W_{ji} is rate of hopping from site *j* to *i*.

The difference between dynamic disordered hopping and ordinary hopping is that the hopping rates W_{ij} are themselves time dependent, and evolve on the time scale of relaxation of the polymer host.

2.3.5 Free Volume Model

The 'free volume theory' was first proposed by Cohen and Turnbull of transport phenomena in the glass forming materials (Cohen et al, 1959). They derive the diffusion coefficient equation, *D*,

$$D = ga^* u \exp\left[-\frac{\gamma V^*}{V_f}\right] \tag{2.5}$$

where *g* is the geometrical factor, *a** is approximately same as molecular diameter, *u* is the average speed of molecules, γ is the numerical factor introduced to correct for overlap of free volume and *V** is the critical volume to permit another molecules to jump in after the displacement. Cohen and Turnbull define the free volume as:

$$V_f = V\text{-}V_0 \tag{2.6}$$

where V is the average volume and V_0 is the Vander Walls volume of the molecule. Using the Nernst- Einstein equation,

$$\sigma = \frac{q^2 nD}{kT} \tag{2.7}$$

It follows that

$$\sigma = \frac{q^2 nga^* u}{kT} \exp\left(\frac{-\gamma V^*}{V_f}\right) \tag{2.8}$$

In this equation, n and q are the concentration carriers and charge carriers respectively; k is the Boltzmann's constant. Theory of free volume in this form has been applied to the polymer electrolytes by several workers (Duclot et al, 2000; Bamford et al, 2001). They predict that at a constant free volume, conductivity should decrease weakly with the increasing temperature because kinetic theory requires that u vary as $T^{1/2}$. Since the remaining terms of Equation (2.8) are approximately temperature independent and can be rewritten as:

$$\sigma = \frac{C}{T^{1/2}} \exp\left(\frac{-\gamma V^*}{V_f}\right) \tag{2.9}$$

where C includes the charge carrier concentration. But the experimental data show that the conductivity increases strongly at constant specific volume with temperature. Conclusion drawn from Equation (2.9) is not supported by the data based on the assumption. Cohen and Turnbull made the assumption that the free volume is proportional to the macroscopic volume and is given as

$$V_f = V_0\left(\exp\left[\int_{T_0}^{T} \alpha dT\right] - 1\right) \tag{2.10}$$

where α is thermal expansion coefficient. A slightly different approximation often made is that the thermal expansion is the difference in thermal expansion coefficient of bulk material above and below T_g of free volume (Bamford et al, 2001). However, when the microscopic volume is held constant, the conductivity increases strongly with temperature. Consequently, if the free volume

varies as microscopic volume, as given in Equation (2.6), free volume theory is not capable of representing the constant volume conductivity for a typical polymer electrolyte. The disagreement between theory and experiment is not surprising since the theory was developed originally for simple Vander Walls liquid and metallic liquids (Cohen et al, 1959). Inability of theory of free volume to account for the phenomena which is governed by segmental motions has been pointed out wisely in literature (Williams, 1997; Mierzwa et al, 2000).

One of the first attempts to modify the theory of free volume to account for the variation in temperature phenomena was made by Macedo and Litovitz (Macedo et al, 1965). They employed the theory of reaction rate of Eyring (Glasstone et al, 1941) to arrive at the following equation for the shear viscosity

$$\eta = \left(\frac{RT}{E_v}\right)^{1/2} \frac{(2mkT)^{1/2}}{V^{2/3}} \exp\left[\frac{\gamma V^*}{V_f} + \frac{E_v}{kT}\right] \tag{2.11}$$

where r is gas constant, E_v is the height of potential barrier between equilibrium positions, V is equal to the volume of a molecule and m is the molecular mass. The Stokes-Einstein equation is given as

$$\eta = \frac{kT}{6\pi Dd} \tag{2.12}$$

where d is the molecular radius. It is well known that Stokes-Einstein equation breaks down for fragile glasses near T_g (Blackburn et al, 1996). The Nernst-Einstein equation is used to obtain the following equation

$$\sigma = \frac{q^2 n V^{2/3}}{6\pi d(2mkT)^{1/2}} \left(\frac{E_v}{kT}\right)^{1/2} \exp\left[-\frac{\gamma V^*}{V_f} - \frac{E_v}{kT}\right] \tag{2.13}$$

At constant volume, Equation (2.13) can be written as

$$\sigma = \frac{B}{T} \exp\left[-\frac{E_v}{kT}\right] \exp\left[-\frac{\gamma V^*}{V_f}\right] \tag{2.14}$$

This equation can account for a strong increase of the conductivity at constant volume and was used by Macedo and Litovitz (Macedo et al, 1965) to successfully reproduce the pressure and temperature dependence of the shear viscosity of several liquids. These include exhibiting VTF or WLF behaviour by several materials. Equation (2.14) can account for VTF or WLF behaviour because both types of behaviour are represented by the factor of free volume.

2.4 Conductivity and Impedance Spectroscopy

Generally, the expression for conductivity 'σ' is given as

$$\sigma = G.\frac{l}{A} = \frac{1}{R}.\left(\frac{l}{A}\right) S\,cm^{-1} \tag{2.15}$$

where G (1/Resistance) is the conductance, R is the resistance, l is the thickness of the sample and A is the area of the electrode.

To measure ionic conductivity is not as easy as is the case for electronic conductors. In the case of electronic conductors, conductivity can be measured directly by applying a d.c. potential using either two-probe or four-probe methods. In the case of ionic conductors, the d.c. potential cannot be applied as it leads to the occurrence of fast interfacial polarization, which results in the continuous increase in resistance as a function of time. In order to avoid these problems, two different methods have been adopted for the measurement of ionic conductivity of solids: d.c. method and a.c. method.

2.4.1 Direct Current Method (D.C. Method)

In this method, constant d.c. potential or current is applied across a cell comprising of electrolyte which is sandwiched between two reversible electrodes and the resulting current or potential are to be monitored. By putting $R = (V/I)$ in the Equation (2.15), the conductivity can be written as

$$\sigma = \frac{I}{V}.\frac{l}{A} \tag{2.16}$$

where V is the voltage and I is the current. There are two techniques that can be used to measure the ionic conductivity i.e. Two probe and Four probe methods. In the two probe method, a known d.c. potential is applied across the cell in which electrolyte material is sandwiched between the two

reversible electrodes and a resulting current is measured to determine the d.c. resistance. Whereas, in case of four probe method, a known d.c. current is applied between two outer electrodes and the potential is measured between two inner electrodes. Conductivity can be calculated by measuring the area of the two inner electrodes and the distance between them. The experimental set-up for the four-probe method is given in Fig. 2.4.

Though the d.c. technique for the measurement of ionic conductivity appears quite simple, it possesses many practical difficulties, e.g. it is very difficult to get reversible electrodes for both the cations and anions, there is also a contribution of electrode-electrolyte interfacial resistances to the overall conductivity, presence of grain boundary conduction, formation of a double layer due to concentration polarization etc. Further, the interpretation of the electrical conductivity data is also very difficult due to the presence of more than one phase in the polymeric materials. Combination of all the above difficulties led the researchers to switch over to a.c. methods rather than the d.c. methods**.**

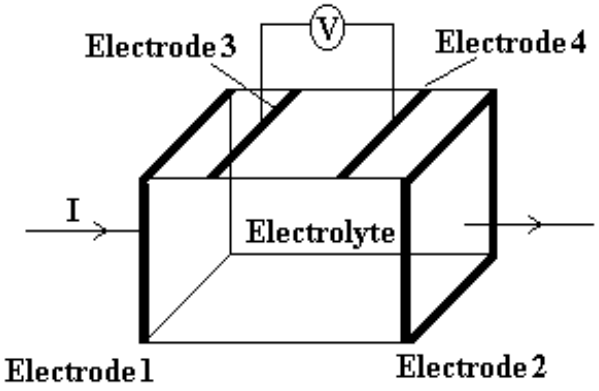

Fig. 2.4: Experimental set-up for four probes method.

2.4.2 Alternating Current Method (A.C. Method)

The a.c. methods are used for the determination of conductivity to minimize the various polarization effects. The technique is called “Impedance Spectroscopy” according to which a sinusoidal voltage is applied to a cell, comprising of an electrolyte which is sandwiched between two blocking or non-blocking electrodes and the resulting current passing through the cell and perturbation is determined. The resulting current is related with the applied sinusoidal voltage by two different parameters, which are:

(i) The ratio of the current and voltage maxima, V_{max}/I_{max} (analogous to d.c resistance measurements), and

(ii) The phase difference 'θ' between voltage and current.

The combination of above two parameters represents the impedance 'Z'. Both the magnitude of impedance ($|Z| = V_{max}/I_{max}$) and the phase angle 'θ' are the functions of applied frequency. The impedance of a cell is measured as a function of applied frequencies, over a wide range of frequencies, typically, 1 mHz - 1 MHz (Glasstone, 1945)**.** The Impedance Spectroscopy enables us to evaluate and separates the contribution of different electrical parameters in different frequency regions such as bulk phenomena, i.e. the movement of ions through the bulk and across the grain boundaries within the electrolyte, interfacial phenomena due to electrode reactions at the electrode-electrolyte interfaces (Donald, 1987; Bruce, 1987) etc. This study was also applied successfully for the study of dielectric properties of the materials by Cole and Cole (Cole, 1941). Bauerle (Bauerle, 1969) was the first to propose a generalized complex impedance plot method to extract the true bulk conductivity from the a.c. conductivity measurement. The subsequent developments in this field have been reviewed extensively in the literature (Gabrielli, 1980; Mellander et al, 1986; Raistrick, 1986; Badwal, 1988). Impedance of a cell is a vector quantity and this vector may be represented by its *x* and *y* components: $|Z| \cos\theta$ and $|Z| \sin\theta$. Z^* represents complex impedance. Z' is the real and Z'' is the imaginary components of the complex impedance Z^*. It can be displayed in a complex plane in several different forms:

Complex impedance, $Z^*(\omega) = Z' - jZ'' = R_s - j/\omega C_s$ (2.17)

Complex admittance, $Y(\omega) = Y' + jY'' = 1 / R_p + j\,\omega C_p = G(\omega) + j\,B(\omega)$ (2.18)

Complex modulus, $M(\omega) = 1 / \varepsilon(\omega) = M' + jM'' = j\,\omega\,C_0\,Z(\omega)$ (2.19)

Complex permittivity (Dielectric constant), $\varepsilon(\omega) = \varepsilon' - j\varepsilon''$ (2.20)

Loss tangent, $\tan\varepsilon = \varepsilon'' / \varepsilon' = M'' / M' = -Z' / Z'' = Y' / Y''$ (2.21)

Complex resistivity, $\varepsilon_0(\omega) = \rho' + j\rho'' = Z \times (C_0 / \rho_0)$ (2.22)

Complex conductivity, $\sigma(\omega) = \sigma' - j\sigma'' = Y \times (\varepsilon_0 / C_0)$ (2.23)

where $j = \sqrt{-1}$, C_0 is vacuum capacitance of the cell, G is the conductance and B is susceptance (subscripts s is for series and p is for parallel combinations of the elements of circuit, respectively). Out of all these parameters, the impedance and admittance plane representations provide useful information when various processes within the cell have different relaxation times as in the case with the solid electrolyte cells. In this regard, Randles was the first to successfully show that the processes occurring within the cell could be entitled by an equivalent circuit comprising of capacitors, resistors, inductors and their series and parallel combinations (Randles, 1947). This equivalent circuit shows almost the same phenomenological processes within the cell. Practically the equivalent circuit consists of resistors and capacitors in terms of which the charge migration and polarization occurring within the cell can be represented. A general practice is to represent one charge polarization or migration process by one parallel *RC* combination. Hence, a model of equivalent circuit for a general solid electrolyte consists of three parallel *RC* circuits which are connected in series. Each of the parallel combinations represents contributions due to the bulk properties of the material, electrode-electrolyte interfacial processes and grain boundary conduction in different frequency ranges respectively as shown in Fig. 2.5.

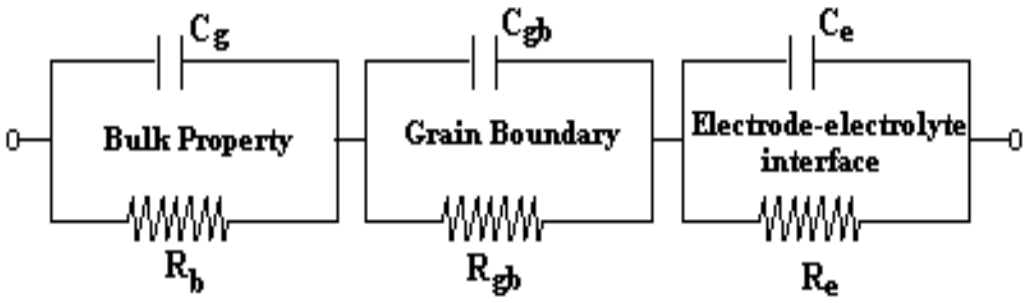

Fig. 2.5: Equivalent circuit model of a typical electrolyte.

The simplest possible circuit in an electrochemical cell consists of an overall resistance (R) which is due to electrolyte, electrodes and lead wires in series with a parallel circuit comprising charge transfer resistance (R_{ct}) at the electrode-electrolyte interface and Warburg impedance (W) representing diffusion polarization in parallel with the double layer capacitance (C_e) is shown in Fig. 2.6.

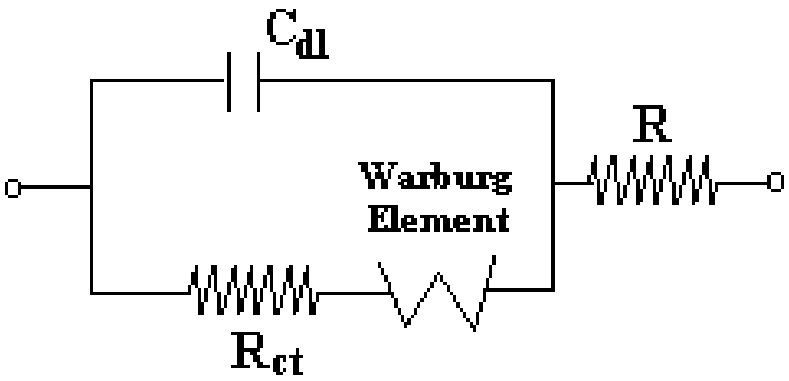

Fig. 2.6: Equivalent circuit representation of an electrochemical cell.

Depending on the types of electrodes used (i.e. either blocking or non-blocking electrodes) and types of electrolytes having single mobile ion species (in conventional solid electrolytes) or double mobile ion species (both cations and anions as observed in the liquid or polymer electrolytes), the behaviour of the cells, their impedance patterns and hence their equivalent circuits are distinctly different, which are described briefly as follows:

2.4.2.1 Blocking Electrodes

Fig. 2.7(a and b) show the cell with blocking electrodes and single ion conducting electrolyte, its ideal impedance pattern and the equivalent circuit representing its a.c. response. The bulk polarization and ion migration in the electrolytes are reflected as a semi-circle in the impedance plot, generally observed in the mid/high frequency range. This semi-circular indicates that the representative components - bulk resistance (R_b) and geometrical capacitance (C_g) are connected in parallel combination. The C_e, built up due to the charge accumulation at electrode-electrolyte interfaces, appears as a spike rising at right angle parallel to imaginary axis in the low frequency region of impedance plot as shown in the Fig. 2.7(b) and connected in series with parallel combination of R_b and C_g as shown in inset of the Fig. 2.7(b).

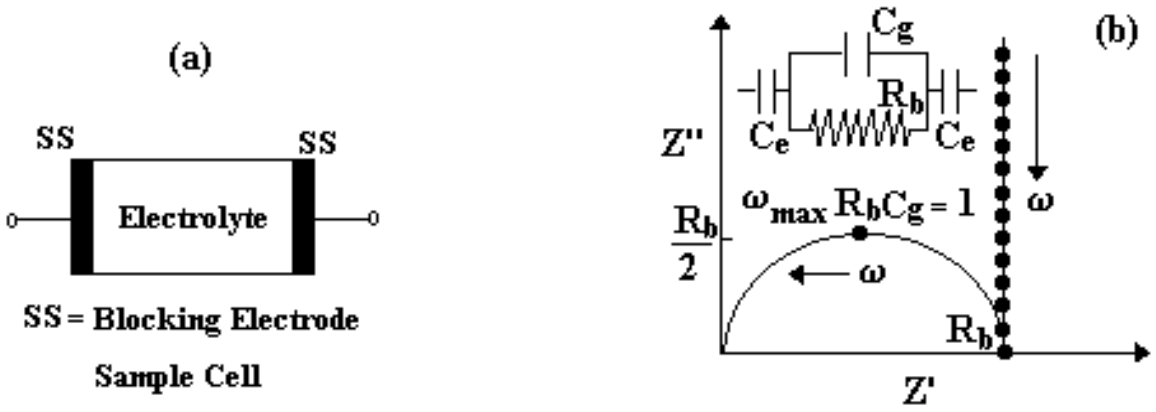

Fig. 2.7: Schematic representation of (a) an electrochemical cell with blocking electrodes; (b) impedance plot with inset showing equivalent circuit.

It is generally observed that the middle/high response of frequency gives information about properties of the electrolyte, whereas the low response of frequency carries information about the electrode-electrolyte interfaces. Overall, the magnitude of all the fundamental properties of the cell may be obtained from the complete impedance data. Particularly, R_b of the electrolyte can easily be evaluated by sandwiching the electrolyte between two blocking electrodes. Generally, the equivalent circuit and the impedance plot, as shown in Fig. 2.7 are equally applicable to the liquid/polymer electrolytes having more than one mobile ionic species, sandwiched between the two blocking electrodes.

2.4.2.2 Non-Blocking Electrodes (Reversible Electrodes)

In the case of non-blocking electrodes, there is a finite reversible electrode reaction at the electrode-electrolyte interfaces, that allow the dissolution of mobile ionic species in the electrodes. Fig. 2.8 show the impedance plots of the cell consisting of (a) single ion conducting electrolyte, and (b) both the cation and anion conducting electrolyte (e.g. liquid / polymeric gel electrolyte). The equivalent circuits are shown in their corresponding insets. In the case of single ion conducting electrolyte, the high frequency semi-circle in the impedance plot is observed due to the parallel combination of R_b and C_g similar to the pattern observed in case of the cell with blocking electrodes. In addition to this another semi-circle is observed in middle region of frequency which represents a.c. response of the electrode/electrolyte interface. This is represented by a parallel combination of a finite charge-transfer resistance (R_e) and charging/discharging C_e.

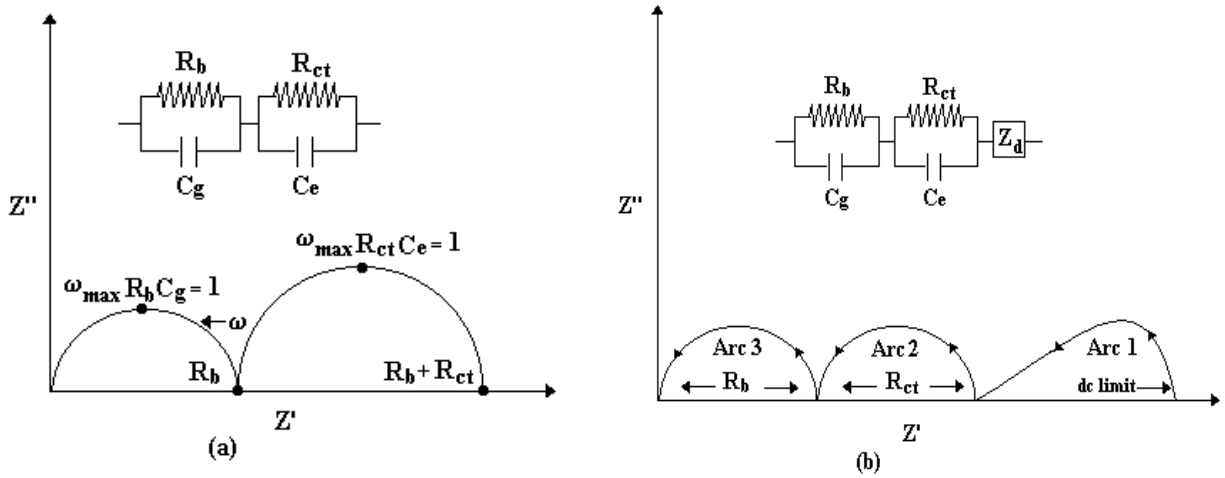

Fig. 2.8: Schematic representation of impedance plots for the cells with non-blocking electrodes consisting of (a) single ion conducting electrolyte, and (b) both the cation and anion conducting electrolyte (e.g. liquid/polymer gel electrolyte). The equivalent circuits are shown in their corresponding insets.

On the other hand, in the case of a cell with non-blocking electrodes and electrolyte having two mobile ions (cation and anion), there appears three semi-circles corresponding to the bulk (high frequency), electrode-electrolyte interfaces (middle frequency), and diffusion impedance due to the concentration gradient of anions developed at sufficiently low frequency, as shown in the above Fig. 2.8(b). The low frequency semi-circle is skewed and is inclined at an angle of 450º to real axis. However, all the three features may not be observed in all the cases (Bruce, 1987).

In actual practice, it is observed that there is a significant flattening of the ideal semi-circular pattern and tilting of the spike in the impedance spectrum contrary to the ideal spectrum obtained from the equivalent circuit model based on the processes within the polymer electrolyte cell as shown in Fig. 2.9(a and b). The effect may be related to the presence of non-conducting crystalline regions interlocked with the conducting amorphous materials within the spherulites of a polymer electrolyte system.

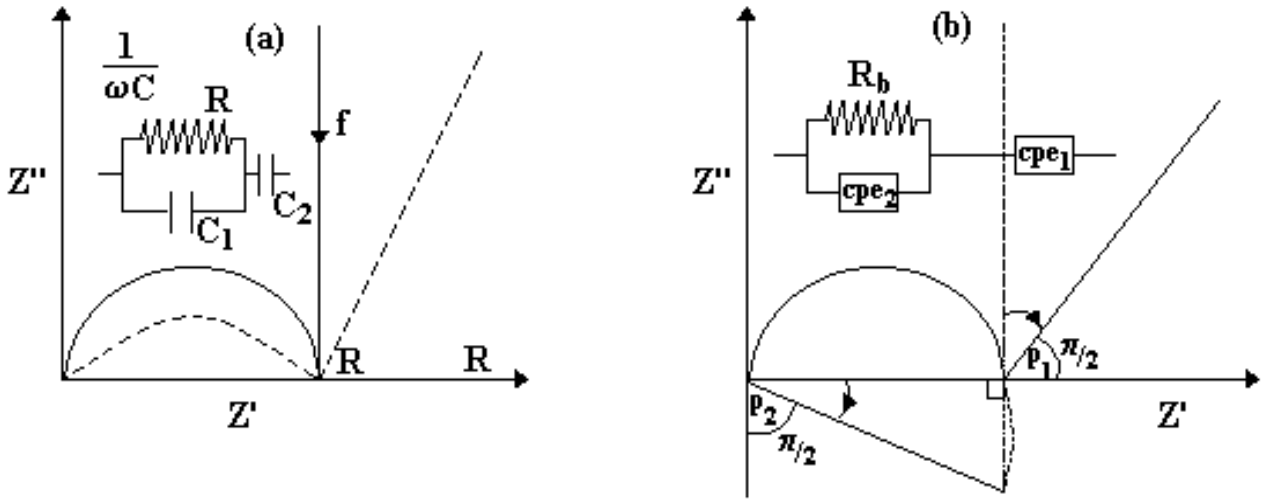

Fig. 2.9: (a) Equivalent circuit and impedance spectrum (solid line = spectrum for ideal equivalent circuit. Dotted line = experimental impedance spectrum for gel electrolytes), (b) depression of semicircle and tilting of spike caused by replacing capacitors by constant phase elements.

The cell behaves as a "leaky capacitor" resulting in the flattening semicircle and tilting of spike as shown in the Fig. 2.9(a). The effect has also been attributed to a variety of physical phenomena such as the coupled or sequence of multiple reactions, frequency dependent ohmic resistances and roughening of the electrode which is produced by a non-uniform charging of the double layer (Raistick et al, 1987). In order to account for such effects, a generalized impedance element known as the "constant phase angle element (CPE)" is introduced into the equivalent circuit model, which is shown in the Fig. 2.9(b) as inset.

The impedance of the constant phase angle element is given by

$$Z_{CPE} = k\,(j\omega)^{-p},\ 0 \leq p \leq 1 \qquad (2.24)$$

where Z is the independent frequency and 'k' represents the resistance (R) for p = 0. When p = 1, ($Z = k/j\omega = -j/\omega k^{-1}$), in such a case Z is now frequency dependent and k^{-1} represents the capacitance. CPE acts as intermediate between resistor and capacitor, which is similar to the case for polymeric materials for $0 \leq p \leq 1$.

2.5 Kinetics of Ion Transport in Gel Polymer Electrolytes

The gel polymer electrolytes are prepared by immobilizing a nonaqueous solution of electrolyte within an inactive structural polymer matrix or by increasing the viscosity of liquid electrolyte by adding a soluble polymer. They are basically called as salt-solvent-polymer systems in which first a salt solution is prepared and then is immobilized with the help of suitable polymer matrix. The salt provides mobile/free ions that take part in the conduction process and solvent helps in dissolving salt and acts as a conducting medium whereas the polymer provides the mechanical stability by increasing the viscosity of the electrolyte (Bruce et al, 1995). The conductivity relation in terms of concentration, charge and mobility can be expressed as

$$\sigma = \sum_i n_i q_i \mu_i \tag{2.25}$$

where n_i is the concentrations of charge carriers of type i, q is the charge and μ the mobility. The conductivity here is also a function of temperature and pressure, and this equation is suitable for homogenous polymer electrolytes. With the assumption that the dissolved salt completely dissociates into cations and anions in the electrolyte system, the determination of ion conductivity depends only on the evaluation of ion mobility. The ionic mobility (μ) can be calculated by using the Stokes-Einstein equation

$$\mu = \frac{q}{6\pi\eta r_s} \tag{2.26}$$

Here q is the electronic charge on each charge carrier, η is the viscosity of the solution, r_s is the effective hydrodynamic (Stokes) radius. Ionic diffusion coefficient D is assumed to relate to the Equation 2.26 and can also be used to evaluate the ionic mobility. This is Nernst-Einstein relationship between the ionic diffusion coefficient and the ionic mobility (Saito et al, 2003)

$$\mu = \frac{qD}{kT} \tag{2.27}$$

where k is the Boltzmann constant. Ionic conductivity from Nernst-Einstein equation is then described as following (Tokuda et al, 2002)

$$\sigma_{diff} = \frac{Nq^2}{kT}(D_+ + D_-) \tag{2.28}$$

where N is the number of charge carriers per cm^3 on the assumption of complete dissociation, and D^+ and D^- are the diffusion coefficient of the cation and anion, respectively. The ionic transfer (transport) number is an important parameter in describing the mechanism of conduction of ions in polymer electrolyte as well as its application. It represents the fraction of the total current moved by the mobile ions. The ionic transfer number of cation (t_+) can be calculated by

$$t_+ = \frac{\mu_+}{\mu_+ + \mu_-} = \frac{q_+ D_+}{q_+ D_+ + q_- D_-} \tag{2.29}$$

where μ_+ (μ_-) and q_+ (q_-) are ionic mobility and electronic charge on the cation (anion), respectively.

2.6 Kinetics of Ion Transport in Nanocomposite Gel Polymer Electrolytes

It has been recognized that in NCGPEs enhancement of ionic conductivity is connected with the existence of a highly conductive layer at the polymer filler interface (Wieczorek et al, 1994) by effective medium approach. Fig. 2.10 shows schematic structure of NCGPEs.

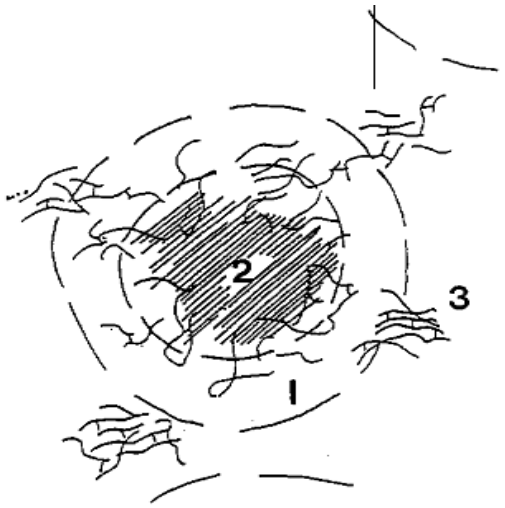

Fig. 2.10: Schematic structure of NCGPEs where 1 represents the highly conductive interface layers coating the surfaces of grains, 2 represents the dispersed insulating grains and 3 represents the matrix polymer ionic conductor. (Wieczorek et al, 1994).

According to Maxwell-Garnett rule, the equivalent conductivity σ_c of the composite unit can be expressed as (Maxwell, 1892)

$$\sigma_c = \sigma_1 \frac{2\sigma_1 + \sigma_2 + 2Y(\sigma_2 - \sigma_1)}{2\sigma_1 + \sigma_2 - Y(\sigma_2 - \sigma_1)} \tag{2.30}$$

where σ_1 and σ_2 are the conductivities of the interface layer and dispersed grain. *Y* is a volume fraction of a dispersed phase for spherical geometry calculated as

$$Y = \frac{1}{\left(1 + \frac{t}{R}\right)^3} \tag{2.31}$$

where *t* is the thickness of interlayer and *R* is the radius of dispersed grain. According to the above assumption, the nanocomposite electrolyte can be treated as a quasi-two phase mixture consisting of an ionically conductive pristine polymer matrix with dispersed nanocomposite units and it can simply be described by the Brugeman equation (Brugeman, 1935) or the effective medium equation which was introduced by Landauer (Landauer, 1952). This ignore local field effects and suitable for the description of quasi two-phase mixture for volume fractions of nanocomposite units which are lower than 0.1. In this system, as the volume fraction of unit increases, nanocomposite grains join each other and form complicated clusters which have to be considered. Therefore, the simple Landauer approach was improved according to the proposed method by Nan (Nan, 1993; Nan et al, 1991) and Nakamura (Nakamura, 1984). Two limiting conditions are considered

(i) The matrix phase is the polymer electrolyte and isolated nanocomposite units are scattered throughout.

(ii) The matrix phase consists of overlapping or touching nanocomposite units with a small amount of dispersed polymer electrolyte in the interstices.

Validating the method by Nakamura (Nakamura, 1984), Wieczorek and co-workers (Wieczorek et al, 1994) showed that *t/R* ratio decreases for nanofiller concentrations higher than the concentration for which the maximum conductivity is reached for polymer electrolytes dispersed with inorganic and organic nanofillers. Moreover, the conductivity of an interface amorphous layer also depends upon the fraction of the additive. They predicted the decrease in conductivity by a model which

considered the decreasing effect in the surface layer conductivity with an increase in concentration of grain. Since the structure of the interface layer is highly amorphous. Therefore, the temperature dependent conductivity was assumed to follow VTF relation

$$\sigma = AT^{-1/2} \exp\left[\frac{-B}{k(T - T_0)}\right] \tag{2.32}$$

Here, B is pseudo activation energy, A is a pre exponential factor and T_0 is a quasi-equilibrium glass transition temperature usually 30-50 K which is lower than T_g. It is assumed that the B and A are independent of the concentration of nanofiller. Therefore, the interface layer conductivity only dependent on T_g and decreases with increase in T_g. From DSC experiments, values of T_g taken were used for the calculation of σ_1 for electrolytes with various concentrations of the filler. To generalize the model, the variation of T_g as a function of grain size and volume fraction of filler should be considered. The T_g effect of the salt which is dissolved should also be taken into account. It was found that for specific nanocomposite systems, T_g could be approximated by the following equation (Bares, 1975; Schneider et al, 1992)

$$T_g = K_0 + K_1[f(V_2 / S_2)] + K_2[f(C_S, V_2)] \tag{2.33}$$

where V_2 and S_2 are volume fraction and surface area of the dispersed phase, C_S is the molar concentration of the salt, and K_0, K_1, and K_2 are adjustable constants. It has been found that for a system with different concentrations of nanofiller and a fixed concentration of salt, the best fit to the experimental data can be obtained when T_g is approximated by the relation

$$T_g = K_0 + K_1 V_2 + K_2 V_2^2 \tag{2.34}$$

The effect of salt is included in K_0 which is similar to the T_g for polymer electrolyte. The influence of filler which are added on T_g of the system describes K_1 and K_2 is connected with polymer-filler-salt interaction.

2.7 Application of Nanocomposite Gel Polymer Electrolytes in Lithium Ion Batteries

As lithium metal is the lightest element that exhibits the highest oxidation potential can safely be handled in various electrochemical processes and ideally suited for high energy density batteries. However, lithium electrodes when comes in contact with the liquid electrolytes can cause a variety

of problems that leads to fires and explosions. Therefore, "rocking chair" cell is the most promising approach in which lithium metal is replaced by a lithium-ion source (Scrosati, 1993). During charging/discharging, lithium ions are "rocked" between lithium-carbon and lithium-metal oxide intercalation compounds. Fig. 2.11 shows an example in which Li_xC_6 is used as anode and $Li_xMn_2O_4$ (a spinel) as cathode. Insertion compounds as electrode materials for rocking chair Li batteries have recently been reviewed by Scrosati (Scrosati, 1994) and Koksberg et al. (Koksberg et al, 1996). Because of the high oxidation potential of cathodes, these batteries may suffer from the decomposition reactions of organic solvents used as electrolyte. Therefore, the replacement of the liquid electrolyte with a thin polymer film would be highly desirable. The electrolyte serves as a medium to transport the ions involved in the charging/discharging cycle of the cell. In addition, a separator has to isolate the anode from the cathode electronically. While polymeric separators have to be placed between the electrodes when liquid electrolytes are used, both functions i.e. ion conduction and separation that can be realized in a single thin film when polymer electrolytes are used. However, in batteries to be used for electrically powered vehicles, such a polymer electrolyte film ought to exhibit ion conductivities better than 10^{-5} Scm^{-1} in the temperature range from –20 ºC to +60 ºC, and they should be mechanically, thermally, and electrochemically stable atleast within that temperature range. A comparison of the electrochemistry of polymer electrolytes and liquid electrolytes was given very recently by Armand and co-workers (Armand et al, 1997).

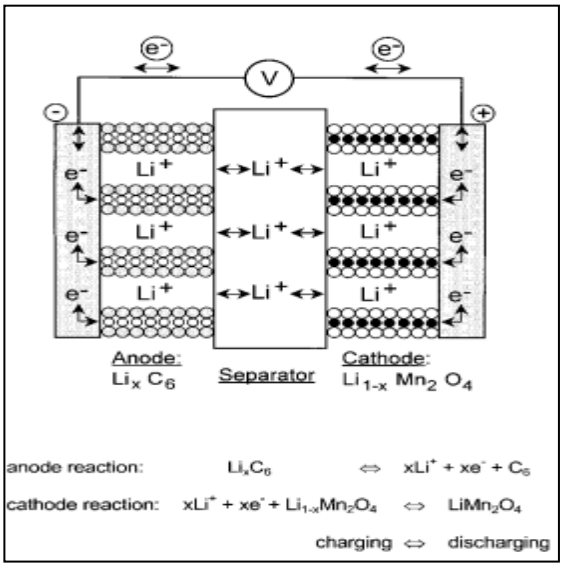

Fig. 2.11: Schematic diagram of a lithium rocking chair battery and its electrode reactions (Scrosati, 1994).

Until now the development of new generation ambient lithium batteries has been exclusively almost based on GPEs. Several organizations including Bellcore (USA), Valence (USA), Mead (USA) and Yuasa (Japan) have announced lithium polymer battery based on gel electrolytes. One of the remaining challenges is to increase the ionic conductivity, mechanical and thermal stability and decrease the interfacial impedance with the metal electrode which makes the use of gel electrolytes in lithium polymer batteries challenging. NCGPEs combines the advantage of both gel and nanocomposite electrolytes and are synthesized by incorporating nanofiller in a polymer matrix that combine the high ambient conductivity of conventional gel electrolytes with the excellent thermal and mechanical behaviour toward the metal electrode of nanocomposite electrolytes (Kwon et al, 2014). The combination of high conductivity, mechanical and thermal strength towards lithium makes the NCGPEs very attractive candidates for practical applications in lithium battery. Lithium polymer batteries are also gaining much attention in electric vehicles such as Hyundai Motor Company uses lithium battery in their hybrid vehicles (Brown, 2011). Kia company uses lithium polymer batteries in their new electric Kia Soul. Other motor companies like Tesla, Chevrolet, Nissan, Renault, Mahindra, GM, Zenn started making car incorporating lithium polymer battery technology. Also lithium polymer batteries are gaining favour in the world of radio-controlled aircraft, radio-controlled cars and large scale model trains where the advantages of lower weight and increased performance capacity and power delivery justify the price.

2.8 Scope of the Thesis and Statement of Thesis Problem

Tremendous research efforts have been made worldwide in the last four decades to develop polymer electrolytes with improved ionic, thermal, mechanical and electrochemical properties. The most widely studied dry polymer electrolytes i.e. PEO complexed with lithium salts have not yet been used for the practical applications because they possess very low ambient conductivity (10^{-7} to 10^{-8} Scm^{-1}) (Armand et al, 1979) despite a high solvating power for the lithium salts and good compatibility with the lithium electrode (Zhang et al, 2004). However, the conductivity still falls far away to be used in practical applications. GPEs have high ionic conductivity at room temperature by immobilizing a large amount of liquid electrolyte in the polymer matrix (Stephan, 2006; Song et al, 1999). The ionic conductivity and mechanical strength of GPEs are mutually exclusive i.e. the ionic conductivity increases at the expense of mechanical stability and vice versa (Stephan et al, 2005). Moreover, leakage of the organic liquid solvents from polymer electrolyte is

yet another big problem for GPEs when used in a working device over a long period of time which leads to a decrease in conductivity and causing damage to the lithium electrode and other components. Addition of nanofiller leads to enhancement of conductivity as well as mechanical strength in the polymer electrolytes. Therefore, NCGPEs combine the high ambient conductivity of gel electrolytes with the excellent stability toward the lithium metal electrode and good mechanical and thermal behaviour (Jacob et al, 2003). NCGPEs can be obtained either from a GPE containing dispersed nanofiller or from NCPEs by incorporating a conventional liquid electrolyte into a porous structure of a nanocomposite polymer. However due to the absence of structure-property correlations in the NCGPEs, an understanding of the phenomenon of ion conduction is still lacking completely. In the present work, an attempt has been made to gain an insight into the ion conduction mechanism (ion-polymer, ion-ion and polymer-filler interfacial interaction) in the polymer electrolytes and develop new NCGPEs with high ionic conductivity, good thermal and electrochemical stability, mechanically strong and flexible, ease of processing and high affinity with organic liquid electrolytes.

To achieve the aforesaid objectives, in the present work the following polymer electrolytes systems have been investigated:

A. PMMA based gel polymer electrolyte systems:

(i) PMMA-(PC+DEC)-$LiClO_4$-MWCNT.

(ii) PMMA-(PC+DEC)-$LiClO_4$-CNF.

(iii) PMMA-(PC+DEC)-$LiClO_4$-SiO_2 nanofiber.

(iv) PMMA-(PC+DEC)-$LiClO_4$-TiO_2 nanofiber.

B. P(VdF-HFP) based gel polymer electrolyte systems:

(v) P(VdF-HFP)-(PC+DEC)-$LiClO_4$-MWCNT.

(vi) P(VdF-HFP)-(PC+DEC)-$LiClO_4$-CNF.

(vii) P(VdF-HFP)-(PC+DEC)-$LiClO_4$-SiO_2 nanofiber.

(viii) P(VdF-HFP)-(PC+DEC)-$LiClO_4$-TiO_2 nanofiber.

Field emission scanning electron microscopy studies were carried out to investigate the microstructure and surface morphology of polymer electrolytes. Transmission electron microscopy studies were carried out to observe the size, shape and distribution of the nanofiller used in the present work. Structural characterization was done by X-ray diffraction analysis. Fourier transform

infrared spectroscopy was carried out to investigate the different bond interactions among polymer-ion-filler so as to understand dynamics of ion conduction processes in the polymer electrolytes. Ionic conductivity of the polymer electrolytes was measured by complex impedance spectroscopy. Wagner polarization technique was employed to measure the total ionic transport number of the polymer electrolytes. Electrochemical analysis i.e. Linear Sweep Voltammetry was done by Arbin Cycler.

Chapter 3

Experimental Techniques

Chapter 3

Experimental Techniques:

This chapter primarily deals with the materials used, synthesis routes for different types of systems and the methods of characterization used. Synthesis techniques for the preparation of composite films using various dispersoids (MWCNT, CNF, SiO_2 nanofiber and TiO_2 nanofiber) have been discussed in detail. This is followed by the discussion of the principles and specifications of different analytical techniques employed for the physico-chemical characterization of the synthesized materials. The synthesis routes of films involve (a) synthesis of GPEs by solution casting method, (b) preparation of NCGPEs dispersing different types of dispersoids/nanofiller by ultrasonication.

The structural characterization of the materials synthesized broadly includes structural and compositional analysis carried out by field emission scanning electron microscope (FESEM) and X-ray diffraction (XRD). The microstructural characterization of the polymer electrolytes has been carried out using transmission electron microscope (TEM). The samples have been characterized by Fourier transform infrared spectroscopy (FTIR) to investigate the bond structure and different interactions that take place among the various constituents of the electrolytes. The ionic conductivity of the polymer electrolytes was determined by electrochemical impedance spectroscopy (EIS). Thermogravimetric analysis (TGA) has been employed to determine the weight loss as a function of temperature of the material. The mechanical properties have been evaluated by stress-strain characteristics for the determination of tensile strength and fracture toughness. The electrochemical characterization of the polymer electrolytes was carried out by linear sweep voltammetry (LSV) for application in Li-ion battery.

3.1 Materials Synthesis

3.1.1 Raw Materials

The polymers, salt and plasticizers used for this study are as follows:

PMMA (M_w = 15000, Alfa Aesar), P(VdF-HFP) (M_w = 400000, Sigma Aldrich), $LiClO_4$ salt (Sigma Aldrich) and PC and DEC plasticizers (Sigma Aldrich). Nanofillers include MWCNT and

CNF were obtained from Chengdu Organic Chemicals Co. Ltd., China. Other oxide nanofillers i.e. SiO_2 nanofiber and TiO_2 nanofiber were purchased from Kertak Nanotechnology, Czech Republic.

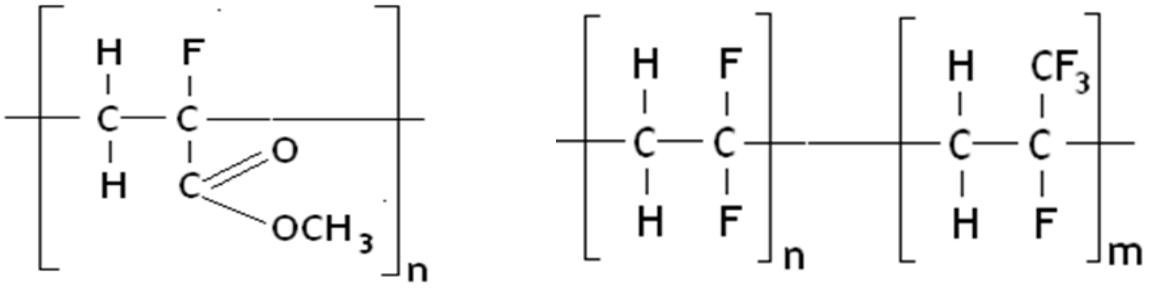

PMMA **P(VdF-HFP)**

Fig. 3.1: Chemical structure of PMMA and P(VdF-HFP) polymers.

Fig. 3.1 and 3.2 show the structure of different polymers and plasticizers, respectively used to synthesize gel polymer electrolytes. Table-3.1, 3.2 and 3.3 represent the basic physical properties of polymers, plasticizers and nanofillers used.

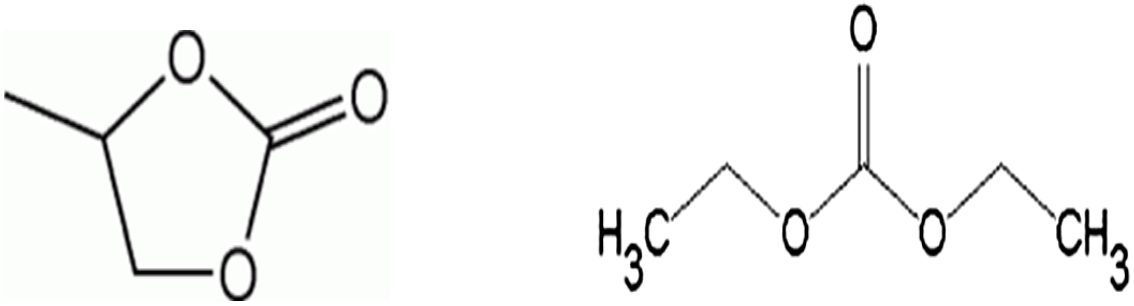

Propylene carbonate (PC) **Diethyl carbonate (DEC)**

Fig. 3.2: Chemical structure of plasticizers, PC and DEC.

Table-3.1: Physical properties of the polymers used for synthesizing GPEs.

Polymer	**Glass transition temperature, T_g (^oC)**	**Melting point (^oC)**	**Tensile strength (N/mm^2)**	**Dielectric constant at 1 MHz**	**Density (g/cm^3)**
PMMA	105	160	2.9-2.3	2.9	1.19
P(VdF-HFP)	–100 - (–90)	140	28-41	7.5	1.78

Table-3.2: Physical properties of the plasticizers used for synthesizing GPEs.

Plasticizer	Mol. Weight (g/mol)	Melting point (^oC)	Boiling point (^oC)	Coefficient of Viscosity η at 25 ^oC (mPa.s)	Density (g/cm^3)	Dielectric constant
PC	102.09	-48.8	242	2.53	1.2047	64.6
DEC	118.13	-43.0	126	0.748	0.9752	2.82

Table-3.3: Some physical properties of nanofillers used for NCGPEs.

Nanofiller	Appearance colour	Physical state-Solid	Fiber diameter (nm)	Solubility in water
MWCNT	Black	Powder	10-20	Insoluble
CNF	Black	Powder	200-600	Insoluble
SiO_2 nanofiber	White	Fiber	100-500	Insoluble
TiO_2 nanofiber	White	Fiber	200-700	Insoluble

3.1.2 Sample Preparation

GPEs were prepared by solution casting method, which involves the following steps:

(i) Drying of PMMA and P(VdF-HFP) polymers and salt ($LiClO_4$) in vacuum oven at 70 ºC temperature for 24 hours prior to their use.

(ii) Dissolution of PMMA and P(VdF-HFP) polymers in acetone or tetrahydrofuran (THF).

(iii) Dissolution of salt ($LiClO_4$) in (PC+DEC). High dielectric constant (ε= 64.6) and high viscosity (η = 2.53 mPas) of PC was combined with DEC having low dielectric constant (ε = 2.82) and low viscosity (η = 0.748 mPas) in ratio of PC:DEC :: 1:1 by volume to obtain high dielectric constant (ε = 33.71) and low viscosity (η = 1.639 mPas) in order to achieve high ionic conductivity.

(iv) Addition of the polymer and salt solutions in a beaker and their mixing using magnetic stirrer at a constant temperature of 50 ^oC for 7-8 hours.

(v) Casting of the viscous solution on glass plates/petri dishes followed by drying under vacuum.

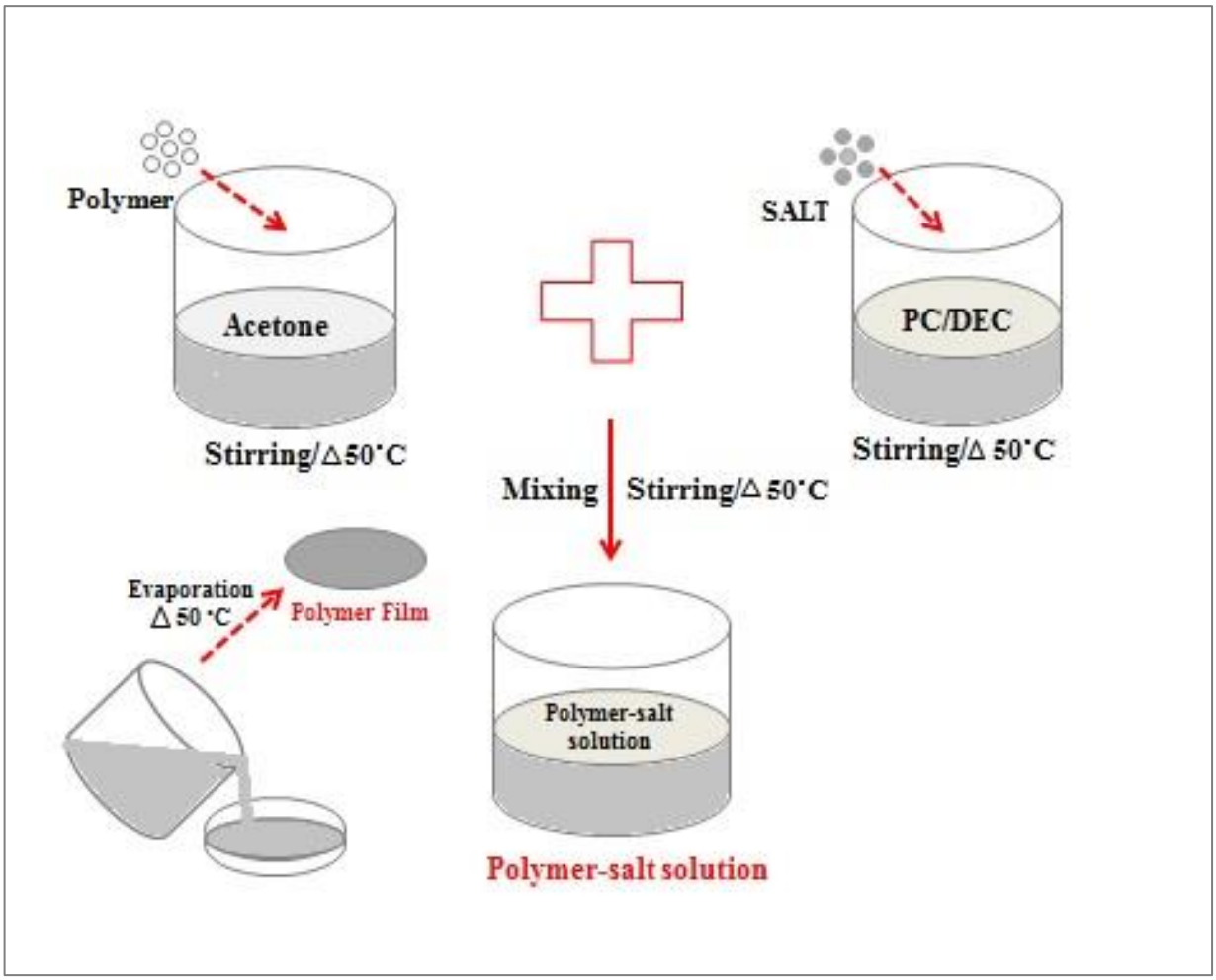

Fig. 3.3: Schematic diagram of the preparation of GPEs.

For preparing NCGPEs, different nanofillers (MWCNT, CNF, SiO_2 nanofiber and TiO_2 nanofiber) were dispersed in solvent by ultrasonication using ultrasonic processor (Sonics and Materials Inc.) with a power output of 750 W. The ultrasonication was carried out for 30 minutes. Fig. 3.3 shows the schematic diagram of the preparation of GPEs and Fig. 3.4 shows the flowchart of the preparation of NCGPEs. These procedures provided free standing, mechanically stable and flexible samples of thickness in the range of ~0.12-0.35 mm.

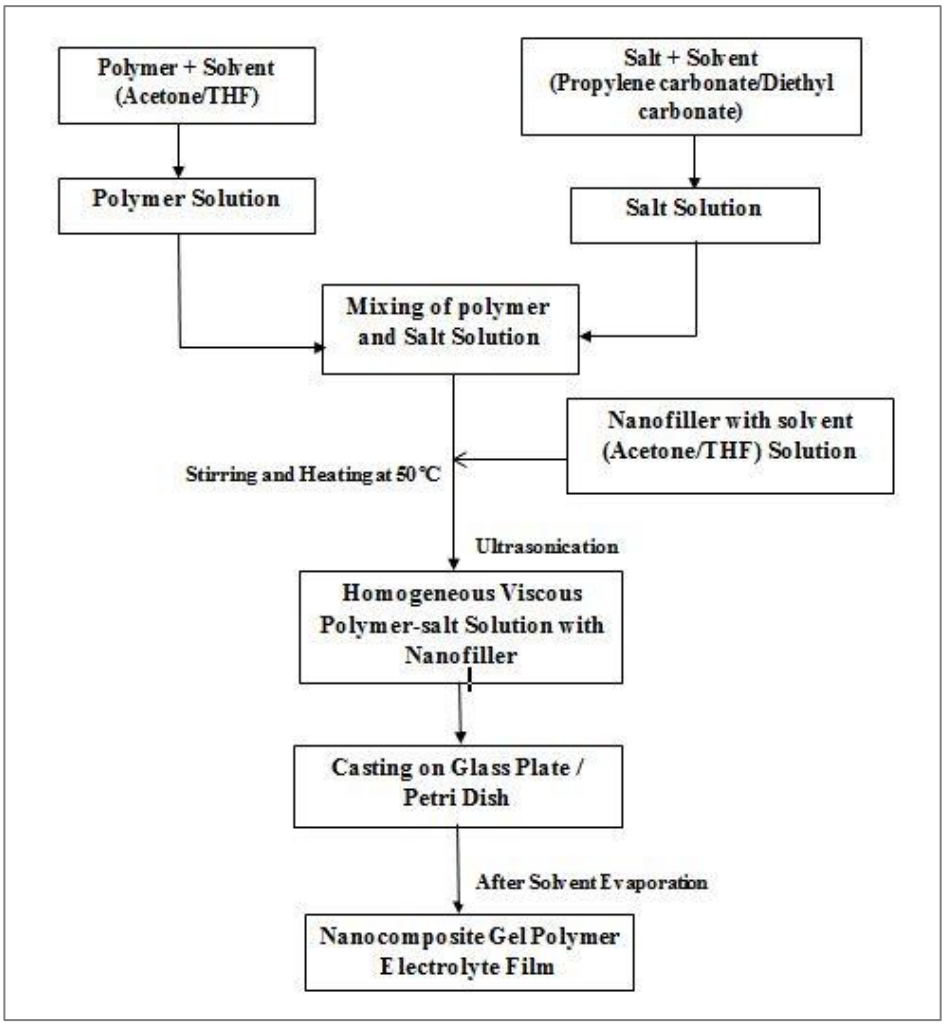

Fig. 3.4: Flowchart of the preparation of NCGPEs.

3.2 Materials Characterization Methods

The following methods were used to characterize materials used in the present study.

3.2.1 X-Ray Diffraction Analysis

X-ray diffraction is one of the most important structural characterization tools used in materials science. XRD patterns give information about different crystal parameters like crystalline size, d-spacing, diffraction planes and structure, phase and lattice constants. The intensities and the angles of diffracted X-ray beams are related to atomic arrangements of the crystal and this method is based on the scattering of X-rays by crystals governed by the Bragg's law:

$$n\lambda = 2d\sin\theta \quad (3.1)$$

In addition to the crystal structure, XRD is applied for various other purposes such as chemical analysis, stress, strain, particle size measurements, phase equilibrium, determination of orientation for single crystals or the ensemble of orientations in a polycrystalline or polymeric aggregate, order-disorder transformation etc. The intensities and angles of the diffracted X-ray beams are related to the atomic arrangement in the crystal. In case of polymeric materials, XRD is used to determine the proportion of the crystalline and amorphous phases in terms of the degree of crystallinity. Polymers are semi-crystalline materials. Their crystallinity is attributed to chain folding or to the formation of single or double helices, for at least part of their chain length (Hussain et al, 2006). The XRD patterns for the films reported in the present work have been recorded using a Bruker AXS, D8 advance (operating at 30 kV and 20 mA) using a CuKα radiation (1.5418 Å). The data were recorded using a scanning rate of 1º min^{-1} in 2θ varying from 10º to 90º. Measured diffraction patterns were compared with the JCPDS database of powder diffraction files. Quantitative estimations of phase composition were made using the semi-quantitative feature present in the X'Pert high score plus (PANalytical) software.

Generally, polymer is neither fully amorphous nor totally crystalline. The degree of crystallinity can be measured by XRD of a polymer. It gives quite a good estimation of the amount of crystalline phase present in a polymer sample. A typical XRD pattern of a polymeric material consists of a broad amorphous hump superimposed with some sharp peaks as shown in the Fig. 3.5(a). The total area under the peaks in the pattern is the sum of the broad amorphous hump and crystalline peaks. If a typical XRD pattern has two crystalline peaks having areas A_1 and A_2 which is superimposed on a broad amorphous hump with an area A_3 as shown in Fig. 3.5(b), then the degree of crystallinity (K) will be calculated by

$$K = \frac{A_1 + A_2}{A_1 + A_2 + A_3} \times 100\% = \frac{A}{A_0} \times 100\% \quad (3.2)$$

where $A = A_1 + A_2$ is the sum of the area of all the crystalline peaks in the diffractogram and A_0 is the total area under the diffractogram. The area has been estimated by counting the number of square grids of suitable size with which the peak areas were filled. The grids size used is 0.5 mm ×

0.5 mm. The degree of crystallinity of the polymer is affected by the structure of the polymer chain (degree of order), the physical treatment and the molecular weight of the polymer.

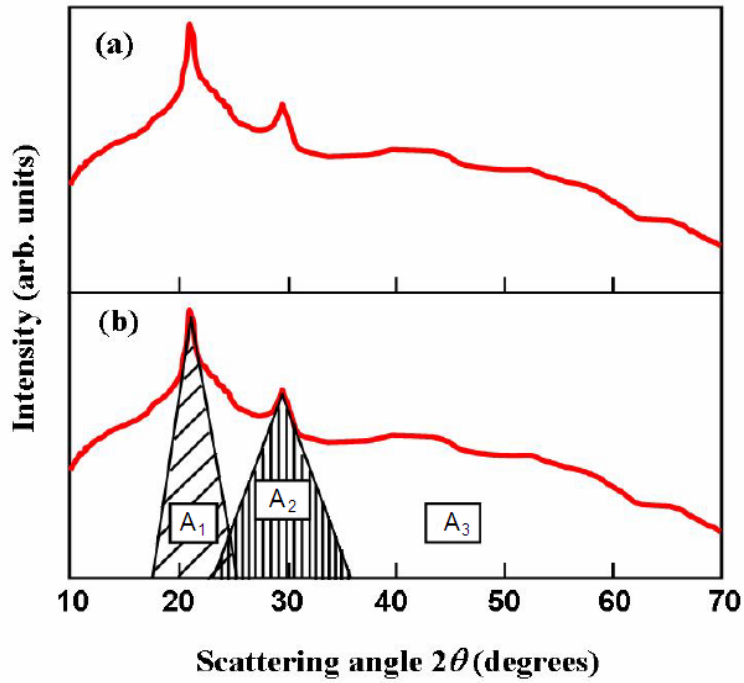

Fig. 3.5: (a) Typical XRD pattern of a semi-crystalline polymer; (b) XRD pattern showing the superposition of crystalline peaks and an amorphous hump.

3.2.2 Microstructure and Phase Composition

The surface morphology of the polymeric films was studied under FESEM and TEM as discussed below:

3.2.2.1 Field Emission Scanning Electron Microscopy

Microstructure observation was made by FESEM. In scanning mode, the interaction of electron beam with sample produces scattering of secondary electrons from atoms in the sample and also causes electrons in the beam to be back-scattered from the sample after collision with atoms in the material, both events occurring mostly on the surface of the sample. These electrons can be detected separately and transformed into magnified images of the sample in secondary electron (SE) and backscattering (BS) modes, respectively. In SE mode, a detailed representation of the surface of a sample can be obtained. Therefore, most scanning electron microscopy (SEM) images showing the morphology of a material are taken in SE mode. In BS mode, the intensity of back-

scattered electrons is proportional to the atomic number of the element involved in the electron collision. Therefore, this mode is usually employed to know about the compositional differences in a sample, observed as intensity variations in the image of the material. Further elemental analysis can be carried out using energy dispersive spectroscopy (EDS) by measuring the energy of photons emitted after scattering of atoms in the sample, which corresponds to energy of transitions in the atoms of the material. After interacting with the sample, the electron beam is magnified and focused to provide an image of the structure of the material, in a manner which is conceptually similar to the acquisition of an optical image with an optical microscope in transmission mode (Kaufmann, 2003).

Samples were examined using FESEM to determine morphologies of planar and cross-sectional microstructure of the GPE and NCGPE samples, and some qualitative elemental analysis was also carried out by EDAX analysis. Samples were prepared by mounting on an aluminium stub with double sided tape and by sputter coating with gold for 60 seconds with a deposition current of 30 mA in BAL-TEC sputter coater (SCD 005). A FEI QUANTA 200F FE-SEM was used with an accelerating voltage varying between 5-15 kV and a working distance of about ~10 mm in most cases, and elemental analysis was also carried out using EDS. Dimensions of the nanofiller were determined by image analysis of FESEM micrographs using Image-J software. Photoshop software was used to correct brightness and contrast in some FESEM and TEM (discussed in the next section) images.

3.2.2.2 Transmission Electron Microscopy

It is a technique in which a beam of high energy electrons are transmitted through an ultra-thin specimen, interacting with the specimen as it passes through it. The interaction of transmitted electrons through the specimen formed magnified image which is to be focused with electromagnetic lenses onto an imaging device i.e. a fluorescent screen or to be detected by a sensor such as CCD camera. The electrons are accelerated at 200 kV, giving wavelength of 0.025 Å much less than that of light. The optical microscope has limited resolution by the wavelength of light but for the electron microscope, it is limited by aberrations inherent in electromagnetic lenses which is about 1-2 Å. For very thin samples, one is looking through many atoms whereas in some cases one does not usually see individual atoms. Rather the high resolution imaging mode of the microscope, images the crystal lattice of a material as an interference pattern between the

transmitted beam and diffracted beam which allows one to observe planar and line defects, interfaces, grain boundaries etc. with atomic scale resolution. The bright/dark field imaging mode operate at intermediate magnification combined with electron diffraction and are also invaluable for providing the morphology, defects and crystal phases in a material. At lower magnification, image contrast is due to absorption of electrons in the material, thickness and composition of the material. At higher magnifications, complex wave interactions modulate the intensity of the image which requires the intense analysis of the observed images. Alternate modes of TEM used to observe modulation in chemical identity, electronic structure, orientation of crystals and shifting of induced electron phase of sample as well as the regular absorption based imaging. The diffraction pattern can be generated by adjusting the magnetic lenses. For the case of single crystal, the diffraction pattern is dependent upon the structure and the orientation of the sample, illuminated by the electron beam. This is typically done at the position where the observed image symmetries and the diffraction spots appear. The morphology of the polymer samples, the distribution of nanofiller within the polymer matrix, the interface between matrix and nanofiller and elemental analysis of nanofiller inside the polymer matrix were obtained using a FEI Technai G2 20 TEM with an acceleration voltage of 200 kV. Samples were prepared for TEM by placing a few drops of the polymer solution on a holey copper grid (carbon-coated) and by allowing it to dry before examination.

3.2.3 Thermogravimetric and their derivative Analysis

Thermal analysis provides information on structural and phase change as well as energy of transformation involved in the materials with increasing temperature. Several methods are commonly used and these are distinguished from one another by the property that is measured. The TGA and their derivative (DTG) are based on weight loss, degradation/decomposition of the materials etc. However, in the present work, the thermal stabilities of GPE and NCGPE samples were studied. Typically, the measurements were carried out in N_2 atmosphere to determine further decomposition or melting that may occur along with weight loss over the temperature range of interest for polymer electrolytes. Measurements were made using a Perkin Elmer (Pyris Diamond) and Exstar TGA 6300 (SII Nanotechnology Inc.) with alumina as the reference material with a heating rate of 10 ^{o}C min^{-1}.

3.2.4 Fourier Transform Infrared Spectroscopy

This is a powerful analytical tool for identifying organic molecules, functional groups (chemical bonds) and the molecular structure of organic compounds by their characteristic peaks. A part of the incident infrared radiation is absorbed by the sample and the rest is transmitted. The wavelength of the infrared radiation gets absorbed if it could excite stretching/bending vibrational modes of a chemical bond in a molecule. The most useful range for identification of the compounds is the near and mid-infrared region as most of the molecular vibrations require energy corresponding to these frequency regions. The resulting spectrum represents the molecular absorption and molecular transmission that creates a fingerprint of the sample with absorption peaks which corresponds to the vibration frequencies of the bonds between the atoms making up the material. Each material is a unique combination of atoms, therefore, no two compounds produce exactly similar spectra. Therefore, FTIR spectroscopy gives a positive identification (qualitative analysis) of various types of materials. A single vibrational energy change is accompanied by a number of rotational energy changes, consequently vibrational spectra appear as bands rather than as discrete lines. FTIR spectroscopy studies of the samples were conducted for understanding the bond structure and different interactions taking place among various constituents of polymer electrolytes. The spectra were recorded using a Perkin Elmer FTIR spectrometer-Spectrum over the wave number range of 400-4000 cm^{-1}.

3.2.5 Mechanical Properties

Testing of mechanical properties under uniaxial tensile loading is used extensively. Sample is subjected to loading along the long axis of the specimen until failure by applying the load necessary for displacing the moving crosshead at a definite rate to correspond to a controlled engineering strain rate. The load is measured by a load cell. The engineering stress developing in the sample of a material due to the application of a given load is calculated by dividing the load by the original area of cross section of the sample. The engineering strain at a given load is measured by dividing the extension of the sample at that load by the original gauge length of the sample (Friedrich, 1985). The stress-strain diagram for the material of the sample is, thus, determined from the load extension diagram recorded during the tensile test. Properties that can be obtained by tensile test are ultimate tensile strength (UTS) and strain-hardening characteristics. Furthermore, it is also possible to determine elongation at fracture, which along with strength gives a measure of

toughness of the material, given by the area under the stress-strain diagram. The tensile testing is carried out commonly using universal testing machine. The samples are held between grips attached to moving and fixed crossheads. The software in the machine does these calculations as the load increases with extension and the data points are recorded to give stress-strain curve. The stress corresponding to maximum load, which could be employed, is the tensile strength of the material.

For polymeric films, the tensile testing was done by Universal Testing Machine (UTM) Hounsfield (H25KS) at a crosshead speed of 10 mm min^{-1} at ambient temperature which helps to determine tensile strength, extension under tensile loading, energy absorbed till failure and elongation at break. The dimensions of the specimens were made as 60 mm (Length) × 20 (Width) mm × 0.5 (Height) mm.

3.3 Electrochemical Studies

The electrochemical measurements of the polymer electrolyte films were carried out as discussed below:

3.3.1 Electrochemical Impedance Spectroscopy

The complex impedance measurements have been done by Hioki 3532-50 LCR HiTester. The instrument is interfaced with a computer to collect the data. It has a built-in frequency synthesizer and has a frequency range 42 Hz to 5 MHz. The impedance measurements were carried out at a temperature interval of 10 ºC from room temperature (25 ºC) to 70 ºC. Sufficient time was allowed at each temperature point for attaining thermal equilibrium and reproducibility of the measurement. The ionic conductivity was calculated using the following relation-

$$\sigma = \frac{L}{R_b A} \tag{3.3}$$

where L is the thickness and A is the cross-sectional area of the polymer electrolyte sample disc, R_b is the bulk resistance obtained from the complex impedance plot.

3.3.2 Transference Number Measurements

Transference number of the NCGPEs was calculated by Wagner's polarization technique (Wagner et al, 1957), which is used to determine the ionic contribution of the electrolytes to the total charge transport by measuring the residual electronic current passing through the electrolytes. The Wagner polarization cell (Ag/PE/Ag) was prepared to measure the total ionic transference number. A fixed small dc potential (300 mV) was applied across the blocking electrodes and the passing current was measured as a function of time to allow the samples to become fully polarized. Initial total current (I_T) is the sum of ionic (I_i) and electronic (I_e) currents i.e. ($I_T = I_i + I_e$) and final current after polarization is only the electronic current (I_e), which were measured. The transference numbers (t_{ion} and t_{ele}) have been calculated using the relations

$$t_{ion} = I_i / I_{total} = (I_T - I_e)/I_T \tag{3.4}$$

$$t_{elc} = I_e / I_T \tag{3.5}$$

3.3.3 Cell Fabrication and Electrochemical Testing

Teflon made cylindrical cells were fabricated for electrochemical testing. The polymer film of area ~ 1 cm^2 was cut and used as solid electrolyte in Li-ion cell, which was then assembled with the film between anode (Lithium) and cathode ($LiFePO_4$) in an argon atmosphere using MBRAUN glove box (MB 200G) having both oxygen and moisture contents less than 0.1 ppm.

NCGPEs with different types of nanofillers viz. MWCNT, CNF, SiO_2 nanofiber and TiO_2 nanofiber have been tested electrochemically. The voltage of a cell depends on the chemical potential of both the electrodes. The electrochemical performance of Li/$LiFePO_4$ polymer cells containing $LiFePO_4$ as cathodes and the GPE was investigated using Teflon cells. Each cell comprised of a lithium metal anode and $LiFePO_4$ as cathode separated by the NCGPE film. The teflon cells were assembled in the glove box and tested galvanostatically on a multichannel battery tester (BT- 2000, Arbin Instruments). The electrochemical stability window of NCGPE was determined by linear sweep voltammetry (LSV) of Teflon type cells which were carried out in the potential range from 2 V to 6 V with a scan rate 0.1 mVs^{-1}. The onset of the current identifies the anodic decomposition voltage of the electrolytes.

Chapter 4

Results and Discussion: Gel Polymer Electrolyte Systems

Chapter 4

Results and Discussion: Gel Polymer Electrolyte Systems

In the present study two types of polymers PMMA and P(VdF-HFP) are used for the preparation of GPEs using solution casting technique followed by the procedure described in the previous chapter (Chapter 3) on experimental procedure. The gel polymers were prepared in the systems comprising of PMMA-(PC+DEC)-$LiClO_4$ and P(VdF-HFP)-(PC+DEC)-$LiClO_4$. Their results on synthesis and characterizations of GPEs have been described in the following section with their comparative study at the end has been discussed.

4.1 Characterizations of the Gel Polymer Electrolytes:

For PMMA-(PC+DEC)-$LiClO_4$ system, required quantity of PMMA (60 wt.%) was dissolved in THF while stirring. The plasticizer, PC+DEC (30 wt.%) were chosen in 1:1 (by vol.) mixture because of its high dielectric constant, high boiling point, low viscosity and low melting point (Sekhon, 2003). The high boiling point of plasticizer is desirable as the evaporation of the liquid will be slow. High dielectric constant (ϵ = 64.4) of PC, helps to dissociate the salt into ions easily and low viscosity of DEC, (η = 0.784) gives rise to high ionic mobility. The salt $LiClO_4$ (10 wt.%) was used due to its low dissociation energy (723 $kJmol^{-1}$) (Watanabe et al, 1985) so that the salt gets easily dissociated in the solvent (PC+DEC). Therefore, liquid electrolyte solution comprising of (PC+DEC) and $LiClO_4$ were further mixed with the polymer solution while stirring at 50 ºC as discussed in Chapter 3. The resulting viscous solution was then cast onto a petri dish to get electrolyte films of thickness ranging from 0.12-0.19 mm.

For P(VdF-HFP)-(PC+DEC)-$LiClO_4$ system, semi-crystalline polymer PVdF is copolymerized with HFP having ratio of 88:12. The degree of crystallinity of the resulting co-polymer is greatly reduced due to the steric hindrance that is provided by bulky -CF_3 pendant group of HFP structural unit which considerably enhances the flexibility of the polymer. The synthesized copolymer P(VdF-HFP) (60 wt.%) was dissolved in THF. PC+DEC (30 wt.%) and salt $LiClO_4$ (10 wt.%) were added into polymer solution as described for the previous system. Therefore, a comparative study has been carried out between PMMA and P(VdF-HFP) based gel polymer electrolytes. Table

4.1 represents the composition of the PMMA and P(VdF-HFP) based gel polymer electrolyte systems.

Table-4.1: Composition of the PMMA and P(VdF-HFP) based gel polymer electrolyte systems.

Sl. No.	Gel Polymer Electrolyte System	Composition (wt.%)
1.	PMMA-(PC+DEC)-$LiClO_4$	60:30:10
2.	P(VdF-HFP)-(PC+DEC)-$LiClO_4$	60:30:10

4.1.1 Morphology and Structure of Gel Polymer Electrolytes

This subsection presents the morphology and structure of gel polymer electrolytes of both the synthesized systems. The FESEM micrographs of PMMA based gel polymer electrolyte system shows the smooth surface as shown in Fig. 4.1(a), whereas P(VdF-HFP) based gel polymer electrolyte system shows a disordered spherical grain structure as shown in Fig. 4.1(b).

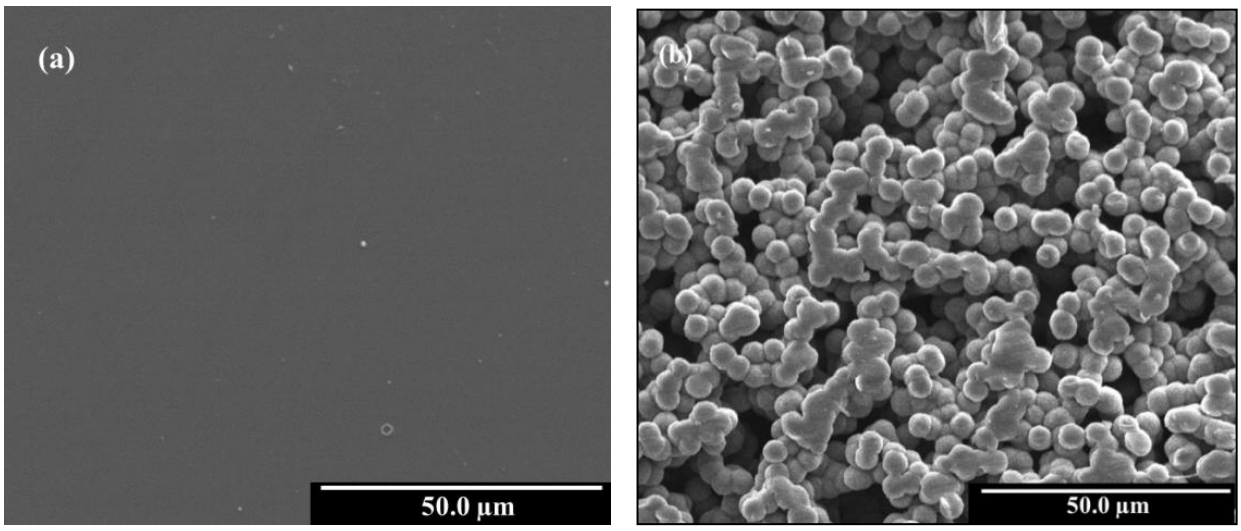

Fig. 4.1: Typical FESEM micrographs of (a) PMMA-(PC+DEC)-$LiClO_4$ system; (b) P(VdF-HFP)-(PC+DEC)-$LiClO_4$ system.

The morphology of the PMMA and P(VdF-HFP) based gel polymer electrolytes have also been examined under TEM and the micrographs are shown in Fig. 4.2(a and b). The diffused rings appeared in selected area diffraction (SAD) patterns given in the inset of Fig. 4.2 are the indication of dominating amorphous region of the polymer material.

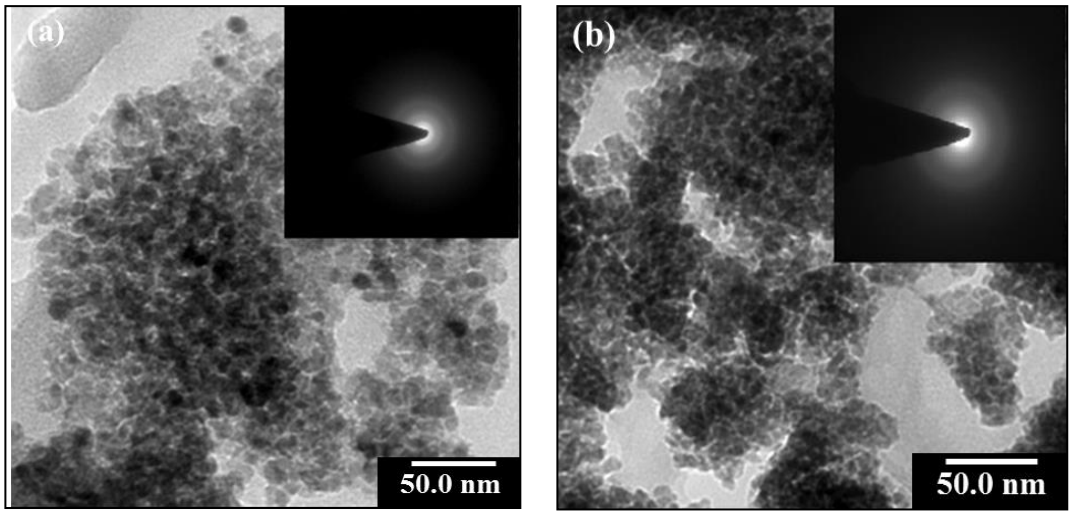

Fig. 4.2: Typical TEM micrographs of (a) PMMA-(PC+DEC)-$LiClO_4$ system; (b) P(VdF-HFP)-(PC+DEC)-$LiClO_4$ system.

The XRD pattern of bare PMMA, bare P(VdF-HFP), $LiClO_4$, PMMA and P(VdF-HFP) based gel polymer electrolytes are shown in Fig. 4.3. For bare PMMA, there is no sharp peak observed as it is amorphous in nature but three humps are observed at $2\theta = 15^o$, 29.9^o and 41.2^o. In the case of pure P(VdF-HFP), the peaks appearing at $2\theta = 20^o$ and 38^o correspond to (020) and (202) peaks of P(VdF) which is a confirmation of partial crystallization of the PVdF units in the co-polymer to give an overall morphology which is semi-crystalline in nature for P(VdF-HFP). The salt $LiClO_4$ is crystalline as observed from its XRD pattern (Abbrent et al, 2001).

Fig. 4.3(d and e) show the XRD pattern of PMMA and P(VdF-HFP) based gel polymer electrolyte systems respectively. Following the relation, $\{K = (A/A_0) \times 100\}$ given in Chapter 3, the degrees of crystallinity (K) for PMMA and P(VdF-HFP) polymers have been found as 31.8% and 30.2% respectively. For PMMA-(PC+DEC)-$LiClO_4$ and P(VdF-HFP)-(PC+DEC)-$LiClO_4$ electrolytes, the degrees of crystallinity are estimated as 26.6% and 22.4% respectively. It is observed that crystallinity of GPE is greatly reduced on addition of plasticizers (PC+DEC) and salt $LiClO_4$. Moreover, the peaks corresponding to salt $LiClO_4$ have disappeared indicating that salt $LiClO_4$ has been mostly dissolved in (PC+DEC) solvents in the polymer gel and no longer exist as a separate phase in the electrolytes. Also the intensity of crystalline peaks is decreased and a noticeable broadening of the area under the peaks was observed is a clear indication of the reduction of crystalline phase in polymer electrolyte (Leo et al, 2001). It is observed that P(VdF-HFP) based gel

polymer electrolytes are more amorphous than PMMA based electrolytes as estimated from the value of degree of crystallinity.

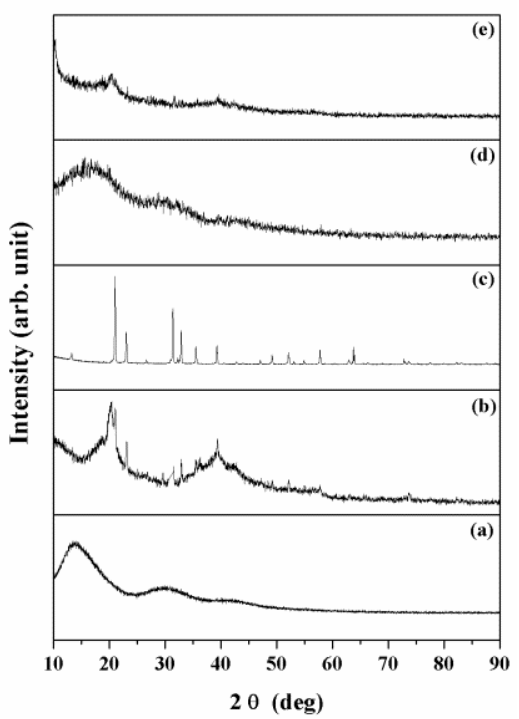

Fig. 4.3: XRD patterns of (a) PMMA, (b) P(VdF-HFP), (c) $LiClO_4$, (d) PMMA based gel polymer electrolytes and (e) P(VdF-HFP) based gel polymer electrolytes.

4.1.2 Fourier Transform Infra-Red Spectroscopy

Fig. 4.4(a) depicts the FTIR spectra of PMMA, $LiClO_4$ and PMMA based gel polymer electrolytes. The characteristic vibration bands of PMMA appear at 1727cm^{-1} and 1450 cm^{-1} corresponds to C=O group and C–O group respectively. The peaks due to the stretching and in plane bending vibrations of the –OH group of molecular H_2O are observed at around 3002 and 1640 cm^{-1}.The bands at 2940 cm^{-1} correspond to the C–H stretching of the methyl group CH_3 while the bands at 1487 and 1386 cm^{-1} are associated with C–H asymmetric and symmetric stretching modes, respectively. The 1264 cm^{-1} band is due to methylene group i.e. CH_2 and 1143 cm^{-1} band corresponds to the vibration of ester group C–O while C–C stretching bands are at 982 and 840 cm^{-1}. For the PMMA based gel polymer electrolyte, the absorption peaks appear at 3548 cm^{-1} and 3002 cm^{-1} corresponding to vibrations involving O–H whereas 2921, 1729, 1446, 1246 cm^{-1} corresponding to vibrations involving CH_3, >C=O symmetric, >C–O–C< symmetric stretching and CH_2 methyl group of PMMA (Rajendran et al, 2000).

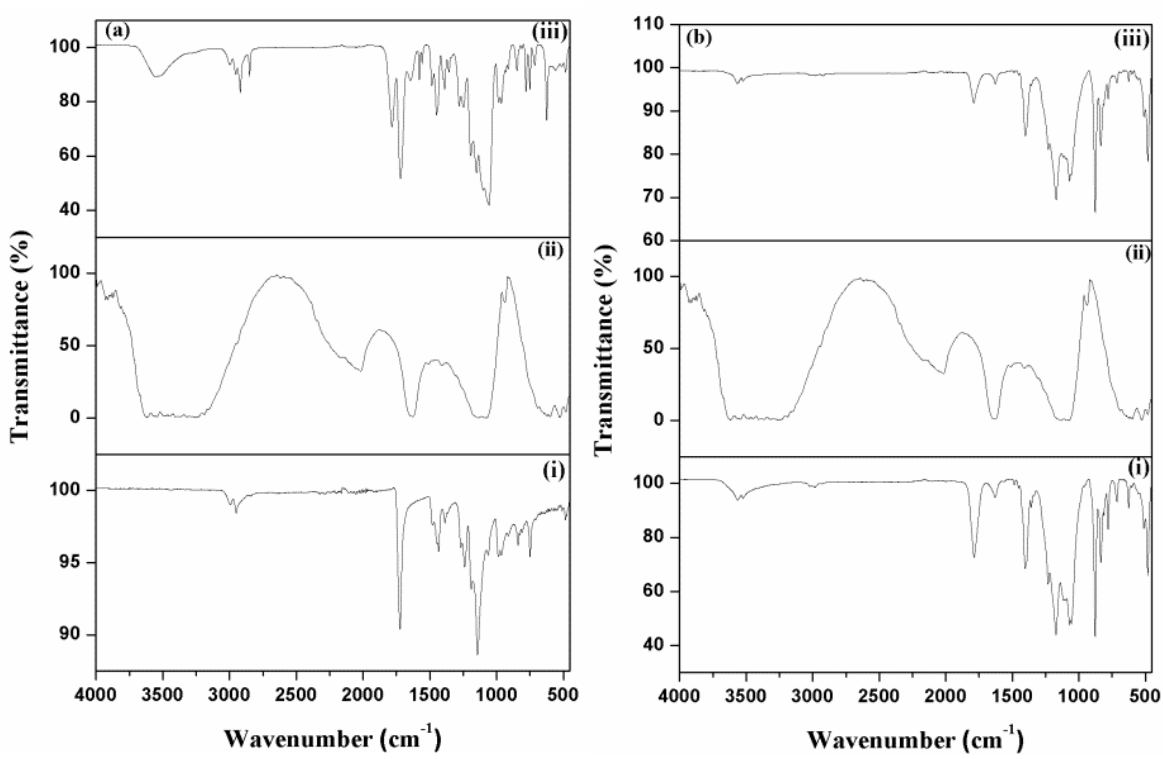

Fig. 4.4: FTIR spectra of (a): (i) PMMA, (ii) $LiClO_4$, (iii) PMMA based gel polymer electrolytes and (b): (i) P(VdF-HFP), (ii) $LiClO_4$, (iii) P(VdF-HFP) based gel polymer electrolytes.

FTIR spectra of P(VdF-HFP), $LiClO_4$ and P(VdF-HFP) based gel polymer electrolytes are shown in Fig. 4.4(b). The wave number 3548 cm^{-1} is assigned to C–H stretching vibrations of PVdF. Frequency 1770 cm^{-1} is assigned to $–CF=CF_2$ group. Peak at 1628 cm^{-1} is assigned to C=O stretching vibration of plasticizer (PC+DEC). Frequencies 1483 cm^{-1} and 1406 cm^{-1} are assigned to $–CH_3$ asymmetric bending and C–F stretching vibration of plasticizers, propylene carbonate and diethyl carbonate respectively. Whereas frequency 1290 cm^{-1} is assigned to –C–F–, 1060 cm^{-1} is assigned to $–CF_2–$ stretching vibrations and 881 cm^{-1} is assigned to vinylidene group of polymer. The vibrational peaks of P(VdF-HFP) appear at 3548, 1770, 1406, 881 and 801 cm^{-1} are shifted respectively to 3568, 1790, 1408, 881 and 820 cm^{-1} in the polymer electrolytes. New absorption peaks at 699 cm^{-1} and 557 cm^{-1} corresponding to C–Cl stretching are observed for the electrolyte material. Appearance of new peaks at 699 and 557 cm^{-1} in P(VdF-HFP) based gel polymer electrolytes could be ascribed to C–Cl stretching vibration indicates that polymer carbon atoms interact with chlorine of ClO_4^- ions (Rajendran et al, 2001). Formation and Shifting of new peaks suggest that the polymer-salt interaction occurs in both PMMA and P(VdF-HFP) based gel polymer electrolytes.

4.1.3 Ionic Conductivity Measurement/Electrochemical Impedance Spectroscopy

The ionic conductivity of as-prepared gel polymer electrolytes was determined from the complex impedance measurements as described in Chapter 2. Fig. 4.5(a and b) show the impedance plot of PMMA and P(VdF-HFP) based gel polymer electrolytes respectively at different temperatures in the range of 25 ºC to 70 ºC. Z' and Z'' represent the real part and imaginary part of the impedance data at different temperatures. The impedance spectra consist of a distorted semi-circular arc in the high frequency region and a spike in the lower frequency region. The bulk resistance R_b is calculated from the intercept at high frequency side on the Z' axis. The ionic conductivity is calculated from the following relation, $\{\sigma = l/(R_b r^2 \pi)\}$, where l is the thickness and r is the radius of the sample. R_b is the bulk resistance of the electrolyte obtained from complex impedance measurements (Abraham et al, 1997; Watanabe et al, 1985).

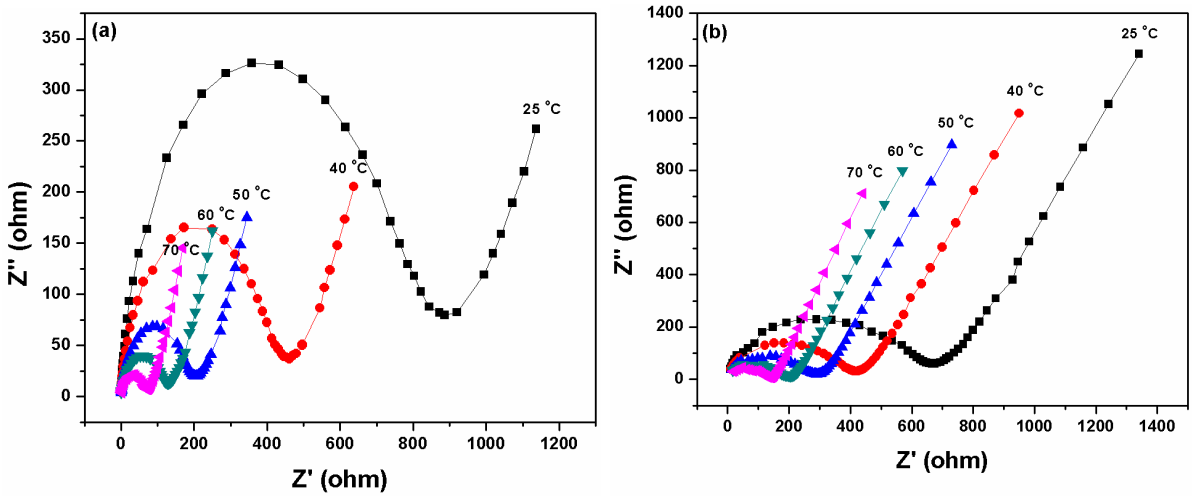

Fig. 4.5: Nyquist plots of (a) PMMA and (b) P(VdF-HFP) based gel polymer electrolytes at different temperatures ranging from 25 ºC to 70 ºC.

The value of conductivity of PMMA and P(VdF-HFP) based gel polymer electrolytes are presented in Table-4.2.

Table-4.2: Conductivity of PMMA and P(VdF-HFP) based gel polymer electrolyte systems.

Sl. No.	Gel Polymer Electrolyte Systems	Conductivity (Scm^{-1})
1.	PMMA based gel polymer electrolyte	0.13×10^{-4}
2.	P(VdF-HFP) based gel polymer electrolyte	1.76×10^{-4}

Fig. 4.6(a and b) show the variation of ionic conductivity as a function of temperature in terms of 1/T for PMMA and P(VdF-HFP) based gel polymer electrolytes in the temperature range of 25 ºC to 70 ºC respectively. The Fig. 4.6(a and b) show that the ionic conduction in GPEs follow the linear variation following the Arrhenius relationship, $\{\sigma = \sigma_0 \exp(-E_a/kT)\}$, where σ, σ_0, E_a, k and T are the ionic conductivity, pre exponential factor, activation energy, Boltzmann constant and absolute temperature, respectively. As expected the increase in temperature leads to increase in ionic conductivity because as the temperature increases the polymer chains expand at increasing rate to produce larger free volume which leads to the enhancement of polymer segmental motion and ionic mobilities. The salt content in the polymer increases the number of charge carriers and results in increase of conductivity. The addition of plasticizer reduces the glass transition temperature of the polymer increasing the segmental mobility thus enhancing the conductivity. The enhancement of ionic conductivity can be explained by the fact that the salt and plasticizer inhibit the recrystallization kinetics, thereby retaining the amorphous phase down to relatively low temperatures (Jeon et al, 2005).

Higher value of conductivity in P(VdF-HFP) based gel polymer electrolyte system could be attributed to the higher amorphicity due to steric hindrance that is provided by CF_3 pendant group in HFP monomer unit which is randomly mixed with the VdF monomers unit in the polymer chain. Higher amorphicity provides mobile Li^+ ion greater free volume giving more freedom to the ionic movement and consequent rise in higher conductivity (Cohen et al, 1959). However, conductivity enhancement is due to the increase in preferred directional movement of the ions. On the other hand pure PMMA consisting of single type of monomer has higher degree of crystallinity providing less free volume to the mobile ions that result in lower conductivity.

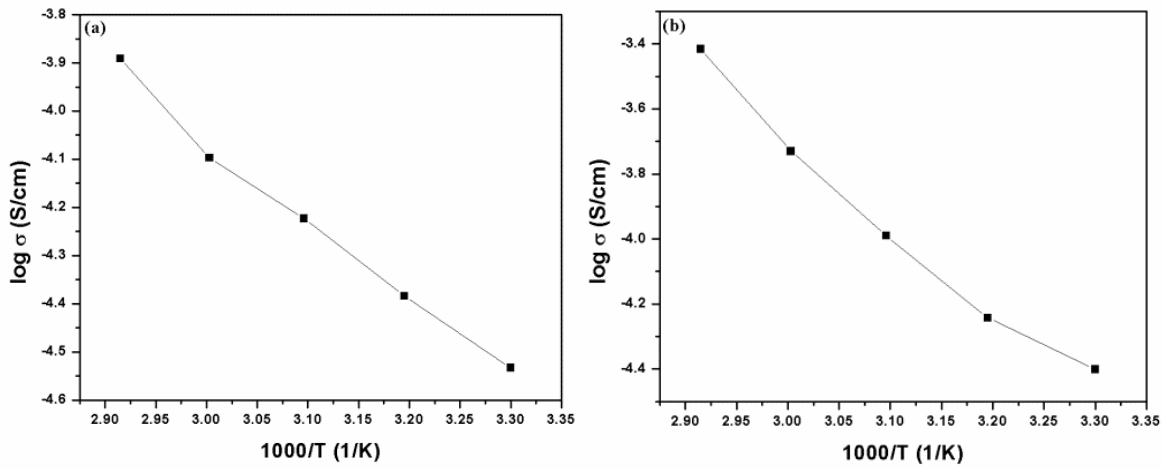

Fig.4.6: Temperature dependent ionic conductivity plots of (a) PMMA and (b) P(VdF-HFP) based gel polymer electrolytes.

The mobility of ionic species is an important parameter to consider when designing new polymer electrolytes for batteries (Ferry et al, 1998). Thus, evaluation of polymer electrolytes requires consideration of transference numbers and ionic conductivities. Total ionic transference number was measured by Wagner's polarization technique of GPEs which is used to determine ionic contribution to the total charge transport by measuring the electronic current passing through the electrolyte (Wagner et al, 1957). Ionic transference number of PMMA based gel polymer electrolyte and P(VdF-HFP) based gel polymer electrolyte systems with varying compositions was measured (with Ag/GPE/Ag) as described in Chapter 3. The ionic transference number was calculated following the relation, $\{t_i = I_i/I_{total} = I_T - I_e/I_T\}$ where t_i is ionic transference number, I_i is the ionic current, I_T is the Initial total current and I_e is the electronic currents (Chandra, 1981). Table-4.3 shows the ionic transference number for the Ag/Electrolyte/Ag cell system using PMMA and P(VdF-HFP) based gel polymer electrolytes.

Table-4.3: Ionic transference number of PMMA and P(VdF-HFP) based gel polymer electrolyte systems.

Sl. No.	Gel Polymer Electrolyte Systems	Transference Number
1.	PMMA based gel polymer electrolyte	0.91
2.	P(VdF-HFP) based gel polymer electrolyte	0.95

Higher transference numbers of 0.91 for PMMA based gel polymer electrolytes and 0.95 for P(VdF-HFP) based gel polymer electrolytes suggest that the transport of charge in these electrolyte

systems is predominantly ionic accompanied by mass transport and electronic contribution to the total current which is negligible.

4.1.4 Thermal Analysis

The TG profiles of bare PMMA, bare P(VdF-HFP), $LiClO_4$, PMMA and P(VdF-HFP) based gel polymer electrolytes are presented in Fig. 4.7(a and b). The influence of salt and plasticizer on the thermal behaviour was studied by comparing the degradation stability of the synthesized PMMA and P(VdF-HFP) polymers. It can be seen from the Fig. 4.7(a) that the bare PMMA is stable up to 240 ºC whereas in case of PMMA based gel polymer electrolyte, it is observed that there is a nominal weight loss of about 8-10% over the temperature range of 100 ºC to 110 ºC which is attributed to the removal of moisture and the major weight loss appears over two temperature ranges of (i) 220 ºC to 330 ºC and (ii) 330 ºC to 485 ºC.

Fig. 4.7(b) shows that there is no weight loss up to 437 ºC in bare P(VdF-HFP) but P(VdF-HFP) based gel polymer electrolytes show initial weight loss of about 10-12% over the temperature range of 100 ºC to 110 ºC which is attributed to the removal of moisture and weight loss appears in three stages (i) 268 ºC to 321 ºC, (ii) 321 ºC to 477 ºC and (iii) 477 ºC to 624 ºC. Therefore, the PMMA based and P(VdF-HFP) based gel polymer electrolytes are thermally stable up to 220 ºC and 268 ºC respectively.

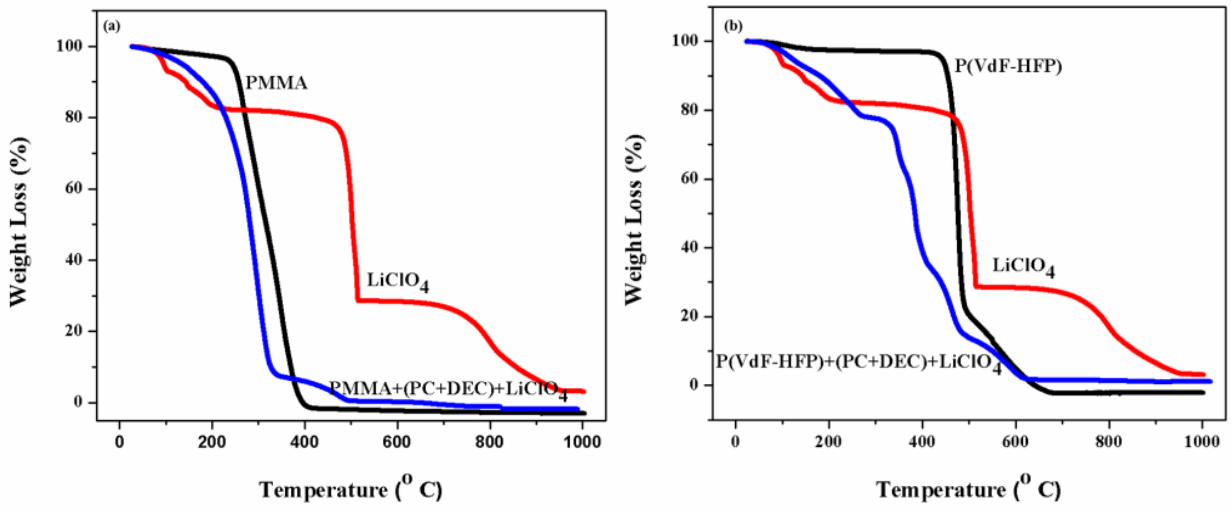

Fig. 4.7: TG traces of (a) PMMA, $LiClO_4$ and PMMA based gel polymer electrolyte and (b) P(VdF-HFP), $LiClO_4$ and P(VdF-HFP) based gel polymer electrolyte.

4.1.5 Mechanical Analysis

Fig. 4.8 shows the stress-strain plots of PMMA and P(VdF-HFP) based gel polymer electrolytes. The films were cast in a rectangular mould of length = 60 mm and width = 20 mm for mechanical testing. The samples after casting were come out to be of thickness of about 0.12-0.19 mm. The tensile strength of samples in both the systems were determined from the stress-strain plots and the values are estimated as 13.4 MPa for PMMA based gel polymer electrolytes and 23.7 MPa for P(VdF-HFP) based gel polymer electrolytes respectively. The area under the stress-strain curve revealing the toughness of 1.032 Jcm^{-3} and 1.424 Jcm^{-3} respectively for PMMA based gel polymer electrolytes and P(VdF-HFP) based gel polymer electrolytes. The elongations at break are 133% and 159% for PMMA based gel polymer electrolytes and P(VdF-HFP) based gel polymer electrolytes systems.

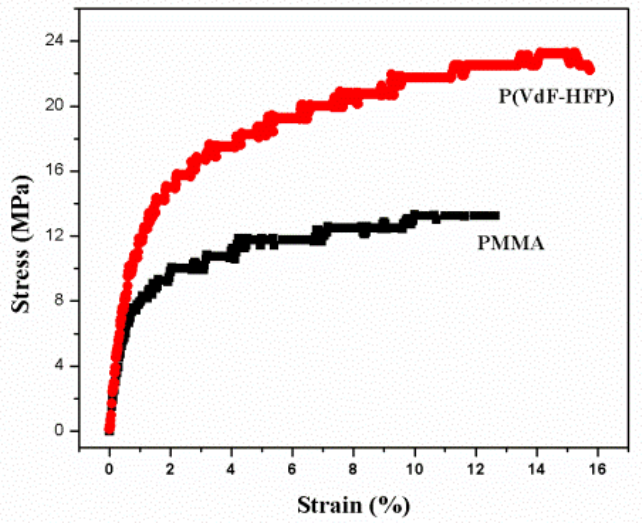

Fig. 4.8: Stress-strain plots of PMMA and P(VdF-HFP) based gel polymer electrolytes.

4.1.6 Electrochemical Analysis

LSV measurements conducted on the Li/GPE/Li cell configuration for the determination of the electrochemical stability window of the electrolytes are presented in Fig. 4.9. The measurements were carried out in the voltage window of 2-6 V at a scan rate of $0.1mVs^{-1}$. The onset of the current identifies the anodic decomposition voltage of the electrolytes. It is observed from the Fig. 4.9(a) that for PMMA based gel polymer electrolyte, the decomposition starts at about 4.2 V. Similarly for P(VdF-HFP) based gel polymer electrolyte the decomposition voltage commences at about 4.5 V as shown in Fig. 4.9(b). Therefore, P(VdF-HFP) based gel polymer electrolyte shows

more stability factor as compared to PMMA based gel polymer electrolyte. It is well known that the anodic stability window is limited by irreversible oxidation of the salt anion (Parka et al, 2003). The Lewis-acid sites on the anionic surface that interact with ClO_4^- (Lewis- base), thereby enhancing the electrochemical potential window by retarding decomposition of the lithium salt anion. This electrochemical potential window (working voltage range) appears to be sufficient for the application of polymer electrolytes as a solid-state electrolyte/separator in Li-ion batteries.

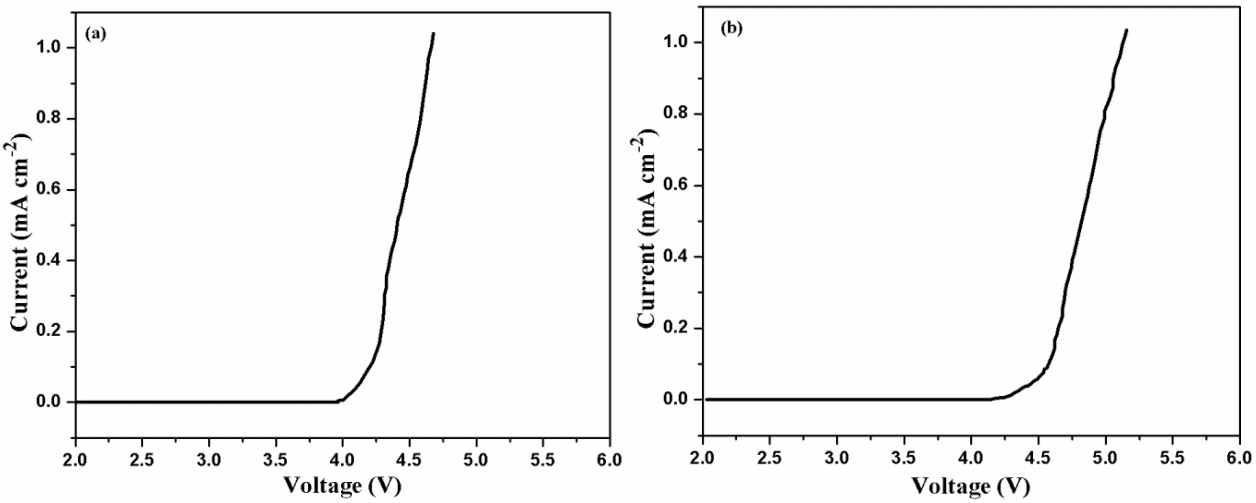

Fig. 4.9: LSV curve of (a) PMMA and (b) P(VdF-HFP) based gel polymer electrolytes.

4.2 Discussion

Formation and breaking of ion-pairs give rise to free ions in the gel polymer electrolyte. Maximum ionic conductivities of PMMA and P(VdF-HFP) based gel polymer electrolytes at ambient temperature are found as 0.13×10^{-4} Scm^{-1} and 1.76×10^{-4} Scm^{-1} respectively. Higher ionic conductivity in P(VdF-HFP) based gel polymer electrolyte in comparison to PMMA based electrolyte could be attributed to higher amorphicity of the former electrolyte system due to steric hindrance by bulky pendant $–CF_3$ group in HFP unit of the copolymer. Higher amorphicity provides higher flexibility to the polymer chains and larger free volume for the mobile ions giving rise to higher conductivity. This result is confirmed by XRD analysis which reveals that degree of crystallinity is reduced from 31.8% in PMMA to 30.2% in PMMA based gel polymer electrolyte system and 26.6% in P(VdF-HFP) to 22.4% in P(VdF-HFP) based gel polymer electrolyte system. Also the transference number was found to be higher for P(VdF-HFP) based electrolytes than that of PMMA based electrolytes. The motion of ions in the gel polymer electrolyte occur in liquid like manner in which the movement of ions through the polymer matrix is assisted by the large

amplitude segmental motion of the polymer backbone as indicated by FTIR analysis which suggests polymer-salt interaction for both PMMA and P(VdF-HFP) based gel polymer electrolyte. FESEM and TEM results are consistent with the view that higher conductivity and ionic transport number in P(VdF-HFP) based gel polymer electrolytes arise from the increased amorphicity and higher solvent retention ability than PMMA based gel polymer electrolytes. The tensile strength of both PMMA and P(VdF-HFP) based gel polymer electrolyte are 13.4 MPa and 23.7 MPa respectively, which is calculated from the stress-strain curves. Also good thermal stability of these polymer electrolyte systems up to 220 ºC in PMMA based electrolytes whereas at 268 ºC in P(VdF-HFP) based electrolyte was confirmed by TG analysis. The anodic decomposition voltage commences at about 4.1 V of PMMA based gel polymer electrolyte but for P(VdF-HFP) based gel polymer electrolyte, the decomposition voltage commences at about 4.5 V.

Chapter 5

Results and Discussion: Nanocomposite Gel Polymer Electrolyte Systems

Chapter 5

Results and Discussion: Nanocomposite Gel Polymer Electrolyte Systems

NCGPEs are prepared with polymer, plasticizer, dissolved salt along with inorganic or organic nano-sized fillers dispersed. This has been the subject of great deal of research in the last decade because of their potential importance in the development of solid state batteries as discussed in previous Chapter 2. It is widely reorganized that the ionic conductivity of gel polymer electrolytes can be considerably enhanced by the introduction of nanofillers which inhibit crystallinity and improves both mechanical and thermal stability of the polymer electrolytes (Croce et al, 1998; Best et al, 1999). The ceramic nanofillers of nanocomposite polymer electrolytes can be classified into two categories such as active and passive. The active components for example are Li_3N and $LiAlO_2$ participate in the conduction process because of the presence of the lithium ion. The passive components comprise of materials such as SiO_2, Al_2O_3 etc. donot have lithium ions so they participate passively in the ion transport process (Khan et al, 1994; Walls et al, 2000).

The enhancement in conductivity is attributed to the disorder caused by the interactions between Lewis-acid sites on the surface of nanofiller and the base species (polymer chain and anion groups) present in the system which leads to a weaker interaction between polymer and Li^+ ions (Forsyth et al, 2002; Weiczorek et al, 1998). Despite all research efforts to investigate the influence of nanofillers on the Li^+ ion conductivity, a few investigations are reported about the interaction of the inorganic fillers with the ions and polymer. The enhancement in conductivity of nanocomposite polymer electrolytes depends upon many factors such as the type of polymer-ceramic system, nanofiller size, annealing parameters (or thermal history), nanofiller concentration and temperature (Kumar et al, 2001).

In this chapter, the following eight types of polymer electrolyte systems have been investigated:

(i) PMMA-(PC+DEC)-$LiClO_4$-MWCNT.

(ii) PMMA-(PC+DEC)-$LiClO_4$-CNF.

(iii) PMMA-(PC+DEC)-$LiClO_4$-SiO_2 nanofiber.

(iv) PMMA-(PC+DEC)-$LiClO_4$-TiO_2 nanofiber.

(v) P(VdF-HFP)-(PC+DEC)-$LiClO_4$-MWCNT.

(vi) P(VdF-HFP)-(PC+DEC)-$LiClO_4$-CNF.

(vii) P(VdF-HFP)-(PC+DEC)-$LiClO_4$-SiO_2 nanofiber.

(viii) P(VdF-HFP)-(PC+DEC)-$LiClO_4$-TiO_2 nanofiber.

In the first four systems, PMMA is blended with four different types of nanofillers and in the remaining four systems, P(VdF-HFP) is used as polymer matrix which is blended with the same nanofillers used in PMMA based electrolytes system. Polymer blends often exhibit properties that are superior compared to the properties of the individual (Rhoo et al, 1997; Tang et al, 2000). The main advantage of the blend systems are simplicity in preparation and ease of control of physical properties by compositional change (Acosta et al, 1996; Rocco et al, 2001). In miscible polymeric blends, there are often specific interactions between groups or polymer segments that lead to a decrease in the Gibbs energy of mixing (Neiro et al, 2000). NCGPEs of various compositions have been prepared by the solution casting technique as described in Chapter 3 (section 3.2). The ionic conductivity of all the samples at different temperatures was obtained by the complex impedance analysis. The nanocomposite gel polymer samples have been investigated by FESEM for microstructural analysis and by XRD and TGA respectively for the determination of crystallinity and thermal stability. FTIR study has also been carried out to investigate the polymer-ion-filler interactions.

5.1 PMMA-(PC+DEC)-$LiClO_4$-MWCNT and PMMA-(PC+DEC)-$LiClO_4$-CNF Systems

An attempt has been made in which the three layered NCGPEs have been prepared using MWCNT (having outer diameter of 10-20 nm and length of 10-30 μm) and CNF (having outer diameter of 200-600 nm and length of 5-50 μm) as dispersoid in the middle layer of the composite with an objective to improve the mechanical strength and thermal stability of the polymer electrolyte. The purpose of constructing the film in three layers is to ensure the avoidance of any possible short circuiting between the electrodes owing to the fact that MWCNT and CNF are electrically conducting.

Various amounts of MWCNT and CNF (0.5, 1.0, 1.5, 2.0 and 2.5 wt.%) were added into the THF solvent and the mixture was ultrasonicated for about 30 minutes to prepare a slurry as discussed in Chapter 3. The NCGPE films of system-I containing 0.5, 1.0, 1.5, 2.0 and 2.5 wt.% MWCNT are

designated as P0.5, P1.0, P1.5, P2.0 and P2.5 respectively and the following codes PC0.5, PC1.0, PC1.5, PC2.0 and PC2.5 were assigned to the NCGPE films containing 0.5, 1.0, 1.5, 2.0 and 2.5 wt.% CNF of system-II respectively. P0 is the film without nanofiller. The composition of polymer base prepared is 0.60PMMA-0.30(PC+DEC)-0.10$LiClO_4$, in which MWCNT and CNF were dispersed separately. Mechanically stable free standing polymer electrolytes were obtained after the solvent evaporation of the as cast films. The three layered nanocomposites were prepared in the form of film with thickness varying between 0.27-0.35 mm.

5.1.1 Morphology and Structure of Nanocomposite Gel Polymer Electrolytes

Microstructural observation on the NCGPE films was made by FESEM. The micrographs are shown in Fig. 5.1. The Fig. 5.1(a) presents the micrographs showing the planar view of the film and Fig. 5.1(b, c and d) show the cross section of the film at different magnifications.

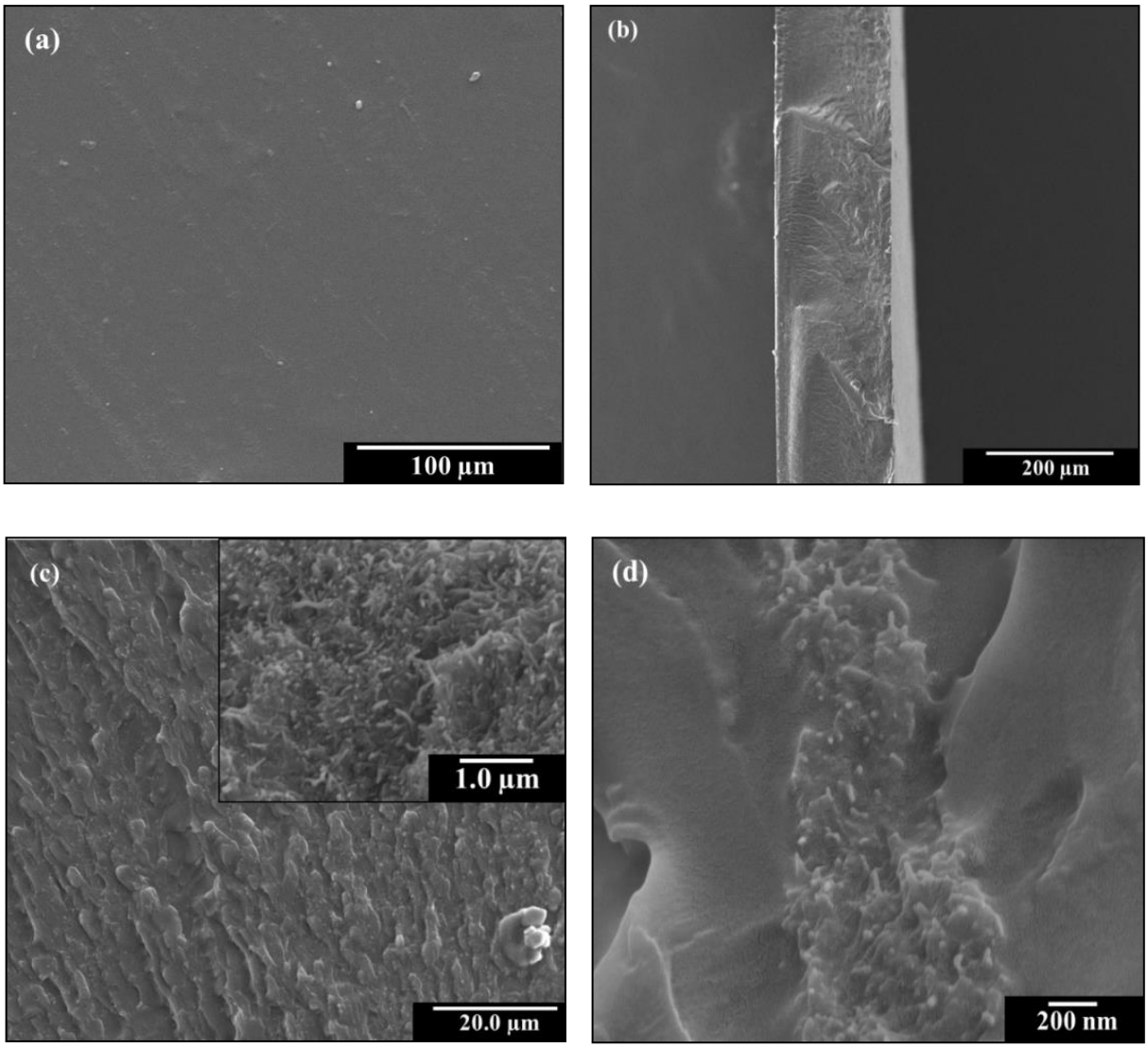

Fig. 5.1: Typical FESEM micrographs of (a) surface of the NCGPE film P2.0; (b), (c) and (d) cross sections of the NCGPE film P2.0 at different magnifications.

The polymer electrolyte investigated in the present study is in the form of three layered polymer electrolyte in which the central layer is dispersed with MWCNT. A cross sectional view of the three layered nanocomposite electrolyte was made by the microstructural observation and the micrograph in Fig. 5.1(b) shows the interface between the layers is perfect. In order to assess the degree of distribution of the dispersoid in the central layer, the microscopic observation was made on a separately prepared layer same as the central layer of the nanocomposite and the micrograph is shown in Fig. 5.1(c). It can be seen from that the micrograph that the distribution of MWCNT in the polymer matrix is nearly uniform. Microstructure of the cross section was observed at higher

magnification to observe the MWCNT matrix interface inside the central layer as shown in Fig. 5.1(d). Dispersion behaviour was further explained with the FTIR studies reported in next section.

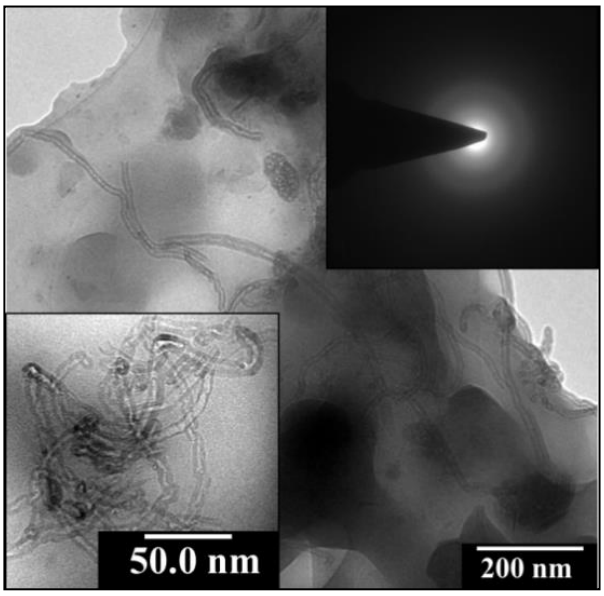

Fig. 5.2: Typical TEM micrograph of NCGPE film P2.0. Inset (above) showing SAD pattern of the film P2.0 and (below) showing the TEM images of the individual MWCNT.

The morphology of the sample P2.0, and the interface between the MWCNT and the polymer matrix have been examined under TEM. Fig. 5.2 shows that MWCNT used as dispersoid having average diameter of about 20 nm. Further it may be observed from the micrograph that the MWCNT are well separated in the polymer matrix. The diffused rings of SAD pattern of MWCNT dispersed polymer electrolyte is an indication of dominating amorphous nature of the polymer material of the composites.

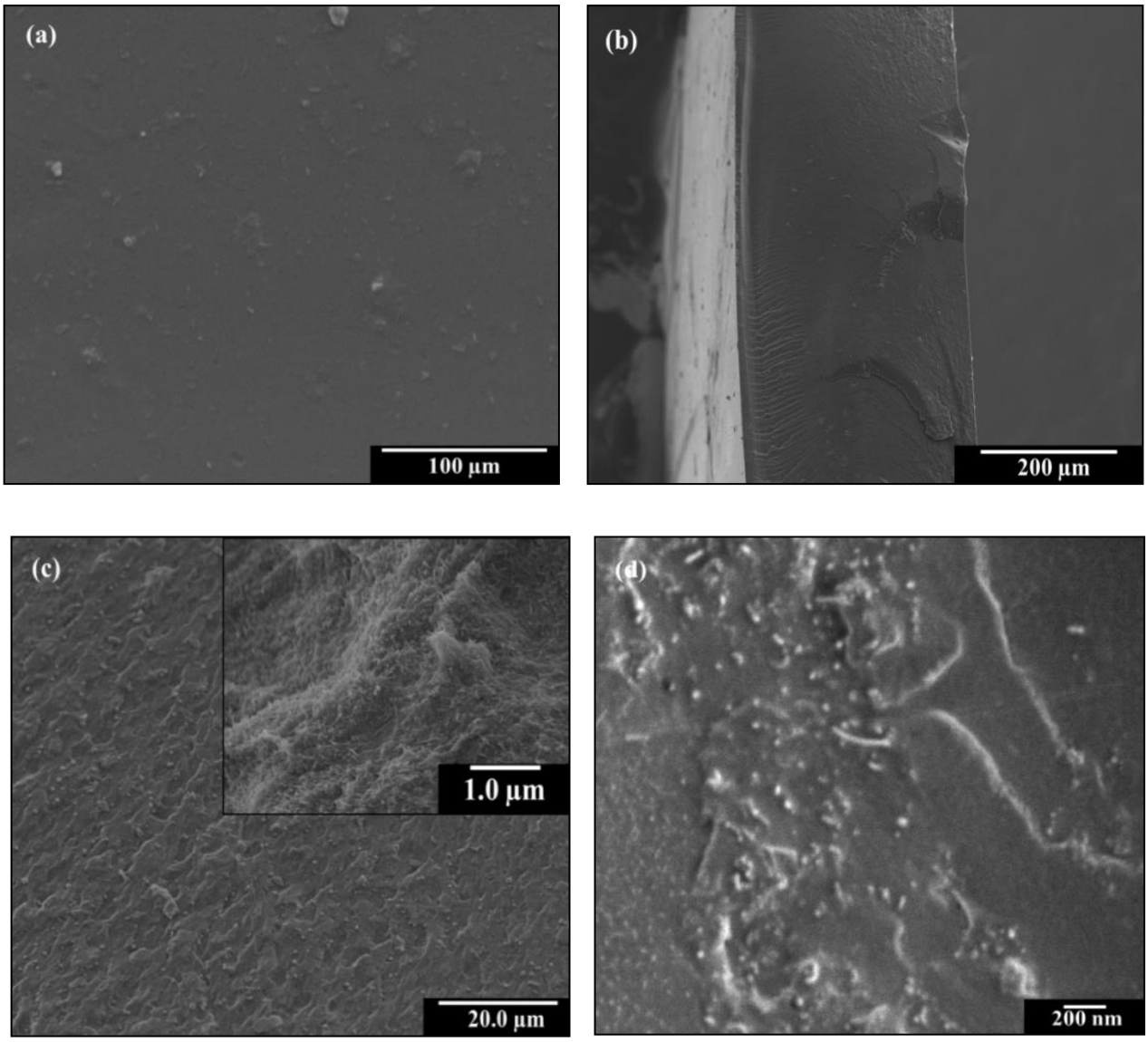

Fig. 5.3: Typical FESEM micrographs of (a) surface of the NCGPE film PC2.0; (b), (c) and (d) cross sections of the NCGPE film PC2.0 at different magnifications.

The micrograph in Fig.5.3(a) shows planar surface of the NCGPEs dispersed with 2.0 wt.% CNF. The cross sectional view of the film shows that degree of dispersion of CNF in the polymer matrix depends upon wettability of nanofiller surface by polymer (Tran et al, 2008; Sengupta et al, 2011). The fact that an adequate amount of surface area of CNF is covered with polymer shows that the wettability of the nanofiller used with polymer compound is good. Aspect ratio and surface roughness are the other important parameters for strong interfacial interaction (Ramanathan et al,

2007). Microstructure of the cross section was observed at higher magnification to observe the interface between CNF and the polymer matrix within the NCGPE tri-layered film.

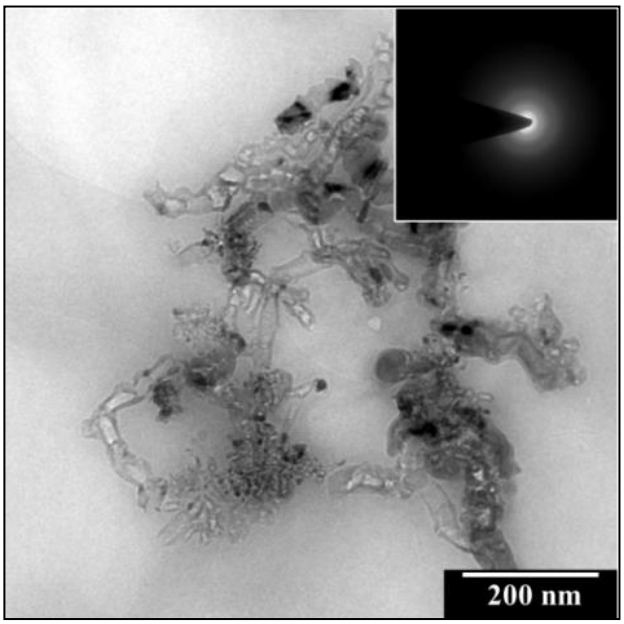

Fig. 5.4: Typical TEM micrograph of NCGPE film PC2.0 and inset showing SAD pattern of the NCGPEs film PC2.0.

The morphology of the sample PC2.0 in Fig. 5.4 shows that CNF are homogeneously dispersed in the polymer matrix with an average diameter of 50-70 nm and the diffused rings of the SAD pattern (inset) is the indication of dominating amorphous region of the polymer electrolyte dispersed with 2.0 wt.% CNF.

The XRD analysis is used to determine the structure and crystallization of polymer electrolytes. Fig. 5.5 shows the XRD patterns of PMMA, $LiClO_4$, MWCNT and CNF. XRD pattern of PMMA matrix shows broad peaks centred around $2\theta = 15^o$, 29.9^o and 41.2^o indicating the polymer PMMA is amorphous. The sharp peaks of the salt $LiClO_4$ in the XRD pattern indicate the salt is crystalline. The XRD pattern of MWCNT and CNF shows sharp (002) diffraction peak at about $2\theta = 26^o$ and one more diffraction peak (101) at $2\theta = 44^o$. The peaks of MWCNT have resulted from the ordered arrangement of the concentric cylinders of graphitic layers (Fang et al, 2005).

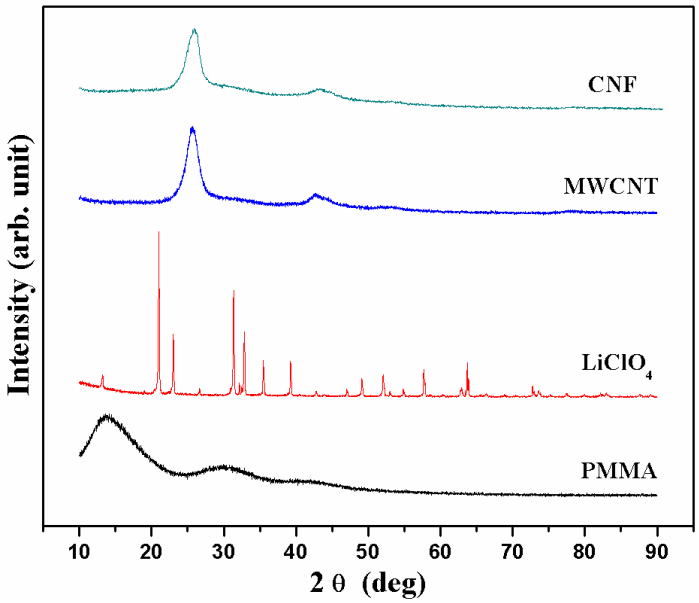

Fig. 5.5: XRD patterns of (a) PMMA, $LiClO_4$ MWCNT and CNF.

On addition of solvent into polymer, resulting in gel polymer electrolyte P0, the diffraction peaks of PMMA broaden further as observed in the XRD pattern shown in Fig. 5.6(a) and this implies that PMMA has large amorphous region. The absence of XRD peaks of the salt indicates its dissociation in the polymer matrix and the complexation of the dissociated ions with polymer molecules. Addition of MWCNT in PMMA based gel polymer electrolytes does not alter the total number of peaks but the first broad peak further broadens and shifts gradually (though marginally) towards the higher diffraction angle for all the nanocomposite samples. Thus, the proportion of amorphous region in the nanocomposite increases as compared to the polymer based matrix without dispersion as well as with the increase in MWCNT (Fang et al, 2005). The absence of characteristic peaks of MWCNT in XRD patterns of P0.5, P1.0, P1.5, P2.0 and P2.5 of system-I may be because of the proportion of the nanotube in the nanocomposites is negligibly small in order to give rise to detectable diffraction peaks. The XRD patterns of nanocomposite films PC0.5, PC1.0, PC1.5, PC2.0 and PC2.5 of system-II in Fig. 5.6(b) shows that the peaks have broadened in relation to those of bare PMMA. Moreover the XRD peaks of the nanocomposites are found shifted towards the higher angles of $2\theta = 17^{o}$, 30.2^{o} and 42.2^{o} as compared to the corresponding peaks of film P0.

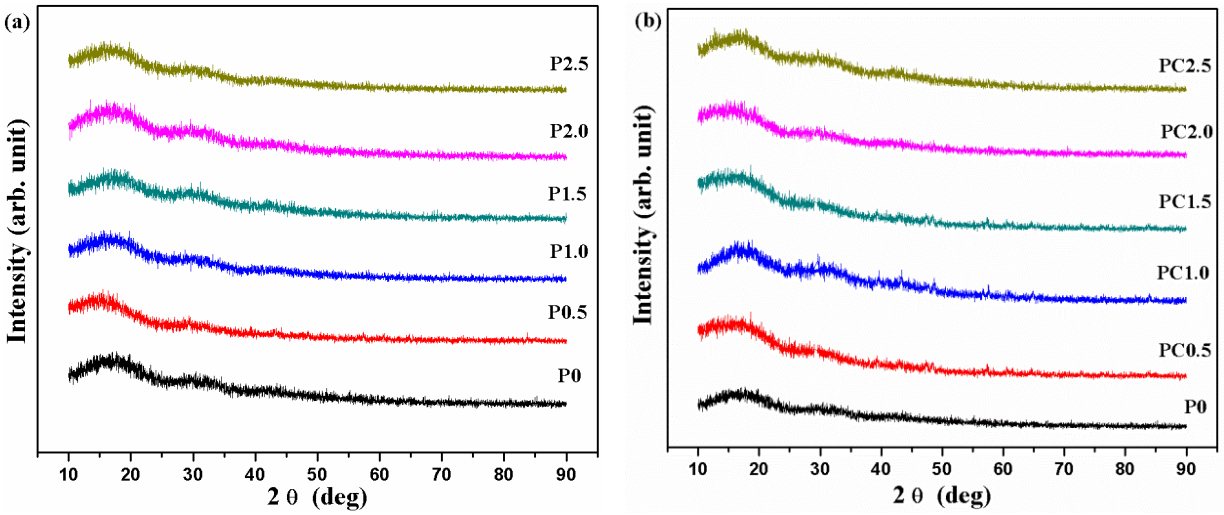

Fig. 5.6: XRD patterns of films (a) P0, P0.5, P1.0, P1.5, P2.0 and P2.5 of system-I; (b) P0, PC0.5, PC1.0, PC1.5, PC2.0 and PC2.5 of system-II.

The degree of crystallinity (K) of the polymer electrolyte is estimated using the following relation, $\{K = (A/A_0) \times 100\}$ mentioned in Chapter 3 (subsection 3.2.1). Table 5.1 shows the estimated value of degree of crystallinity for all the films of system-I and system-II.

Table-5.1: Estimated value of degree of crystallinity for all the films of system-I and system-II.

Sl. No.	Sample Name	Degree of Crystallinity of system-I	Sample Name	Degree of Crystallinity of system-II
1.	P0	26.6%	P0	26.6%
2.	P0.5	24.8%	PC0.5	24.4%
3.	P1.0	22.3%	PC1.0	22.9%
4.	P1.5	19.1%	PC1.5	20.2%
5.	P2.0	17.9%	PC2.0	18.6%
6.	P2.5	19.3%	PC2.5	21.1%

The degree of crystallinity of NCGPE films decreases to a greater extent in the sample P2.0 of system-I and PC2.0 of system-II than that of P0 respectively. The peaks corresponding to $LiClO_4$ are not observed in the electrolytes suggesting that the $LiClO_4$ is perhaps got dissolved in the polymer matrix and is no longer existent as a separate phase so as to give rise to detectable signal. Higher amorphicity in the electrolyte is attributed to the steric hindrance provided by the bulky

pendant $–CH_3COO$ ester group of PMMA upon formation of nanocomposites in PMMA and consequently will give rise to higher ionic conductivity (Stephan et al, 2002).

5.1.2 Fourier Transform Infra-Red Spectroscopy

FTIR investigation has been carried out to understand structural changes taking place due to interaction between constituents of the nanocomposite electrolyte (Pavia, 2001). FTIR spectra of PMMA and the other constituents such as salt $LiClO_4$, MWCNT and CNF are shown in Fig. 5.7. It can be seen that the characteristic absorption peaks for the host polymer PMMA are at (i) 2987 and 2994 cm^{-1} (split peak), corresponding to symmetric and asymmetric vibrations of CH bond due to stretching of CH_3, (ii) 1724 cm^{-1} corresponding to >C=O stretching vibration, (iii) 1436 cm^{-1} corresponding to CH_3 and CH_2 deformation vibrations, (iv) 1261 cm^{-1} corresponding to >C-O-C< symmetric stretching, (v) 979 cm^{-1} corresponding to asymmetric CH_2 transformation, (vi) 727 cm^{-1} corresponding to CH_2 twisting vibration and (vii) 581 cm^{-1} corresponding to CH_2 rocking vibration while $LiClO_4$ has broad peak in between (3600-3400) cm^{-1}, 1627, 1069 and 758 cm^{-1}, corresponding to inter and intra molecular stretching vibration of –OH bond (due to chemisorbed moisture), stretching vibration of pure $LiClO_4$, asymmetric stretching vibration of ClO_4^- ion and symmetric stretching vibration of ClO_4^- ion respectively (Rajendran et al, 2000). The absorption bands of MWCNT appear at 2996, 2819, 2657, 2334, 1774, 1683, 1538, 1406, 1332, 1185, 1053, 787 and 552 cm^{-1} whereas the absorption bands of CNF appear at 3008, 2680, 2332, 2107, 1922, 1738, 1512, 1349, 1225, 713 and 529 cm^{-1} are shown in Fig 5.7.

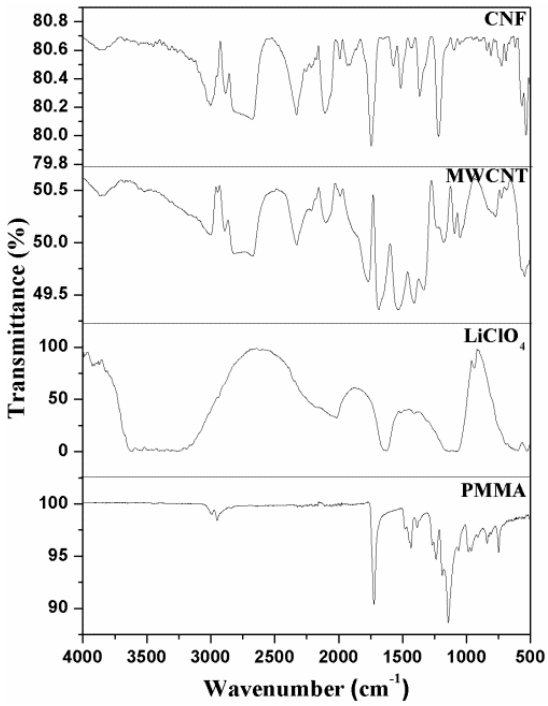

Fig. 5.7: FTIR spectra of (a) PMMA, $LiClO_4$, MWCNT and CNF.

FTIR spectra of films designated as P0, P0.5, P1.0, P1.5, P2.0 and P2.5 are shown in Fig 5.8(a). For the film P0, the absorption peaks appear at 3547, 2994, 2987, 2963, 1717, 1627, 1443, 1268, 1065, 979, 758 and 727 cm^{-1}. The peak in between (3600-3400) cm^{-1} appears to have come from $LiClO_4$ but it has become relatively broader compared to that obtained in the case of pure $LiClO_4$ for which the peak is at 3538 cm^{-1}. However, the peaks corresponding to stretching vibration of CH_3 at 2994 and 2987 cm^{-1} in pure PMMA has an additional peak appearing for the sample P0 at a lower frequency of 2963 cm^{-1}, which is due to vibration of CH_2 bond. The position of the peak of pure $LiClO_4$ at 1627 cm^{-1}, attributed to its stretching vibration remains unchanged in P0 at 1717 cm^{-1} but the ones belonging to PMMA just above and below this peak have moved closer at 1717 cm^{-1} (1724 cm^{-1} in pure PMMA corresponding to >C=O stretching vibration) and at 1443 cm^{-1} (1436 cm^{-1} in pure PMMA corresponding to CH_3 and CH_2 deformation vibration). However, the peak of PMMA at 1261 cm^{-1} corresponding to >C–O–C< symmetric stretching moves to a slightly higher frequency of 1268 cm^{-1} while that at 1069 cm^{-1} in pure $LiClO_4$, corresponding to asymmetric stretching vibration of ClO_4^- ion, has moved slightly lower to 1065 cm^{-1}. The peaks of pure PMMA at 979 cm^{-1} and727 cm^{-1} corresponding to asymmetric CH_2 transformation and CH_2 twisting vibration remain at the same position as found for P0 while that at 581 cm^{-1} corresponding

to CH_2 rocking vibration shifts to 590 cm^{-1}. The peaks at 1627 and 758 cm^{-1} of $LiClO_4$, however, appear at the same wave number in P0 as in pure salt.

The split sharp peaks in pure $LiClO_4$ at 3538 cm^{-1} and 3547 cm^{-1} corresponding respectively to inter and intra molecular stretching vibrations of –OH bond (due to chemisorbed moisture) has merged into a broad single peak at 3547 cm^{-1}. Thus, intermolecular stretching vibration of –OH has disappeared. An additional peak appeared in P0 at 2963 cm^{-1}, which is due to vibration of CH_2 bond. It could be due to change in local environment due to the presence ionic species from $LiClO_4$, which also has contributed to the shift in peaks due to local ionic fields. Since all the peaks corresponding to vibrations of $LiClO_4$ and ClO_4^- have been detected there is no doubt that these species are intact and distributed in the structure of PMMA in locations affecting the vibrations due to >C=O stretching, CH_3 and CH_2 deformations, >C-O-C< symmetric stretching.

With the addition of MWCNT to PMMA, the C=O stretching band width broadens and the interface gets modified and the peak shifts to higher wave number 1719 cm^{-1} for the nanocomposite films P0.5, P1.0, P1.5,P2.0 and P2.5 indicating the increase in bond strength of carbonyl group (C=O) due to the dispersion of MWCNT. This indicates that there is an interaction between the carbonyl group of PMMA ester and O–H bond via a coordinate bond leading to the complexation formation. The bands appear at 2996, 2334, 1185, 1531 and 552 cm^{-1} correspond to –OH stretching, CH_3 stretching, >C–O–C< symmetric stretching, $–OCH_3$ asymmetric bending, and CH_2 twisting of PMMA, respectively. The peak at 2996 cm^{-1} of –OH stretching gets shifted to 3439 cm^{-1} indicating a weak interaction between various constituents of polymer electrolytes. Also the >C-O-C< symmetric stretch bands of PMMA at 1266 cm^{-1} are shifted to 1268 cm^{-1} wave number in the polymer complexes. The other bands of PMMA based polymer electrolytes appeared at the same wavenumber after adding MWCNT in them, indicating the coordination to the tubes did not occur.

With the addition of CNF to PMMA as shown in Fig 5.8(b), the pattern of FTIR with dispersion of CNF in PMMA based electrolytes is quite similar to system-I. The C=O stretching band broadens and the interface between the PMMA and CNF gets modified resulting in the peak shift to higher wave number of 1718 cm^{-1} for all the films as discussed in system-I.

The bands appear at 3570, 2934, 1627, 1081and 603 cm^{-1} correspond to C–H stretching, CH_3 stretching, >C–O–C< symmetric stretching, $–OCH_3$ asymmetric bending, and CH_2 twisting of PMMA, respectively. Also the >C–O–C< stretching vibration band of PMMA at 1124 cm^{-1} is shifted to 1170 cm^{-1} wave number for all the films P0, P0.5, P1.0, P1.5, P2.0 and P2.5 as shown in Fig. 5.8(a). The wave number of the other bands of nanocomposite films on the addition of CNF remains unchanged indicating the complexation has not occurred. The formation and shifting of new peaks suggest that the polymer-salt-filler interaction has occurred in NCGPEs.

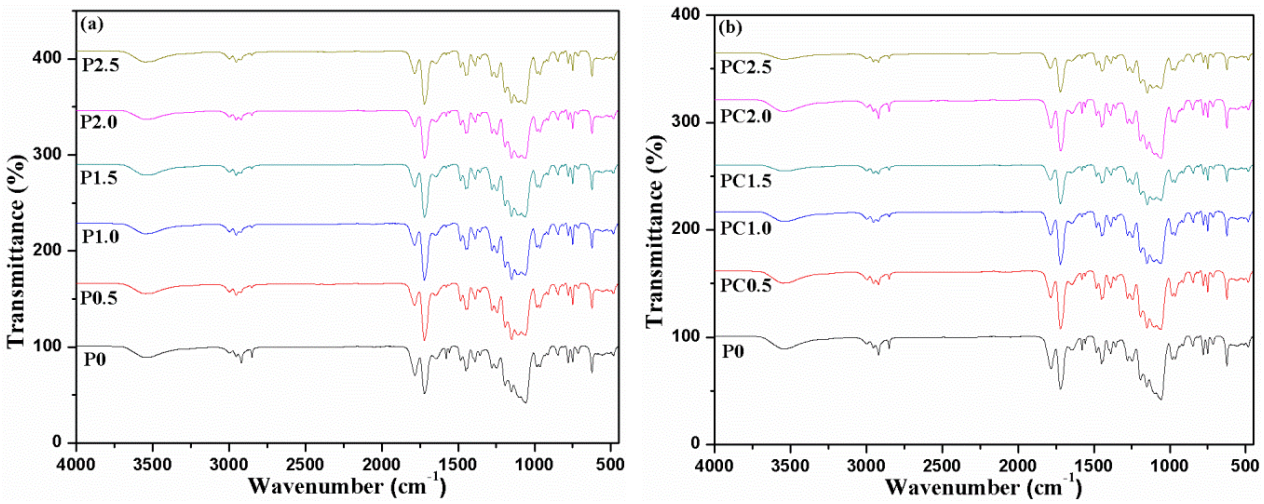

Fig. 5.8: FTIR spectra of films (a) P0, P0.5, P1.0, P1.5, P2.0 and P2.5 of system-I and (b) P0, PC0.5, PC1.0, PC1.5, PC2.0 and PC2.5 of system-II.

5.1.3 Ionic Conductivity Measurement/Electrochemical Impedance Spectroscopy

Impedance spectra of the samples were collected over a frequency range of 42 Hz-1MHz. The bulk electrical resistance (R_b) of the samples is estimated from the intercept of the extrapolated semi-circular impedance plot towards the lower frequency on the real (Z′) axis. The ionic conductivity (σ) of the materials is calculated from the following equation, $\{\sigma = l/(R_b \times A)\}$, where l is the thickness (cm) of the sample and A is the flat surface area (cm^2) of the electrode.

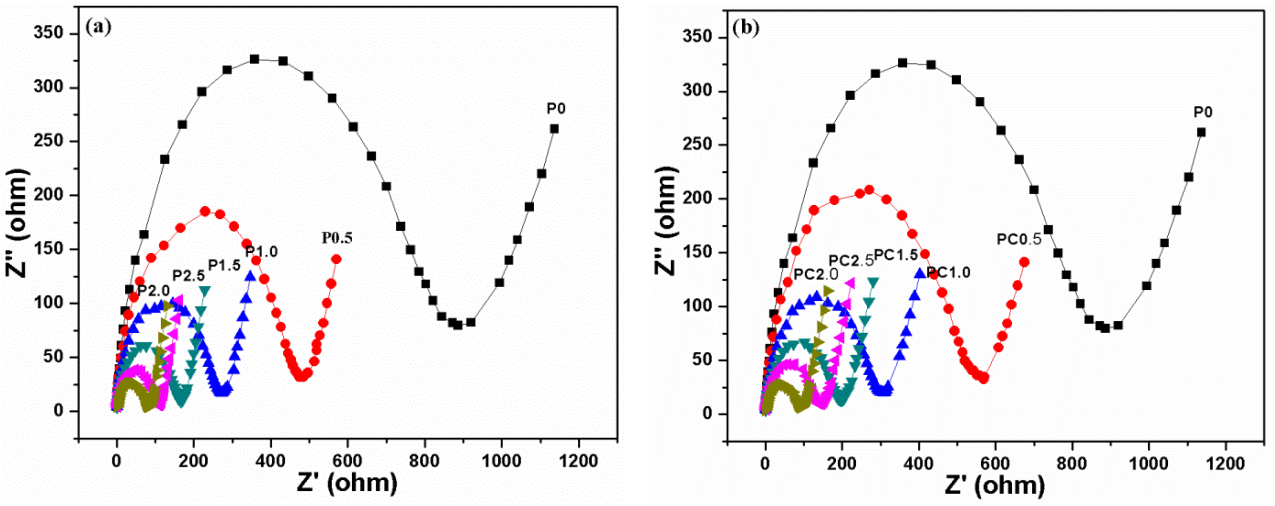

Fig. 5.9: Nyquist plot of films (a) P0, P0.5, P1.0, P1.5, P2.0 and P2.5of system-I and (b) P0, PC0.5, PC1.0, PC1.5, PC2.0 and PC2.5 of system-II.

The complex impedance spectra have two well-defined segments comprising of a semi-circular arc in the high frequency region and an oblique line in the low frequency region. The high frequency semicircle can be ascribed to the bulk resistance of the electrolytes whereas the low frequency oblique line is due to the capacitance of electric double layer formed at the electrode/electrolyte interface. The ionic conductivity enhancement in nanocomposite is attributed to the combined effect of ionic mobility increase owing to increase in segmental mobility of the polymer chains induced by dissociated Li^+ ions in the PMMA. Further, the increase in free volume with the increase in temperature of the electrolyte leads to the increase in ion mobility and segmental mobility (MacDonald, 1987). The calculated value of ionic conductivity of P0 at room temperature is 0.13×10^{-4} Scm^{-1} as shown in Table-5.2. It may be seen that maximum value of ionic conductivity 2.52×10^{-4} Scm^{-1} can be achieved with the dispersion of 2.0 wt.% MWCNT of system-I as shown in Fig. 5.9(a) and 2.18×10^{-4} Scm^{-1} for film PC2.0 at room temperature of system-II as shown in Fig. 5.9(b) and the conductivity increases to 2.74×10^{-3} Scm^{-1} at 70 ^oC.

Table-5.2: Estimated value of conductivity for all the films of system-I and system-II.

Sl. No.	Sample Name	Conductivity (Scm^{-1}) of system-I	Sample Name	Conductivity (Scm^{-1}) of system-II
1.	P0	0.13×10^{-4}	P0	0.13×10^{-4}
2.	P0.5	1.02×10^{-4}	PC0.5	0.76×10^{-4}
3.	P1.0	1.64×10^{-4}	PC1.0	1.42×10^{-4}
4.	P1.5	2.18×10^{-4}	PC1.5	1.76×10^{-4}
5.	P2.0	2.52×10^{-4}	PC2.0	2.18×10^{-4}
6.	P2.5	2.21×10^{-4}	PC2.5	1.73×10^{-4}

The variation in conductivity as a function of nanofiller content of NCGPEs in the system-I and II at ambient temperature which has been considered up to 2.5 wt.% with an interval of 0.5 wt.% as shown in Fig. 5.10(a and b). It is observed that conductivity increases with the increase in nanofiller content up to 2.0 wt.% and thereafter the conductivity decreases. However, the nanocomposite electrolytes become fragile and brittle with higher nanofiller content i.e. more than 2.0 wt.% in both the systems of I and II.

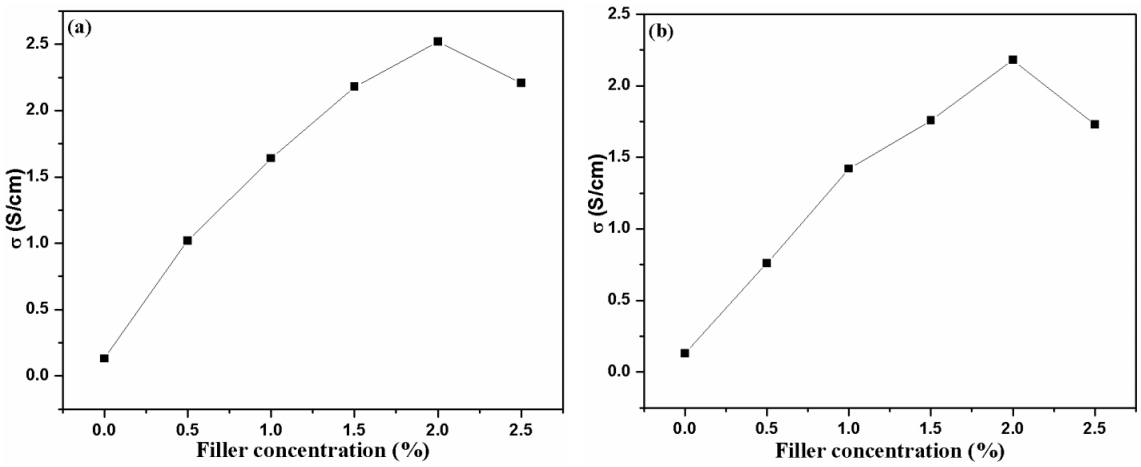

Fig. 5.10: Conductivity (Scm^{-1}) versus filler concentration (wt.%) of (a) system-I and (b) system-II.

As polymer electrolytes are widely disorganized heterogeneous systems and the temperature dependence ionic conductivity (σ) was determined from impedance spectra of the films which are measured at five different temperature between 25 ºC (room temperature) and 70 ºC. Fig. 5.11(a and b) show that the ionic conduction in NCGPEs obeys the following Arrhenius relation:

{$\sigma = \sigma_0 \exp(-E_a/kT)$}, where σ is the ionic conductivity, σ_0 is the pre exponential factor, E_a is the activation energy, k is the Boltzmann constant and T is the absolute temperature at which the measurement was made, respectively. The addition of plasticizer (PC+DEC) into the system causes viscosity reduction and facilitates the dissociation of salt into ions, thereby increasing the ionic conductivity. The addition of nanofiller increases the conductivity by creating more amorphous path (inhibiting crystallization) of the PMMA chains and providing a Li^+ conducting pathway at the dispersoid-matrix interface. The migration of lithium ion mainly depends on the segmental motion of the polymer chain in the amorphous region. The decrease in segmental mobility arises from virtual cross-linking and has an obvious signature in the enhancement of glass transition temperature (Johan et al, 2010).

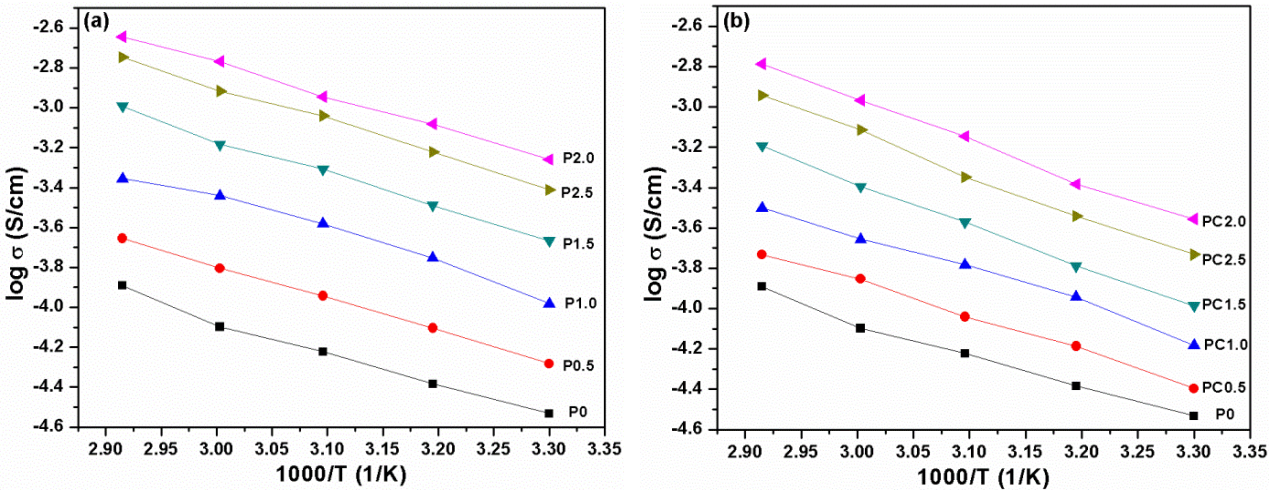

Fig. 5.11: Temperature dependent ionic conductivity plots of (a) system-I and (b) system-II.

Generally, in polymer electrolytes, cationic transport number is smaller than anionic transport number because anionic species are more coupled to the polymeric structure than the cationic species. The motion of large anionic species and vibrational frequencies of polymer chains are expected to be more in phase than those of cationic species. As a result, when materials with high anionic transport number are used in battery then extensive concentration gradients are set up during use affects its electrical performance. Total ionic transference number was measured by Wagner's polarization technique (Wagner et al, 1957; Chandra, 1981) as described in Chapter 3. Wagner polarization cell was prepared by coating silver (Ag) paste as blocking electrodes on both the sides of sample (Ag/electrolyte/Ag). Table-5.3 shows the ionic transference number of both the systems of I and II.

Table-5.3: Ionic transference number for all the films of systems-I and system-II.

Sl. No.	Sample Name	Transference Number of System-I	Sample Name	Transference Number of System-II
1.	P0	0.91	P0	0.91
2.	P0.5	0.93	PC0.5	0.92
3.	P1.0	0.93	PC1.0	0.92
4.	P1.5	0.93	PC1.5	0.93
5.	P2.0	0.95	PC2.0	0.93
6.	P2.5	0.92	PC2.5	0.91

High transport number lying in the range of 0.91-0.95 suggests that the charge transport in both the systems of I and II are predominantly ionic accompanied by mass transport and electronic contribution to the total current negligible.

5.1.4 Thermal Analysis

The thermal stability is an important parameter to assess in-situ performance of the electrolyte in lithium ion battery especially when the operating temperature of the battery is increased and the safety is a serious concern. The thermal stability of the films is investigated by TG/DTG analysis. The weight loss of the samples is recorded as a function of increasing temperature.

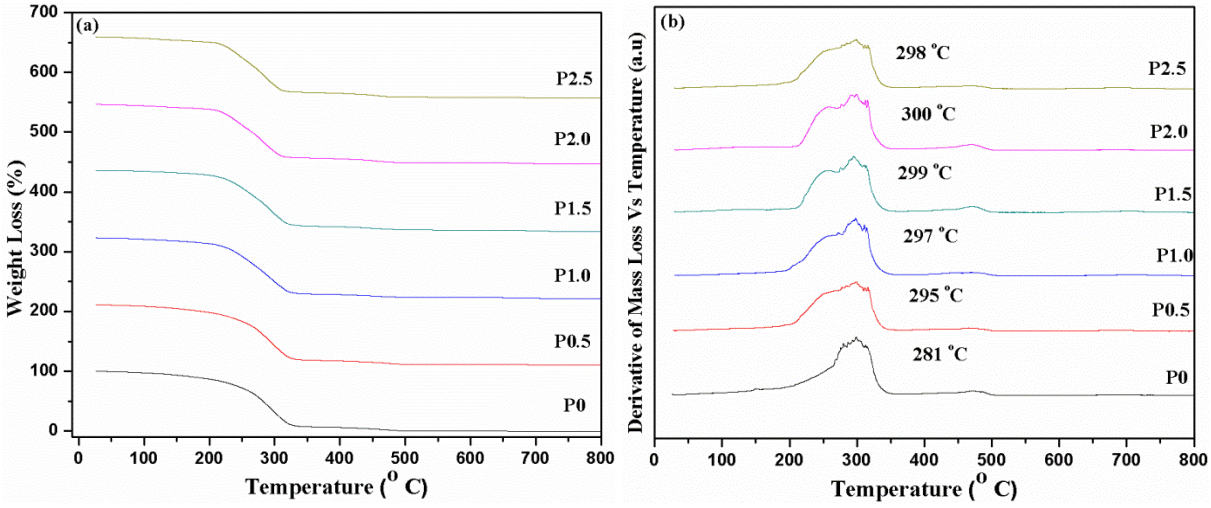

Fig. 5.12: (a) TG traces of films P0, P0.5, P1.0, P1.5, P2.0 and P2.5; (b) DTG of films P0, P0.5, P1.0, P1.5, P2.0 and P2.5 of system-I.

The TG traces of films of system-I are shown in Fig. 5.12(a). The first weight loss at around 100 º-110 ºC in all the films is attributed to the removal of moisture from the sample. The PMMA based gel polymer electrolyte is stable up to 220 ºC. When MWCNT are added to the PMMA based gel polymer electrolyte, the decomposition temperature of gel polymer electrolyte increases from 220 ºC to 230 ºC. The increased thermal stability of NCGPEs as compared to PMMA based gel polymer is perhaps the constraints that are imposed by the MWCNT for the movement of polymer chain segments. The derivative of the mass loss of the films as a function of temperature is presented in Fig. 5.12(b). The broad peak in each plot indicating the maximum change in mass w.r.t temperature corresponds to the thermal stability. There is an increase in decomposition temperature with increase in nanofiller content upto 2.0 wt.% in the PMMA based electrolytes afterwards it decreases. It may be seen that the decomposition temperature varies from 281 ^{o}C for film P0 to 300 ^{o}C for film P2.0. Therefore, the NCGPEs having 2.0 wt.% MWCNT have better thermal stability than that of film without MWCNT.

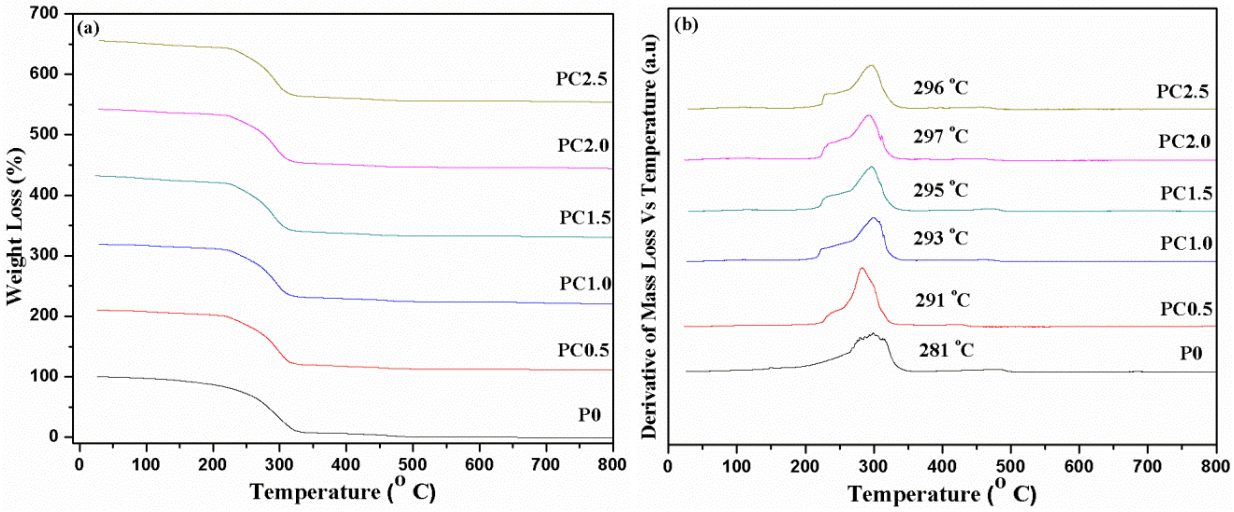

Fig. 5.13: (a) TG traces of films P0, PC0.5, PC1.0, PC1.5, PC2.0 and PC2.5; (b) DTG of films P0, PC0.5, PC1.0, PC1.5, PC2.0 and PC2.5 of system-II.

In system-II, the observed initial weight loss of 2 to 6 wt.%, in the temperature range 50 º-150 ^{o}C for all the films is presumably due to the evaporation of low molecular weight species such as absorbed moisture, unreacted monomer (acrylonitrile), and residual solvent viz. THF used in the electrolyte synthesis. In the temperature range 250 º-500 ºC, the films show three significant weight loss regions as revealed from the respective plots. As film P0 gets reduced at ~ 200 ºC and

for PC2.0, the decomposition occurs at 220 ºC. Therefore, it may be inferred that CNFs dispersion has caused an enhancement in electrolyte decomposition temperature. The weight loss over (~ 220 º-330 ºC) corresponds to the thermal decomposition of ester (CH_3COO) group in the polymer network. A rapid weight loss of 70-80 wt.% takes place over the temperature range of 330 º-470 ºC. Degradation above 470 ºC is most likely due to the advanced fragmentation of the chain segments formed in the different stages of degradation. The decomposition region for all the NCGPE films with the percentage of weight loss is shown in Fig. 5.13(a). It can be inferred that the percentage of weight loss is minimum for PC2.0 showing maximum thermal stability as compared with other films. The derivative of the mass loss as a function of temperature for all the films is presented in Fig. 5.13(b). It may be seen that the decomposition temperature varies from 281 ºC of P0 to 297 ºC of PC2.0. Therefore, the nanocomposite electrolyte PC2.0 has better thermal stability than P0.

5.1.5 Mechanical Analysis

Fig. 5.14(a) shows the stress-strain plots of films P0, P0.5, P1.0, P1.5, P2.0 and P2.5. The tensile strength of film P0 is estimated as 13.4 MPa and 68.4 MPa of film P2.0 which is nearly five times more than that of P0. The higher strength is owing to the reinforcement of MWCNT having large aspect ratio in the matrix. The area under the stress-strain curve per unit volume i.e. toughness of P0 is 1.032 Jcm^{-2} and with the increasing MWCNT content, the energy increases up to 3.402 Jcm^{-2} for film dispersed with 2.0 wt.% MWCNT.

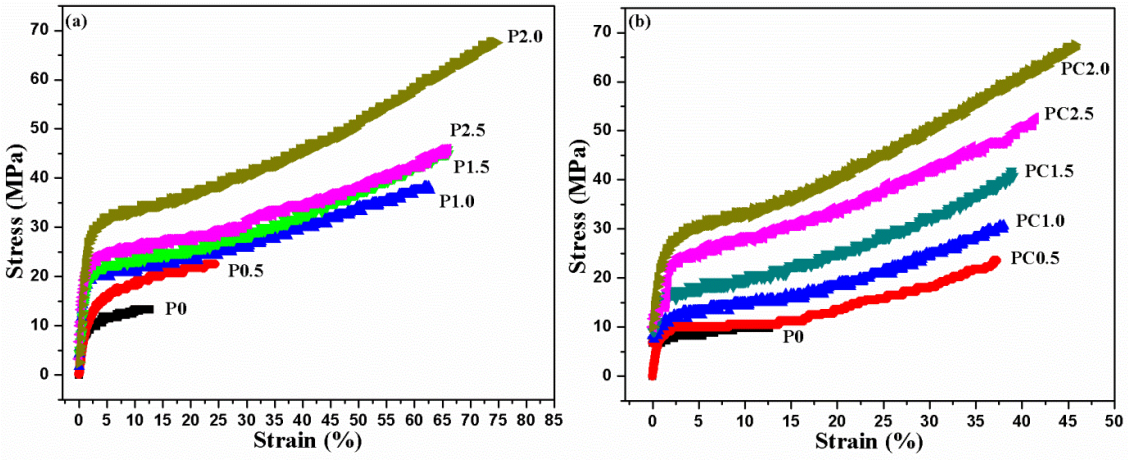

Fig. 5.14: Stress-strain plots of films (a) P0, P0.5, P1.0, P1.5, P2.0 and P2.5 of system-I; (b) P0, PC0.5, PC1.0, PC1.5, PC2.0 and PC2.5 of system-II.

For system-II, the stress-strain curves of films P0, PC0.5, PC1.0, PC1.5, PC2.0 and PC2.5 are shown in Fig. 5.14(b). The film PC2.0 has maximum tensile strength of 66.7 MPa with an elongation-at-break value of 457% which is quiet high. Also, the area per unit volume i.e. toughness of PC2.0 is 3.012 J. The nanofiller wrap well the polymer chains resulting in strong interface between nanofiller and polymer as confirmed by TEM micrograph. The films P2.0 and PC2.0 also have the highest ionic conductivity as confirmed in Table-5.2 which suggests that the dispersion of 2.0 wt.% nanofiller (MWCNT and CNF) in gel polymer electrolytes offers maximum ionic conductivity with good mechanical strength.

5.1.6 Electrochemical Analysis

LSV measurements were carried out using the Li|NCGPE|Li cell configuration over the voltage range of 2-6 V at a scan rate of 0.1mVs^{-1} for determination of the electrochemical stability window of the electrolytes are presented in Fig. 5.15. The onset of the current identifies the anodic decomposition voltage of the electrolytes. It is observed that for P0, the decomposition voltage is 4.1 V. The film PC2.0 gives the decomposition voltage at about 4.3 V. The electrochemical stability is enhanced for film P2.0 which gives good anodic stability above 4.4 V. Thus there is an improvement in the voltage stability factor in the polymer electrolytes containing nanofiller.

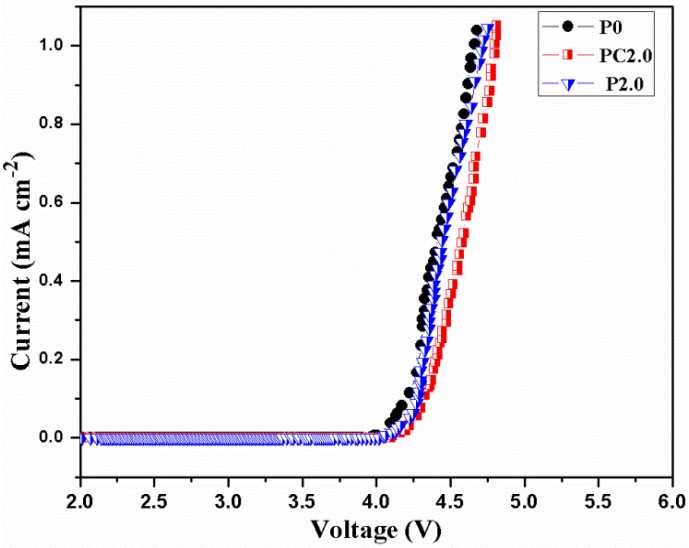

Fig. 5.15: LSV curve of films P0, P2.0 and PC2.0.

5.2 PMMA-(PC+DEC)-$LiClO_4$-SiO_2 nanofiber and PMMA-(PC+DEC)-$LiClO_4$-TiO_2 nanofiber Systems

In this section, an attempt has been made using different type of inorganic nanofibers i.e. SiO_2 nanofiber (having diameter 100-500 nm) and TiO_2 nanofiber (having diameter of 200-700 nm) which are dispersed in PMMA based gel polymer electrolyte. The NCGPE films were identified as PS2.0, PS4.0, PS6.0, PS8.0, PS10.0 and PS12.0 containing 2.0, 4.0, 6.0, 8.0, 10.0 and 12.0 wt.% SiO_2 nanofiber of system-III respectively. For system-IV, NCGPE films containing 2.0, 4.0, 6.0, 8.0 and 10.0 wt.% TiO_2 nanofiber were assigned as PT2.0, PT4.0, PT6.0, PT8.0 and PT10.0 respectively. The reason for dispersing SiO_2 nanofiber up to 12.0 wt.% and TiO_2 nanofiber up to 10.0 wt.% is that they become brittle after 10.0 wt.% and 8.0 wt.%. The physical and electrochemical properties of NCGPEs were investigated using various characterization techniques to examine its suitability for application in Li-ion batteries. The synthesized film thickness varies between 0.15-0.19 mm.

5.2.1 Morphology and Structure of Nanocomposite Gel Polymer Electrolytes

The surface and cross-sectional images of the electrolyte films designated as PS10.0, as observed under field emission scanning electron microscope (FESEM), are shown at different magnifications in Fig. 5.16. The micrograph in Fig. 5.16(a) reveals that the surface of the film is smooth while Fig. 5.16(b) shows the morphology of the TiO_2 nanofiber and the energy dispersive X-ray analysis (EDAX) (inset) confirms the presence of constituent elements in the polymer matrix. It can be observed from the cross-sectional view that the SiO_2 nanofiber are well distributed in the polymer matrix and the dispersion of SiO_2 nanofiber plays an active role in the growth of highly porous microstructures with a completely different morphology as shown in Fig. 5.16(c and d).

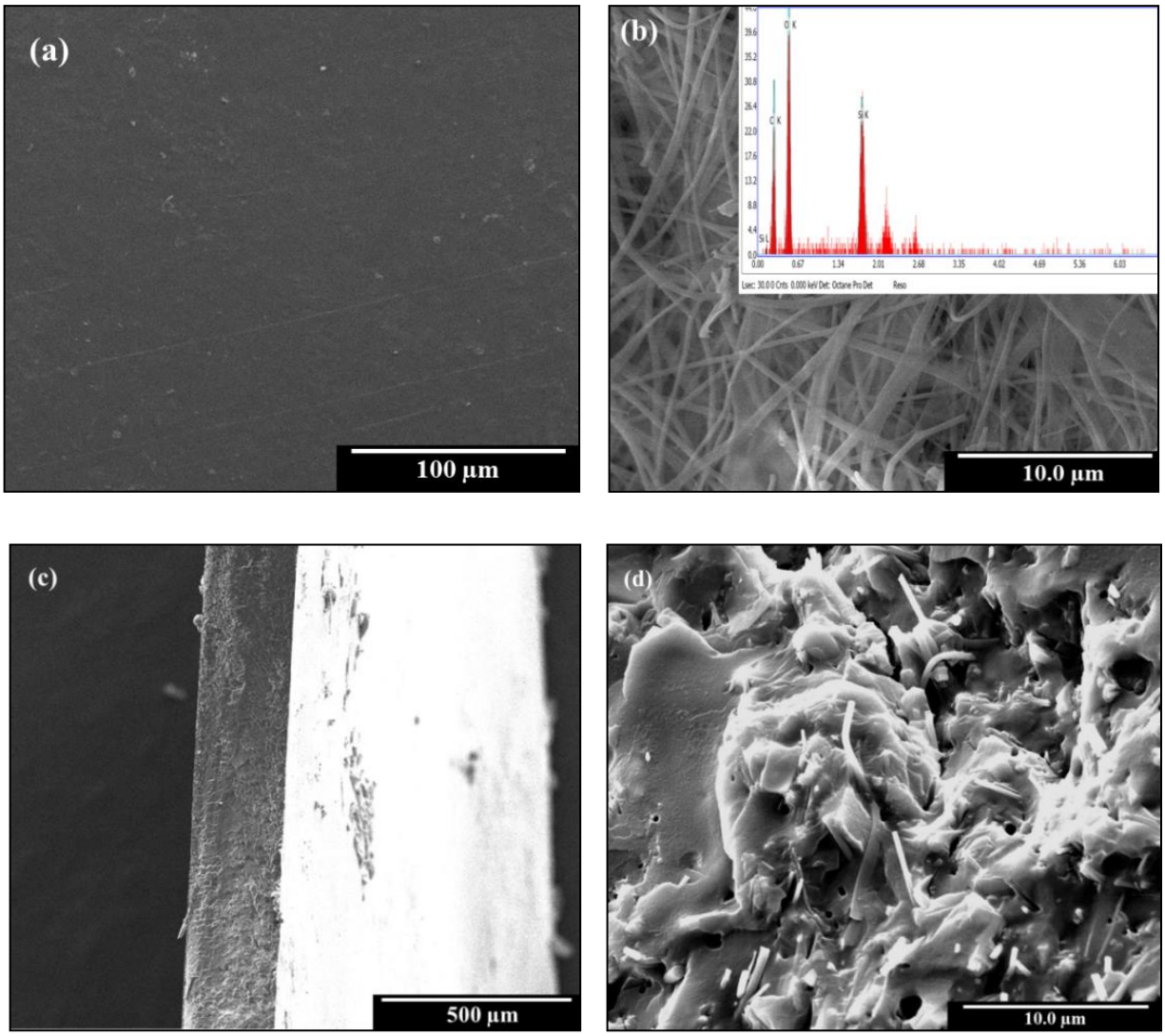

Fig. 5.16: Typical FESEM micrographs of (a) surface of the NCGPE film PS10.0; (b) SiO_2 nanofiber with EDAX (inset); (c) and (d) cross sections of the NCGPE film PS10.0 at higher magnifications.

Fig. 5.17 represents the transmission electron microscope (TEM) image of the NCGPE film having 10.0 wt.% SiO_2 nanofiber. Entangled fiber can be seen in this image, with sizes ranging from 100-300 nm in diameter. The SAD pattern shows only diffused rings, which confirm intimate interaction between the SiO_2 nanofiber and the amorphous matrix of GPE.

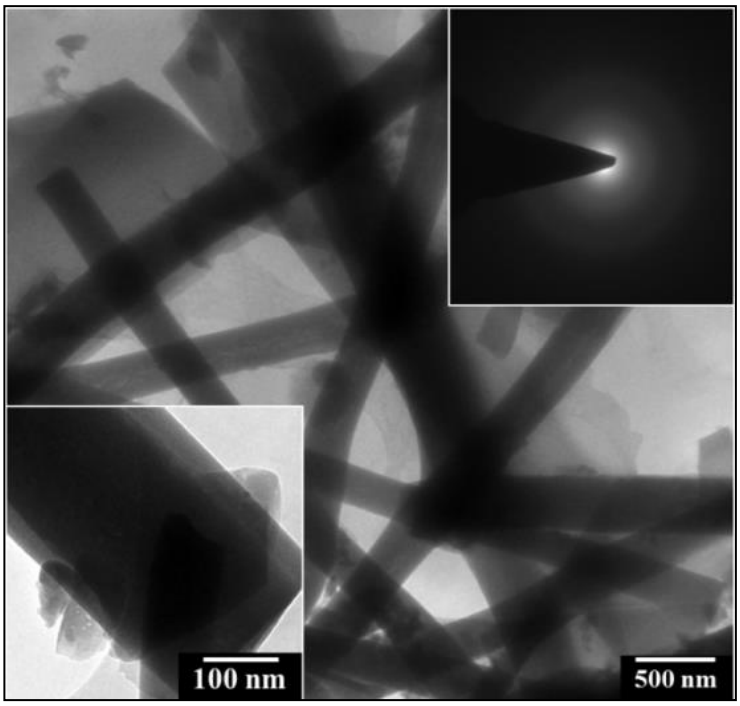

Fig. 5.17: Typical TEM micrographs of film PS10.0. Inset (above) showing SAD pattern of the film PS10.0 and (below) showing the TEM image of the individual SiO_2 nanofiber dispersed in polymer electrolyte.

Fig. 5.18 shows the planar surface and cross-sectional view micrographs of the NCGPE film PT8.0 at higher magnifications. It is observed that the surface micrograph reveals smooth surface as shown in Fig 5.18(a). Fig. 5.18(b) shows the morphology of TiO_2 nanofiber with EDAX (inset) which confirms the presence of constituent elements in polymer electrolytes. Fig. 5.18(c) shows the cross-sectional view of film PT8.0. Moreover, it can clearly be seen from Fig. 5.18(d) that the TiO_2 nanofiber were spread across the polymer electrolyte surface leading to the improved generation of charge carriers which helps in enhancing the conductivity value.

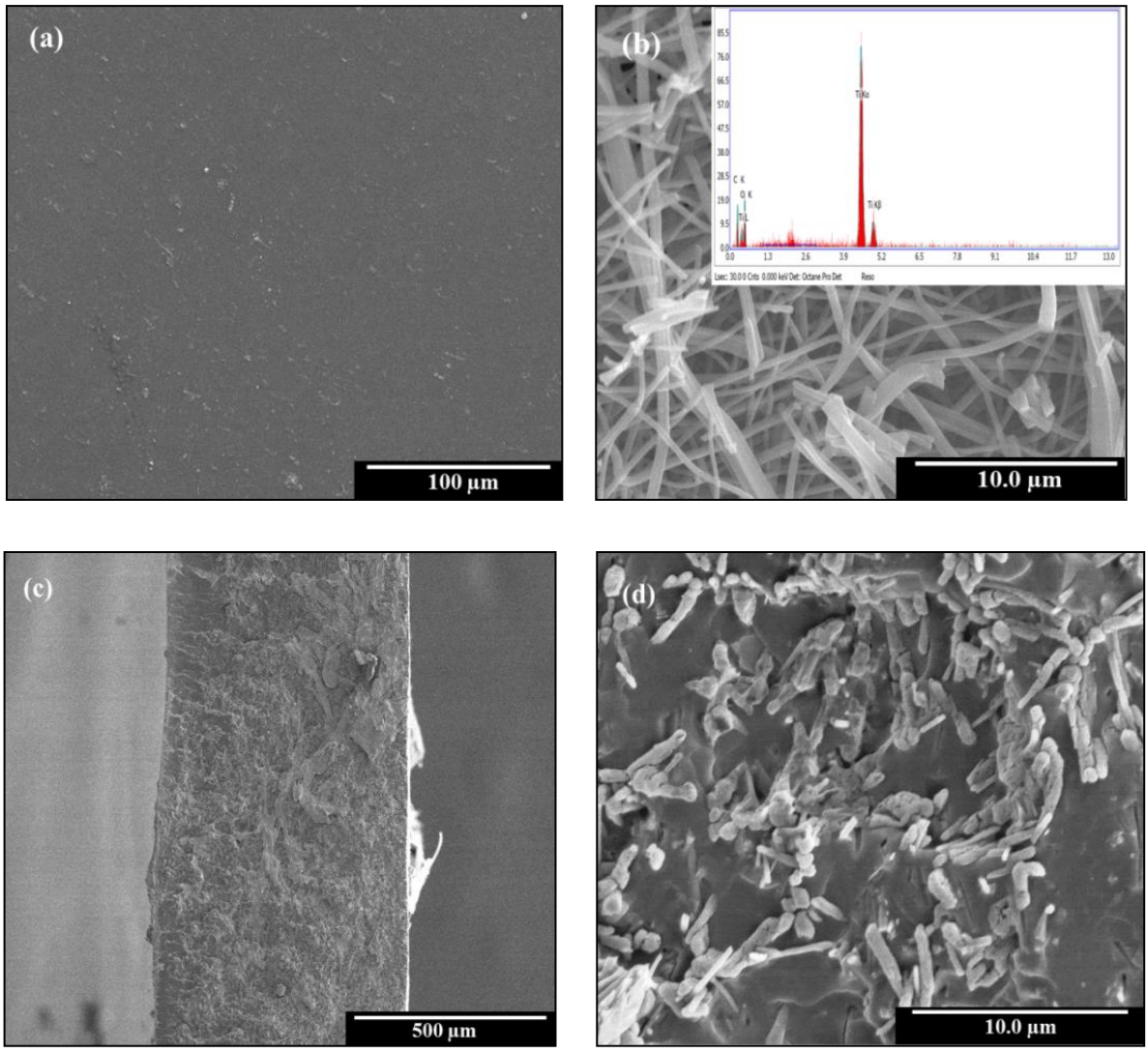

Fig. 5.18: Typical FESEM micrographs of (a) surface of the NCGPE film PT8.0; (b) TiO_2 nanofiber with EDAX (inset); (c and d) cross sections of the NCGPE film PT8.0 at higher magnifications.

The interface between the nanofiber and the polymer matrix has been examined under TEM of film PT8.0. Fig. 5.19 shows that TiO_2 nanofiber are well dispersed in the polymer matrix with an average diameter of 200-500 nm and the diffused ring of the SAD pattern (inset) is an indication of dominating amorphous region of the polymer material of the composites with TiO_2 nanofiber.

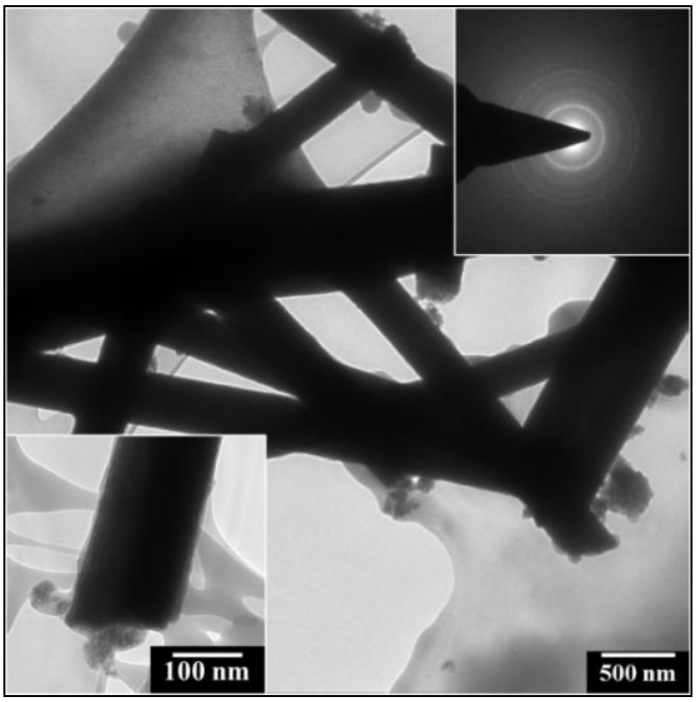

Fig. 5.19: Typical TEM micrographs of sample PT8.0. Inset (above) showing SAD pattern of the film PT8.0 and (below) showing the TEM image of the individual TiO_2 nanofiber dispersed in polymer electrolyte.

In order to investigate the effect of SiO_2 nanofiber on the structure of the NCGPE films, XRD studies has been carried out. Fig. 5.20 shows the XRD pattern of individual constituents used in the nanocomposite which reveals that the polymer PMMA has broad peaks centered on $2\theta = 15^o$, 29.9^o and 41.2^o indicating its amorphous nature. The salt $LiClO_4$ indicates sharp peaks which confirm its crystalline nature as discussed before. The XRD pattern of SiO_2 nanofiber shows broad humps indicating its amorphous nature and the XRD peaks at $2\theta = 24.5^o$, 38.3^o, 47.5^o, 54.4^o, 62.5^o, 69.4^o, 74.6^o and 82.7^o of TiO_2 nanofiber correspond to the (110), (101), (004), (200), (111), (210), (211) and (220) reflections of semi-crystalline nature.

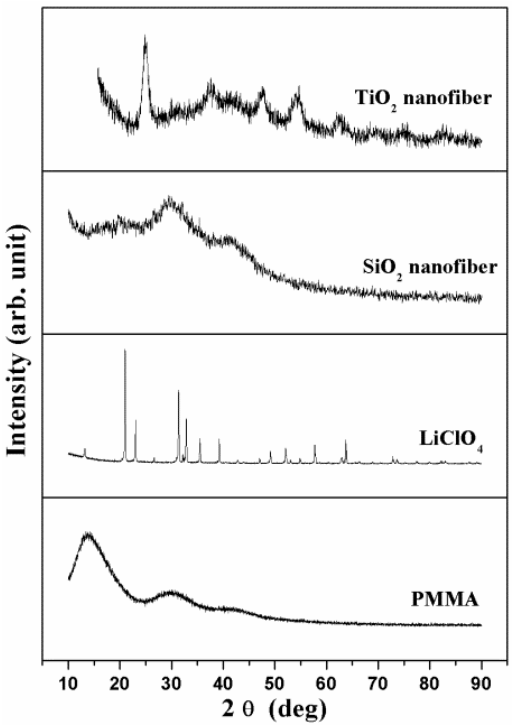

Fig. 5.20: XRD pattern of PMMA, $LiClO_4$, SiO_2 nanofiber and TiO_2 nanofiber.

When plasticizers of PC and DEC were added to PMMA along with $LiClO_4$, the PMMA peaks broadened and shifted to higher 2θ, particularly in respect of the first and the third peaks when one compares the peaks obtained in the film P0. The XRD patterns of nanocomposite films in Fig 5.21(a) shows that the peaks corresponding to PMMA have broadened and shifted compared to those in pure PMMA as noted in Table-5.4. Addition of nanofiber of SiO_2 further shifts these two peaks (29.9º and 41.2º) along with the first peak (15º) of PMMA to still higher 2θ. The major peak of SiO_2 nanofiber is near the second peak of PMMA.

Table-5.4: Shift of PMMA peaks (2θ) in nanocomposite electrolytes.

PMMA peaks	P0	PS2.0	PS4.0	PS6.0	PS8.0	PS10.0	PS12.0
15	16.41	16.52	16.83	16.83	16.83	17.21	16.83
29.9	29.9	31.14	31.14	31.14	31.14	31.34	31.14
41.2	42.1	42.5	43.4	43.4	43.4	43.83	43.4

Addition of TiO_2 nanofiber also shifts the major peaks of PMMA to the higher number as compared to P0 i.e. 16.41º, 29.9º and 42.1º and PT8.0 gives 16.8º, 32.01º and 43.79º indicating

reduction of crystallinity of PT8.0. Therefore, increases amorphicity further helps to achieve higher ionic conductivity.

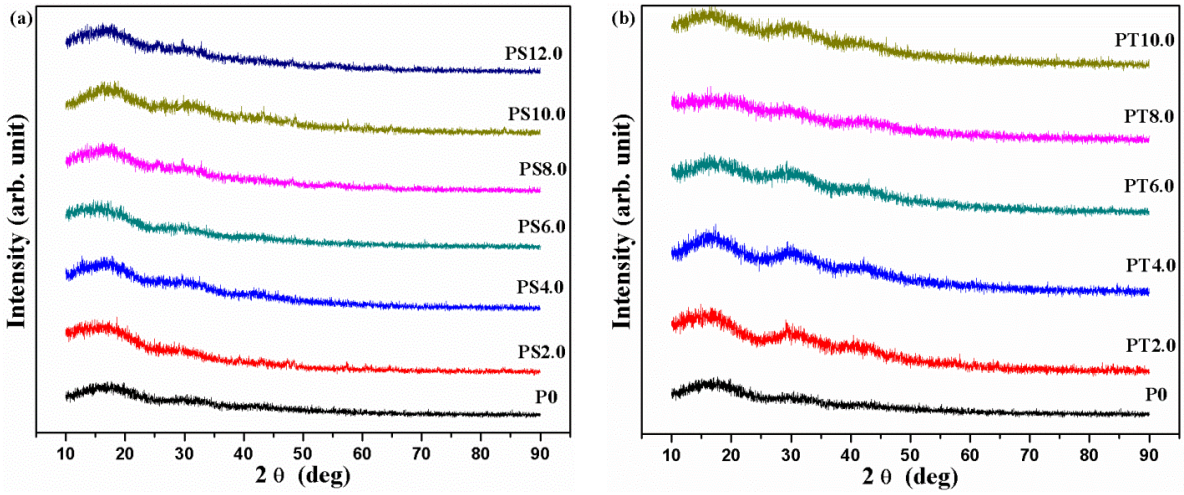

Fig. 5.21: XRD pattern of films (a) P0, PS2.0, PS4.0, PS6.0, PS8.0, PS10.0 and PS12.0 of system-III and (b) P0, PT2.0, PT4.0, PT6.0, PT8.0 and PT10.0 of system-IV.

The degree of crystallinity (K) of the polymer electrolyte for both the system-III and IV is estimated by the following relation as given in the previous subsection (5.1.1).

Table-5.5: Estimated value of degree of crystallinity for all the films of systems-III and system-IV.

Sl. No.	Sample Name	Degree of Crystallinity of system-III	Sample Name	Degree of Crystallinity of system-IV
1.	P0	26.6%	P0	26.6%
2.	PS2.0	22.4%	PT2.0	23.8%
3.	PS4.0	20.7%	PT4.0	21.9%
4.	PS6.0	18.1%	PT6.0	19.2%
5.	PS8.0	16.3%	PT8.0	16.5%
6.	PS10.0	13.8%	PT10.0	18.9%
7.	PS12.0	15.3%	-	-

It is observed that the characteristic peaks corresponding to the lithium salts are absent in gel electrolyte which possibly confirms dissolution of the salt in the polymer matrix. Further loss of crystallinity with the addition of nanofiber may be attributed to obstruction to chain mobility for

reorganization caused by oxide nanofiber which also facilitates for higher ionic conduction (Wieczorek et al, 1996).

5.2.2 Fourier Transform Infra-Red Spectroscopy

FTIR spectra of PMMA and $LiClO_4$ were same as discussed earlier (subsection 5.1.2). The absorption bands of SiO_2 nanofiber appear at 1127 and 807 cm^{-1} corresponding to stretching of Si–O–Si bond and stretching mode of Si–O bond in Si–OH and bands of TiO_2 nanofiber appear at 1082 and 734 cm^{-1} corresponding to stretching mode of Ti–O–Ti and Ti–O bond as shown in Fig. 5.22.

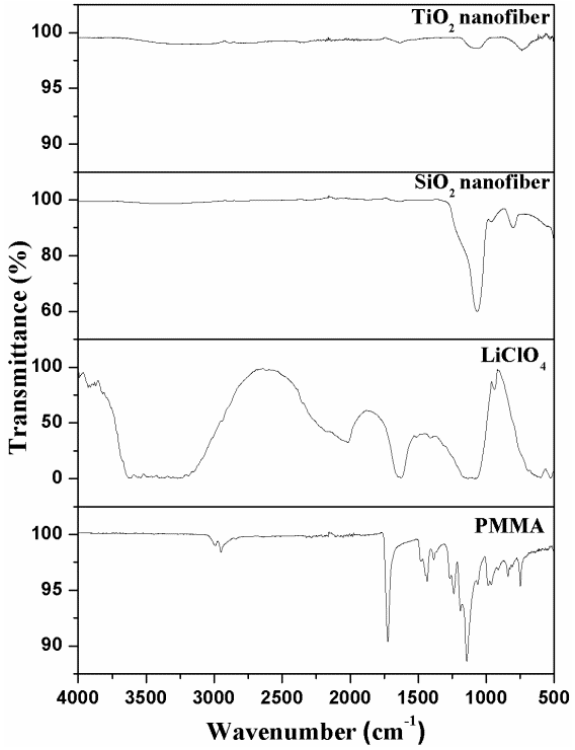

Fig. 5.22: FTIR spectra of PMMA, $LiClO_4$, SiO_2 nanofiber and TiO_2 nanofiber.

When one adds SiO_2 nanofiber to PMMA and $LiClO_4$ as in nanocomposite electrolytes designated as PS2.0, PS4.0, PS6.0, PS8.0, PS10.0 and PS12.0, the FTIR spectra shows interesting changes from that of P0 as shown in Fig. 5.23(a) but these changes are insensitive to increasing addition of SiO_2 nanofiber. Interestingly, all the vibration peaks associated with $LiClO_4$ remain unchanged and its associated –OH bonds at (3600-3400), 1627 and1069 cm^{-1} disappear while the peak at 758 cm^{-1}, corresponding to the symmetric stretching vibration of ClO_4^- ion only remains. It is an indication

of significantly increased ionization of $LiClO_4$ in presence of only 2.0 wt.% silica nanofiber. This enhanced ionisation does not cause any change in PMMA vibration peaks compared to those in P0 except disappearance of the vibration peak at 727 cm^{-1} which corresponds to CH_2 twisting vibration, and that at 979 cm^{-1} corresponding to asymmetric CH_2 transformation. Nanofiber may have frozen these vibrations directly or through the enhanced amount of ionization products. The peak of SiO_2 nanofiber corresponding to stretching of Si–O–Si bond does not change its vibration frequency of 1127 cm^{-1} position while the second peak is attributed to stretching mode of Si-O bond in Si–OH shifts to a higher value from 807 cm^{-1} to 890 cm^{-1} and there could be some bonding of dissociation products at these locations either with ionization products or with the bonds of PMMA for which the vibration peaks may have disappeared.

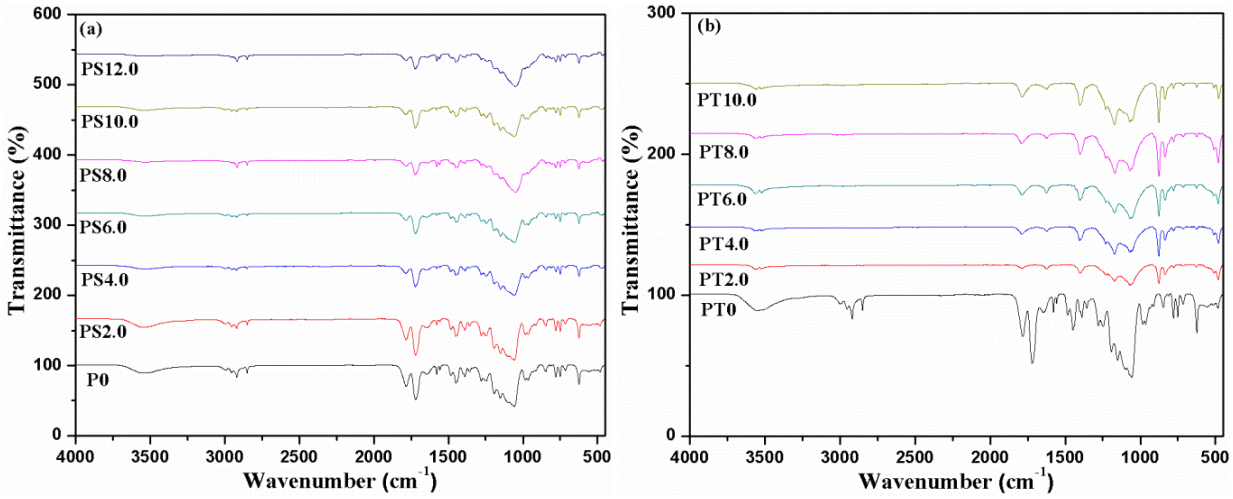

Fig. 5.23: FTIR spectra of films (a) P0, PS2.0, PS4.0, PS6.0, PS8.0, PS10.0 and PS12.0 of system-III and (b) P0, PT2.0, PT4.0, PT6.0, PT8.0 and PT10.0 of system-IV.

With the addition of TiO_2 nanofiber in PMMA based electrolyte, a change takes place as shown in Fig. 5.23(b). The stretching mode of TiO_2 at 1082 cm^{-1} shifted to lower wavenumber of 1058 cm^{-1} in all the nanocomposite electrolyte films PT2.0, PT4.0, PT6.0, PT8.0 and PT10.0. The bond stretching frequency corresponding to O–H of P0 at 3547 cm^{-1} is further shifted to 3559 cm^{-1} in all the nanocomposite electrolyte films. The vibration mode of TiO_2 at 734 cm^{-1} has shifted and merged with the peak of PMMA based electrolyte at 759 cm^{-1}. Also, the peak at 1717 cm^{-1} corresponding to C=O stretching has shifted to higher wave number of 1784 cm^{-1} in nanocomposite electrolytes indicating that there is an interaction between the carbonyl group of PMMA and TiO_2 via a coordinate bond leading to the complexation formation.

5.2.3 Ionic Conductivity Measurement/Electrochemical Impedance Spectroscopy

Ionic conductivity of the NCGPEs was obtained from the complex impedance measurements as described in Chapter 2. Fig. 5.24(a and b) show the impedance plots of system-III with PMMA-(PC + DEC)-$LiClO_4$-x% SiO_2 nanofiber (x = 2.0, 4.0, 6.0, 8.0, 10.0 and 12.0) at room temperature and system-IV having PMMA-(PC + DEC)-$LiClO_4$-x% TiO_2 nanofiber (x = 2.0, 4.0, 6.0, 8.0 and 10.0) at room temperature, respectively.

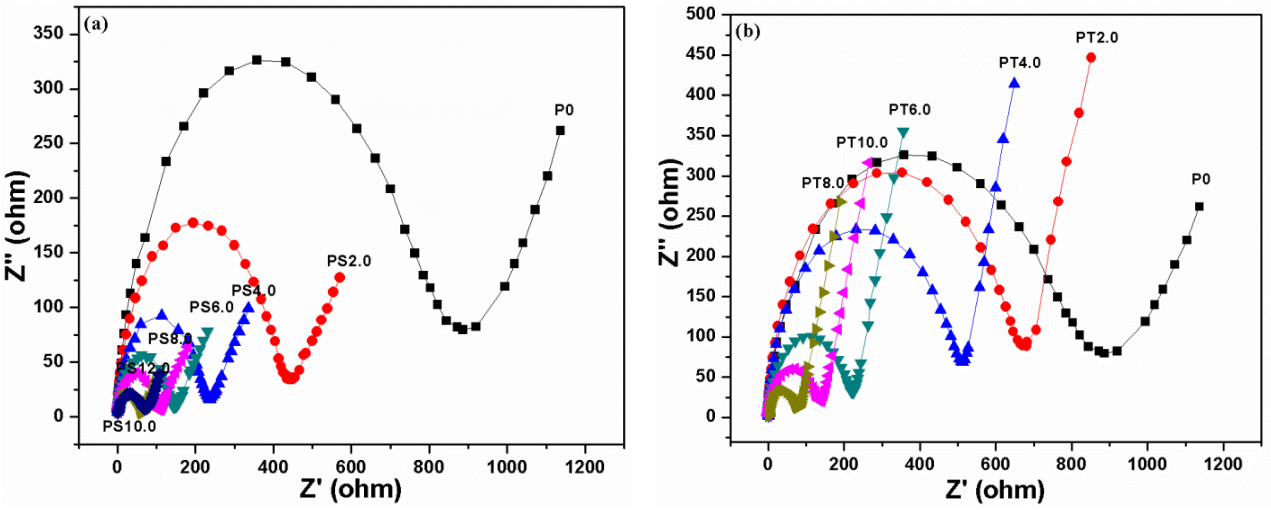

Fig. 5.24: Nyquist plots of films (a) P0, PS2.0, PS4.0, PS6.0, PS8.0, PS10.0 and PS12.0 of system-III and (b) P0, PT2.0, PT4.0, PT6.0, PT8.0 and PT10.0 of system-IV.

It is observed from the Fig. 5.24(b) that bulk resistance decreases i.e. ionic conductivity increases with increase of SiO_2 nanofiber loading and attains a maximum conductivity 3.19×10^{-3} Scm^{-1} of film PS10.0 and 2.38×10^{-3} $Scm^{-1}$of film PT8.0 as shown in Table-5.6.

Table-5.6: Estimated value of Conductivity for all the films of systems-III and system-IV.

Sl. No.	Sample Name	Conductivity Value (Scm^{-1}) of system-III	Sample Name	Conductivity Value (Scm^{-1}) of system-IV
1.	P0	0.13×10^{-4}	P0	0.13×10^{-4}
2.	PS2.0	1.28×10^{-3}	PT2.0	1.04×10^{-4}
3.	PS4.0	2.09×10^{-3}	PT4.0	1.52×10^{-3}
4.	PS6.0	2.43×10^{-3}	PT6.0	1.83×10^{-3}
5.	PS8.0	3.01×10^{-3}	PT8.0	2.38×10^{-3}
6.	PS10.0	3.19×10^{-3}	PT10.0	1.69×10^{-3}
7.	PS12.0	2.86×10^{-3}	-	-

The variation in ionic conductivity as a function of nanofiber content in nanocomposite electrolytes at room temperatures is shown in Fig. 5.25(a and b). It is observed that the conductivity increases with increasing SiO_2 nanofiber content and above 10.0 wt.% nanofiber content the conductivity decreases whereas in case of TiO_2 nanofiber the conductivity decreases above 8.0 wt.% of nanofiber content. However, the nanocomposite electrolytes become fragile and brittle with higher nanofiber content. According to Croce et al., the Lewis-acid groups of the nanofiber is added in the electrolyte which may compete with the lithium cations for the formation of complexes with polymer chains as well as the anions of the lithium salt (Croce et al, 2001). This structural modifications on the surface of nanofiber may be due to the specific actions of the polar surface groups of the inorganic nanofiber. The Lewis acid-base interaction centre reacts with the electrolytic species thus lowering the ionic coupling and promotes the dissociation of salt with the formation of ion-nanofiber complex. In the present study, the SiO_2 nanofiber of system-III and TiO_2 nanofiber of system-IV have a basic centre which can react with the Lewis-acid centres of the polymer chains and these interactions lead to the reduction in the crystallinity of the polymer host and indeed, this effect could be one of the reason for the observed enhancement in the conductivity (Wieczorek et al, 1996).

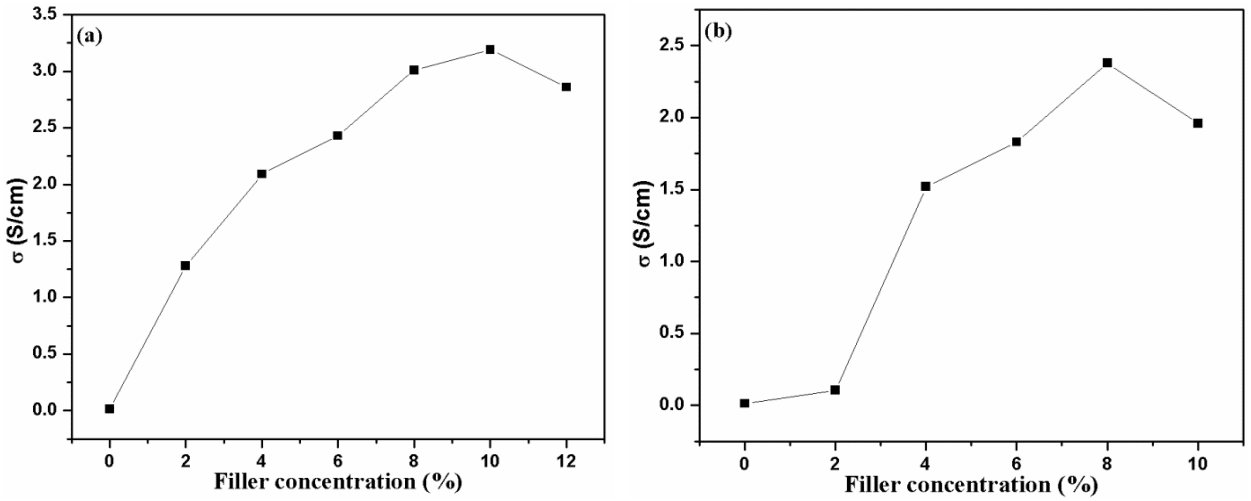

Fig. 5.25: Conductivity (Scm^{-1}) versus filler concentration (wt.%) of (a) system-III and (b) system-IV.

Fig. 5.26(a and b) shows the temperature dependant conductivity for NCGPEs of system-III and system-IV revealing that ionic conductivity increase with the increase of oxide nanofiber concentration up to some content depending upon nature of nanofibers.

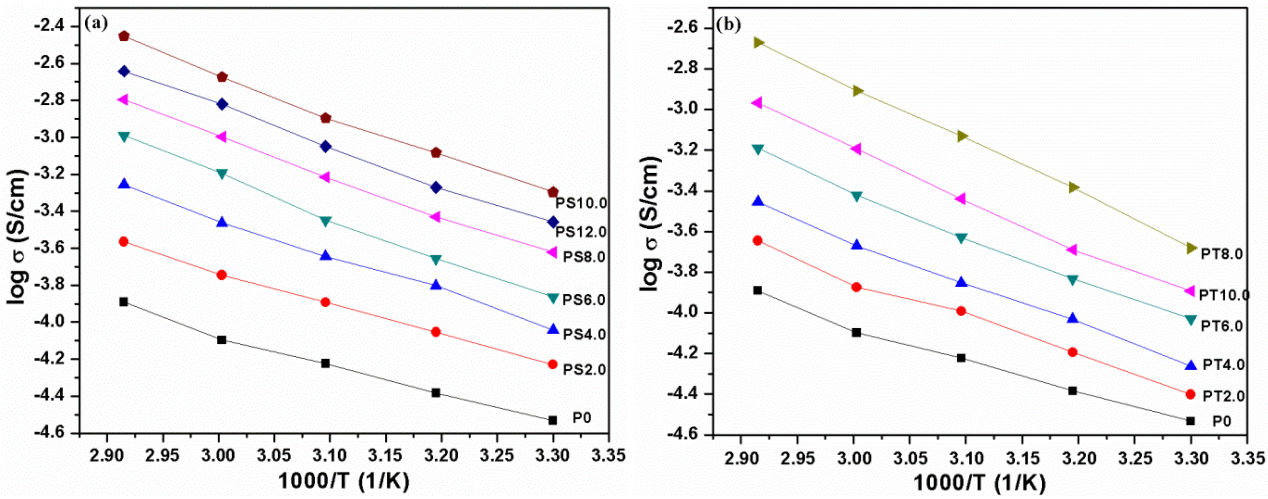

Fig. 5.26: Temperature dependent ionic conductivity plots of (a) system-III and (b) system-IV.

Both the curves of Fig. 5.26(a and b) follows a linear trend i.e. Arrhenius behaviour governed by the equation, $\{\sigma = \sigma_0 \exp(-E_a/kT)\}$ as discussed earlier. It has been reported that ionic transport in gel polymer electrolytes obeys the VTF relation, $\{\sigma = B \exp(-E_a/k(T-T_0))$, where B is a constant and T_0 is the idealized glass transition temperature and is typically 20-50 K below the glass

transition temperature of the polymer}, describes the transport properties in a viscous polymer matrix (Saikia et al, 2005). However after addition of liquid plasticizer the glass transition temperature (T_g) drops abruptly in case of GPEs. In that case T_0 will be far below the temperature regions of measurements from ambient to higher temperature. As expected the increase in temperature leads to the increase in conductivity due to increase in the flexibility of the polymer chain that provides more free volume resulting enhanced polymer segmental mobility.

Table 5.7: Ionic transference numbers for all the films of system-III and system-IV.

Sl. No.	Sample Name	Transference Number of system-III	Sample Name	Transference Number of system-IV
1.	P0	0.91	P0	0.91
2.	PS2.0	0.93	PT2.0	0.92
3.	PS4.0	0.93	PT4.0	0.93
4.	PS6.0	0.94	PT6.0	0.93
5.	PS8.0	0.95	PT8.0	0.95
6.	PS10.0	0.96	PT10.0	0.93
7.	PS12.0	0.93	-	-

High value of transport number lying in the range 0.91-0.96 for different compositions of system-III and system-IV nanofiber dispersed in PMMA based gel polymer electrolytes suggests that the transport of charge in polymer electrolyte systems is predominantly ionic accompanied by mass transport and electronic contribution to the total current negligible.

5.2.4 Thermal Analysis

The thermal stability of the NCGPE films PS2.0, PS4.0, PS6.0, PS8.0, PS10.0 and PS12.0 was investigated by TG analysis and the TG traces are shown in Fig. 5.27(a). The film P0 is stable up to 220 ºC as discussed before. When SiO_2 nanofiber dispersed into the PMMA based gel polymer electrolyte, the decomposition temperature increases from 220 ºC to 245 ºC for film PS10.0. The volatility of the decomposed products obtained may be hindered by the nanofiber and limit the continuous decomposition of PMMA content because of the dispersion and good thermal transmission properties whose effect could result in the enhancement of the thermal decomposition temperature (Yu et al, 2009). Also, the presence of SiO_2 nanofiber in the films forming materials

strengthened the inorganic SiO_2 network of the PMMA, which led to a corresponding enhancement in their thermal stability (Yu et al, 2009). The derivative of the mass loss of the films as a function of temperature is presented in Fig 5.27(b). It may be seen that the decomposition temperature varies between 281 ^oC for film P0 and 344 ^oC for film PS10.0 which is quite high. The highest peak in each plot indicating the maximum change in mass with the temperature change corresponds to the thermal stability.

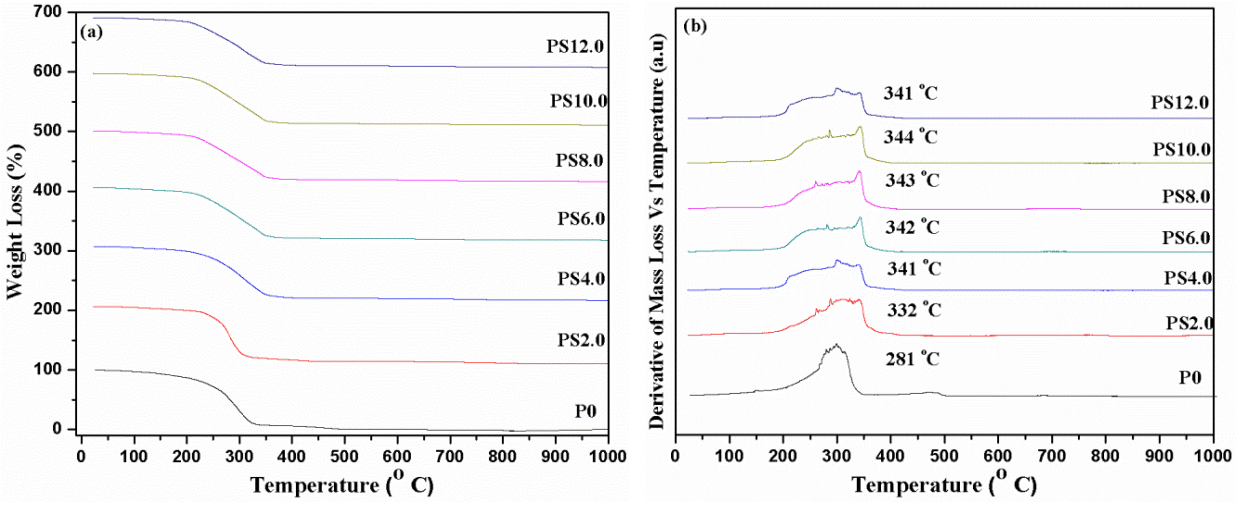

Fig. 5.27: (a) TG traces of films P0, PS2.0, PS4.0, PS6.0, PS8.0, PS10.0 and PS12.0 of system-III; (b) DTG of films P0, PS2.0, PS4.0, PS6.0, PS8.0, PS10.0 and PS12.0 of system-III.

Fig. 5.28(a) shows the TG traces of films P0, PT2.0, PT4.0, PT6.0, PT8.0 and PT10.0 by varying wt. % of TiO_2 nanofiber indicates that the prepared films degrade in three steps. The first step degradation takes place in the temperature range of 110 °C to 150 °C which is due to presence of moisture and trapped solvent in polymer electrolytes. The second step of degradation takes place from 200 °C to 350 °C which is due to degradation of PMMA and scissioning of the polymer chains in the first step. The third step degradation is observed between 340 °C and 460 °C. It is observed that there is not much change in degradation temperature with the addition of TiO_2 nanofiber. But the amount of polymer degraded in the first step is decreased in the case of PT8.0 as compared to P0 indicating PT8.0 is thermally more stable than P0**.** The derivative thermogravimetry (DTG) curve in Fig. 5.28(b) shows important peak at 281 °C for film P0 and 307 °C for film PT8.0 indicating that the maximum decomposition process occurs at ~ 307 °C with 8.0 wt.% TiO_2 nanofiber.

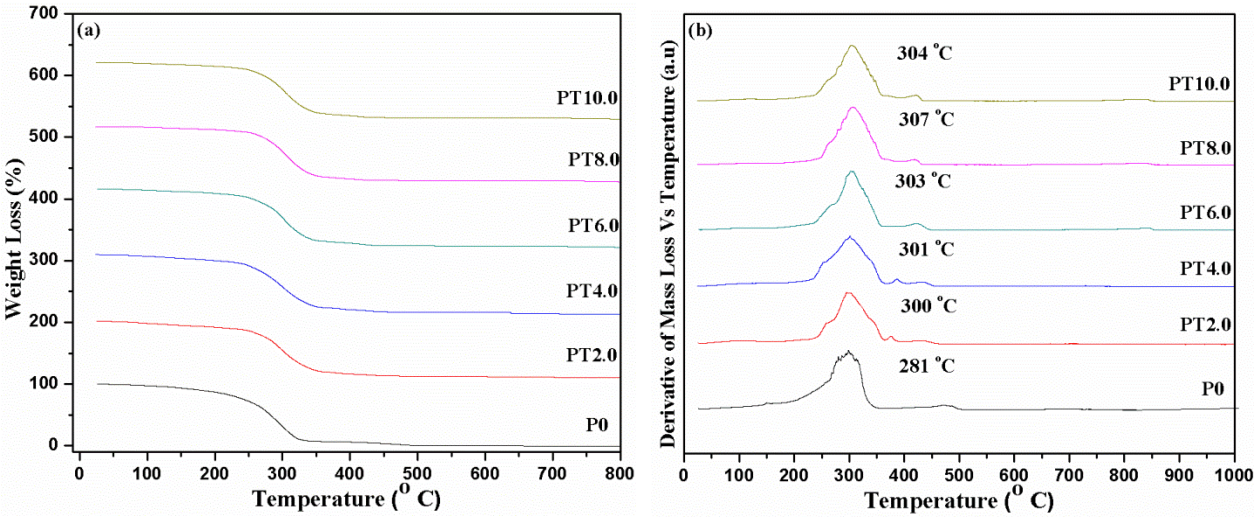

Fig. 5.28: (a) TG traces of films P0, PT2.0, PT4.0, PT6.0, PT8.0 and PT10.0 of system-IV; (b) DTG of films P0, PT2.0, PT4.0, PT6.0, PT8.0 and PT10.0 of system-IV.

5.2.5 Mechanical Analysis

The stress-strain curves of the films PS2.0, PS4.0, PS6.0, PS8.0, PS10.0 and PS12.0 of system-III and PT2.0, PT4.0, PT6.0, PT8.0 and PT10.0 of system-IV are shown in Fig. 5.28(a). The tensile strength 28.4 MPa with an elongation-at-break value of 256% for film PS10.0 is found maximum. The film PT8.0 has tensile strength of 28.2 MPa with an elongation-at-break of 248%. Also, the area per unit volume which is toughness for PT8.0 is 2.784 Jcm^{-2}. As already confirmed with FESEM and FTIR studies, interactions exist between the polymer matrix and the oxide nanofiber as discussed earlier. Therefore, the nanocomposite films obtained are more flexible and can tolerate high strength than sample without dispersion.

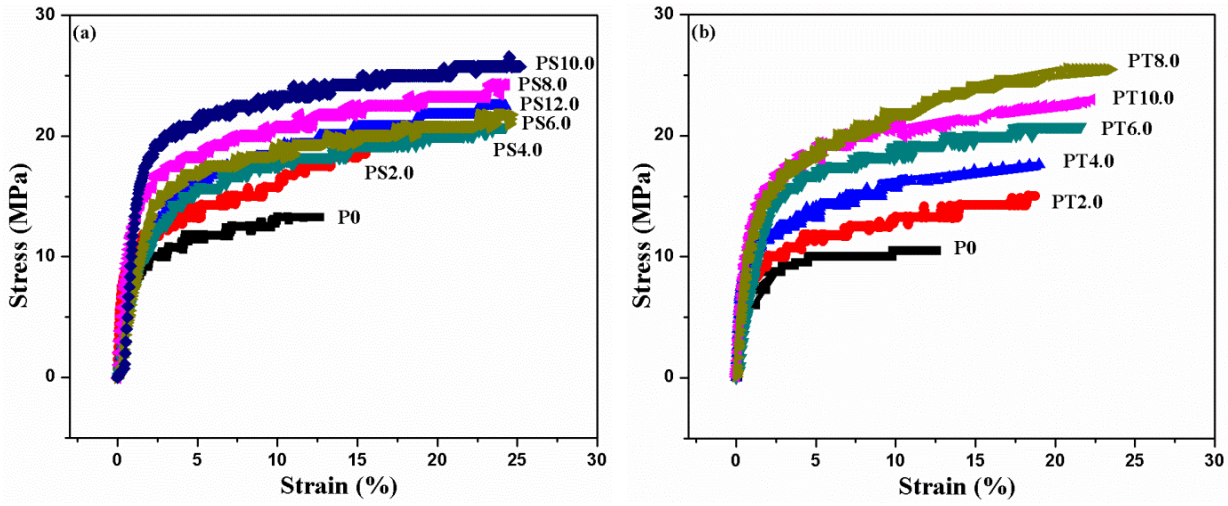

Fig. 5.29: Stress-strain plots of films (a) P0, PS2.0, PS4.0, PS6.0, PS8.0, PS10.0 and PS12.0 of system-III and (b) P0, PT2.0, PT4.0, PT6.0, PT8.0 and PT10.0 of system-IV.

5.2.6 Electrochemical Analysis

Fig. 5.30 presents the LSV curve of films P0, PS10.0 and PT8.0. The irreversible onset of the current determines the electrolyte breakdown voltage, which only extends to about 4.1 V versus lithium in film P0. The decomposition voltage of the film PS10.0 extends to 4.6 V whereas 4.5 V for film PT8.0, indicating that the addition of oxide nanofiber improves electrochemical stability of the gel polymer electrolytes.

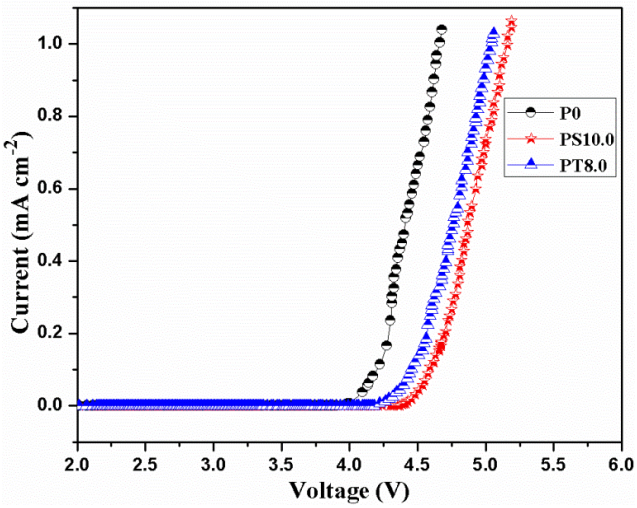

Fig. 5.30: LSV curve of films P0, PS10.0 and PT8.0.

5.3 P(VdF-HFP)-(PC+DEC)-$LiClO_4$-MWCNT and P(VdF-HFP)-(PC+DEC)-$LiClO_4$-CNF Systems

In this section, P(VdF-HFP) based gel polymer electrolyte is used which is dispersed with two different types of nanofillers, MWCNT (having outer diameter of 10-20 nm and length of 10-30 μm) with small volume fraction and high surface area (>200 m^2g^{-1}) and CNF (having outer diameter of 200-600 nm and length of 5-50 μm) with high surface area (>18 m^2g^{-1}) to characterize its morphology, ionic conductivity, thermal and mechanical behaviour. The NCGPE films have been identified with PH0.5, PH1.0, PH1.5 and PH2.0 corresponding to 0.5, 1.0, 1.5 and 2.0 wt.% MWCNT of system-V and PHC0.5, PHC1.0, PHC1.5 and PHC2.0 corresponding to CNF loading of 0, 0.5, 1.0, 1.5 and 2.0 wt.% of system-VI respectively. PH0 is the film without dispersion. The composition of polymer base prepared is 0.60P(VdF-HFP)-0.30(PC+DEC)-0.10$LiClO_4$, in which both MWCNT and CNF were dispersed as a separate systems. The NCGPEs were prepared in the form of film with thickness varying between 0.17-0.21 mm.

5.3.1 Morphology and Structure of Nanocomposite Gel Polymer Electrolytes

Fig. 5.31 shows FESEM images of the cross section of the film PH1.5 at different magnifications. The micrograph images reveal that MWCNT are properly embedded in the polymer matrix. The porous structure of P(VdF-HFP) can be reduced by using MWCNT which occupied the pores of P(VdF-HFP) matrix and resulted in improved morphology as can be observed in Fig 5.31(c and d). A mass of entangled MWCNT can be seen in Fig 5.31(d) image, ranging from 10-50 nm in diameter and about 15 μm in length.

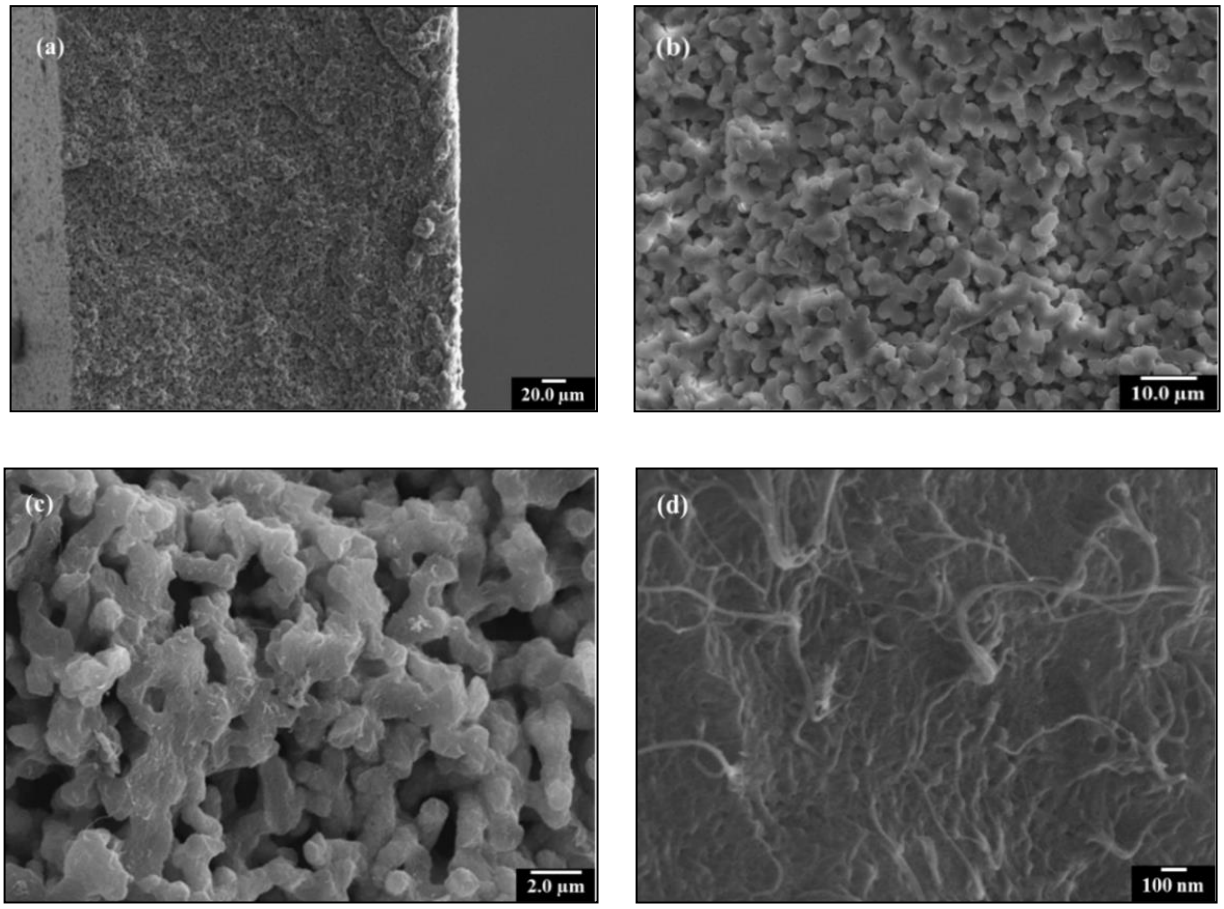

Fig. 5.31: (a-d) Typical FESEM micrographs of cross section of NCGPE film PH1.5 at different magnifications.

Fig. 5.32 shows an TEM image of film PH1.5 in which the distribution pattern of the MWCNT layers inside the matrix of P(VdF-HFP) is seen. It has been observed that most of the MWCNT layers are well dispersed and are found to be disordered in a random fashion in the polymer matrix with sizes ranging from 10-30 nm in diameter. The inset SAD pattern shows only diffused rings which confirm the amorphous pattern.

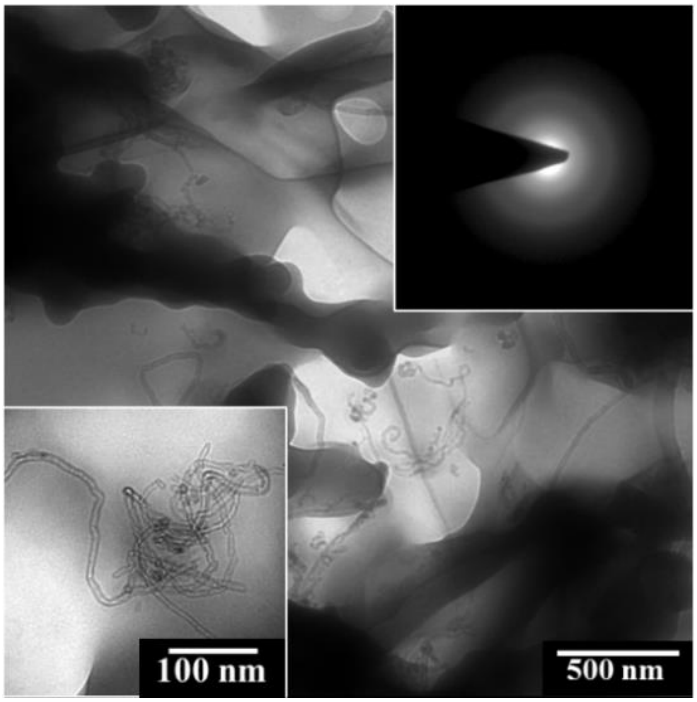

Fig. 5.32: Typical TEM micrograph of film PH1.5. Inset (above) showing SAD pattern of the film PH1.5 and (below) showing the TEM image of the individual MWCNT.

Fig. 5.33 shows the FESEM micrograph of cross section of P(VdF-HFP) based gel polymer electrolyte having 1.5 wt.% CNF in it at different magnifications. The film is composed of numerous randomly oriented continuous fiber having diameter in the range of 60-100 nm. Importantly, CNF are distributed within the P(VdF-HFP) matrix in straight and aligned orientations along the fiber axis.

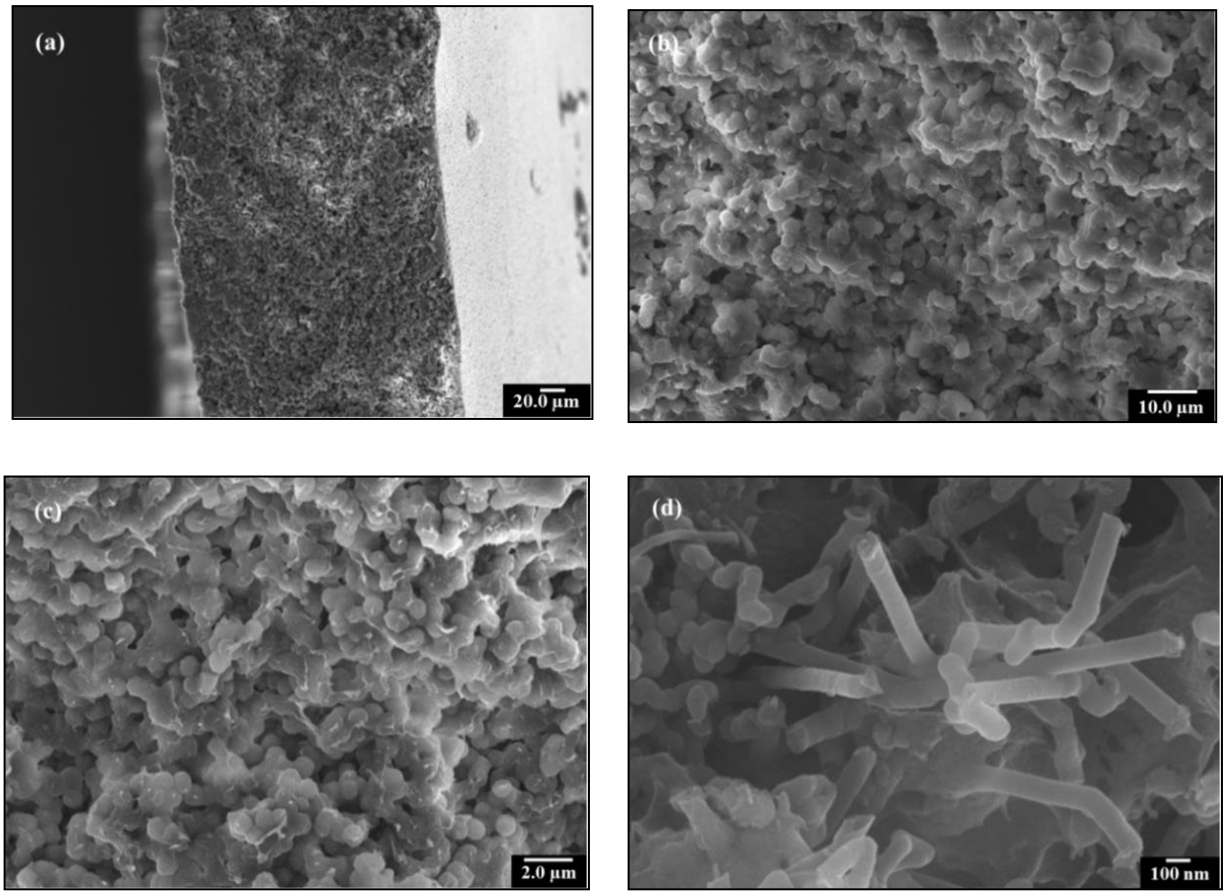

Fig. 5.33: (a-d) Typical FESEM micrographs of cross section of NCGPE film PHC1.5 at different magnifications.

Fig. 5.34 shows the TEM image of sample PHC1.5 having diameter of the CNF is in the range of 20-80 nm. Also CNFs are homogeneously dispersed in the polymer matrix of P(VdF-HFP) and the inset SAD pattern shows that the film is amorphous in nature which is in good agreement with XRD as discussed in the next section.

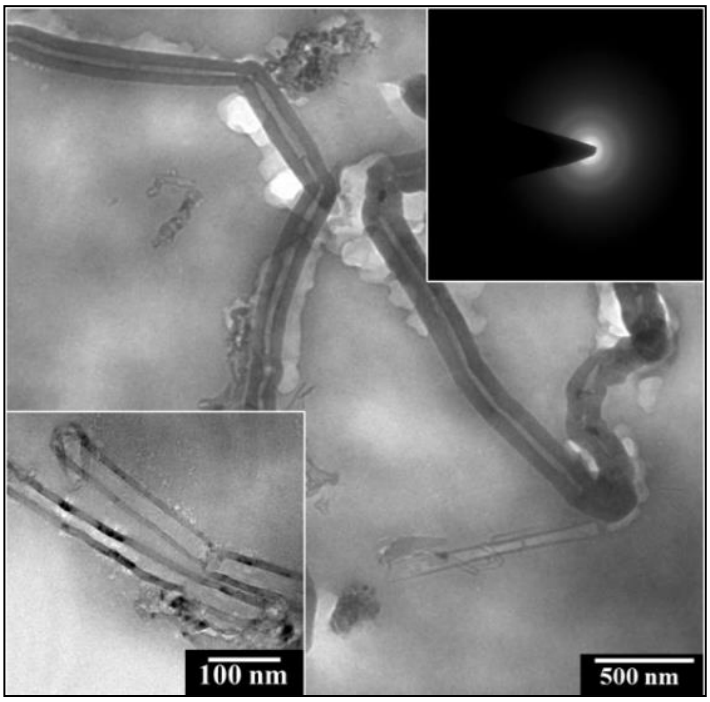

Fig. 5.34: Typical TEM micrographs of film PHC1.5. Inset (above) showing SAD pattern of the film PHC1.5 and (below) showing the TEM image of the individual CNF.

The XRD pattern of P(VdF-HFP), $LiClO_4$, MWCNT and CNF are shown in Fig. 5.35. The peaks of pure P(VdF-HFP) at 2θ = 18.8º, 20.4º, 26.6º and 39.9º matches well with the (100), (020), (110) and (021) reflections of crystalline PVdF which confirms semi-crystalline morphology for P(VdF-HFP). The sharp peaks of the salt $LiClO_4$ in the XRD pattern indicating its crystalline nature. The XRD pattern of MWCNT has diffraction peaks (002) and (101) at about 2θ = 26º and 44º and CNF also having peaks at same position at about 2θ = 26º and 44º respectively.

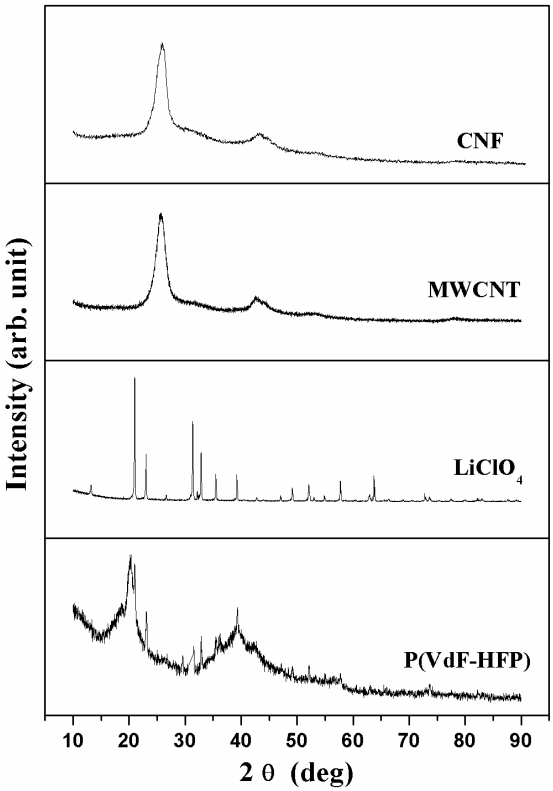

Fig. 5.35: XRD pattern of P(VdF-HFP), $LiClO_4$, MWCNT and CNF.

Addition of MWCNT in P(VdF-HFP) based gel polymer electrolytes further broadens and shifts nominally towards the higher diffraction angle for all the nanocomposite films as shown in Fig 5.36(a). Thus, the proportion of amorphous region in the nanocomposite increases as compared to the polymer based matrix without dispersion of MWCNT. The absence of characteristic peaks of MWCNT in films PH0.5, PH1.0, PH1.5 and PH2.0 may be because of the proportion of the nanotube in the nanocomposite films is negligibly smaller to give rise to detectable diffraction peaks. Fig 5.36(b) shows XRD pattern of films PH0, PHC0.5, PHC1.0, PHC1.5 and PHC2.0. With the addition of CNF, it has been observed that there is an absence of characteristic peaks of CNF in all NCGPE films which confirms that CNF surface structure having many graphitic edges which assist in making stronger bonding with polymer matrix (Tibbetts et al, 2007).

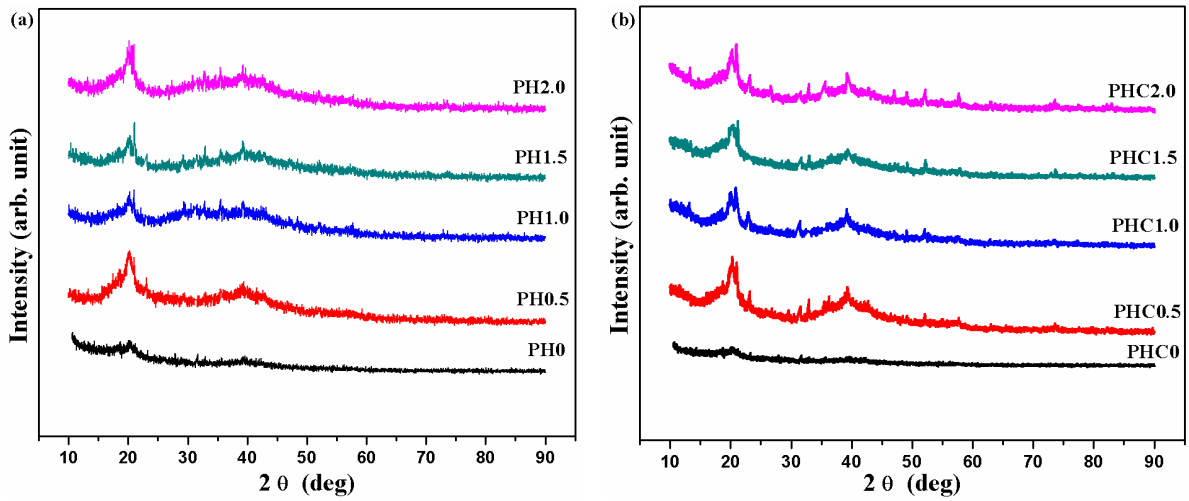

Fig. 5.36: XRD pattern of films (a) PH0, PH0.5, PH1.0, PH1.5 and PH2.0 of system-V; (b) PH0, PHC0.5, PHC1.0, PHC1.5 and PHC2.0 of system-VI.

Following the relation, $\{K = (A/A_0) \times 100\}$, the calculated values of degree of crystallinity for both the system-V and system-VI are shown in below Table-5.8.

Table-5.8: Estimated degree of crystallinity for all films of system-V and system-VI.

Sl. No.	Sample Name	Degree of Crystallinity of system-V	Sample Name	Degree of Crystallinity of system-VI
1.	PH0	22.4%	PH0	22.4%
2.	PH0.5	20.6%	PHC0.5	21.6%
3.	PH1.0	18.9%	PHC1.0	19.8%
4.	PH1.5	15.6%	PHC1.5	16.1%
5.	PH2.0	17.4%	PHC2.0	18.4%

As there is a tendency in the literature on polymer based nanocomposites to consider that nanofiller have a complex behaviour, acting as nucleating agents, reducing the induction time, decreasing the crystallization temperature, lowering the enthalpy of fusion, increasing the crystallization speed, resulting in larger crystallites leading to a higher degree of crystallinity (Chen et al, 2011). Therefore, the degree of crystallinity of NCGPEs is greatly reduced in all the films of system-V and system-VI which increases its amorphicity and further helps in increasing ionic conductivity.

5.3.2 Fourier Transform Infra-Red Spectroscopy

FTIR spectra of P(VdF-HFP), $LiClO_4$, MWCNT and CNF are shown in Fig. 5.37. The wave number 3548 cm^{-1} corresponds to C–H stretching vibrations of PVdF. Frequency 1770 cm^{-1} is assigned to $–CF=CF_2$ group. Peak at 1628 cm^{-1} is assigned to C=O stretching vibration of plasticizer (PC+DEC). Frequencies 1483 cm^{-1} and 1406 cm^{-1} are assigned to $–CH_3$ asymmetric bending and C–F stretching vibration of plasticizer, propylene carbonate and diethyl carbonate and P(VdF-HFP) respectively. Frequency 1290-1060 cm^{-1} assigned to –C–F– and $–CF_2–$ stretching vibrations and at 881 cm^{-1} is assigned to vinylidene group of polymer while $LiClO_4$ has broad peak in between (3600-3400) cm^{-1}, 1627, 1069 and 758 cm^{-1}, corresponding respectively to inter and intra molecular stretching vibration of –OH bond (due to chemisorbed moisture), stretching vibration of $LiClO_4$, asymmetric stretching vibration of ClO_4^- ion and symmetric stretching vibration of ClO_4^- ion (Rajendran et al, 2001). The absorption bands of MWCNT appear at 2996, 2819, 2657, 2334, 1774, 1683, 1538, 1406, 1332, 1185, 1053, 787 and 552 cm^{-1} whereas the absorption bands of CNF appear at 3008, 2680, 2332, 2107, 1922, 1738, 1512, 1349, 1225, 713 and 529 cm^{-1} are shown in Fig 5.37.

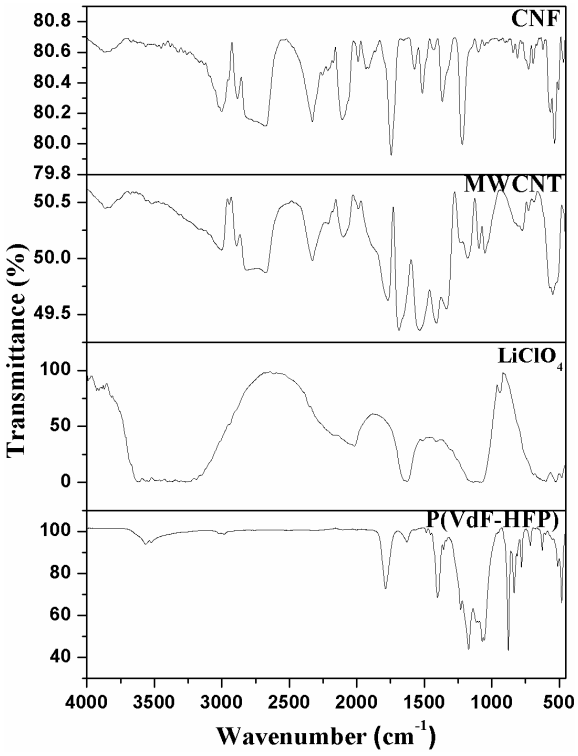

Fig. 5.37: FTIR spectra of P(VdF-HFP), $LiClO_4$, MWCNT and CNF.

FTIR spectra of NCGPEs PH0.5, PH1.0, PH1.5 and PH2.0 are shown in Fig. 5.38(a) in which some of the vibrational peaks of P(VdF-HFP) (3548, 1770, 1406, 881 and 801 cm^{-1}) are shifted to (3568, 1786, 1408, 886 and 820 cm^{-1}) in the film P0. New absorption peaks at 633 cm^{-1} and 557 cm^{-1} corresponding to C–Cl stretching are observed for the electrolyte material. Absorption peaks at frequency 2985 cm^{-1} is assigned to C–H stretching vibration. Peak at frequency 1786 cm^{-1} is assigned to $–CF=CF_2$ group and the frequency 1408 cm^{-1} is assigned to C–F stretching vibration of P(VdF-HFP) and 1169 cm^{-1} and 1070 cm^{-1} are assigned to C–F and CF_2 stretching vibration. Frequency 886 cm^{-1} is shifted in NCGPEs could be attributed to ionic association through redissociation of charge accompanying the formation of ionic pairs assigned to vinylidene group of polymer. Some peaks (1718, 1365, 1225, 1084, 788, 521 cm^{-1}) are appeared in NCGPEs which are found to be shifted to lower side indicating increase of polymer-nanofiller-ion interaction with increasing MWCNT content (Stephan et al, 2000).

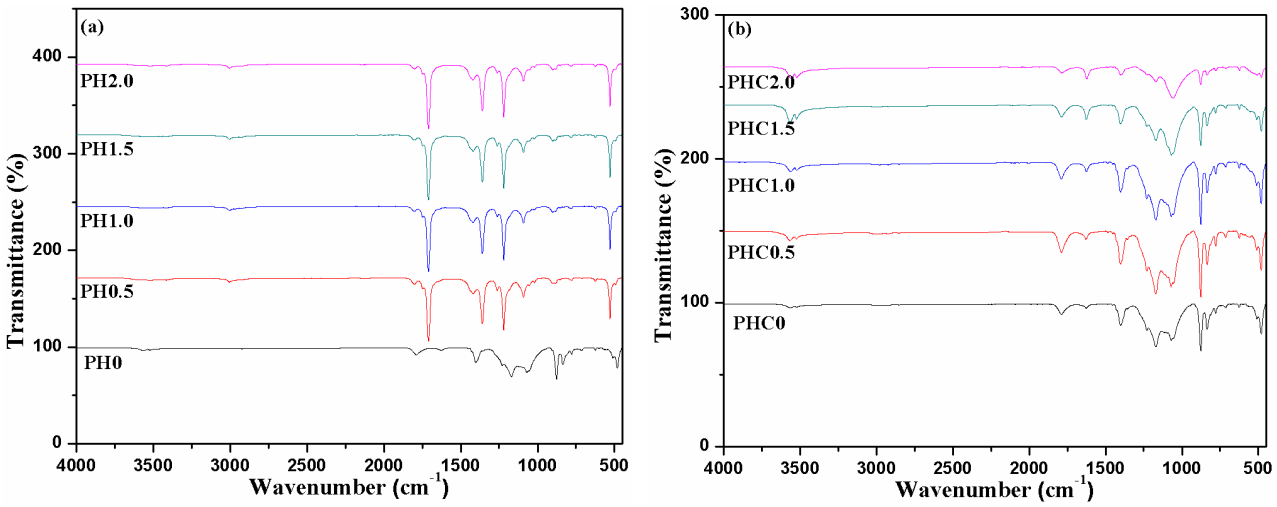

Fig. 5.38: FTIR spectra of films (a) PH0, PH0.5, PH1.0, PH1.5 and PH2.0 of system-V; (b) PH0, PHC0.5, PHC1.0, PHC1.5 and PHC2.0 of system-VI.

With the incorporation of CNF in the P(VdF-HFP) based gel polymer electrolytes, the free ions increase to a maximum at 1.5 wt.% CNF content and the peaks appears at 3571, 3534, 1784, 1634, 1409, 1171, 1068,871, 783 and 546 cm^{-1} which suggests that the CNF can effectively facilitate the dissociation of lithium salt by weakening the bond between the contact ion pairs shifting to higher wavenumber, resulting in the increased charge carrier concentration. There are no obvious changes in the degree of lithium salt dissociation upon further increase in CNF content beyond 1.5 wt.%.

5.3.3 Ionic Conductivity Measurement/Electrochemical Impedance Spectroscopy

The typical Nyquist plots of system-V and system-VI at room temperature are shown in Fig. 5.39 (a and b). All plots comprise a semi-circular arc in the high frequency region and an oblique line in the low frequency region similar to the earlier Nyquist plot. The high frequency semicircle can be ascribed to the bulk polymer electrolytes, whereas the low frequency spike is due to the capacitance of electric double layer formed at the electrode/electrolyte interface. The impedance spectra can be modeled by an equivalent circuit having a parallel combination of a capacitor and a resistor in series or parallel with a constant phase element (CPE). The impedance of CPE is given by $\{Z_{CPE} = k\ (j\omega)^{-p}$ where $0 < p < 1\}$. When $p=0$, Z is frequency independent and k is just the resistance and when p=1, $Z = k/j\omega = -j/\omega(k)$, the constant k^{-1}corresponds to the capacitance. When p is between 0 and 1, the CPE acts in a way intermediate between a resistor and capacitor. The use of series CPE terms tilts the spike and parallel CPE terms depress the semicircle.

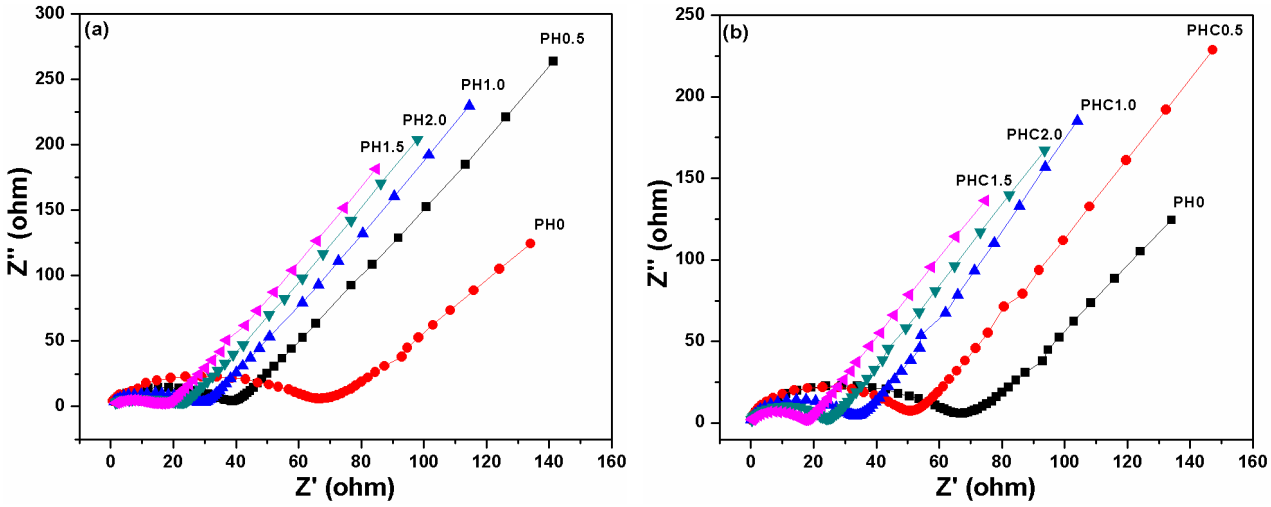

Fig. 5.39: Nyquist plots of films (a) PH0, PH0.5, PH1.0, PH1.5 and PH2.0 of system-V; (b) PH0, PHC0.5, PHC1.0, PHC1.5 and PHC2.0 of system-VI.

The bulk resistance (R_b) is determined from the intercept of the slanted line with the real-axis value. Then the conductivity σ can be obtained from $\{\sigma = l/R_bA\}$, where l is the thickness of the polymer electrolyte film and A its area. It is observed from the Fig. 5.39(a) that ionic conductivity increases (i.e. bulk resistance decreases) with increase of MWCNT loading and attains a maximum value of 1.41×10^{-3} Scm^{-1} at 1.5 wt.% MWCNT content. This value of ionic conductivity at room temperature is better than that reported in literature for P(VdF-HFP)/MWCNT systems where

conductivity values were found to be of the order of 10^{-4} Scm^{-1} (Lee et al, 2007). Fig. 5.39(b) gives Nyquist plots of system-VI which gives a maximum value of ionic conductivity of 1.01×10^{-3} Scm^{-1} for film PHC1.5. The enhancement in ionic conductivity depend upon the surface areas which is more in MWCNT than CNF so the interface region will be more enhances amorphicity and further ionic conductivity (Xi et al, 2000).

Table-5.9: Estimated value of conductivity for all the films of system-V and system-VI.

Sl. No.	Sample Name	Conductivity Value (Scm^{-1}) of system-V	Sample Name	Conductivity Value (Scm^{-1}) of system-VI
1.	PH0	1.76×10^{-4}	PH0	1.76×10^{-4}
2.	PH0.5	7.73×10^{-4}	PHC0.5	2.63×10^{-4}
3.	PH1.0	1.03×10^{-3}	PHC1.0	5.87×10^{-4}
4.	PH1.5	1.41×10^{-3}	PHC1.5	1.01×10^{-3}
5.	PH2.0	0.95×10^{-3}	PHC2.0	8.19×10^{-4}

The value of conductivity decreases with further increase in content of nanofiller (MWCNT and CNF) content as shown in Fig. 5.40(a and b). The decrease in ionic conductivity after 1.5 wt.% content of nanofiller (or at higher fraction) can be attributed to the blocking effect on the transport of charge carriers due to the phase separation of nanofiller in system-V and VI.

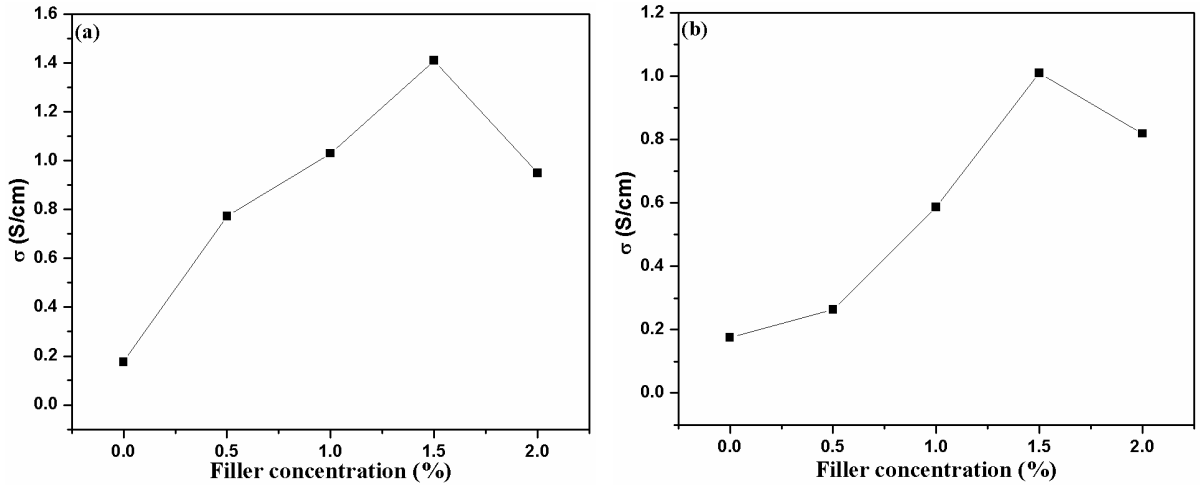

Fig. 5.40: Conductivity (Scm^{-1}) versus filler concentration of (a) system-V; (b) system-VI.

Fig. 5.41(a and b) shows the temperature dependent ionic conductivity follows a linear trend i.e. Arrhenius behaviour. The conductivity enhancement behaviour with temperature can be

understood by free volume model. As the temperature increases, the polymer chains flex and expand at increasing rate and produce free volume leading to an increase in ion and segmental mobility, which facilitates ion transport (Jeon et al, 2005).

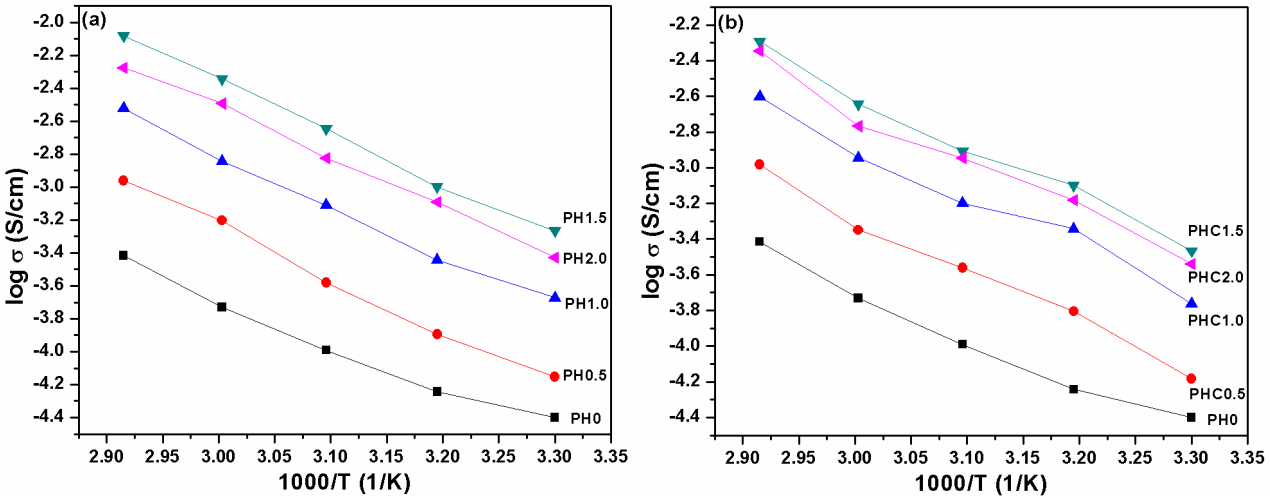

Fig. 5.41: Temperature dependent ionic conductivity plots of (a) PH0, PH0.5, PH1.0, PH1.5 and PH2.0 of system-V; (b) PH0, PHC0.5, PHC1.0, PHC1.5 and PHC2.0 of system-VI.

Table-5.10 shows the ionic transference number for all the films of system-V and system-VI using Wagner's polarization technique as discussed in Chapter 3 in which the value lies in between 0.95-0.97 which suggests that the charge transport in this system is predominantly ionic and contribution of electronic current to the total is negligible. Larger value of the transference number indicates that charge transport is dominant by ions in the NCGPE films.

Table-5.10: Ionic transference number for all the films of system-V and system-VI.

Sl. No.	Sample Name	Transference Number of system-V	Sample Name	Transference Number of system-VI
1.	PH0	0.95	PH0	0.95
2.	PH0.5	0.96	PHC0.5	0.95
3.	PH1.0	0.96	PHC1.0	0.96
4.	PH1.5	0.97	PHC1.5	0.96
5.	PH2.0	0.96	PHC2.0	0.96

5.3.4 Thermal Analysis

Fig. 5.42(a) shows that the initial weight loss of about 5-6 % discloses the evaporation process of the residual THF and acetone with elimination of impurities which is mainly due to fluorine compound from $LiClO_4$. Besides, the dehydration of moisture is also a contributor to this phenomenon as the tendency of polymer to absorb water from surrounding is quite high. According to the curves, the degradation of the electrolyte film PH1.5 starts at 340 °C with 21% weight loss. The second degradation occurs at 420 °C with 33% weight loss. The observed results indicate that upon increasing MWCNT content, the decomposition of film PH2.0 takes place at three stages. The thermal stability drops to temperature around 300 °C with 25% weight loss. The second decomposition occurs at 380 °C with modest weight loss of 19% which is followed by the final decomposition at 460 °C. Fig. 5.42(b) shows the DTG of the mass loss of system-V as a function of temperature which shows two important peaks at 349 °C and 467 °C for films PH1.5 indicating that the maximum decomposition process occurs at approximately 467 °C. There is an increase in the decomposition temperature with increase in the filler content from 0 to 1.5 wt.% in the P(VdF-HFP) based electrolytes.

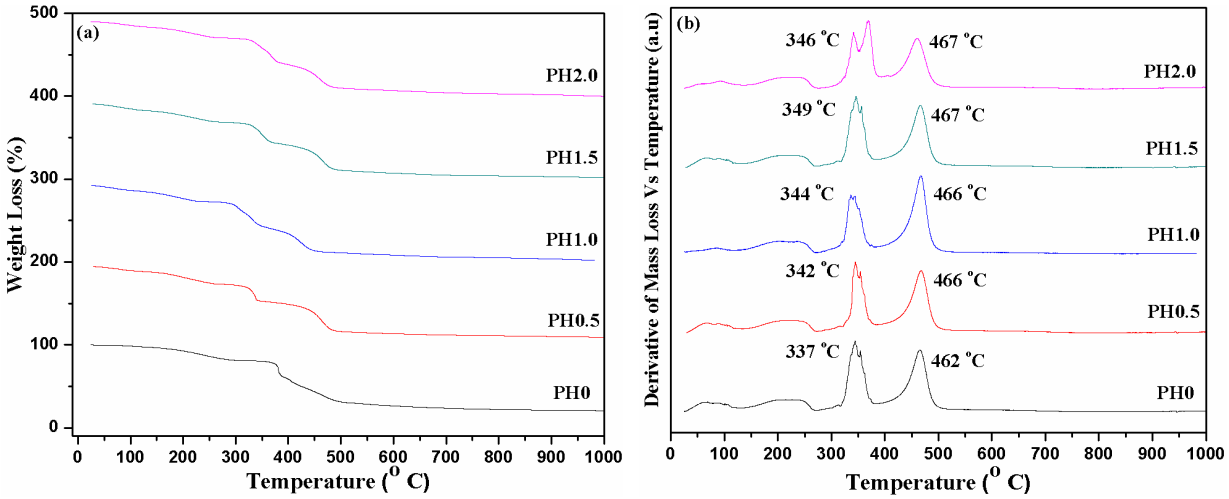

Fig. 5.42: (a) TG traces of films PH0, PH0.5, PH1.0, PH1.5 and PH2.0 of system-V; (b) DTG of films PH0, PH0.5, PH1.0, PH1.5 and PH2.0 of system-V.

Fig. 5.43(a) shows the TG analysis of system-VI. It is noticed that the degradation of film PHC1.5 starts at about 175 ºC and becomes stronger in the temperature range from 225 ºC to 350 ºC. Between 350 ºC and 425 ºC, there is a weak decrease of the mass of these samples as the

temperature is increased (below 5%). As the temperature is further increased, a secondary degradation process is ignited which is occurring in the temperature range from 425 ºC to 500 ºC. Further increase of the temperature of the sample above 500 ºC (up to 650 ºC) does not result in a significant drop of the mass of the film (Zhang et al, 2002). The derivative of weight loss versus temperature curves are given in Fig. 5.43(b) where the two important peaks at 346 °C and 466 °C, for the sample PHC1.5, indicating that the maximum decomposition process occurs at approximately 466 °C which is quite high as compared to film P0. In case of thermal degradation, the shift in the peak value is in accordance with the rule of mixture as one of the components (CNF) is having higher thermal stability. Enhancement of degree of crystallinity and restriction of molecular mobility around nanofiller will also play a role in this phenomenon.

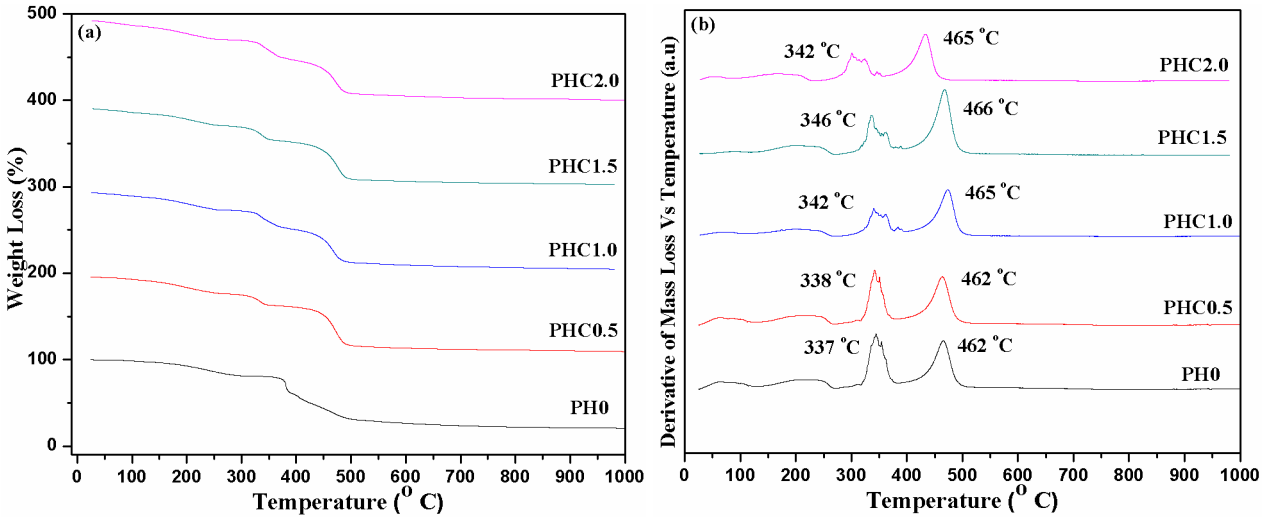

Fig. 5.43: (a) TG traces of films PH0, PHC0.5, PHC1.0, PHC1.5 and PHC2.0 of system-VI; (b) DTG of films PH0, PHC0.5, PHC1.0, PHC1.5 and PHC2.0 of system-VI.

5.3.5 Mechanical Analysis

Fig. 5.44(a) shows the stress-strain curves of films PH0, PH0.5, PH1.0, PH1.5 and PH2.0 of system-V in which film PH1.5 has maximum tensile strength of 39.4 MPa with elongation at break at 520% as compared to P0. Also, the area per unit volume i.e. toughness for PH1.5 is 2.989 Jcm^{-2}. Fig. 5.44(b) shows the stress-strain curves of films PH0, PHC0.5, PHC1.0, PHC1.5 and PHC2.0 of system-VI shows the maximum tensile strength of 43.2 MPa with an elongation of 362% and toughness of 2.891 Jcm^{-2} which is quiet high as compared to other samples of system-VI. Therefore, stress-strain measurements show a large enhancement of the yield strength and

toughness when passing from filler-free (P0) to NCGPE films. Here, both the sample PH1.5 of system-V and PHC1.5 of system-VI improves the adhesion between the polymer and nanofiller that exhibit excellent strength and % elongation properties.

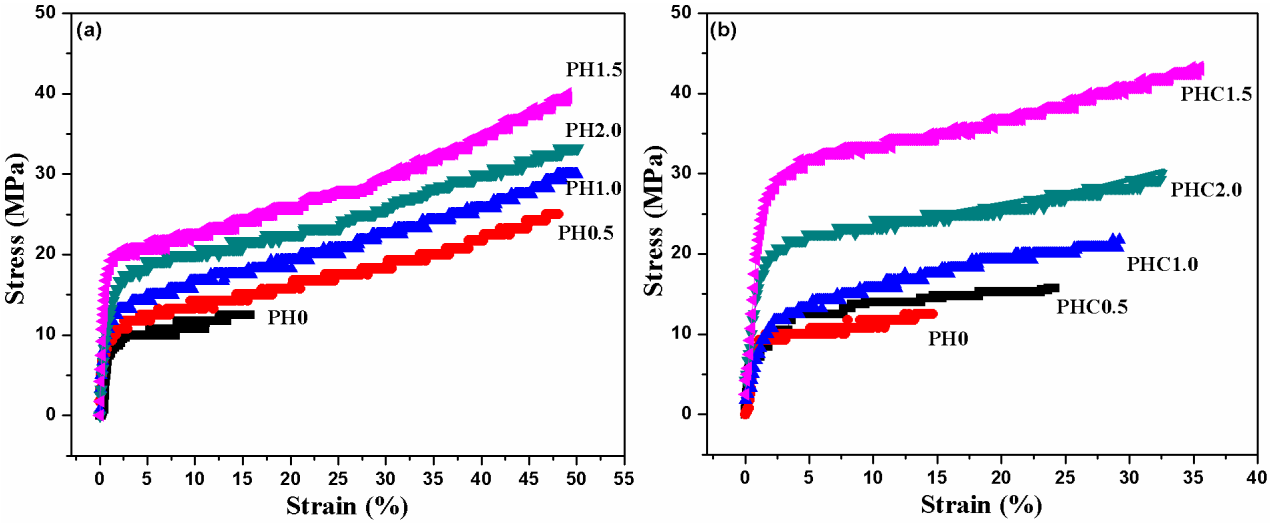

Fig. 5.44: Stress-strain plots of films (a) PH0, PH0.5, PH1.0, PH1.5 and PH2.0 of system-V; (b) PH0, PHC0.5, PHC1.0, PHC1.5 and PHC2.0 of system-VI.

5.3.6 Electrochemical Analysis

Fig 5.45 shows two important features that can be recognized from the trend of LSV curve. First, the current onset occurs at > 4.5 V versus Li, suggesting that polymer film has a high anodic stability. The second one is the very low current (0.0058 µA cm^{-2}) prior to the onset of anodic breakdown. Above this cell voltage, the current increased steeply as the applied voltage increased. This low residual current level up to 4.6 V for film PHC1.5 and 4.7 V for film PH1.5 with the absence of any peak on the low voltage range confirms the high purity of the electrolyte.

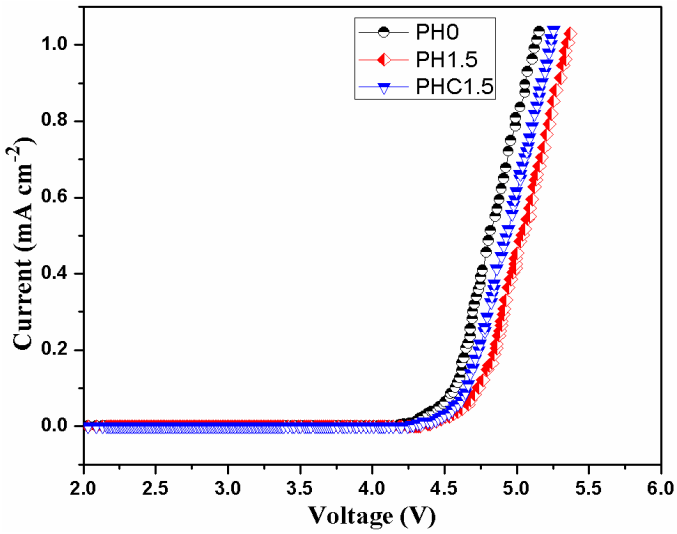

Fig. 5.45: LSV curve of films PH0, PH1.5 and PHC1.5.

5.4 P(VdF-HFP)-(PC+DEC)-$LiClO_4$-SiO_2 nanofiber and P(VdF-HFP)-(PC+DEC)-$LiClO_4$-TiO_2 nanofiber Systems

An attempt has been made in which P(VdF-HFP) based nanocomposite gel polymer electrolytes are synthesized using solution casting method using dispersoid SiO_2 nanofiber (diameter, 100-500 nm) in system-VII and TiO_2 nanofiber (diameter, 200-700 nm) in system-VIII. Following codes PHS2.0, PHS4.0, PHS6.0, PHS8.0, PHS10.0 and PHS12.0 were assigned to the films containing 2.0, 4.0, 6.0, 8.0, 10.0 and 12.0 wt.% SiO_2 nanofiber and other codes were PHT2.0, PHT4.0, PHT6.0, PHT8.0 and PHT10.0 assigned to the films containing 2.0, 4.0, 6.0, 8.0 and 10.0 wt.% of TiO_2 nanofiber respectively. The reason for dispersing SiO_2 nanofiber up to 12.0 wt.% and TiO_2 nanofiber up to 10.0 wt.% is that they become brittle after 10.0 wt.% and 8.0 wt.%. Mechanically stable free standing polymer electrolyte films of thickness from 0.17-0.22 mm were obtained after the solvent evaporation of as cast films.

5.4.1 Morphology and Structure of Nanocomposite Gel Polymer Electrolytes

Fig. 5.46(a and b) shows the FESEM micrographs of the cross section of film PHS10.0. The SiO_2 nanofiber are dispersed in disordered manner in the P(VdF-HFP) based polymer matrix with diameter ranging from 100-200 nm as shown in Fig 5.46(b).

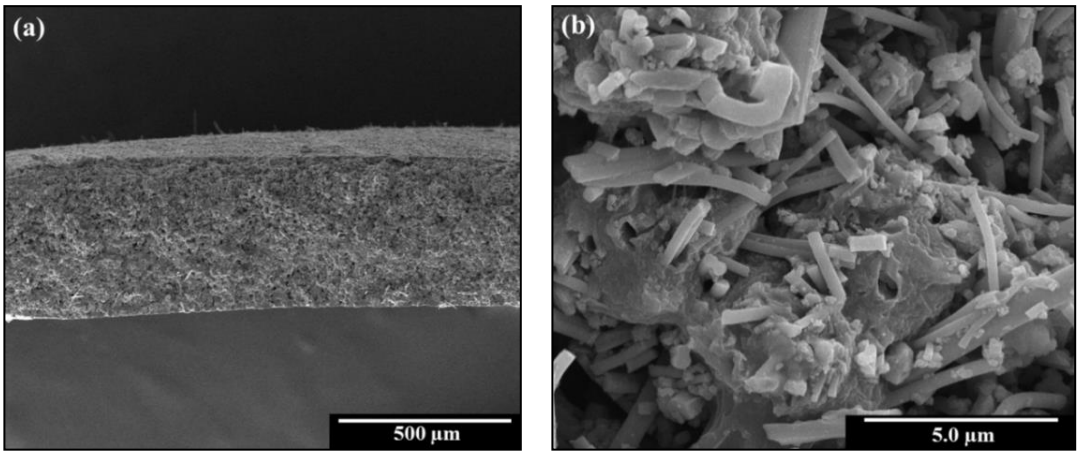

Fig. 5.46: (a and b) Typical FESEM micrographs of cross section of NCGPE film PHS10.0 at different magnifications.

Fig 5.47(a) shows that SiO_2 nanofiber are well dispersed in the matrix and SAD pattern (inset) shows amorphous nature of the film PHS10.0. Fig 5.47(b) shows the EDAX from TEM confirming the presence of constituent elements without any other impurities with inset of individual SiO_2 nanofiber.

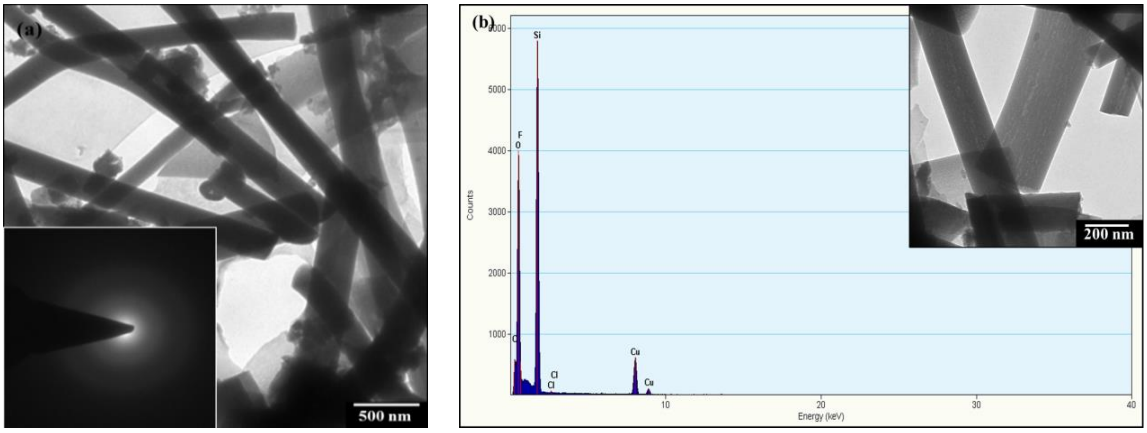

Fig. 5.47: (a) Typical TEM micrographs of film PHS10.0 with SAD pattern (inset); (b) EDAX pattern of film PHS10.0 with inset of individual SiO_2 nanofiber.

Fig 5.48(a and b) shows the cross section of film PHT8.0 The morphology indicating in Fig 5.48(b) shows that TiO_2 nanofiber is dispersed in disordered manner within the polymer matrix. The dispersed TiO_2 nanofiber play active role in the growth of highly porous microstructure with completely different morphology. Besides polymer-ion interaction, TiO_2 nanofiber with liquid

electrolyte (salt+plasticizer) interaction provides additional mechanism of ionic conductivity enhancement along the interface giving higher conductivity in NCGPE film (Maier, 1985; Kim et al, 2003).

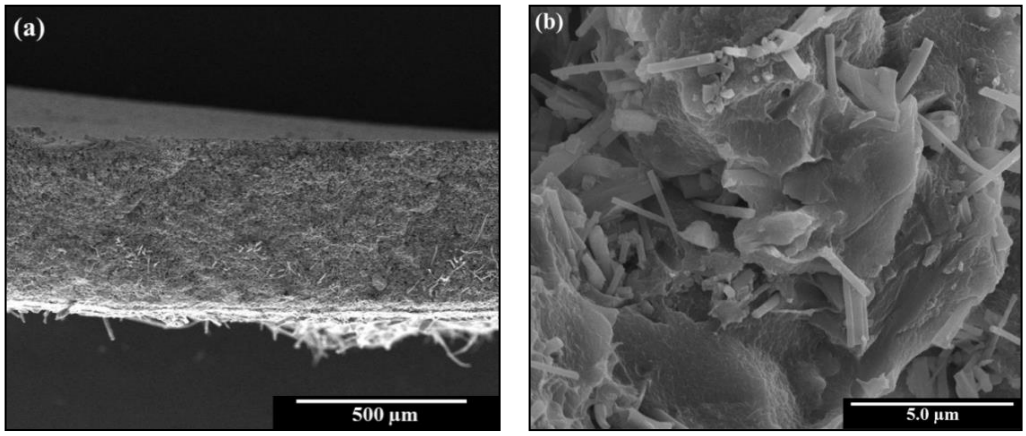

Fig. 5.48: (a and b) Typical FESEM micrographs of cross sections of the NCGPE film PHT8.0 at different magnifications.

The morphology and the interface between the TiO_2 nanofiber and the polymer matrix of the film PHT8.0 have been examined under TEM as shown in Fig. 5.49. TiO_2 nanofiber used as dispersoid is well dispersed in the polymer matrix and the SAD pattern (inset) in Fig 5.48(a) shows its amorphous nature. Fig 5.49(b) shows the EDAX of film PHT8.0 from TEM confirms the presence of constituent elements and inset showing diameter of 200-300 nm of TiO_2 nanofiber in the polymer matrix.

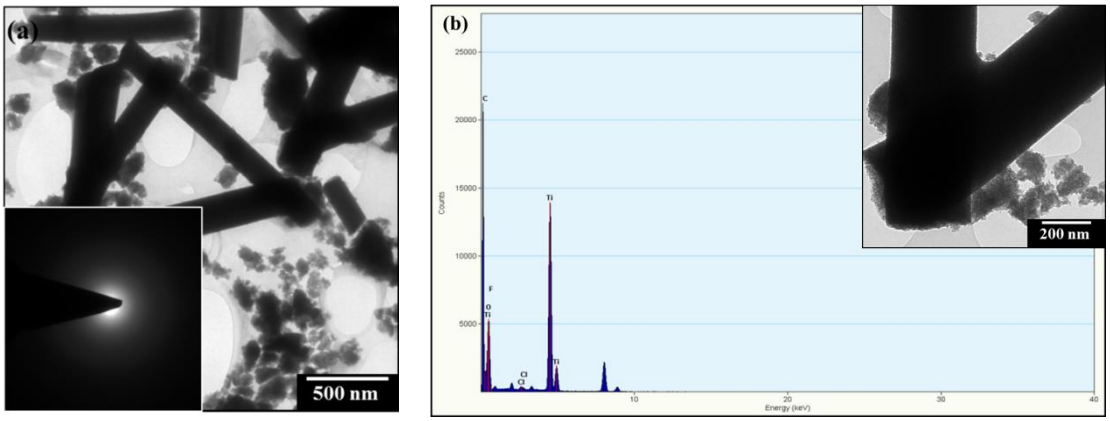

Fig. 5.49: (a) Typical TEM micrographs of film PHT8.0 with SAD pattern (inset); (b) EDAX pattern of the film PHT8.0 with inset at higher magnification.

Fig. 5.50 shows the XRD pattern of P(VdF-HFP), $LiClO_4$, SiO_2 nanofiber and TiO_2 nanofiber respectively. The XRD pattern of P(VdF-HFP) and salt $LiClO_4$ is same as discussed in previous subsection (5.3.1). The XRD pattern of SiO_2 nanofiber shows broad humps indicating its amorphous nature. The XRD peaks at 2θ = 24.5º, 38.3º, 47.5º, 54.4º, 62.5º, 69.4º, 74.6º and 82.7º for TiO_2 nanofiber correspond well with the (110), (101), (004), (200), (111), (210), (211) and (220) reflections of crystalline nature respectively (Abbrent et al, 2001).

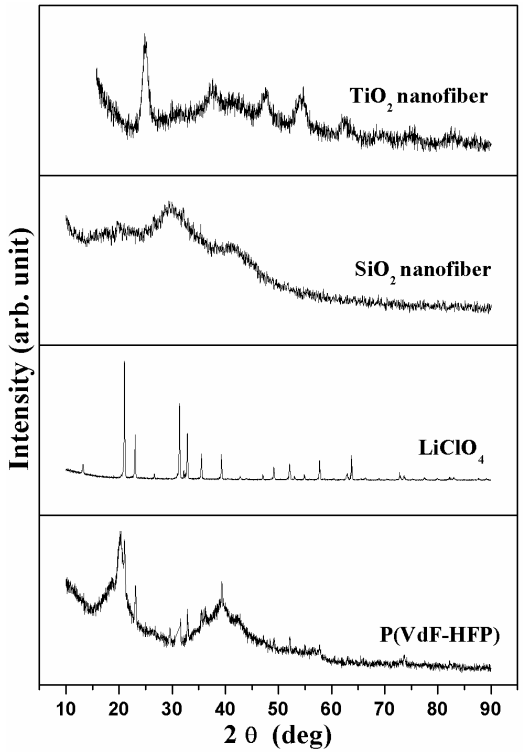

Fig. 5.50: XRD pattern of P(VdF-HFP), $LiClO_4$, SiO_2 nanofiber and TiO_2 nanofiber.

The X-ray diffraction pattern of NCGPE films with varying content of SiO_2 nanofiber are presented in Fig. 5.51(a) and with TiO_2 nanofiber are presented in Fig. 5.51(b) . It shows that the relative intensity decreases with increasing concentration of nanofibers, which suggests that the added nanofibers can lower the crystallinity of the polymer electrolytes. Moreover, the XRD pattern shows broad humps after adding nanofibers into polymer matrix which suggests that the NCGPE films may possess more amorphous areas for lithium-ion transfer. The interaction of P(VdF-HFP) chains between nanofibers may lead to lower crystallinity and rich amorphous phase for the NCGPEs.

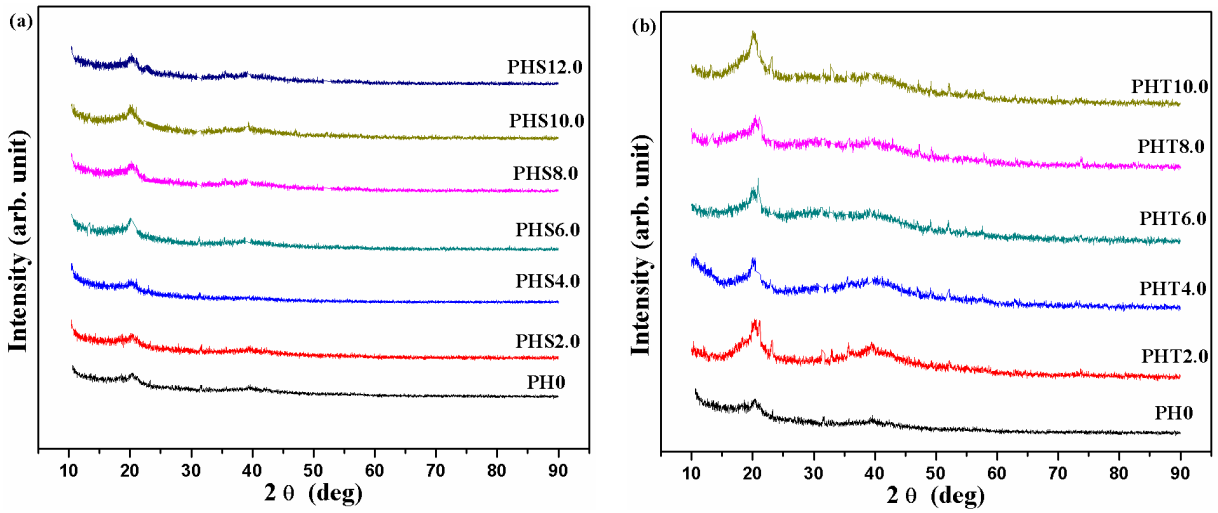

Fig. 5.51: XRD pattern of films (a) PH0, PHS2.0, PHS4.0, PHS6.0, PHS8.0, PHS10.0 and PHS12.0 of system-VII; (b) PH0, PHT2.0, PHT4.0, PHT6.0, PHT8.0 and PHT10.0 of system-VIII.

Following the relation, $\{K = (A/A_0) \times 100\}$, the calculated values of degree of crystallinity for both the system-VII and system-VIII are shown in below Table-5.11.

Table 5.11: Estimated value of degree of crystallinity for all the films of system-VII and system-VIII.

Sl. No.	Sample Name	Degree of Crystallinity of system-VII	Sample Name	Degree of Crystallinity of system-VIII
1.	PH0	22.4%	PH0	22.4%
2.	PHS2.0	19.5%	PHT2.0	20.1%
3.	PHS4.0	17.3%	PHT4.0	17.8%
4.	PHS6.0	14.9%	PHT6.0	15.2%
5.	PHS8.0	11.5%	PHT8.0	12.6%
6.	PHS10.0	6.9%	PHT10.0	14.4%
7.	PHS12.0	9.8%	-	-

5.4.2 Fourier Transform Infra-Red Spectroscopy

Fig. 5.52 shows the FTIR spectra of P(VdF-HFP), $LiClO_4$, SiO_2 nanofiber and TiO_2 nanofiber. The spectra of P(VdF-HFP) and $LiClO_4$ is same as discussed earlier in subsection (5.3.2). The

absorption bands of SiO_2 nanofiber appear at 1127 and 807 cm^{-1} corresponding to stretching of Si–O–Si bond and stretching mode of Si–O bond in Si–OH and bands of TiO_2 nanofiber appear at 1082 and 734 cm^{-1} corresponding to stretching mode of Ti–O–Ti and Ti–O bond.

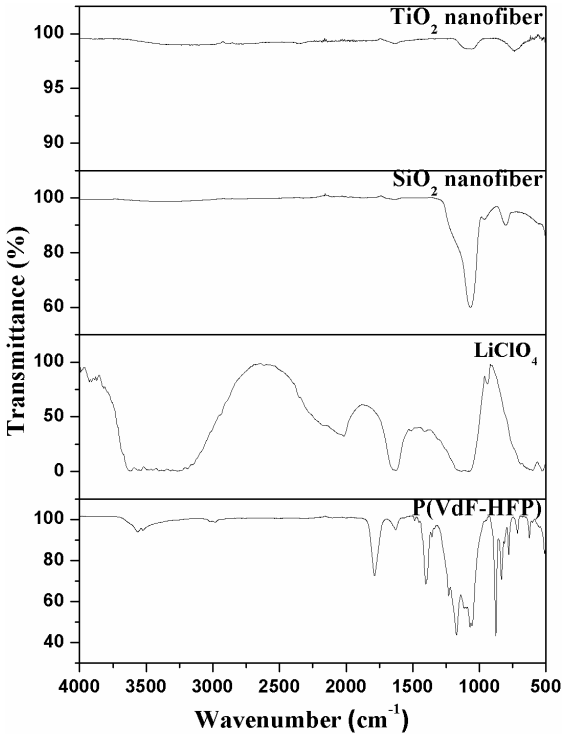

Fig. 5.52: FTIR spectra of P(VdF-HFP), $LiClO_4$, SiO_2 nanofiber and TiO_2 nanofiber.

It has been observed in Fig. 5.53(a) that for film P0, the vibrational peaks of P(VdF-HFP) appear at 3548, 1770, 1406, 881 and 801 cm^{-1} are shifted to 3568, 1790, 1408, 881 and 820 cm^{-1} respectively in the polymer electrolytes. The absorption peaks at 699 cm^{-1} and 557 cm^{-1} corresponding to C–Cl stretching are observed for the electrolyte material (Rajendran et al, 2001). Appearance of new peaks at 699 and 557 cm^{-1} in P0 indicates that polymer carbon atoms interact with chlorine of ClO_4^- ions. If one compares the FTIR response of P(VdF-HFP), $LiClO_4$ and SiO_2 nanofiber as such with the FTIR response of the SiO_2 dispersed P(VdF-HFP) based nanocomposite polymer electrolytes, the peak at 1790 cm^{-1} corresponding to $–CF=CF_2$ has shifted to a lower wave number i.e. 1784 cm^{-1} in nanocomposite electrolyte samples. The stretching of Si-O-Si bond at frequency 1127 cm^{-1} shifted to lower wavenumber i.e. 1046 cm^{-1} in all the nanocomposite electrolyte samples. The bond stretching frequency corresponding to O-H of P0 at 3547 cm^{-1} is further shifted to 3571 cm^{-1} in case of nanocomposite electrolyte films. The stretching mode of Si–O bond in Si–

OH bending vibrations at frequency 807 cm^{-1} has shifted to 771 cm^{-1}. The stretching mode of TiO_2 at frequency 1082 cm^{-1} shifted to a higher wavenumber i.e. 1084 cm^{-1} in all the nanocomposite samples as shown in Fig. 5.53(b). The bond stretching frequency corresponding to O–H of P(VdF-HFP) based electrolyte at 3547 cm^{-1} is further shifted to 3550 cm^{-1} in case of nanocomposite samples. The vibration mode of TiO_2 at frequency 734 cm^{-1} has shifted and merged with the peak of P(VdF-HFP) based electrolyte at 749 cm^{-1}. Shifting and appearance of new peaks suggest that the polymer-salt-filler interaction occurs in P(VdF-HFP) based gel polymer electrolytes.

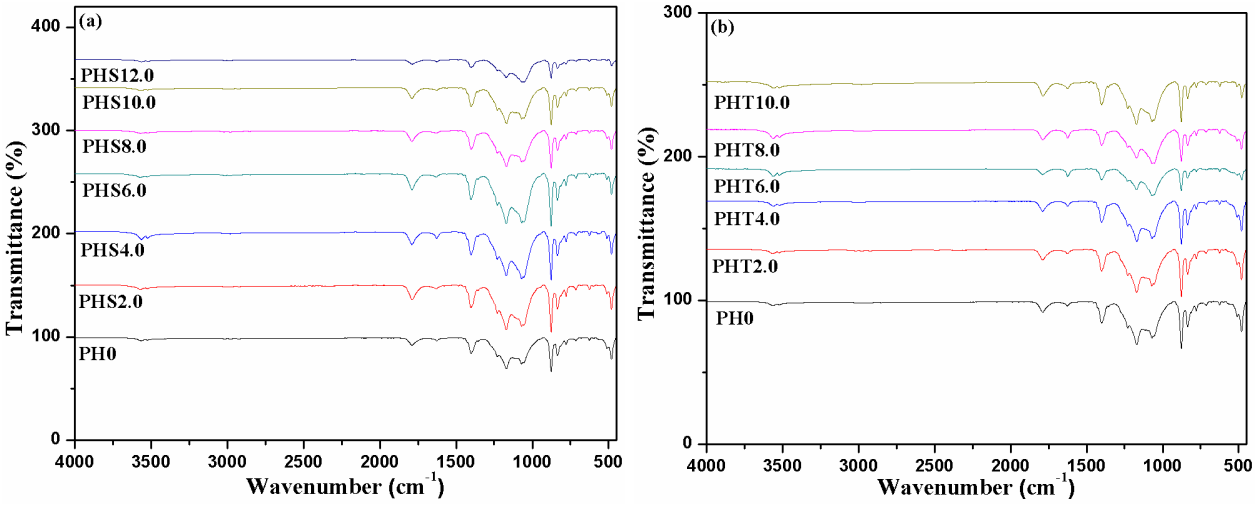

Fig. 5.53: FTIR spectra of films (a) PH0, PHS2.0, PHS4.0, PHS6.0, PHS8.0, PHS10.0 and PHS12.0 of system-VII; (b) PH0, PHT2.0, PHT4.0, PHT6.0, PHT8.0 and PHT10.0 of system-VIII.

5.4.3 Ionic Conductivity Measurement/Electrochemical Impedance Spectroscopy

The typical Nyquist plots of P(VdF-HFP) based nanocomposite gel polymer electrolytes at room temperature are shown in Fig. 5.54(a and b). As discussed in the previous subsection (5.3.3) that the use of series CPE terms tilts the spike and parallel CPE terms depress the semicircle. The ionic conductivity of polymer electrolytes is calculated from $\{\sigma = l/(R_b r^2 \pi)\}$, where l and r represent thickness and radius of the electrolyte discs respectively. R_b is the bulk resistance of the gel electrolyte obtained from complex impedance measurements (Abraham et al, 1997).

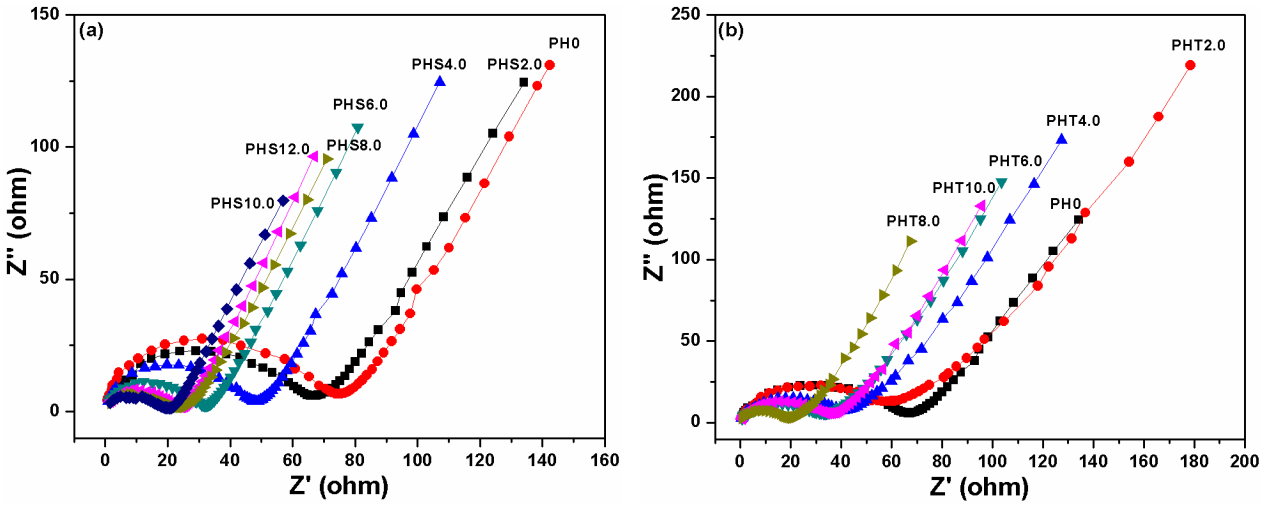

Fig. 5.54: Nyquist plots of films (a) PH0, PHS2.0, PHS4.0, PHS6.0, PHS8.0, PHS10.0 and PHS12.0 of system-VII; (b) PH0, PHT2.0, PHT4.0, PHT6.0, PHT8.0 and PHT10.0 of system-VIII.

It was found that for system-VII, the highest ionic conductivity achieved for the film PHS10.0 is 4.39×10^{-2} Scm^{-1} whereas film PHT8.0 gives maximum conductivity 1.52×10^{-2} Scm^{-1} for system-VIII at room temperature which is quite high. These conductivity values are over one order higher as compared to that for polymer electrolyte without nanofiber (PH0) as shown in Table-5.12.

Table-5.12: Estimated value of conductivity for all the films of system-VII and VIII.

Sl. No.	Sample Name	Conductivity Value (Scm^{-1}) of system-VII	Sample Name	Conductivity Value (Scm^{-1}) of system-VIII
1.	PH0	1.76×10^{-4}	PH0	1.76×10^{-4}
2.	PHS2.0	6.98×10^{-4}	PHT2.0	3.77×10^{-4}
3.	PHS4.0	3.58×10^{-3}	PHT4.0	2.42×10^{-3}
4.	PHS6.0	7.65×10^{-3}	PHT6.0	6.88×10^{-3}
5.	PHS8.0	2.07×10^{-2}	PHT8.0	1.52×10^{-2}
6.	PHS10.0	4.39×10^{-2}	PHT10.0	7.03×10^{-3}
7.	PHS12.0	9.76×10^{-3}	-	-

At low ceramic nanofiber concentrations up to 10.0 wt.% as shown in Fig. 5.55(a), the conductivity increases with SiO_2 nanofiber content basically due to the increase in amount of the conductive layers. When the content of the SiO_2 nanofiber exceeds 10.0 wt.% then the value of

conductivity of NCGPE reduced because it becomes brittle. The variation of ionic conductivity as a function of TiO_2 nanofiber is shown in Fig. 5.55(b). The enhancement up to a certain concentration (8.0 wt.%) seems to be correlated with the fact that the dispersion of TiO_2 nanofiber to the polymer matrix prevents chain reorganization due to the high aspect ratio of nanofiber resulting in reduction in polymer crystallinity that gives rise to an increase in ionic conductivity. The reduction in crystallinity upon addition of TiO_2 nanofiber up to 8.0 wt.% is consistent with XRD results which were discussed before. Increased amorphicity in the electrolytes, which gives rise to higher conductivity, is also attributed to addition of salt, nanofiber and solvent (Stephan, 2002).

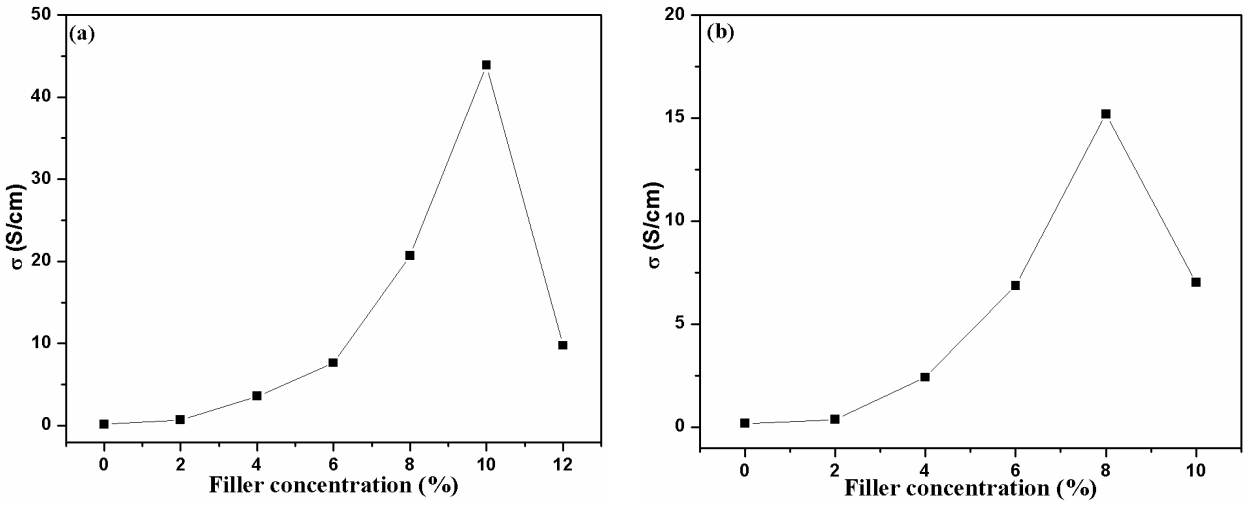

Fig. 5.55: Conductivity (Scm^{-1}) versus filler concentration (wt.%) of (a) system-VII; (b) system-VIII.

Fig. 5.56(a) shows the conductivity versus temperature inverse plots of films PH0, PHS2.0, PHS4.0, PHS6.0, PHS8.0, PHS10.0 and PHS12.0 of system-VII and Fig 5.56(b) shows the conductivity versus temperature inverse plots of films PH0, PHT2.0, PHT4.0, PHT6.0, PHT8.0 and PHT10.0 of system-VIII. Slightly bent pattern of the curves in both the system-VII and VIII indicates that ionic conduction in NCGPEs that obeys the VTF relation, which describes the transport properties in amorphous matrix (Hayamizu et al, 2000).

It supports the idea that the ions move through the solvent rich phase, which provides the conducting path and involves the salt and oxide nanofiber. An increase in conductivity with the addition of up to 10.0 wt.% of SiO_2 nanofiber and 8.0 wt.% of TiO_2 nanofiber could be attributed

to the enhancement of the capability of holding the liquid electrolytes since nanofiber supports the formation of porous microstructure (Lee et al, 2003). The enhancement in ionic conductivity due to the addition of oxide nanofiber has been explained by an improved effective-medium theory (Wieczorek et al, 1998).

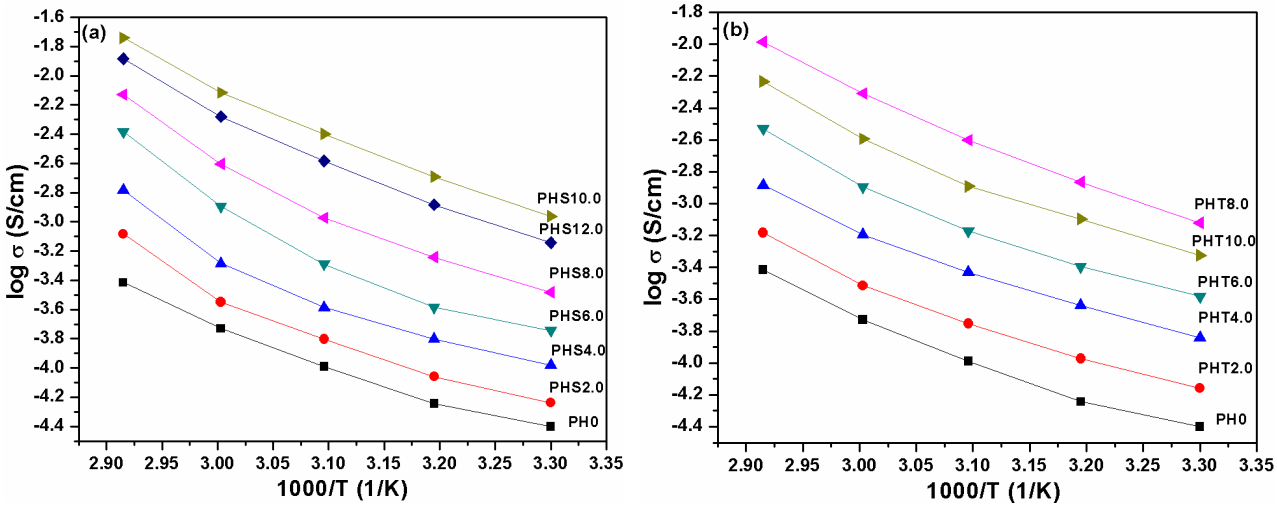

Fig. 5.56: Temperature dependent ionic conductivity of films (a) PH0, PHS2.0, PHS4.0, PHS6.0, PHS8.0, PHS10.0 and PHS12.0 of system-VII; (b) PH0, PHT2.0, PHT4.0, PHT6.0, PHT8.0 and PHT10.0 of system-VIII.

Total ionic transference number for all the films of system-VII and VIII was measured by Wagner's polarization technique which is used to determine the ionic contribution to the total charge transport by measuring the residual electronic current passing through the electrolytes. High value of transport number from 0.95 to 0.99 as shown in Table-5.13 suggests that the charge transport in this polymer electrolyte systems is predominantly ionic accompanied by mass transport and electronic contribution to the total current negligible.

Table-5.13: Ionic transference number for all the films of system-VII and VIII.

Sl. No.	Sample Name	Transference Number of system-VII	Sample Name	Transference Number of system-VIII
1.	PH0	0.95	PH0	0.95
2.	PHS2.0	0.95	PHT2.0	0.96
3.	PHS4.0	0.97	PHT4.0	0.96
4.	PHS6.0	0.98	PHT6.0	0.97
5.	PHS8.0	0.98	PHT8.0	0.97
6.	PHS10.0	0.99	PHT10.0	0.95
7.	PHS12.0	0.97	-	-

5.4.4 Thermal Analysis

Fig 5.57(a) shows the TG traces of films PH0, PHS2.0, PHS4.0, PHS6.0, PHS8.0, PHS10.0 and PHS12.0. The film PH0 is stable up to 268 ºC as discussed in Chapter 4. But with the addition of SiO_2 nanofiber, the first step of degradation for film PHS10.0 occurred roughly from 120 ºC to 370 ºC and the maximum decomposition temperature was at 250 ºC to 360 ºC. The second step degradation occurred from about 370 ºC to 600 ºC and the maximum decomposition temperature from 420 ºC to 470 ºC. The above discussion indicates that the thermal stability of NCGPEs was improved. It was believed that the SiO_2 nanofiber on the surface of the polymer could create a passive layer during thermal degradation process. Additionally, SiO_2 nanofiber could also act as mass transport barrier to the volatile by-products generated during the thermal decomposition, leading to the improvement on thermal stability of nanocomposite electrolytes. Fig. 5.57(b) shows DTG curve for film PHS10.0 which shows two important peaks at 356 °C and 466 °C indicating that the maximum decomposition process occurs at approximately 466 °C. There is an increase in the decomposition temperature with increase in the nanofiber content from 2.0 to 10.0 wt.% in the P(VdF-HFP) based gel polymer electrolytes and film PHS10.0 shows maximum thermal stability.

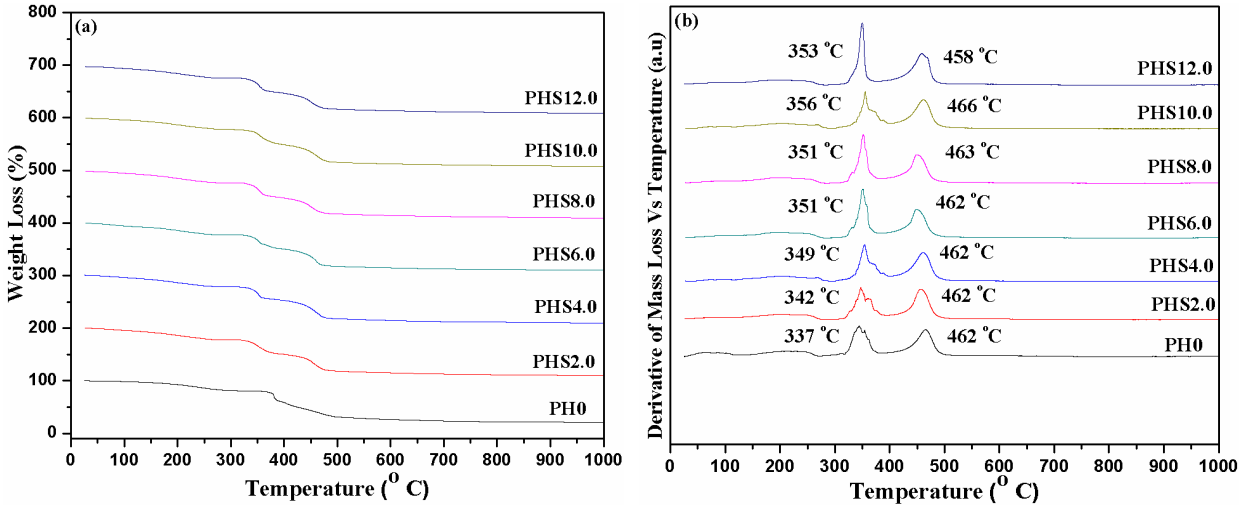

Fig. 5.57: (a) TG traces of films PH0, PHS2.0, PHS4.0, PHS6.0, PHS8.0, PHS10.0 and PHS12.0 of system-VII and (b) DTG of films PH0, PHS2.0, PHS4.0, PHS6.0, PHS8.0, PHS10.0 and PHS12.0 of system-VII.

Fig. 5.58(a) presents TG traces of films PH0, PHT2.0, PHT4.0, PHT6.0, PHT8.0 and PHT10.0. It has been found that there are three steps ranging from 150 °C to 500 °C of film PHT8.0. At approximately 150 °C, there is a 15 % weight loss in TG curve. Such weight loss can be ascribed to the volatilization of solvent THF. The further weight loss is approximately 12-19 % which occurs at 300 °C to 380 °C. From 380 °C to 500 °C, there exists a continuous and broad weight loss process which is about 23% of weight loss. TG characterization shows that there is no phase transition in the studied temperature range from 600 °C to 1000 °C. Fig. 5.58(b) shows the derivative of the mass loss of the films PH0, PHT2.0, PHT4.0, PHT6.0, PHT8.0 and PHT10.0 as a function of temperature. The curve of film PHT8.0 shows important peaks at 348 °C and 465 °C indicating that the maximum decomposition process occurs at ~ 465 °C. Therefore, film PHT8.0 has better thermal stability than film P0.

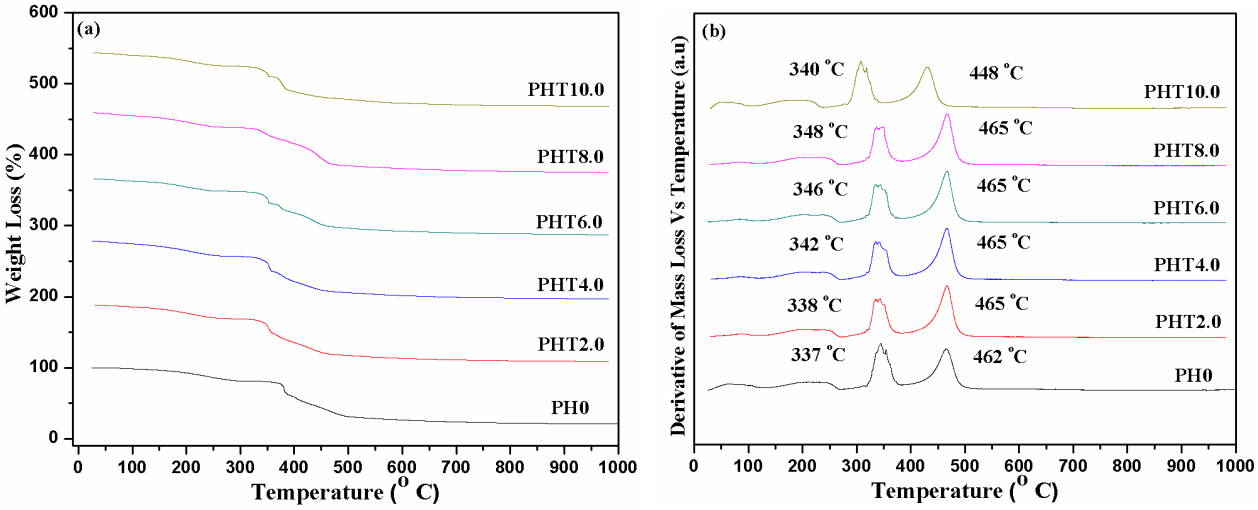

Fig. 5.58: (a) TG traces of films PH0, PHT2.0, PHT4.0, PHT6.0, PHT8.0 and PHT10.0 of system-VIII; (b) DTG of films PH0, PHT2.0, PHT4.0, PHT6.0, PHT8.0 and PHT10.0 of system-VIII.

5.4.5 Mechanical Analysis

Fig. 5.59(a) shows the stress-strain curves of all films of system-VII. The film PHS10.0 exhibited tensile strength of 39.9 MPa with an elongation-at-break value of 29.9% which is quite high. Also the area under curve i.e. toughness value of film PHS10.0 is 2.987 Jcm^{-2} which means films containing SiO_2 nanofiber (10.0 wt.%) is more flexible in nature and can tolerate more stress. In system VIII as shown in Fig. 5.59(b), the film PHT8.0 shows maximum tensile strength of 39.7 MPa with an elongation-at-break value of 324%. With the character of small size and large surface, the TiO_2 nanofiber can contact with the polymer chains adequately, which can absorb the impact forces and prevent further expansion of the crack of the materials. Therefore, NCGPE films have got good mechanical stability with the addition of nanofiber in both the system-VII and VIII.

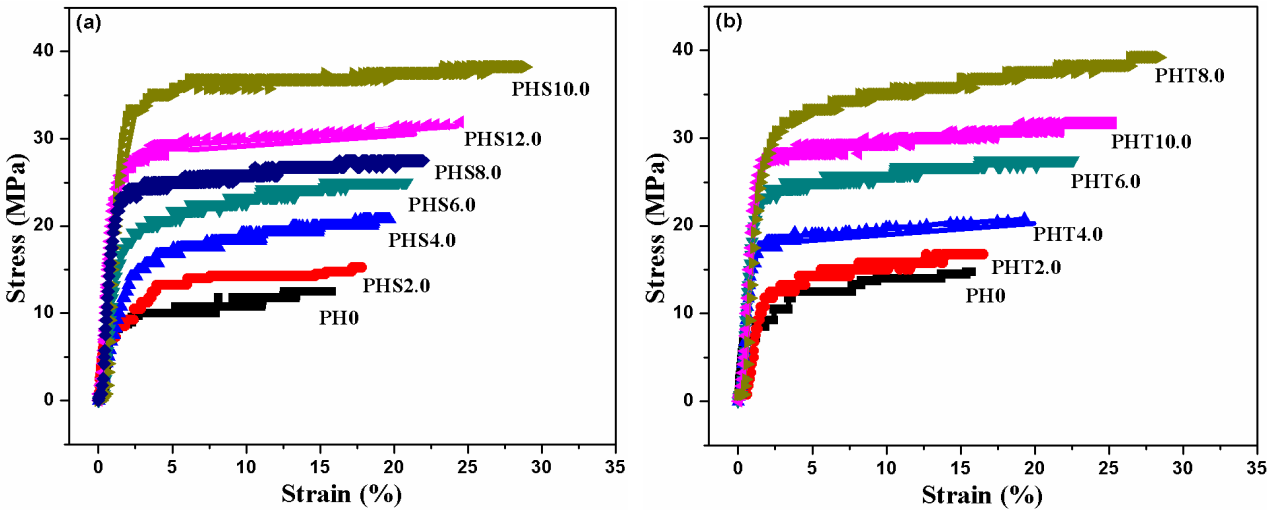

Fig. 5.59: Stress-strain plot of films (a) PH0, PHS2.0, PHS4.0, PHS6.0, PHS8.0, PHS10.0 and PHS12.0 of system-VII; (b) PH0, PHT2.0, PHT4.0, PHT6.0, PHT8.0 and PHT10.0 of system-VIII.

5.4.6 Electrochemical Analysis

For rechargeable Li-ion batteries, the instability in the electrolyte is known to bring out irreversible reactions and capacity fading. Therefore, the electrochemical stability of an electrolyte is one of the essential parameter. It is evident from Fig. 5.60 that there is no electrochemical reaction in the potential range 3.0-4.5 V. It is found that the current onset of film PHS10.0 occurs at around 4.9 V vs. Li/Li^+, slightly higher than the data of the film PH0 (around 4.5 V), which means it has a high anodic stability and the film PHT8.0 gives 4.8 V. Therefore, it may be concluded that the addition of nanofiber can improve the electrochemical stability of the NCGPEs due to its electrochemical inertness.

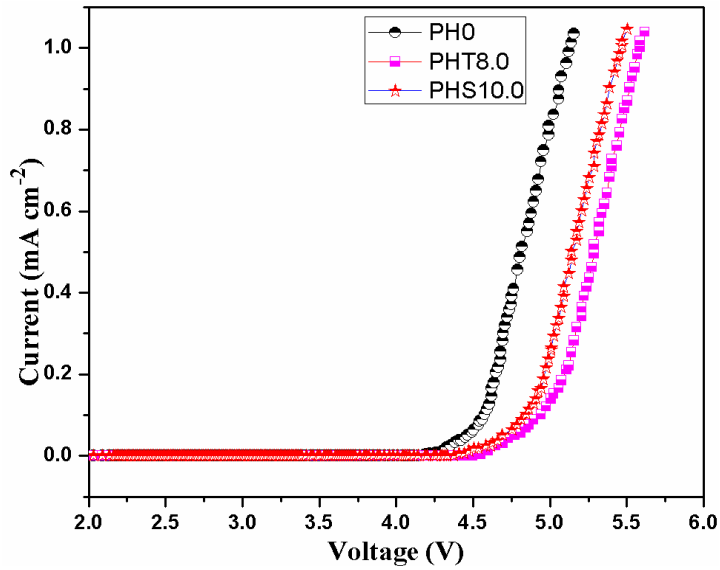

Fig. 5.60: LSV curve of films PH0, PHS10.0 and PHT8.0.

5.5 Discussion

The ionic conductivities presented in Table-5.2 and 5.6 confirm that the films P2.0 (with 2.0 wt.% MWCNT dispersion), PC2.0 (2.0 wt.% CNF), PS10.0 (10.0 wt.% SiO_2 nanofiber) and PT8.0 (8.0 wt.% TiO_2 nanofiber) show highest value of ionic conductivity in the respective systems with enhanced thermal stability. The plot between filler concentration and stress for a given strain of 10% as shown in Fig 5.61(a and b) shows that with the increase in nanofiller content, the stress bearing capacity of the NCGPEs increases. The electrochemical stabilities of NCGPEs show the improvement in the following order of sequence PC2.0 < P2.0 < PT8.0 < PS10.0. Therefore, the electrochemical potential window 4.6 V for PS10.0 is quite good for the application in Li-ion batteries.

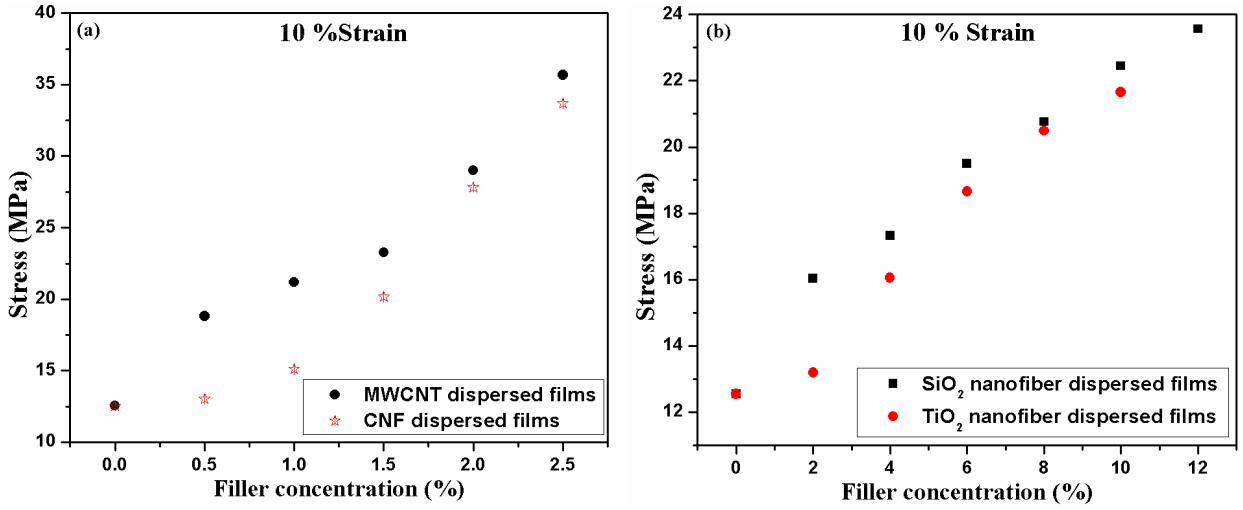

Fig. 5.61: Filler concentration (%) vs Stress (MPa) at constant strain of 10% for PMMA based gel polymer electrolytes dispersed with (a) MWCNT and CNF; (b) SiO_2 and TiO_2 nanofibers.

In last four systems, P(VdF-HFP) is dispersed with four different types of dispersoids (MWCNT, CNF, SiO_2 nanofiber, TiO_2 nanofiber). The ionic conductivities presented in Table-5.9 and 5.12 confirm that the films PH2.0 (with 2.0 wt.% MWCNT dispersion), PHC2.0 (2.0 wt.% CNF), PHS10.0 (10.0 wt.% SiO_2 nanofiber) and PHT8.0 (8.0 wt.% TiO_2 nanofiber) show highest value of ionic conductivity in the respective systems with enhanced thermal stability. The plot between filler concentration and stress for a given strain of 10% as shown in Fig 5.62(a and b) shows that with the increase in nanofiller content, the stress bearing capacity of the NCGPEs increases. The electrochemical stabilities of NCGPEs show the improvement in the following order of sequence PHC2.0 < PH2.0 < PHT8.0 < PHS10.0. Therefore, the electrochemical potential window 4.9 V for PHS10.0 is quite good for the application in Li-ion batteries.

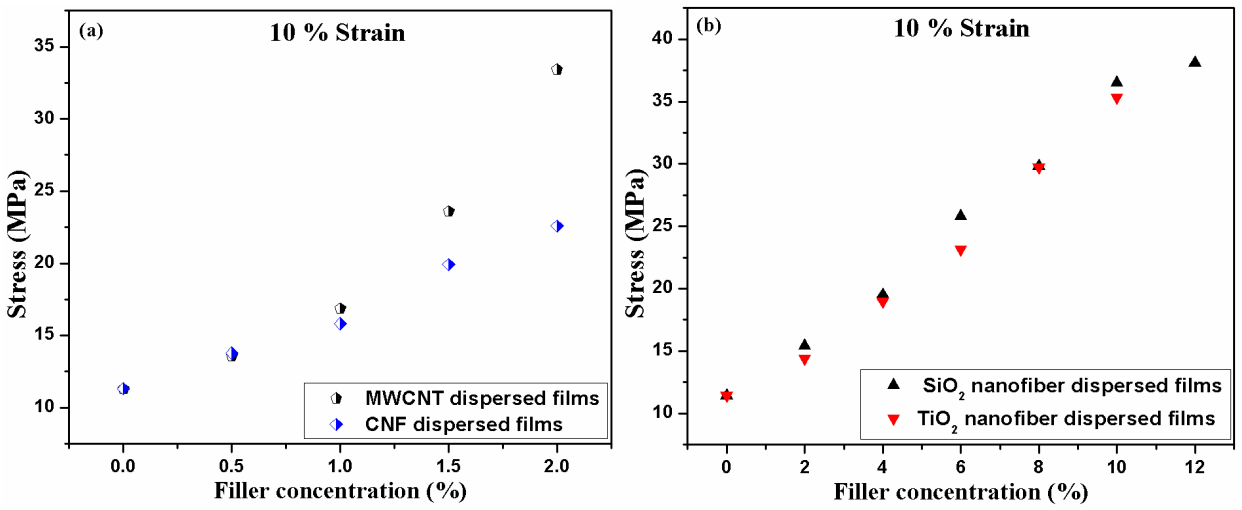

Fig. 5.62: Filler concentration (%) vs Stress (MPa) at constant strain of 10 % for P(VdF-HFP) based gel polymer electrolytes dispersed with (a) MWCNT and CNF; (b) SiO_2 and TiO_2 nanofibers.

From the above discussion of all the total eight systems, it is summarised that the systems having P(VdF-HFP) based nanocomposite gel polymer electrolytes have more ionic, thermal, mechanical and electrochemical properties than that of PMMA based gel polymer electrolytes.

Chapter 6

Conclusions and Future Scope

Chapter 6

Conclusions and Future Scope:

This present investigation is on GPEs in the systems PMMA-(PC+DEC)-$LiClO_4$ and P(VdF-HFP)-(PC+DEC)-$LiClO_4$ which were synthesized by solution casting method. NCGPEs are prepared using various types of dispersoids (MWCNT, CNF, SiO_2 nanofiber and TiO_2 nanofiber) by ultrasonication and solution casting in order to explore their potential for application in the electrolyte of Li-ion batteries in place of liquid electrolytes. The results have been discussed in Chapter 4 and Chapter 5. This chapter presents the major conclusions with a possible future scope of research in this area. The major conclusions are as follows:

A. Gel Polymer Electrolytes

1. The porous structure of P(VdF-HFP) based system shows higher ionic conductivity due to its solvent retention ability.
2. XRD analysis reveals that GPEs have lower degree of crystallinity than their corresponding base polymers. Reduction of crystallinities from 31.8% to 30.2% and from 26.6% to 22.4% are found for PMMA based and P(VdF-HFP) based electrolytes respectively. Therefore, amorphicity is relatively larger in P(VdF-HFP) based electrolyte than PMMA based electrolyte.
3. The peaks in the FTIR spectra at 2921 and 1729cm^{-1} in PMMA based gel polymer electrolytes and at 699 and 557 cm^{-1} in P(VdF-HFP) based gel polymer electrolytes could be ascribed to C–Cl stretching vibration. This indicates that carbon atoms in the polymer chains interact with chlorine of ClO_4^- ions suggesting interaction between polymer and the salt.
4. Ionic conductivities of PMMA based and P(VdF-HFP) based gel polymer electrolytes are found 0.13×10^{-4} Scm^{-1} and 1.76×10^{-4} Scm^{-1} respectively. Higher ionic conductivity in P(VdF-HFP) based electrolyte is attributed to higher amorphicity due to steric hindrance provided by bulky pendant $–CF_3$ group in HFP monomer unit of the copolymer. Higher amorphicity also provides higher flexibility to the polymer chains which may facilitate the conductivity rise.

5. PMMA based and P(VdF-HFP) based gel polymer electrolytes show thermal stabilities up to 220 ºC and 268 ºC, maximum tensile strength of 13.4 MPa and 23.7 MPa and electrochemical stabilities at 4.2 V and 4.5 V respectively. Therefore, the thermal, mechanical and electrochemical properties of P(VdF-HFP) based gel polymer electrolyte are superior to PMMA based gel polymer electrolyte.

B. **Nanocomposite Gel Polymer Electrolyte Systems**

NCGPEs were prepared on the two types of GPEs mentioned in the previous section with different types of dispersoids (MWCNT, CNF, SiO_2 nanfiber and TiO_2 nanofiber) with several compositions to study the effect of dispersoid type and its quantity on the properties under investigation of the NCGPEs. In all the cases NCGPEs show enhancment in ionic conductivity, thermal stability and mechanical strength along with desirable electrochemical characteristics in relation to their GPEs bases. A total of eight systems were prepared for NCGPEs and studied. Four systems identified as I, II, III and IV using MWCNT, CNF, SiO_2 nanofiber and TiO_2 nanofiber respectively are on PMMA based gel polymer electrolytes and the other four systems named as V, VI, VII and VIII using MWCNT, CNF, SiO_2 nanofiber and TiO_2 nanofiber respectively are of P(VdF-HFP) based gel polymer electrolytes.

1. In the systems I and II, NCGPE films P2.0 (with 2.0 wt.% MWCNT dispersion) and PC2.0 (2.0 wt.% CNF) show highest conductivities of 2.52×10^{-4} Scm^{-1} and 2.18×10^{-4} Scm^{-1} along with highest transference numbers of 0.95 and 0.93 respectively. The degrees of crystallinity are found 17.9% and 18.6% for the films of P2.0 and PC2.0 respectively. The maximum tensile strengths of 68.4 MPa and 66.7 MPa, thermal stabilities up to 300 ºC and 297 ºC and electrochemical stabilities window at 4.4 V and 4.3 V are found for P2.0 and PC2.0 respectively.
2. In the systems III and IV, NCGPE films PS10.0 (10.0 wt.% SiO_2 nanofiber) and PT8.0 (8.0 wt.% of TiO_2 nanofiber) show highest conductivities of 3.19×10^{-3} Scm^{-1} and 2.38×10^{-3} Scm^{-1} along with highest transference numbers of 0.96 and 0.95 respectively. The degrees of crystallinity are found 13.8% and 16.5% for the films of PS10.0 and PT8.0 respectively. The maximum tensile strength of 28.4 MPa and 28.2 MPa, thermal stabilities up to 347 ºC and 304 ºC and electrochemical stabilities window at 4.6 V and 4.5 V are found for PS10.0 and PT8.0 respectively.

3. In the systems V and VI, NCGPE films PH1.5 (1.5 wt.% MWCNT) and PHC1.5 (1.5 wt.% CNF) show highest ionic conductivities of 1.41×10^{-3} Scm^{-1} and 1.01×10^{-3} Scm^{-1} along with highest transference numbers of 0.97 and 0.96 respectively. The degrees of crystallinity are found 15.6% and 16.1% for the films of PH1.5 and PHC1.5 respectively. The maximum tensile strength of 39.4 MPa and 43.2 MPa, thermal stabilities up to 467 ºC and 466 ºC and electrochemical stabilities window at 4.7 V and 4.6 V are found for PH1.5 and PHC1.5 respectively.
4. In the systems VII and VIII, NCGPE films PHS10.0 (10.0 wt.% SiO_2 nanofiber) and PHT8.0 (8.0 wt.% of TiO_2 nanofiber) show highest ionic conductivities of 4.39×10^{-2} Scm^{-1} and 1.52×10^{-2} Scm^{-1} along with highest transference numbers of 0.99 and 0.97 respectively. The degrees of crystallinity are found 6.9% and 12.6% for the films of PHS10.0 and PHT8.0 respectively. The maximum tensile strength of 39.9 MPa and 39.7 MPa, thermal stabilities up to 466 ºC and 465 ºC and electrochemical stabilities window at 4.9 V and 4.8 V are found for PHS10.0 and PHT8.0 respectively.
5. P(VdF-HFP) based nanocomposite gel polymer electrolyte systems give better ionic conductivity, thermal stability, mechanical strength and electrochemical performance than those of PMMA based nanocomposite gel polymer electrolyte systems.

Future Scope:

There is a vast scope of further development of high ion conducting gel polymer electrolyte materials for high energy density lithium battery. Undesired reactions that may take place between the battery components and the liquid organic electrolyte. Such reactions may lead to unpredictable events such as short circuiting or local overheating. It has been contemplated by the researchers that ionic-liquid based lithium-ion-conducting polymer electrolytes may greatly reduce the risk of thermal runaway since ionic liquids are practically non-flammable. It provides the lithium battery the level of safety which is required for their large-scale applications. Extensive work for testing of ionic liquids as new electrolyte media for the future is in progress worldwide. In polymer electrolytes both cation and anion contribute to the overall conductivity, where not only lithium ions but also their counter ions migrate during the charging and discharging processes of a battery. This causes concentration polarization by accumulation of anions on the anode and ultimately leads to the premature failure of the battery. Intensive research on single cationic polymer

electrolytes is under way, but researchers are far away from achieving the goal. Also to achieve a better property of the nanocomposite polymer electrolytes, the nanofillers have to be dispersed uniformly within the polymer matrix. Sometimes use of high energy ultrasonication is not sufficient to develop the uniform dispersion of nanofillers. Agglomeration of the nanofillers can be avoided by using of surfactant and or functionalization of the fillers. Swift heavy ion irradiation on nanocomposite gel polymer electrolytes has another great avenue for enhancing their properties and is a potential research field both from theoretical and practical points of view.

References

[1] Abbrent, S., Plestil, J., Hlavata, D., Lindgren, J., Tegenfeldt, J. and Wendsjo, A., Crystallinity and morphology of PVdF-HFP-based gel electrolytes, Polymer, 42 (2001) 1407.

[2] Abraham, K.M. and Alamgir, M., Li^+-conductive solid polymer electrolytes with liquid-like conductivity, J. Electrochem. Soc., 137 (1990) 1657.

[3] Abraham, K.M. and Alamgir, M., Solid electrolytes, US Patent No. 5219679, (1993).

[4] Abraham, K.M., Jiang, Z. and Carroll, B., Highly conductive PEO-like polymer electrolytes, Chem. Mater., 9 (1997) 1978.

[5] Adam, G. and Gibbs, J.H., On the temperature dependence of cooperative relaxation properties in glass forming liquids, J. Chem. Phys., 43 (1965) 139.

[6] Agrawal, R.C. and Pandey, G.P., Solid polymer electrolytes: materials designing and all-solid-state battery applications: an overview, J. Phys. D: Appl. Phys., 41 (2008) 223001.

[7] Alagarasi, A., Introduction to nanomaterials, Vishwanathan, B., ed., Nanomaterials, Narosa Publishing House (2009).

[8] Alamgir, M. and Abraham, K.M., Lithium batteries:new materials, development and perspectives, G. Pistoia, ed., Elsevier, Amsterdam, (1994) 93.

[9] Angell, C.A. and Sichina, W., Thermodynamics of glass transition: Empirical aspects, Ann. N.Y. Acad. Sc., 279 (1976) 53.

[10] Angell, C.A., Liu, C. and Sanchez, E., Rubbery solid electrolytes with dominant cationic transport and high ambient conductivity, Nature, 362 (1993) 137.

[11] Appetecchi, G.B. and Scrosati, B., A lithium ion polymer battery, Electrochim. Acta, 43 (1998) 1105.

[12] Appetecchi, G.B., Croce, F. and Scrosati, B., Kinetics and stability of the lithium electrode in poly(methylmethacrylate)-based gel electrolytes, Electrochim. Acta, 40 (1995) 991.

[13] Appetecchi, G.B., Croce, F., Persi, L., Ronci, F. and Scrosati, B., Transport and interfacial properties of composite polymer electrolytes, Electrochim. Acta, 45 (2000) 1481.

[14] Armand, M.B., Chabagno, J.M. and Duclot, M.J., Poly-ethers as solid electrolytes in Fast ion transport in solids, Vashishta, P., Mundy, J.N. and Shenoy, G.K., eds., Elsevier, New York, (1979) 131.

[15] Armand, M.B., Chabagno, J.M. and Duclot, M.J., Polymer solid electrolytes, Second International Conference on Solid Electrolytes, St. Andrews (1978).

[16] Arvindan,V., Vickraman, P., Madhavi, S., Sivashanmugan, A., Thirunakaran, R. and Gopukumar, S., Improved performance of polyvinylidenefluoride-hexafluorpropylene based nanocomposite polymer membranes containing lithium bis(oxalato)borate by phase inversion for lithium batteries, Solid State Sc., 13 (2011) 1047.

[17] Badwal, S.P.S., Solid state ionics devices, Chowdari, B.V.R. and Radhakrishna, S., eds., World Scientific Publishing Co., Singapore (1988) 165.

[18] Bamford, D., Dlubek, G., Reiche, A., Alam, M.A., Meyer, W., Galvosas, P. and Rittig, F., The local free volume, glass transition, and ionic conductivity in a polymer electrolyte: a positron lifetime study, J. Chem. Phys., 115 (2001) 7260.

[19] Bares, J., Glass transition of the polymer microphase, Macromolecules, 8 (1975) 244.

[20] Baril, D., Michot, C. and Armand, M., Electrochemistry of liquids vs. solids: polymer electrolytes, Solid State Ionics, 94 (1997) 35.

[21] Bauerle, J.E., Study of solid electrolyte polarization by a complex admittance method, J. Chem. Phys., 30 (1969) 2657.

[22] Berthier, C., Gorecki, W., Minier, M., Armand, M.B., Chabango, J.M. and Rigaud, P., Microscopic investigation of ionic conductivity in alkali metal salts-poly(ethylene oxide) adducts, Solid State Ionics, 11 (1983) 91.

[23] Blackburn, F.R., Wang, C.Y. and Ediger, M.D., Translational and rotational motion of probes in supercooled 1,3,5-tris(naphthyl)benzene, J. Phys. Chem., 100 (1996) 18249.

[24] Blonsky, P.M., Shriver, D.F., Austin, P. and Allcock, H.R., Polyphosphazene solid electrolytes, J. Am. Chem. Soc., 106 (1984), 6854.

[25] Bohnke, O., Frand, G., Rezrazi, M., Rousselot, C. and Truche, C., Fast ion transport in new lithium electrolytes gelled with PMMA. 2. Influence of lithium salt concentration, Solid State Ionics, 66 (1993) 105.

[26] Bohnke, O., Rousselot, C., Gillet, P.A. and Truche, C., Gel electrolyte for solid-state electrochromic cell, J. Electrochem.Soc., 139 (1992) 1862.

[27] Bruce, P.G. and Gray, F.M., Solid state electrochemistry, Bruce, P.G., ed., Cambridge University Press, New York, USA (1995) 119.

[28] Bruce, P.G., ed., Solid state electrochemistry, Cambridge University Press, Cambridge, (1995).

[29] Bruce, P.G., Polymer Electrolyte Reviews-I, MacCallum, J.R. and Vincent, C.A., eds., Elsevier Applied Sciences, London (1987).

[30] Capiglia, C., Saito,Y., Yamamoto,H., Kageyama, H. and Mustarelli, P., Structure and transport properties of polymer gel electrolytes based on PVdF-HFP and $LiN(C_2F_5SO_2)_2$, Solid State Ionics, 131 (2001) 291.

[31] Capuano, F., Croce, F. and Scrosati, B., Composite polymer electrolytes, J. Electrochem. Soc., 138 (1991) 1918.

[32] Carol, P., Ramakrishnan, P., John, B. and Cheruvally, G., Preparation and characterization of electrospun poly(acrylonitrile) fibrous membrane based gel polymer electrolytes for lithium-ion batteries, J. Power Sources, 196 (2011) 10156.

[33] Chandra, A., Srivastava, P.C. and Chandra, S., Ion transport studies in PEO-NH_4I polymer electrolytes with dispersed Al_2O_3, J. Mater. Sci., 30 (1995) 3633.

[34] Chandra, S., Sekhon, S.S. and Arora, N., PMMA based protonic polymer gel electrolytes, Ionics, 6 (2000) 112.

[35] Chandra, S., Superionic solids - principle and application, Elsevier Science, (1981).

[36] Chen, X., Wei, S., Yadav, A., Patil, R., Jiahua Zhu, J., Ximenes, R., Sun, L. and Guo, Z., Poly(propylene)/Carbon Nanofiber Nanocomposites: Ex Situ Solvent-Assisted Preparation and Analysis of Electrical and Electronic Properties, Macromolecular Materials and Engineering, 296 (2011) 434.

[37] Cheradame, H., IUPAC Macromolecules, Benoit, H. and Rempp, P., eds., Pergamon, New York, (1982).

[38] Choe, H.S., Carroll, B.G., Pasquariello, D.M. and Abraham, K.M., Characterization of some polyacrylonitrile based electrolytes, Chem. Mater., 9 (1997) 369.

[39] Choi, S.W., Kim, J.R., Ahn, Y.R., Jo, S.M. and Cairns, E.J., Characterization of electrospun PVdF fiber-based polymer electrolytes, Chem. Mater., 19 (2007) 104.

[40] Cohen, M.H. and Grest, G.S., Liquid-glass transition: dependence of the glass transition on heating and cooling rates, Phys. Rev. B, 21 (1980) 4113.

[41] Cohen, M.H. and Trunbull, D., Molecular transport in liquids and glasses, J. Chem. Phys., 31 (1959) 1164.

[42] Cole, K.S. and Cole, R.H., Dispersion and absorption in dielectrics I. Alternating current characteristics, J. Chem. Phys., 9 (1941) 341.

[43] Croce, F., Appetecchi, G.B., Persi, L. and Scrosati, B., Nanocomposite polymer electrolytes for lithium batteries, Nature, 394 (1998) 456.

[44] DeSimone, T., Stratt, R.M. and Demoulini, S., Continuum percolation in an interacting system: Exact solution of the Percus-Yevick equation for connectivity in liquids, Phys Rev. Lett., 56 (1986) 1140.

[45] Druger, S.D., Nitzan, A. and Ratner, M.A., Dynamic bond percolation theory: A microscopic model for diffusion in dynamically disordered systems. I. Definition and one dimensional case, J. Chem. Phys., 79 (1983) 3133.

[46] Duclot, M., Alloin, F., Brylev, O., Sanchez, J.Y. and Souquet, J.L., New alkali ionomers: transport mechanism from temperature and pressure conductivity measurements, Solid State Ionics, 136/137 (2000) 1153.

[47] Fang, W., Chu, H.Y., Hsu, W.K., Cheng, T.W. and Tai, N.H., Polymer-Reinforced, Aligned Multiwalled Carbon Nanotube Composites for Microelectromechanical Systems Applications, Adv. Mater., 17 (2005) 2987.

[48] Faraday, M., Experimental researches in electricity, Bernard Quaritch, London (1839).

[49] Fenton, B.E, Parker J.M. and Wright P.V., Complexes of alkali metal ions with poly(ethylene oxide), Polymer, 14 (1973) 589.

[50] Fergus, J.W., Ceramic and polymeric solid electrolytes for lithium-ion batteries, J. Power Sources, 195 (2010) 4554.

[51] Ferry, A., Doeff, M.M. and DeJonghe, L.C. Transport property measurements of polymer electrolytes, Electrochim. Acta, 43 (1998) 1387.

[52] Florjanczyk, Z., W. Krawiec, D. Greszta, W. Wieczorek and M. Siekierski, Blend based polymeric electrolytes: a review, Bull. Eolectrochem., 8 (1992) 524.

[53] Friedrich, K., Microstructural efficiency and fracture toughness of short fiber/ thermoplastic matrix composites, Comp. Sc. Tech., 22 (1985) 43.

[54] Fujinami, T., Siloxyaluminate polymers with high Li^+ ion conductivity, Chem. Mater., 9 (1997) 2236.

[55] Fulcher, G.S., Analysis of recent measurements of the viscosity of glasses, J. Am. Ceram. Soc, 8 (1925) 339.

[56] Gabrielli, C., Identification of electrochemical processes by frequency response analysis, Solartron Instrumentation Group (1980).

[57] Gibbs, J.H. and DiMarzio, E.A., Nature of the glass transition and the glassy state, J. Chem. Phys., 28 (1958) 373.

[58] Glasstone, S., Laidler, K.J. and Eyring, H., The theory of rate processes, McGraw-Hill, New York (1941).

[59] Goldstein, M.J., Viscous liquids and the glass transition IV. Thermodynamic equations and the transition, J. Phys. Chem. 77 (1973) 667.

[60] Gozdz, A.S., Chmutz, C.N., Tarascon, J.M. and Warren, P.C., Lithium secondary battery extraction method, US patent No. 5540741, (1997).

[61] Gray, F.M., Polymer Electrolytes: Fundamentals and technological applications, VCH, New York, 1991.

[62] Gray, F.M., Polymer Electrolytes, Royal Chemical Society, Cambridge, (1997).

[63] Hall, P.G., Davies, G.R., McIntyre, J.E., Ward, I.M., Bannister, D.J. and Le Brocq, K.M.F., Ion conductivity in polysiloxane comb polymers with ethylene glycol teeth, Polym. Commun., 27 (1986) 98.

[64] Hashmi, S.A., Kumar, A. and Tripathi, S.K., Experimental studies on poly methyl methacrylate based gel polymer electrolytes for application in electrical double layer capacitors, J. Phys. D: Appl. Phys., 40 (2007) 6527.

[65] Hayamizu, K., Aihara, Y. and Price, W.S., Correlating the NMR self-diffusion and relaxation measurements with ionic conductivity in polymer electrolytes composed of cross-linked poly (ethylene oxide-propylene oxide) doped with $LiN(SO_2CF_3)_2$, Journal of Chemical Physics, 113 (2000) 4785.

[66] He, X., Shi, Q., Zhou, X., Wan, C. and Jiang, C., In situ composite of nano SiO_2–P(VDF-HFP) porous polymer electrolytes for Li-ion batteries, Electrochim. Acta, 51 (2005) 1069.

[67] Hwang, J.J. and Liu, H.J., Influence of organophilic clay on the morphology, plasticizer-maintaining ability, dimensional stability and electrochemical properties of gel polyacrylonitrile (PAN) nanocomposite electrolytes, Macromolecules, 35 (2002) 7314.

[68] Hwang, Y.J., Jeong, S.K., Nahm, K.S. and Stephan, A.M., Electrochemical studies on poly(vinylidene fluoride-hexafluoropropylene) membranes prepared by phase inversion method, Eur. Polym. J., 43 (2007) 65.

[69] Iijima, T., Toyoguchi, Y. and Eda, N., Quasi-solid organic electrolytes gelatinized with poly(methylmethacrylate) and their applications for lithium batteries, Denki Kagaku 53 (1985) 619.

[70] Ito, Y., Kanehori, K., Miyauchi, K. and Kudo, T., Ionic conductivity of electrolytes formed from PEO-$LiCF_3SO_3$ complex low molecular weight poly(ethylene glycol), J. Mater. Sci., 22 (1987) 1845.

[71] Itoh, T., Mitsuda, Y., Ebina, T., Uno, T. and Kubo, M., Solid polymer electrolytes based on comblike polymers, J. Power Sources, 163 (2006) 252.

[72] Jacob, M.M.E., Hackett, E. and Giannelis, E.P., From nanocomposite to nanogel polymer electrolytes, J. Mater. Chem., 13 (2003) 1.

[73] Jeon, J.D., Cho, B.W. and Kwak, S.Y., Solvent-free polymer electrolytes based on thermally annealed porous P(VdF-HFP)/P(EO-EC) membranes, J. Power Sources, 143 (2005) 219.

[74] Ji, K.S., Moon, H.S., Kim, J.W. and Park, J.W., Role of functional nano-sized inorganic fillers in poly(ethylene) oxide-based polymer electrolytes, J. Power Sources, 117 (2003) 124.

[75] Jiang, Z., Carroll, B. and Abraham, K.M., Studies of some poly(vinylidene fluoride) electrolytes, Electrochim. Acta, 42 (1997) 2667.

[76] Johan, M.R. and Fen, L.B., Combined effect of CuO nanofillers and DBP plasticizer on ionic conductivity enhancement in the solid polymer electrolyte PEO–$LiCF_3SO_3$, Ionics, 16 (2010) 335.

[77] Johan, M.R., Shy, O.H., Ibrahim, S., Yassin, S.M.M. and Hui, TY., Effects of Al_2O_3 nanofiller and EC plasticizer on the ionic conductivity enhancement of solid PEO–$LiCF_3SO_3$ solid polymer electrolyte, Solid State Ionics, 196 (2011) 41.

[78] Kaufmann, E.N., Characterization of materials, John Wiley & Sons Inc., Hoboken, New Jersey (2003).

[79] Killis, A., Le Nest, J.F., Gandini, A., Cheradame, H. and Addad, J.P.C., Correlation among transport properties in ionically conducting cross-linked networks, Solid State Ionics, 14 (1984) 231.

[80] Kim, C.S. and Oh, S.M., Importance of donor number in determining solvating ability of polymers and transport properties in gel-type polymer electrolytes, Electrochim. Acta, 45 (2000) 2101.

[81] Kim, C.S. and Oh, S.M., Spectroscopic and electrochemical studies of PMMA-based gel polymer electrolytes modified with interpenetrating networks, J. Power Sources, 109 (2002) 98.

[82] Kim, K.M., Ko, J.M., Park, N.G., Ryu, S. and Chang, S.H., Characterization of poly(vinylidenefluoride-co-hexafluoropropylene)-based polymer electrolyte filled with rutile TiO_2 nanoparticles, Solid State Ionics, 161 (2003) 121.

[83] Kim, S., Hwang, E.J, Jung, Y., Han, M. and Park, S.J., Ionic conductivity of polymeric nanocomposite electrolytes based on poly(ethylene oxide) and organo-clay materials, Colloids Surf. A: Physicochem. Engg. Aspects, 313/314 (2008) 216.

[84] Koksberg, R., Barker, J., Shi, H. and Saidi, M.Y., Cathode materials for lithium rocking chair batteries, Solid State Ionics, 84 (1996) 1.

[85] Kovac, M., Gaberscek, M. and Grdadolnik, The effect of plasticizer on the microstructural and electrochemical properties of a $(PEO)_n$ $LiAl(SO_3Cl)_4$ system, Electrochim. Acta, 44 (1998) 863.

[86] Kuila, T., Acharya, H., Srivastava, S.K., Samantaray, B.K. and Kureti, S., Enhancing the ionic conductivity of PEO based plasticized composite polymer electrolyte by $LaMnO_3$ nanofiller, Mater. Sc. Engg. B, 137 (2007) 217.

[87] Kumar, B. and Scanlon, L.G., Composite electrolytes for lithium rechargeable batteries, J. Electroceramics, 5 (2000) 127.

[88] Kumar, D., Suleman, Md. and Hashmi, S.A., Studies on poly(vinylidene fluoride-co-hexafluoropropylene) based gel electrolyte nanocomposite for sodium-sulfur batteries, Solid State Ionics, 202 (2011) 45.

[89] Kwon, Y.H., Chang, S.K., Hong, S.T., Kim, J.Y. and Oh, B.H., Novel polymer electrolyte and lithium secondary battery including the same, US patent 0106236 A1, (2014).

[90] Lalia, B.S., Fujita, T., Yoshimoto, N., Egashira, M. and Morita, M., Electrochemical performance of nonflammable polymeric gel electrolyte containing triethylphosphate, J. Power Sources, 186 (2009) 211.

[91] Lan, T. and Pinnavaia, T., Clay-reinforced epoxy nanocomposites, Chem. Mater. 6 (1994) 2216.

[92] Landauer, R., The electrical resistance of binary metallic mixtures, J. Appl. Phys., 23 (1952) 779.

[93] Lee, C.C. and Wright, P.V., Morphology and ionic conductivity of complexes of sodium iodide and sodium thiocyanate with poly(ethylene oxide), Polymer, 23 (1982) 681.

[94] Lee, K.P., Gopalan, A.I., Manesh, K.M., Santhosh, P. and Kim, K.S., Influence of Finely Dispersed Carbon Nanotubes on the Performance Characteristics of Polymer Electrolytes for Lithium Batteries, IEEE Transactions on Nanotechnology, 6 (2007) 362.

[95] Lee, W.J., Jung, H.R., Lee, M.S., Kim, J.H. and Yang, K.S., Preparation and ionic conductivity of sulfonated-SEBS/SiO_2/plasticizer composite polymer electrolyte for polymer battery, Solid State Ionics, 164 (2003) 65.

[96] Leo, C.J., Rao, G.V.S. and Chowdhari, B.V.R., Studies on plasticized PEO-lithium triflate-ceramic filler composite electrolyte system, Solid State Ionics, 148 (2001) 159.

[97] Li, Y., Wang, J., Tang, J., Liu, Y. and He, Y., Conductive performances of solid polymer electrolyte films based on PVB/$LiClO_4$ plasticized by PEG_{200}, PEG_{400} and PEG_{600}, J. Power Sources, 187 (2009) 305.

[98] Li, Z.H., Zhang, H.P., Zhang, P., Wu, Y.P. and Zhou, X.D., Macroporous nanocomposite polymer electrolyte for lithium-ion batteries, J. Power Sources, 184 (2008) 562.

[99] Linford, R.G., Applications of electroactive polymers, Scrosati, B. eds., Chapman and Hall London (1993) 1.

[100] Liquan, C., Materials for solid state batteries, Chowdari, B. and Radhakrishna, S., eds., World Scientific, Singapore, (1988) 69.

[101] Mac Donald, J.R., ed., Impedance spectroscopy, John Wiley & Sons, Inc. NewYork (1987).

[102] MacCallum, J.R. and Vincent, C.A. eds., Polymer electrolyte review-I, Elsevier Applied Science Publishers, London, (1987) 185.

[103] Macedo, P.B. and Litovitz, T.A., On the relative roles of free volume and activation energy in the viscosity of liquids, J. Chem. Phys, 42 (1965) 245.

[104] Maier, J., Heterogeneous doping of silver bromide (AgBr:Al_2O_3), Mat. Res Bull., 20 (1985) 383.

[105] Maxwell, J.C., A treatise on electricity and magnetism, Vol. 1, Chap. 11, Clerendon Press, London (1892).

[106] Mellander, B.E. and Lunden, A., Materials for solid state batteries, Chowdari, B.V.R. and Radhakrishna, S., eds., World Scientific Publ. Co. Pvt. Ltd., Singapore (1986) 161.

[107] Meyer, W.H., Polymer electrolytes for lithium-ion batteries, Adv. Mater.,10 (1998) 439.

[108] Mierzwa, M., Floudas, G. Štepánek, P. and Wegner, G., Effect of pressure on the side-chain crystallization of poly(n-octadecyl methacrylate) studied by dielectric spectroscopy, Phys. Rev. B, 62 (2000) 14012.

[109] Nagasubramanian, G. and Di Stefano, S., 12-Crown-4 ether-assisted enhancement of ionic conductivity and interfacial kinetics in polyethylene oxide electrolytes, J. Electrochem. Soc., 137

[110] Nakamura, M., Conductivity for the site-percolation problem by an improved effective-medium theory, Phys. Rev. B, 29 (1984) 3691.

[111] Nan, C.W. and Smith, D.M., A.c. electrical properties of composite solid electrolytes, Mat. Sci. Eng. B, 10 (1991) 99.

[112] Nan, C.W., Fan, L., Lin, Y. and Cai, Q., Enhanced ionic conductivity of polymer electrolytes containing nanocomposite SiO_2 particles, Phy. Rev. Lett., 91 (2003) 266104.

[113] Nan, C.W., Physics of inhomogeneous inorganic materials, Prog. Mater. Sci., 37 (1993) 1.

[114] Nemanich, R.J. and Solin, S.A., First- and second-order Raman scattering from finite-size crystals of graphite, Phys. Rev. B, 20 (1979) 392.

[115] Nicholas, C.V., Wilso, D.J., Booth, C. and. Giles, J.R.M., Improved synthesis of oxymethylene-linked poly(oxyethylene), Br. Polym. J., 20 (1988) 289.

[116] Osman, Z. Ghazali, M.I., Othman, L. and Isa, K.B., AC ionic conductivity and DC polarization method of lithium ion transport in PMMA-$LiBF_4$ gel polymer electrolytes, Results in Physics, 2 (2012) 1.

[117] Owens, B.B. and Argue, G.R., High-conductivity solid electrolytes: MAg_4I_5, Science, 157 (1967) 308.

[118] Panero, S., Scrosati, B. and Greenbaum, S.G., Ionic conductivity and ^7Li NMR Study of Poly(ethylene glycol) complexed with lithium salts, Electrochim. Acta, 37 (1992) 1533.

[119] Parka, C.H., Kim, D.W., Prakash, J. and Sun, Y.K., Electrochemical stability and conductivity enhancement of composite polymer electrolytes, Solid State Ionics, 159 (2003) 111.

[120] Pavia, D.L., Lampman, G.M., Kriz, G.S. and Vyvyan, J.A., Introduction to spectroscopy, Brooks Cole, Belmont, CA (2009).

[121] Payne, D.R. and Wright, P.V., Morphology and ionic conductivity of some lithium ion complexes with poly(ethylene oxide), Polymer 23 (1982) 690.

[122] Pradhan, D.K., Samantaray B.K., Choudhary R.N.P. and Thakur A.K., Effect of plasticizer on structure-property relationship in composite polymer electrolytes, J. Power Sources, 139 (2005) 384.

[123] Przyluski J. and Wieczorek, W., Solid state ionics: materials and applications, Chowdari, B.V.R. and Radakrishna, S., eds., World Scientific Publ. Co., Singapore (1992) 209.

[124] Przyluski, J., Siekierski, M. and Wieczorek, W., Effective medium theory in studies of conductivity of composite polymeric electrolytes, Electrochim. Acta, 40 (1995) 2101.

[125] Raistrick, I.D., Application of impedance spectroscopy to problems in solid state ionics, Solid State Ionics, 18/19 (1986) 40.

[126] Raistrick, I.D., Macdonald, J.R. and Franceschetti, D.R., Impedance spectroscopyc characterizing solid materials and analysis, Macdonald, J.R., ed., Chap. 2, John Wiley & Sons Inc., New York (1987).

[127] Rajendran, S. and Sivakumar, P., An investigation of PVdF/PVC-based blend electrolytes with EC/PC as plasticizers in lithium battery applications, Physica B, 403 (2008) 509.

[128] Rajendran, S. and Uma, T., Conductivity studies on PVC/PMMA polymer blend electrolyte, Mater. Lett., 44 (2000) 242.

[129] Rajendran, S., Kannan, R. and Mahendran, O., An electrochemical investigation on PMMA/PVdF blend-based polymer electrolytes, Mater. Lett., 49 (2001) 172.

[130] Rajendran, S., Kesavan, K., Nithya, R. and Ulaganathan, M., Transport, structural and thermal studies on nanocomposite polymer blend electrolytes for Li-ion battery applications, Current Appl. Phys., 12 (2012) 789.

[131] Ramanathan, T., Stankovich, S., Dikin, D.A., Liu, H., Shen, H., Nguyen, S.T. and Brinson, L.C., Graphitic nanofillers in PMMA nanocomposites-An investigation of particle size and dispersion and their influence on nanocomposite properties, J. Polymer Sci.: Part B: Polymer Phy., 45 (2007) 2097.

[132] Randles, J.E.B., Kinetics of rapid electrode reactions, Discuss. Faraday Soc., 1 (1947) 11.

[133] Ratner, M.A. and Nitzan, A., Conductivity in polymer ionics. Dynamic disorder and correlation, Faraday Discuss. Chem. Soc., 88 (1989) 19.

[134] Ratner, M.A., Polymer electrolyte reviews, MacCallum, J.R. and Vincent, C.A., eds., Elsevier, London (1987).

[135] Ray, S.S., Polymer Nanocomposites, J. Nanosc. Nanotech., 8 (2008) 1557.

[136] Roelofs, M.G., Choudhury, B., Siddiqui, J.A. and Banerjee, S., Composite electrolyte membrane, US patent 0120431 A1, (2014).

[137] Russell, C.A., The determination of the relative isotactic content of polypropylene by extraction, J Appl Polym Sci, 4 (1960) 219.

[138] Saikia, D., and Kumar, A., Ionic conduction in P(VDF-HFP)/PVDF–(PC+DEC)–$LiClO_4$ polymer gel electrolytes, Electrochim. Acta, 49 (2004) 2581.

[139] Sander, B., Steurich, T., Wiesner, K. and Bischoff, H., Solid polymer electrolytes based on oligo(ethyleneglycol)methacrylates, Polym. Bull., 28 (1992) 355.

[140] Schneider, H.A. and DiMarzio, E.A., The glass temperature of polymer blends:comparison of both the free volume and the entropy predictions with data, Polymer, 33 (1992) 3453.

[141] Scrosati, B. ed., Applications of electroactive polymers, Chapman and Hall, London (1993).

[142] Scrosati, B., ed., Second international symposium on polymer electrolytes, Elsevier, Amsterdam, (1990) 339.

[143] Scrosati, B., Electrochemistry of novel materials, Lipkowski, J. and Ross, P.N., eds., VCH, Weinheim, Germany (1994) 111.

[144] Scrosati, B., JEC battery newsletters, 6, 44 (1993) 53.

[145] Scrosati, B. and Vincent, C.A., Polymer electrolytes: The key to lithium polymer batteries, MRS Bulletin, 25 (2000) 28.

[146] Sekhon, S.S., Conductivity behaviour of polymer gel electrolytes: role of polymer, Bull. Mater. Sc., 26 (2003) 321.

[147] Sengupta, R., Bhattacharya, M., Bandyopadhyay, S., and Bhowmick, A.K., A review on the mechanical and electrical properties of graphite and modified graphite reinforced polymer composites, Prog. Pol. Sc., 36 (2011) 638.

[148] Shah, D., Maiti, P., Jiang, D. and Giannelis, E.P., Effect of nanoparticle mobility on toughness of polymer nanocomposites, Adv. Mater., 17 (2005) 525.

[149] Shodai, T., Owens, B.B., Ohtsuka, H. and Yamaki, J., Thermal stability of the polymer electrolyte $(PEO)_8\,LiCF_3SO_3$, J. Electrochem. Soc., 141 (1994) 2978.

[150] Singh, J., Mimani, T., Patil, K.C. and Bhatt, S.V., Enhanced lithium-ion transport in PEG-based composite polymer electrolyte with $Mn_{0.03}Zn_{0.97}Al_2O_4$ nanoparticles, Solid State Ionics 154/155 (2002) 21.

[151] Smedly, S., The interpretation of ionic conductivity in liquids, Springer (1980).

[152] Song, J.Y., Cheng, C.L., Wang, Y.Y. and Wan, C.C., Microstructure of poly(vinylidene fluoride)-based polymer electrolyte and its effect on transport properties, J. Electrochem. Soc., 149 (2002) A1230.

[153] Song, J.Y., Wang, Y.Y. and Wan C.C., Conductivity study of porous plasticized polymer electrolytes based on poly(vinylidene fluoride) A comparison with polypropylene separators, J. Electrochem Soc., 147 (2000) 3219.

[154] Song, J.Y., Wang, Y.Y. and Wan C.C., Review of gel-type polymer electrolytes for lithium-ion batteries, J. Power Sources, 77 (1999) 183.

[155] Stallworth, P.E., Greenbaum, S.G., Croces, F., Slant, S. and Salomon, M., Lithium-7 NMR and ionic conductivity studies of gel electrolytes based on poly(methylmethacrylate), Electrochim. Acta., 40 (1995) 2137.

[156] Stephan, A.M. and Nahm, K.S., Review on composite polymer electrolytes for lithium batteries, Polymer, 47 (2005), 5952.

[157] Stephan, A.M. and Saito, Y., Ionic conductivity and diffusion coefficient studies of PVdF–HFP polymer electrolytes prepared using phase inversion technique, Solid State Ionics,148 (2002) 475.

[158] Stephan, A.M., Kumar, S.G., Renganathan, N.G. and Kulandainathan, M.A., Characterization of poly(vinylidenefluoride-hexafluoropropylene) (PVdF–HFP) electrolytes complexed with different lithium salts, Eur. Polym. J., 41 (2005) 15.

[159] Stephan, A.M., Nahm, K.S., Kumar, T.P., Kulandainathan, M.A., Ravi, G. and Wilson, J., Nanofiller incorporated poly(vinylidene fluoride-hexafluoropropylene) (PVdF–HFP) composite electrolytes for lithium batteries, J. Power Sources, 159 (2006) 1316.

[160] Stephan, A.M., Review on gel polymer electrolytes for lithium batteries, Eur. Polym. J., 42 (2006) 21.

[161] Sun, H.Y., Sohn, H.J., Yamamoto, O., Takeda, Y. and Imanishi, N., Enhanced lithium-ion transport in PEO-based composite polymer electrolytes with ferroelectric $BaTiO_3$, J. Electrochem. Soc., 146 (1999) 1672.

[162] Tarascon, J.M., GozdzA,. S, Schmutz, C., Shokoohi, F. and Warren, P.C., Performance of Bellcore's plastic rechargeable Li-ion batteries, Solid State Ionics, 86 (1996) 49.

[163] Tibbetts, G.G., Lake, M.L., Strong, K.L. and Rice, B.P., A review of the fabrication and properties of vapor-grown carbon nanofiber/polymer composites, Compo. Sci. Tech., 67 (2007) 1709.

[164] Tien, C.P., Liang, W.J., Kuo, P.L. and Teng, H.S., Electric double layer capacitors with gelled polymer electrolytes based on poly(ethylene oxide) cured with poly(propylene oxide) diamines, Electrochimica Acta, 53 (2008) 4505.

[165] Torrel, L.M. and Angell, C.A., Ion matrix coupling in polymer electrolytes from relaxation time studies, Br. Polym. J., 20 (1988) 173.

[166] Tran, M.Q., Cabral, J.T., Shaffer, M.S.P. and Bismarck, A., Direct measurement of the wetting behavior of individual carbon nanotubes by polymer melts:The key to carbon nanotube-polymer composites A., Nano Letters, 8 (2008) 2744.

[167] Tsuchida, E., Ohno, H. and Tsunemi, K., Conduction of lithium ions in polyvinylidene fluoride and its derivatives, Electrochim. Acta., 28 (1983) 591.

[168] Vallee, A., Besner, S. and Prud'homme, J., Comparative study of poly(ethylene oxide) electrolytes made with $LiN(CF_3SO_2)_2$, $LiCF_3SO_3$ and $LiClO_4$: Thermal properties and conductivity behavior, Electrochim. Acta, 37 (1992) 1579.

[169] Wagner, J.B. and Wagner, C., Electrical conductivity measurements on cuprous halides, J. Chem. Phys., 26 (1957) 1597.

[170] Wagemaker, M. and Mulder, F.M., Properties and Promises of Nanosized Insertion Materials for Li-Ion Batteries, Acc. Chem. Res., 46 (2013) 1206.

[171] Watanabe, M. and Ogata, N., Polymer electrolytes reviews-I, MacCallum, J.R. and Vincent, C.A., eds., Elsevier, London, (1987) 39.

[172] Watanabe, M., Kanba, M., Matsuda, H., Tsunemi, K., Mizoguchi, K., Tsuchida, E. and Shinohara, I., High lithium ion conductivity of polymeric solid electrolytes, Die Makromolekulare Chemie, 2 (1981) 741.

[173] Watanabe, M., Kanba, M., Nagaoka, K. and Shinohara, I., Ionic conductivity of hybrid films based on polyacrylonitrile and their battery application, J. Appl. Polym. Sci., 27(1982) 4191.

[174] Watanabe, M., Kanba, M., Nagaoka, K. and Shinohara, I., Ionic conductivity of hybrid films composed of polyacrylonitrile, ethylene carbonate and $LiClO_4$, J. Polym. Sci. Part B: Polym. Phys., 21 (1983) 939.

[175] Watanabe, M., Sanui, K., Ogata, N., Kobayashi, T. and Ohtaki, Z., Ionic conductivity and mobility in network polymers from poly(propylene oxide) containing lithium perchlorate, J. Appl. Phys., 57 (1985) 123.

[176] Weston, J.E. and Steele, B.C.H., Effects of inert fillers on the mechanical and electrochemical properties of lithium salt-poly(ethylene oxide) polymer electrolytes, Solid State Ionics, 7 (1982) 75.

[177] Wieczorek, W. and Siekierski, M., A description of the temperature dependence of the conductivity for composite polymeric electrolytes by effective medium theory, J. Appl. Phys., 76 (1994) 2220.

[178] Wieczorek, W., Raducha, D., Zalewska, A. and Stevens, J.R., Effect of Salt Concentration on the Conductivity of PEO-Based Composite Polymeric Electrolytes, J. Phys. Chem. B 102 (1998) 8725.

[179] Wieczorek, W., Stevens, J.R. and Florjańczy, Z., Composite polyether based solid electrolytes. The Lewis acid-base approach, Solid State Ionics, 85 (1996) 67.

[180] Wieczorek, W., Such, K., Chung, S.H. and Stevens, J.R., Comparison of properties of composite polymeric electrolytes based on the oxymethylene-linked poly(ethylene oxide) $NaClO_4$ electrolyte with polyacrylamide or α-Al_2O_3 Additives, J. Phys. Chem., 98 (1994) 9047.

[181] Wieczorek, W., Such, K., Florjanczyk, Z. and Stevens, J. R., Polyether, polyacrylamide, $LiClO_4$ composite electrolytes with enhanced conductivity, J. Phys. Chem. 98 (1994), 6840.

[182] Wieczorek, W., Such, K., Wycislik, H. and Plocharski, J., Modifications of crystalline structure of PEO polymer electrolytes with ceramic additives, Solid State Ionics, 36 (1989) 255.

[183] Wieczorek, W., Zalewska, A., Raducha, D., Florjanczyk, Z. and. Stevens, J.R., Polyether, poly(N,N-dimethylacrylamide) and $LiClO_4$ composite polymeric electrolytes, Macromolecules, 29 (1996) 143.

[184] Williams, G., Dielectric spectroscopy of polymeric materials, fundamentals and applications, Runt, J.P. and Fitzgerald, J.J., eds., Am. Chem. Soc., Washington (1997).

[185] Williams, M.L., Landel, R.F. and Ferry, J.D., The temperature dependence of relaxation mechanisms in amorphous polymers and other glass-forming liquids, J. Am. Chem. Soc., 77 (1955) 3701.

[186] Wu, C.G., Lu, M.I., Tsai, C.C. and Chuang, H.J., PVdF-HFP/metal oxide nanocomposites: The matrices for high-conducting, low-leakage porous polymer electrolytes, J. Power Sources, 159 (2006) 295.

[187] Xiao, Q., Wang, X., Li, W., Li, Z., Zhang, T. and Zhang, H., Microporous polymer electrolytes based on PVdF/PEO-b-PMMA block copolymer blends for rechargeable lithium battery, J. Membr. Sci., 334 (2009) 117.

[188] Xi, J., Qiu, X., Li, J., Tang, X., Zhu, W. and Chen, L., PVDF–PEO blends based microporous polymer electrolyte: Effect of PEO on pore configurations and ionic conductivity, J. Power Sources, 157 (2000) 501.

[189] Yamamoto, T., Hara, T., Segawa, K., Honda, K. and Akashi, H., 4.4 V lithium-ion polymer batteries with a chemical stable gel electrolyte, J. Power Sources, 174 (2007) 1036.

[190] Zhang, M., Yudasaka, M., Koshio, A. and Iijima, S., Thermo-gravimetric analysis of single-wall carbon nanotubes ultrasonicated in monochlorobenzene, Chemical Physics Letters, 364 (2002) 420.

[191] Zhang, S., Lee, J.Y. and Hong, L., Visualization of particle distribution in composite polymer electrolyte systems, J. Power Sources, 126 (2004) 125.

[192] Zhou, J. and Fedkiw, P.S., Cycling of lithium/metal oxide cells using composite electrolytes containing fumed silica, Electrochim. Acta, 48 (2003) 2571.